Mono and Bimetallic Transition Metal Complexes That Bind to DNA

by

Clive Metcalfe

A Thesis Submitted for the Degree of Doctor of Philosophy

March 2002

Department of Chemistry
University of Sheffield
Sheffield
S3 7HF

Abstract

This thesis reports the syntheses and DNA binding properties of a number of novel DNA binding complexes.

A library of ruthenium(II) and rhenium(I) complexes incorporating extended terpyridine type ligands has been synthesised **(1)**.

The library consists of a series of structurally related complexes in which we have varied the number of hydrogen bonding sites, charge, chirality and steric demand on the complexes. Experimental data offers clear evidence that these complexes interact with DNA, possibly in an intercalative mode, and that varying the characteristics above has significant effects on the nature of the interaction with DNA.

Furthermore a series of achiral mono **(2)** and bimetallic complexes of ruthenium(II) **(3)** and rhenium(I) **(4)** incorporating the well-characterised intercalating domain dppz have been assembled. The novel achiral ruthenium system shows good affinity for CT-DNA and there is a 13-fold increase in binding affinity for the di-cationic complex over the mono-cationic complex. The binding of the di-rhenium and bis-ruthenium complexes show increased affinity for CT-DNA however bis-intercalation is not seen and the major contribution to the interaction comes from electrostatic and groove binding interactions.

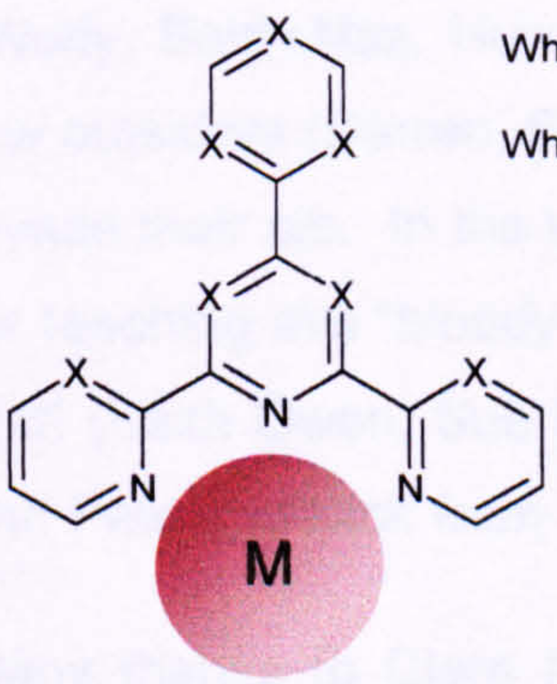

Where X = C or N

Where M = $(phen)_2 Ru^{2+}$
= $(terpy) Ru^{2+}$
= $(CO)3L Re^{+}$

(1)

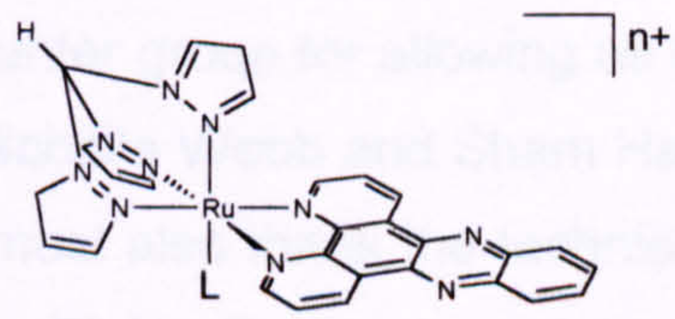

L = Cl, n=1
L = Py or MeCN, n = 2

(2)

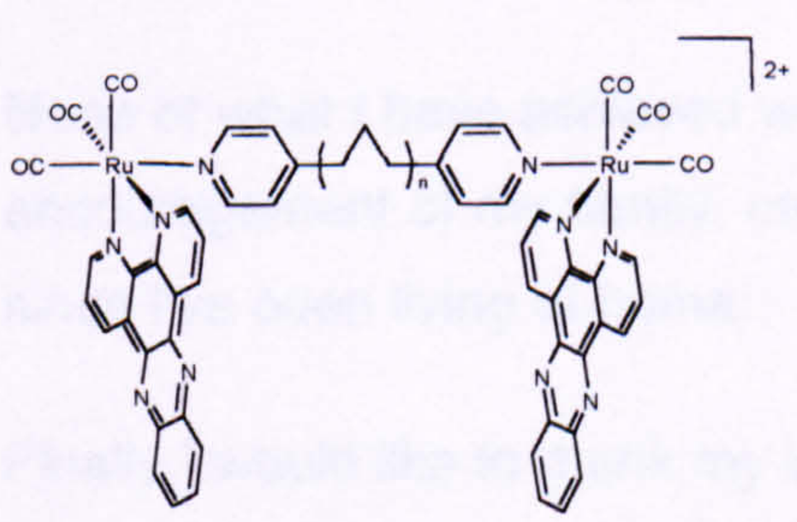

(3)

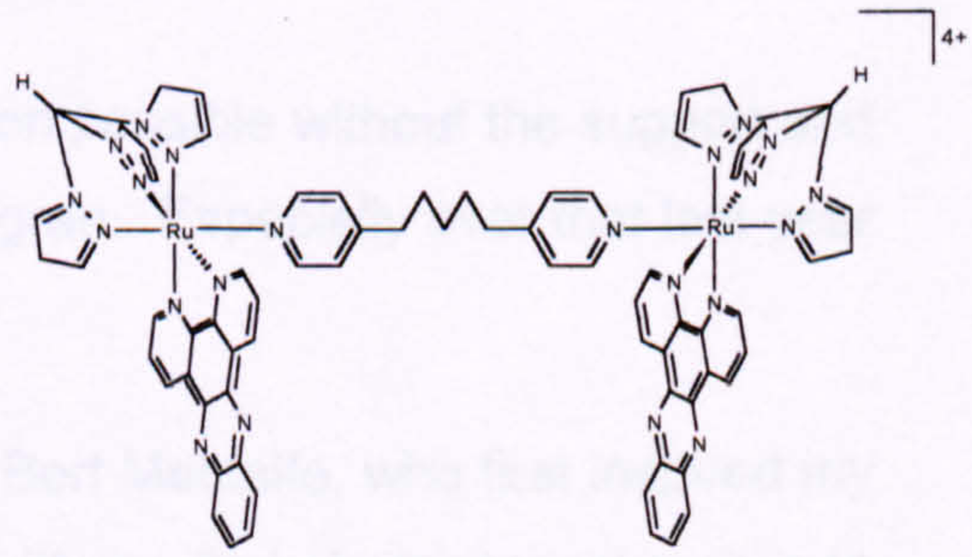

(4)

Acknowledgments

Although this passage resides at the front of this thesis, the fact that I am writing it means that my three and a half years in the chemistry department at Sheffield are drawing to a close. Many people have helped supported and encouraged me throughout my Ph.D. and I would like to thank a few of them personally. My apologies for those I have omitted, but not forgotten.

First I would like to thank the many friends I have made over the years. In particular many thanks to Wolfy, Isabel, Mark, Glarves, Tony and Sue. Thanks for all the beer, curry, football, whinging and emails.

I also express sincere gratitude to my supervisor Jim Thomas for his constant encouragement, endless enthusiasm and incredible ability to invent new ideas, Although one always worries when you hear the words “It will definitely work” or “money for old rope”. In the early days I owe much to Sue Roche and Tony Johnson, as they taught me all I know about chemistry, football, beer and talking rubbish. I express thanks to all those who have worked in the Thomas group (Wolfy, Baldy,Naz, Huw and the many 4th year and Erasmus students), plus a few outsiders (Darren, Scott and Barney) and the Hunter group for allowing us to invade their lab. In the latter stages I must thank Michelle Webb and Sham Haq for teaching this “bloody chemist” some biology. I must also thank the technical staff (Keith Owen, Sue Bradshaw, Denise Richards, Elaine Frary, Harry Adams and Pete and Nick from stores) whose knowledge and expertise is unsurpassed.

Many thanks to Clare for her encouragement and support and thanks to her family for making me so welcome.

None of what I have achieved would have been possible without the support and encouragement of my family, mum, dad and gran. Especially over that last year since I’ve been living at home.

Finally I would like to thank my late grandad, Bert Metcalfe, who first inspired my interest in practical things. He supplied me with my first chemistry set so it is to him that I dedicate this thesis.

Abbreviations

A	Adenine
bipy	2,2'-bipyridine
Bp	Base pairs
bpm	2,2'-bipyrimidine
C	Cytosine
CD	Circular dichroism
Chrysi	5,6-chrysinequinone diimine
COSY	Correlation spectroscopy
CT-DNA	Calf thymus DNA
CV	Cyclic Voltammetry
DABCO	1,4-diazobicyclo[2.2.2]octane
DCM	Dichloromethane
DMF	Dimethylformamide
DMSO	Dimethylsulfoxide
DNA	Deoxyribose nucleic acid
dNTP	Deoxynuleotide triphosphate
dpb	2,3-bis(2-pyridyl)benzo[g]quinoxaline
dpe[2]	1,2-di(4-pyridyl)-ethane
dpp[3]	1,3-di(4-pyridyl)-propane
dpp[5]	1,5-di(4-pyridyl)-pentane
dpphen	4,7-diphenyl-1,10-phenanthroline
dppn	Benzodipyridophenazine
dppz	Dipyrido[3,2-a:2',3'-c]phenazine
dpq	Dipyrido-[3,2-d:2',3'-f]-quinoxaline
dpqc	Dipyrido-[3,2-a:2',3'-c]-(6,7,8,9-tetrahydro)-

	phenazine)
en	Ethylenediamine
FAB-MS	Fast atom bombardment mass spectrometry
G	Guanine
HOMO	Highest occupied molecular orbital
ITC	Isothermal titration calorimetry
LD	Linear dichroism
LUMO	Lowest unoccupied molecular orbital
m-AMSA	Amsacrin
Me_2bipy	4,4'-dimethyl-2,2'-bipyridine
Me_2trien	diamino-4,7-diazodecane
MLCT	Metal to ligand charge transfer
Mp	Melting point
mRNA	Messenger RNA
MS	Mass spectrometry
NMR	Nuclear magnetic resonance
ORTEP	Oak Ridge Thermal Ellipsoid Parameters
P-terpy	4'-phenyl-2,2':6',2''-terpyridine
pdo	1,10-phenanthroline-5,6-dione
ph	Phenyl
PHEHAT	1,10-phenanthroline-[5,6-b]-1,4,5,8,9,12-hexaazatriphenylene
phen	1,10-phenanthroline
phi	9,10-phenanthrinequinone diimine
ppy	2-phenylpyridine
Py	Pyridine
Pyr	Pyrimidine
Qtpy	2,2':4,4'':6,2''-quaterpyridine
rac	Racemic
RNA	Ribose nucleic acid
rRNA	Ribosomal RNA

sat	Saturated
snRNA	Small nuclear RNA
T	Thymine
Terpy	2,2':6',2''-terpyridine
THF	Tetrahydrofuran
TLC	Thin layer chromatography
Tpm	Tris-(1-pyrazolyl)methane
Tpp	tetra-2-pyridyl-1,4-pyrazine
Tpt	2,4,6-tris(2-pyridyl)1,3,5-triazine
Tpymt	2,4,6-tris(2-pyrimidyl)1,3,5-triazine
tRNA	Transfer RNA
U	Urasil
UV	Ultra violet

Contents

Figures

Reaction Schemes

Tables

Chapter 1

Introduction

1.1 DNA-the molecule of life

Deoxyribose nucleic acid (DNA) is described as a chemical repository for the genetic information of an organism[1]. This apparently "simple" bio-polymer, consisting of four distinct building blocks, is capable of storing, retrieving and processing immense amounts of genetic information quickly and efficiently upon cellular demand. The information stored within the DNA in the form of the genetic code, governs every characteristic of every living species on earth.

DNA is designed in such a way that it can be easily copied, allowing vital information to be passed on from generation to generation. Although the information is never lost it is sometimes altered, either as a result of breeding where the individual genetic characteristic from the father and the mother is mixed, or as a result of a physical alteration such as miss-copying or damage sustained from an external source. These alterations are called mutations and often trigger a cascade of events that eventually lead to the host developing a disadvantageous condition such as some form of disease or a characteristic that will enable it to become fitter and stronger than before.

Over the last half-century, scientists have begun to unlock many of the mechanisms of the processes surrounding the function of DNA, such as replication, damage repair, transcription and its function in the cell cycle. It is now the ultimate goal of genetic scientists to gain control of the

functions of DNA by designing novel molecular scale tools and probes that can be easily introduced to the cell and perform specific pre-determined tasks. One such goal is to be able to selectively switch a gene on or off in a process called 'gene modulation' and this thesis describes a small step towards this goal through the use of metal-based DNA binding agents.

If a mutation occurs in a gene, which has a marked negative affect on its host, the ability to switch this gene off and stop it being replicated throughout the host, or even repair the gene on the chromosome would be a priceless commodity in the fight against disease.

The primary feature of any natural or synthetic molecule that interacts with DNA is its ability to form a tight pre-defined complex with the DNA molecule. That means that the targeting molecule must be able to read the genetic code for itself, so that it can be sure to bind to the correct site or gene on a DNA molecule that contains many hundreds of thousands of potential binding sites. In order to achieve this, one must have an understanding of the structural and physical characteristics of DNA that can be exploited in the design of site-specific DNA binding molecules.

1.2 The structure of DNA[2]

DNA is a biopolymer made from four code-dependant alternating sub units of nucleotides, consisting of a nucleoside bonded through a 5' phosphate ester linkage to phosphoric acid. A nucleoside is a 2' deoxy ribose sugar with a heterocyclic amine base bonded to the C1 carbon of the ribose sugar (Figure 1.1).

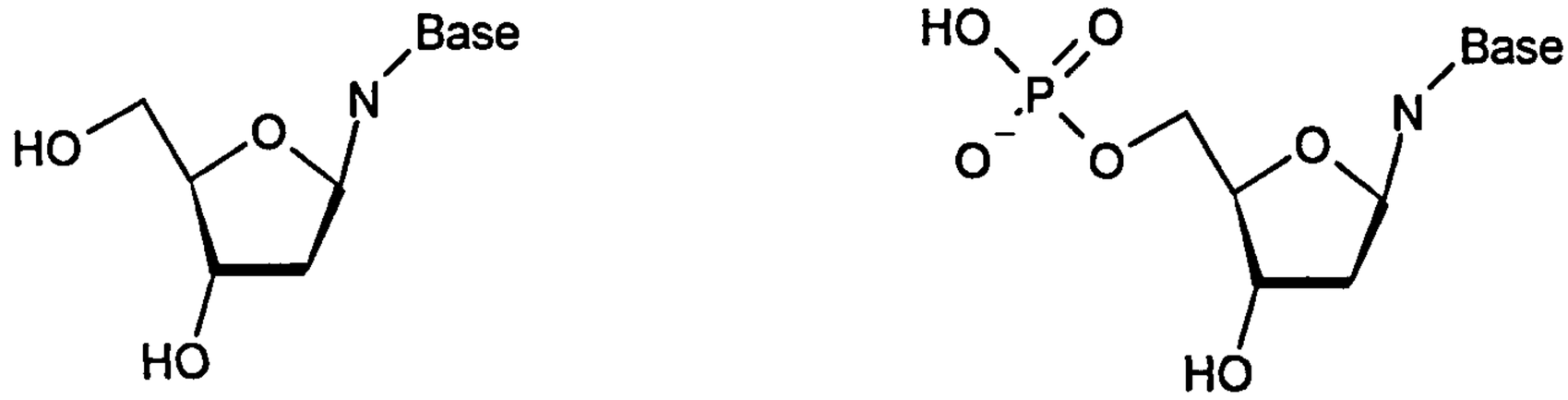

Figure 1.1:- *A nucleoside (A) and a nucleotide (B)*

The polymer is formed by the 5' phosphoric acid forming another phosphate ester linkage to 3' hydroxyl of an adjacent nucleotide.

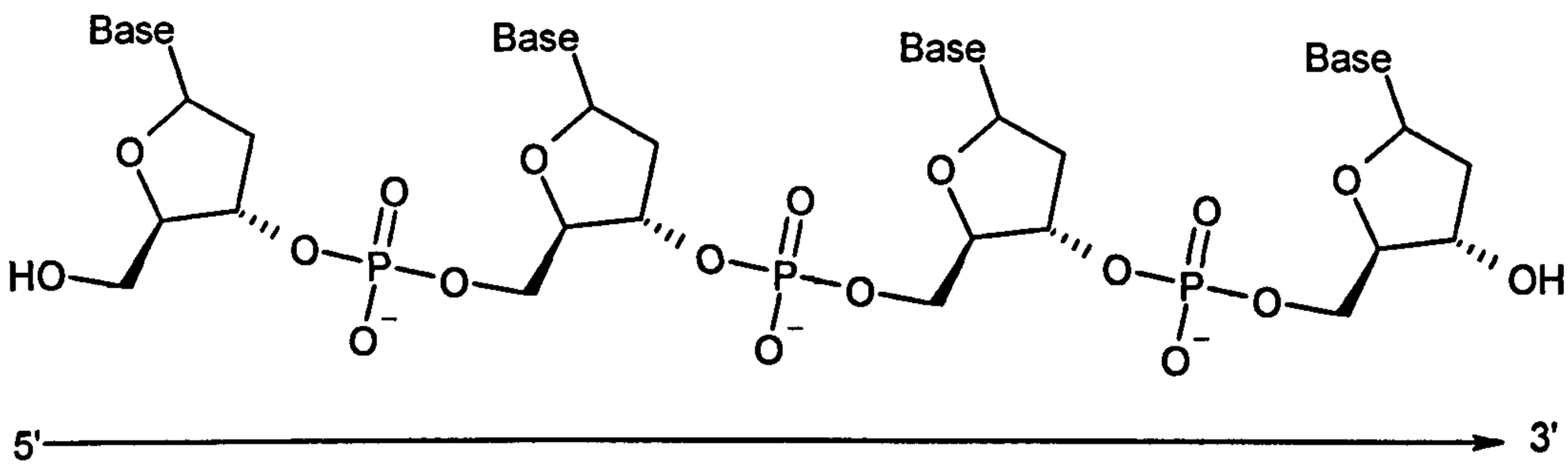

Figure 1.2:- *Schematic of DNA showing the 5'→3' polarity of the structure*

1.2.1 The DNA bases and Watson-Crick base pairing[1]

The code that DNA stores so effectively is made up of four "letters" which represent the four DNA bases. The purine bases are adenine (A) and guanine (G) and pyrimidine bases are thymine (T) and cytosine (C) (Figure 1.3).

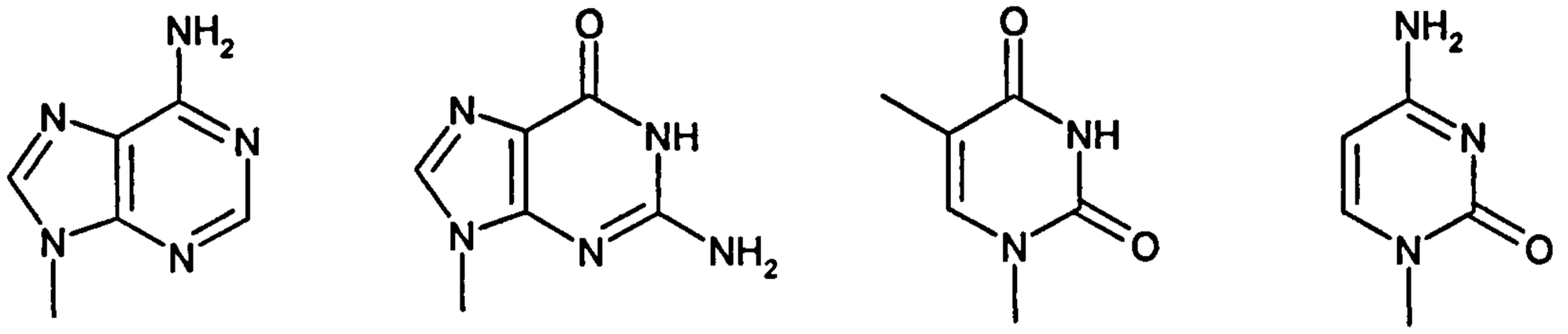

Figure 1.3:- *The DNA bases*

In the early 1950s when Watson and Crick were working investigating the structure of DNA, they made the observation that wherever an A appeared in the sequence it was always paired with T. Likewise wherever G appeared it was always paired with C. This led them to propose that DNA consisted of two complementary strands which were held together through hydrogen bonds between complementary base pairs TA and GC (Figure 1.4).

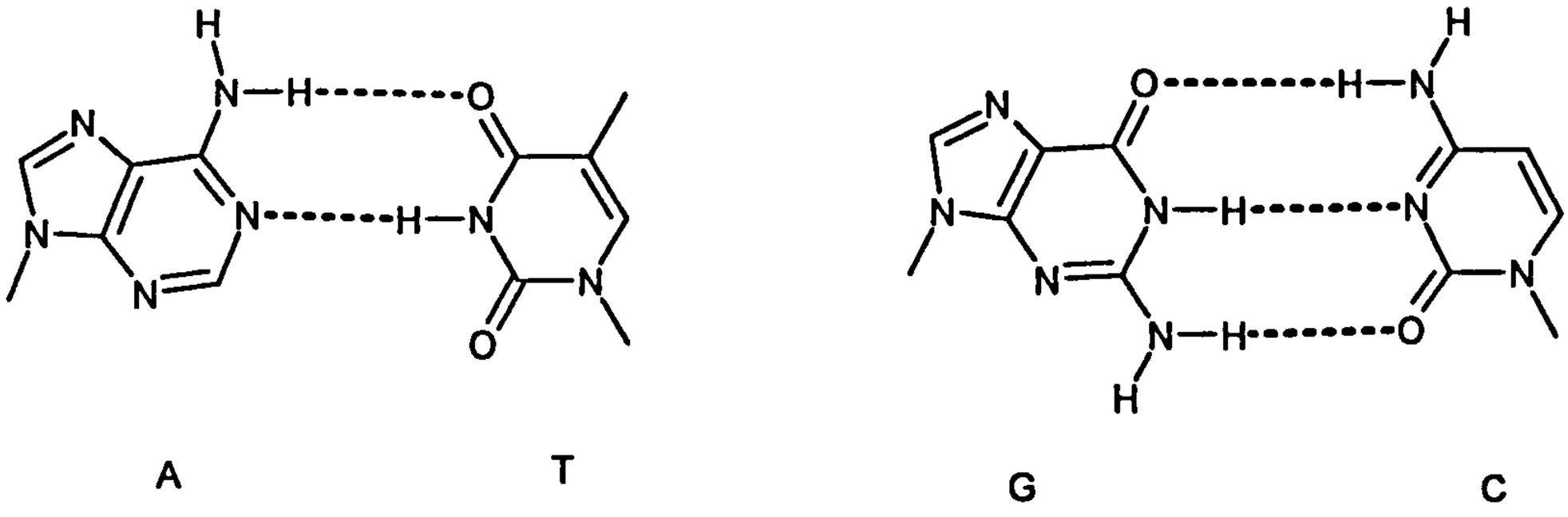

Figure 1. 4:- *The complementary hydrogen bonding in DNA base pairs*

1.2.2 The DNA helix[1]

With the help of an X-ray diffraction pattern and the knowledge of DNA base-pairing Watson and Crick were able to propose a complete structural model of DNA.

The important features of their model are:

1. Two helical polynucleotide chains are coiled around a common core.

2. The purine and pyrimidine bases are stacked along the central axis of the helix whereas the phosphate and deoxyribose units are on the outside of the helix. The planes of the bases are perpendicular to the central axis

3. The diameter of the helix is 20 Å. Adjacent bases are separated by 3.4 Å along the helical axis and are offset by a rotation of 36°. Hence the helical structure repeats after ten residues on each chain.

4. The two chains run in opposite directions and are held together by hydrogen bonds between the base pairs. Each base pair consists of one pyrimidine and one purine.

5. The sequence of bases along a polynucleotide chain is not restricted in any way. The precise sequence of bases carries the genetic code.

Due to steric restrictions, each base pair consists of a purine and a pyrimidine base. The regular nature of the helical phosphate backbone means that the glycosidic bonds that attach the deoxyribose sugars to the bases are always 10.85 Å apart. A purine-pyrimidine base pair fits perfectly into this space. There is insufficient space for two purines but

too much for two pyrimidines meaning they would be placed too far apart for any hydrogen bonding interaction to occur.

1.2.3 The major and minor grooves[2]

A consequence of the helical structure of DNA is that there are two helical grooves that run the entire length of the DNA molecule. These are called the major and the minor groove (Figure 1.5). The major groove is wider (12 Å) than the minor groove (6 Å). The bases themselves can be accessed from both the major and the minor groove, allowing molecules such as proteins and other small molecules to read the code and bind to the DNA molecule sequence specifically.

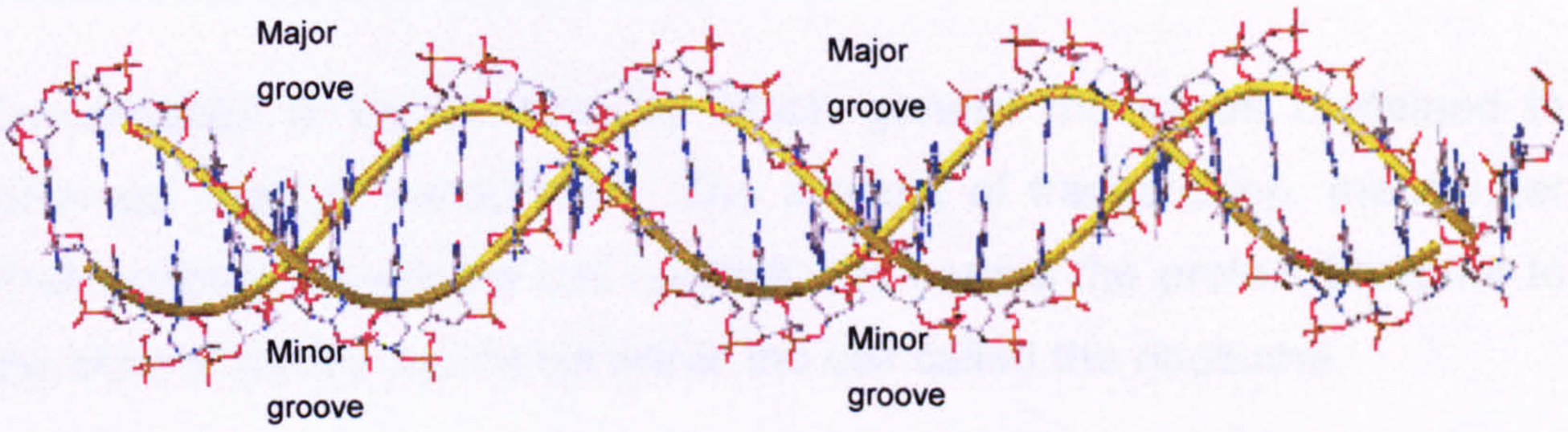

Figure 1.5:- *Picture of DNA showing the major and minor grooves*

1.3 The function of DNA[1,2]

The information stored in the genetic code needs to be replicated upon demand, conserved through generations and decoded in order to carry out everyday cellular functions. The overall process of copying, and decoding has been termed the "central dogma" of molecular genetics.

1.3.1 The central dogma of molecular genetics

According to the central dogma of molecular genetics, the function of DNA is to store genetic information and pass it onto RNA, and the function of RNA is to read, decode and use the information to make proteins.

Replication is the process by which a identical copy of DNA is made. Replication occurs every time a cell divides so that the information can be preserved and passed onto the new cell.

Transcription is the process by which genetic messages contained in DNA are read or transcribed. The product of transcription, messenger RNA (mRNA) leaves the cell nucleus and carries the protein blueprint to the sites of protein synthesis within the cell called the ribosome.

Translation is the process by which genetic messages carried in the mRNA is decoded and used to build proteins.

1.3.2 DNA replication

DNA replication begins with a partial unwinding of the DNA double helix, at an area known as the replication fork. One of the DNA strands is first of all nicked and broken by DNA topoisomerase, which results in the loss of tension that keeps the DNA in its coiled and super-coiled state within the chromosome. Then the unwinding of the original DNA double helix is accomplished by DNA helicase. The unwound section of the DNA appears as a bubble when viewed under an electron microscope and is

thus known as the replication bubble. The starting point for the DNA synthesis is a small RNA primer, which is placed in position by RNA primase. DNA polymerase is an aggregate of several different protein subunits, called a holoenzyme. The holoenzyme then recruits free deoxynuclotide triphosphates (dNTP's) to hydrogen bond to their complementary bases on the template strand. DNA polymerase is described as being template dependent. It will read the sequence of bases on the template strand, then synthesise the complementary information strand, but it can only read the template strand in the 3→ 5' directions. The dNTP's are then joined together by the reaction of the free 3' hydroxyl of the primer with the triphosphate on the 5' end of the adjacent dNTP. The result is that the new complementary DNA strand can only grow in the 5'→3' direction. Because the parent DNA strands are complementary and run anti-parallel only one new strand can begin with its 3' end adjacent to the replication fork and grow continuously as the replication fork moves along the DNA. This is called the leading strand. The other strand (the lagging strand) must grow in the opposite direction. This is achieved by the formation of a number of short sections of DNA called Okazaki fragments. These fragments are ligated together by DNA ligase to form a continuous strand of DNA. In the final step of the process DNA polymerase III removes the RNA primer and replaces it with DNA bases to form the full DNA strand, which will be exactly complementary to the original template strand (Figure 1.6).

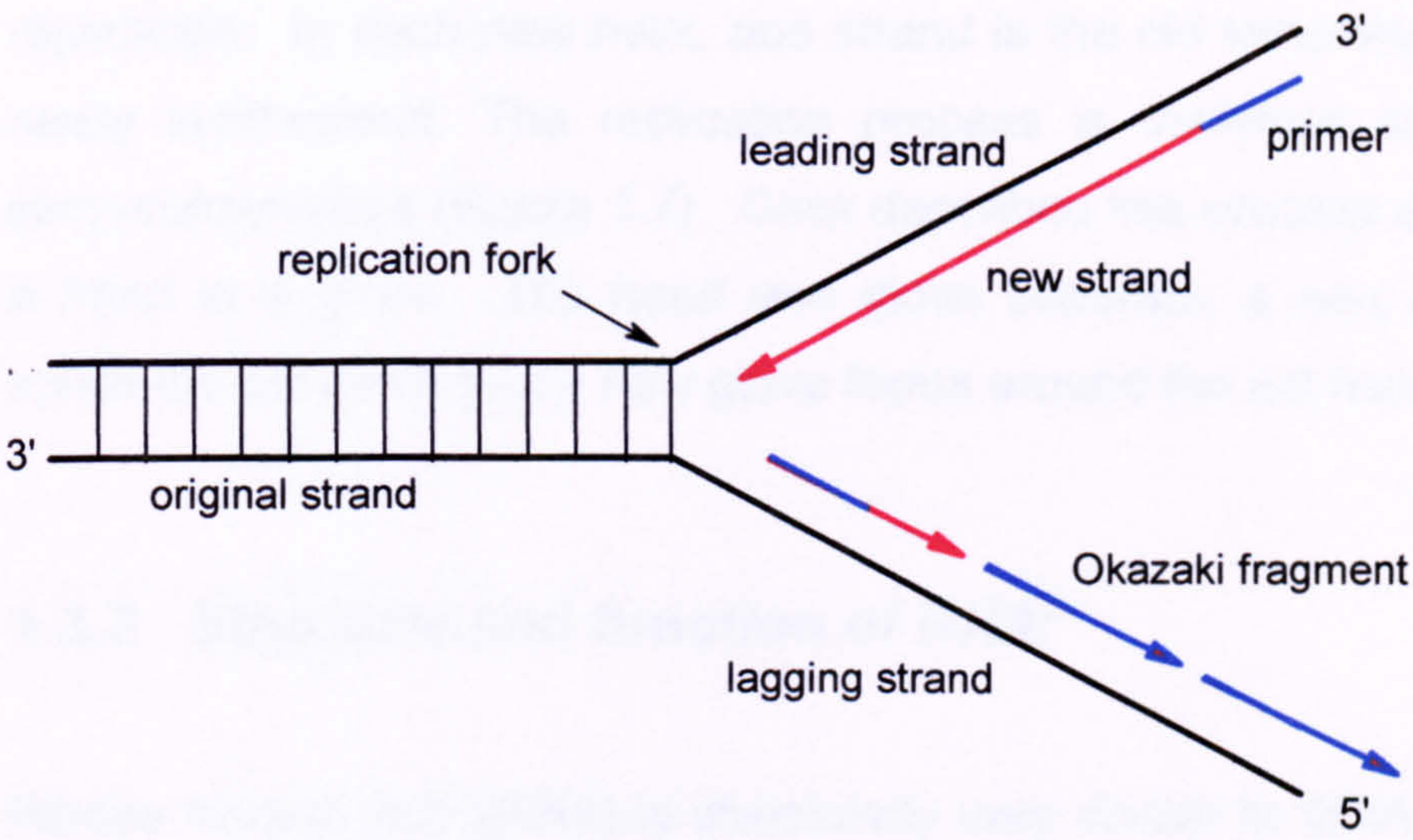

Figure 1.6:- *Schematic of replication*

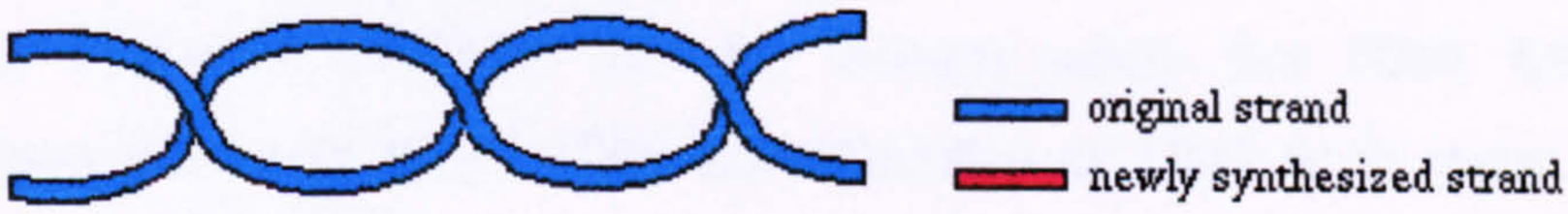

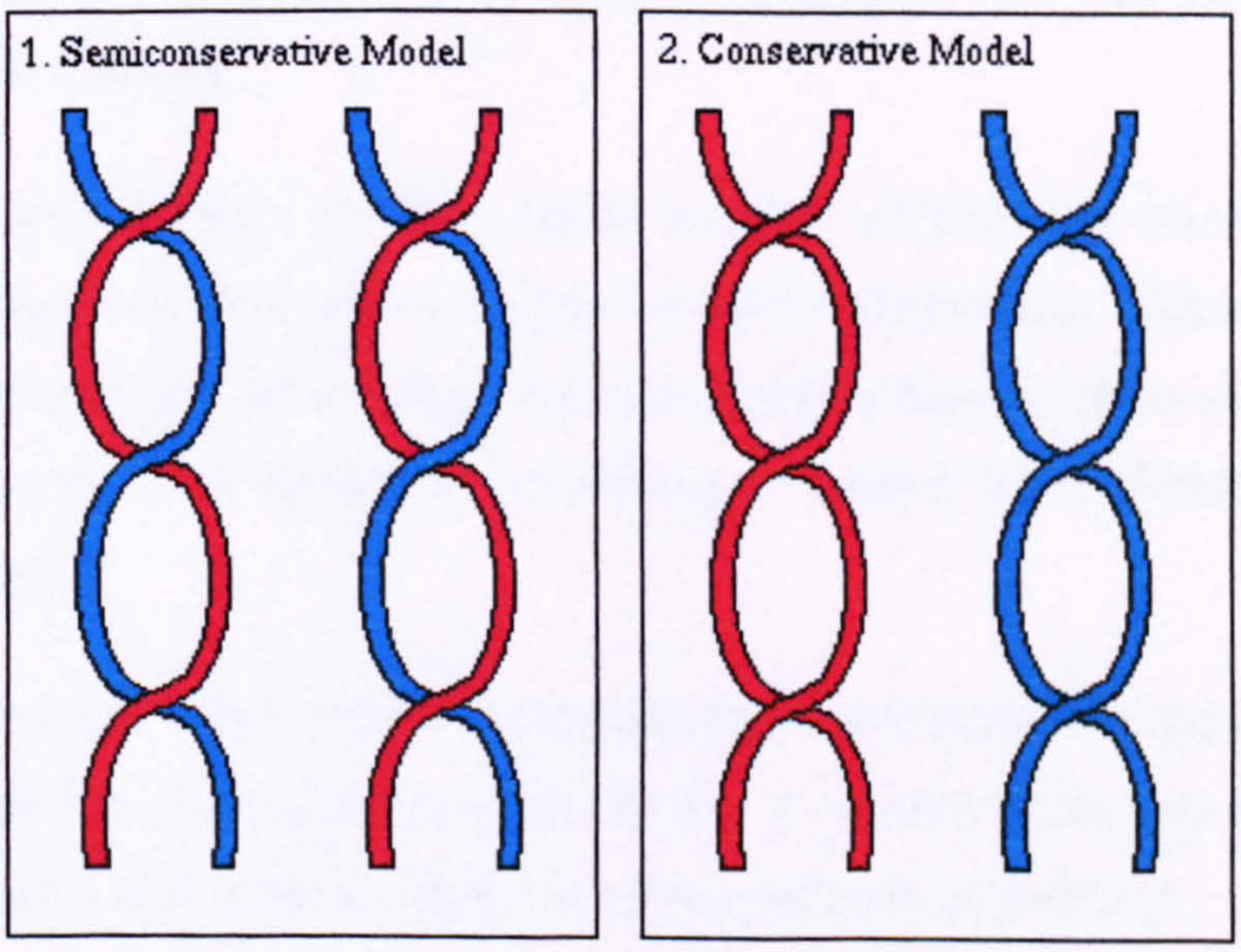

Figure 1.7:- *Conservative, and semi-conservative modes of replication*

Since each new strand is complementary to its template strand, two identical new copies of the DNA double helix are produced during

replication. In each new helix, one strand is the old template and one is newly synthesised. The replication process is therefore described as semi-conservative (Figure 1.7). Crick described this process as being like a hand in a glove. The hand and glove separate, a new hand forms inside the old glove and a new glove forms around the old hand[2].

1.3.3 Structure and function of RNA[2]

Ribose nucleic acid (RNA) is structurally very similar to DNA, with a few significant differences. The sugar in RNA is ribose rather than 2'-deoxyribose and the base thymine is replaced by urasil in RNA. RNA molecules are also shorter and exist only as single strands, although double stranded portions can be formed when the RNA folds and hydrogen bonds to itself. The sole function of DNA is to store genetic information, but there are a number of types of RNA all with differing functions in the cell.

1. Ribosomal RNA (rRNA) exists outside of the cell nucleus in the cytoplasm of the cell in structures called ribosomes. Ribosomes are small granular structures where protein synthesis takes place. Each ribosome is a complex consisting of about 60% rRNA and 40% protein.

2. Messenger RNA (mRNA) records the information stored in the DNA within the cell nucleus and carries it to the ribosome where it is decoded and used to direct the biosynthesis of proteins.

3. Transfer RNA (tRNA) is used to deliver the correct amino acids one by one to protein chains growing at ribosomes.

4. Small nuclear RNA (snRNA) is used to process the mRNA as it is transferred from the cell nucleus to the ribosome.

1.3.4 RNA synthesis: Transcription[2]

Messenger RNA is synthesised in the cell by transcription of DNA, a process similar to DNA replication. Again a small segment of the DNA unwinds which exposes the bases of the two DNA strands. A DNA dependent RNA polymerase then lines up the ribonucleotides with their complementary bases on the DNA strand and then ligates them together to form mRNA.

Unlike DNA replication where both strands of the DNA are copied, only one of the strands is transcribed into mRNA. The DNA strand that is transcribed is called the template strand or the antisence strand, and its complement is called the information strand (also called the coding or sense strand). Since the template strand and the information strand are complementary, and as the template strand and the mRNA molecule are also complementary, it follows that the mRNA produced during transcription is a copy of the DNA information strand.

The synthesis of RNA by RNA-polymerase takes place in three distinct stages; 1) initiation, 2) elongation, and 3) termination. Transcription starts at specific sites called promoters. These promoters are regions of DNA rich in AT bases. RNA-polymerase is a holoenzyme consisting of four subunits. The sigma subunit recognises the promoter sequence and initiates mRNA synthesis. RNA synthesis proceeds in the 5'→3' direction analogous to DNA synthesis for the same reasons. The termination of transcription is as strictly governed as its initiation. The DNA template strand contains stop signals that stop the synthesis of the mRNA at the end of the gene, so that only information specific to any one given gene is transcribed to the mRNA. The termination signals for mRNA synthesis are normally denoted as a GC rich region of DNA, followed by an AT rich sequence. There is also a two-fold symmetry of the CG rich region, which allows the formation of a hairpin.

1.3.2 Groove binding interactions

When a molecule associates either in the major or minor groove of DNA it is said to be a groove-binding agent[3]. Because the DNA bases can be accessed through both of the grooves, there is enormous scope for sequence specific interactions. Figure 1.9 shows the recognition sites of A-T and G-C base pairs that are accessible in the major and minor grooves[6].

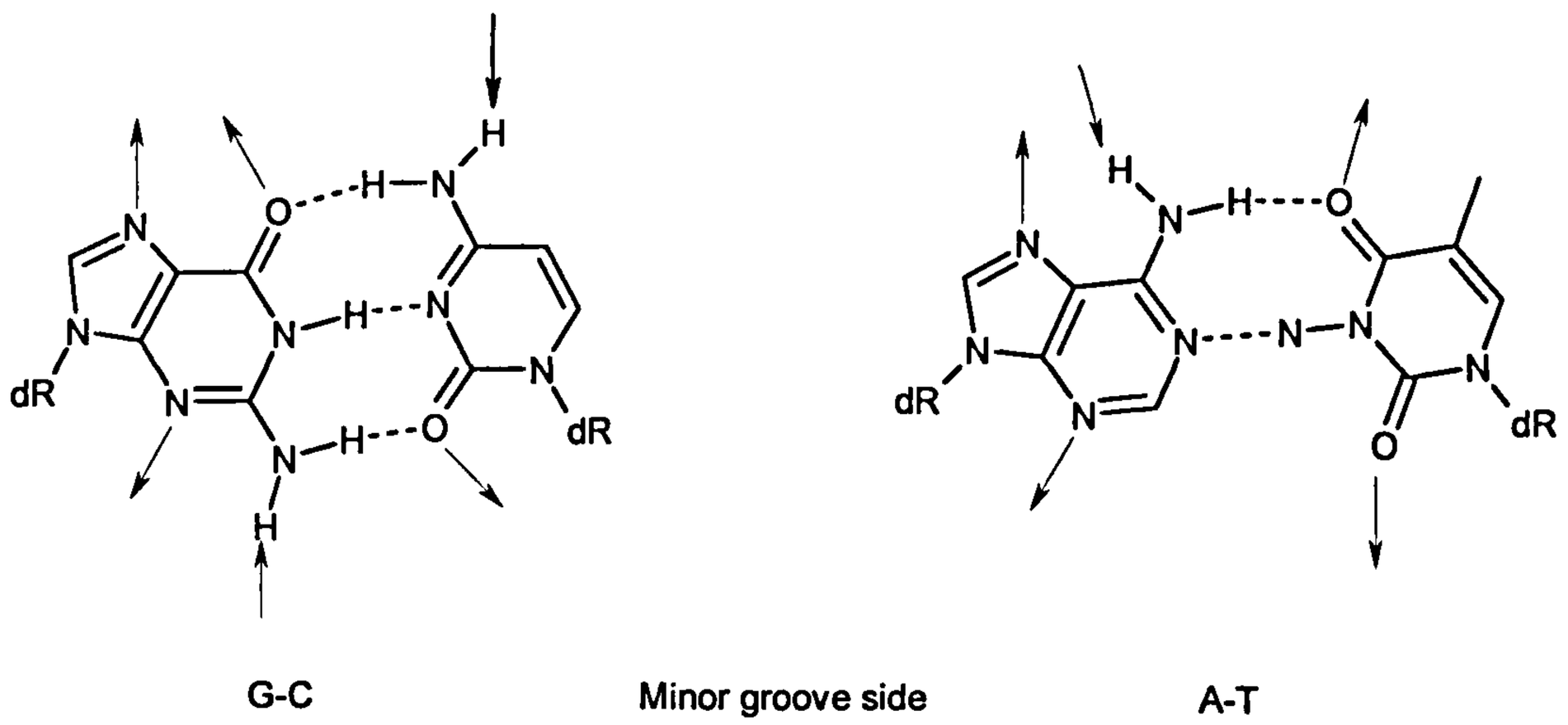

Figure 1.9:- *Recognition sites accessible from the grooves of DNA*

The major groove contains the largest number of recognition sites. For A-T base pairs these include the adenine N-7 and thymine C-4 carbonyl as hydrogen bond acceptors, the adenine C-6 amine as a hydrogen bond donor and the thymine methyl group as stabilisation for van der Waals' interactions. For the G-C base pair, guanine N-7 and the guanine C-6 carbonyl can function as hydrogen bond acceptors and the cytosine C-4 amine can act as a hydrogen bond donor. The minor groove has far fewer recognition sites than the major groove. Despite this most minor groove-binding agents bind in the minor groove[7]. The G-C base pair contains guanine N-3 and the cytosine C-2 carbonyl as hydrogen bond

acceptors and the guanine C-2 amine as a hydrogen bond donor. The A-T base pair only has the adenine N-3 and the thymine C-2 carbonyl are available to act as hydrogen bond acceptor sites. The sequence selectivity of the binding has been shown to depend on a combination of hydrogen bonding, van der Waals' interactions and hydrophobic contacts with the bases and the walls of the groove[3,6].

Most minor groove binding ligands show an enhanced preference for A-T rich regions of DNA. This has been contributed to the steric protrusion of the C-2 amine of guanine above the floor of the minor groove, along with the narrower groove in A-T rich regions, which helps to maximise hydrophobic, and van der Waals' contacts between the molecule and the groove walls[8].

1.3.3 Netropsin and Distamycin as minor groove binders[3]

The two naturally occurring minor groove binding anti-tumour antibiotics, Netropsin and Distamycin have been extensively studied. They provide a good example of the non-covalent interactions, which are important in directing sequence specific binding.

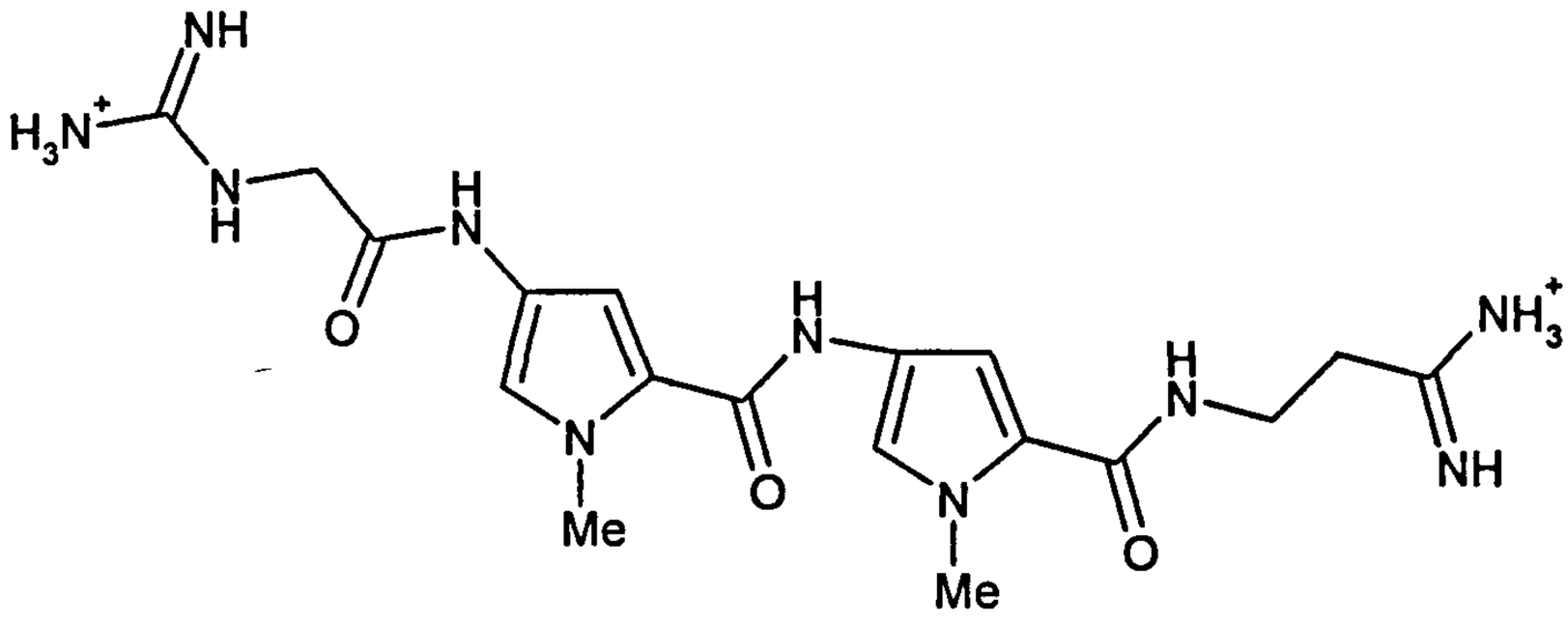

Netropsin

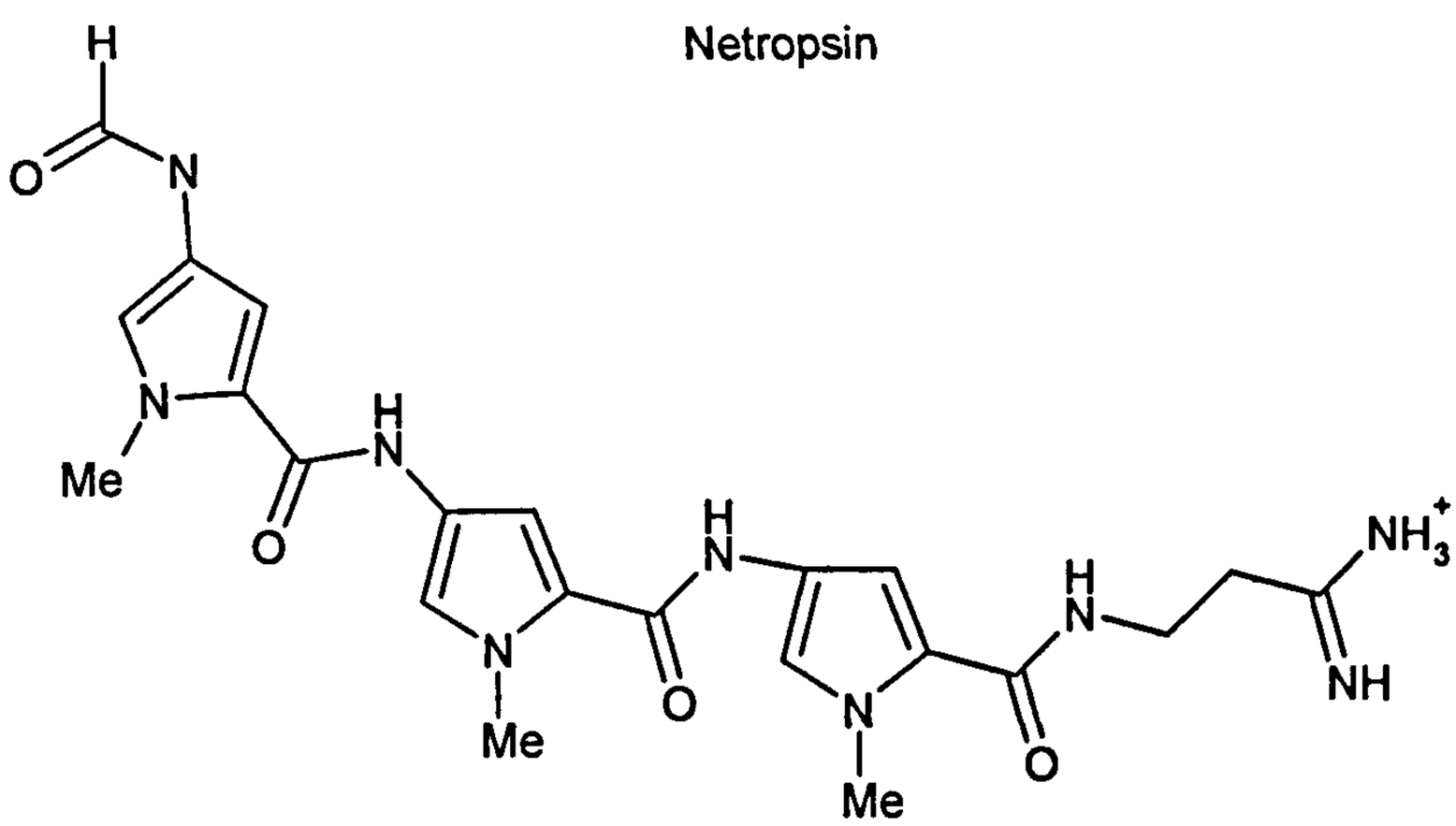

Distamycin

Netropsin and Distamycin are both crescent shaped ligands containing two and three N-methylpyrrole carboxamides respectively. Foot printing and NMR experiments along with analysis of crystal structures has shown that Netropsin targets 5'-AATT-3' whilst Distamycin binds as a head to tail dimer and targets 5'-AAATT-3' (Figure 1.10).

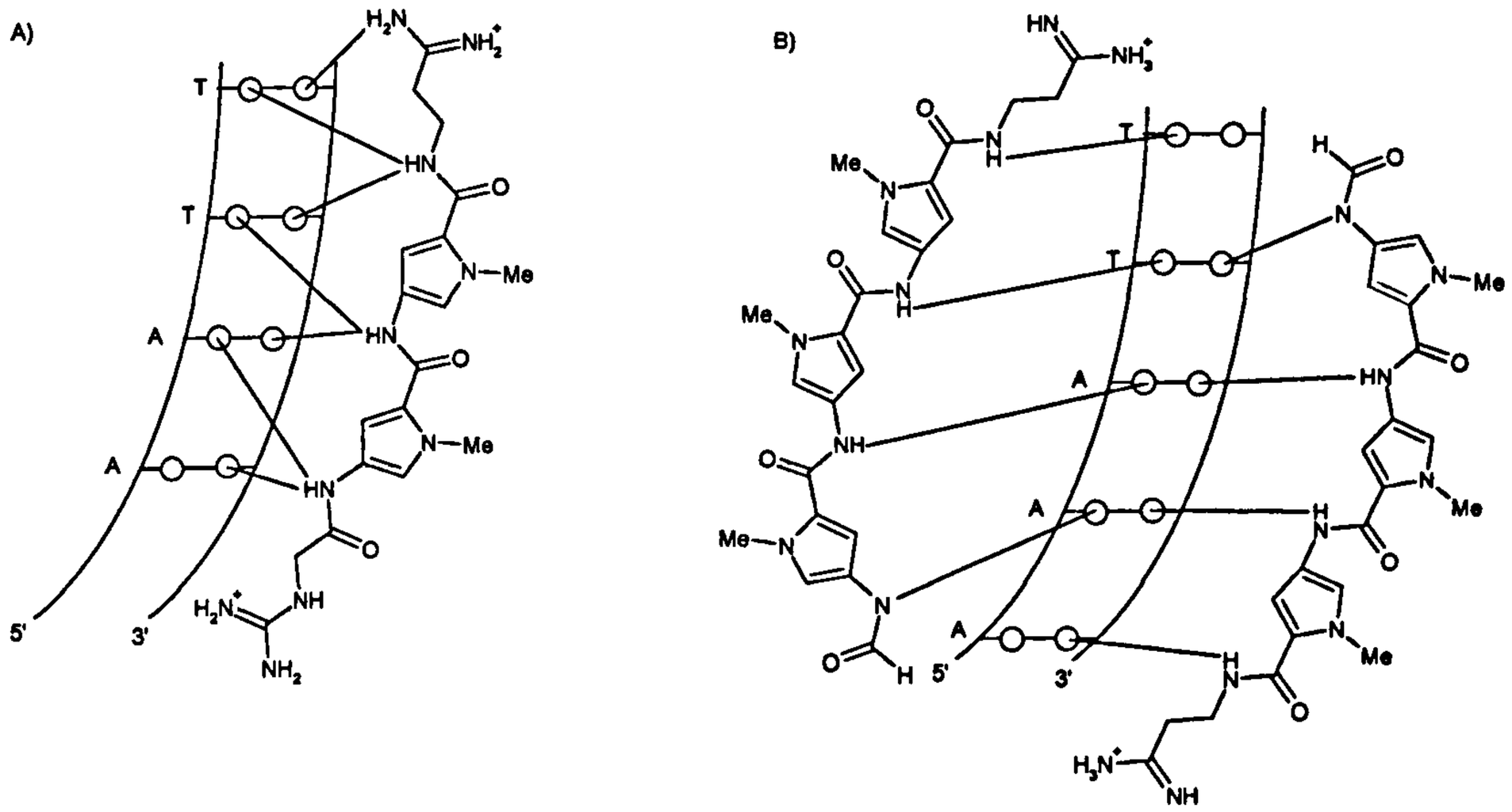

Figure 1.10:- *Key hydrogen bonding interactions for A) Netropsin and B) Distamycin binding to AT rich DNA*

The crystal structure of Netropsin binding to the Dickerson dodecamer, 5'-d(CGCGAATTCGCG)$_2$ shows van der Waals' interactions with the deoxyribose backbone lining the groove. The selectivity comes from three hydrogen bonds between the hydrogens on Netropsin and adenine N-3 or thymine C-2 carbonyl on adjacent base pairs of opposite strands. The two positive charges interact with the N-3 of the adenines flanking the binding site as well as forming a salt bridge secondary interaction with the phosphate backbone. Distamycin shows similar interaction to Netropsin.

The high binding affinities ($K=10^9$ M) and selectivity of Netropsin and Distamycin have been attributed to the local short-range ligand DNA interactions rather than from any entropy driven process resulting from the displacement of ordered water from the minor groove and desolvation of the ligand itself.

1.3.6 Intercalation

Intercalation describes the process in which planar aromatic compounds insert between two adjacent base pairs in the DNA double helix. This stabilizes, lengthens, stiffens and unwinds duplex DNA. Interactions involved in intercalation are π-π stacking interactions, dipole-dipole electronic interactions and hydrophobic interactions. The energetic cost of distorting the helix and disrupting the existing base pair stacks has a profound effect on the binding affinity and selectivity of the intercalating ligand. An informative account by Barton and Long addresses many of the confusing experimental criteria required to establish intercalation[9].

Simple intercalators such as ethidium bromide show little or no selectivity in their binding although they have a slight preference for G-C rich sequences of DNA[3].

Most intercalators bind best to mixed sequences of alternating purine pyrimidine bases. The neighbour exclusion principle states that intercalators can, at most, only bind at alternate base pair sites on DNA. However in practice the binding site size is larger than two base pairs due to the local disruption in the DNA duplex upon intercalation[3].

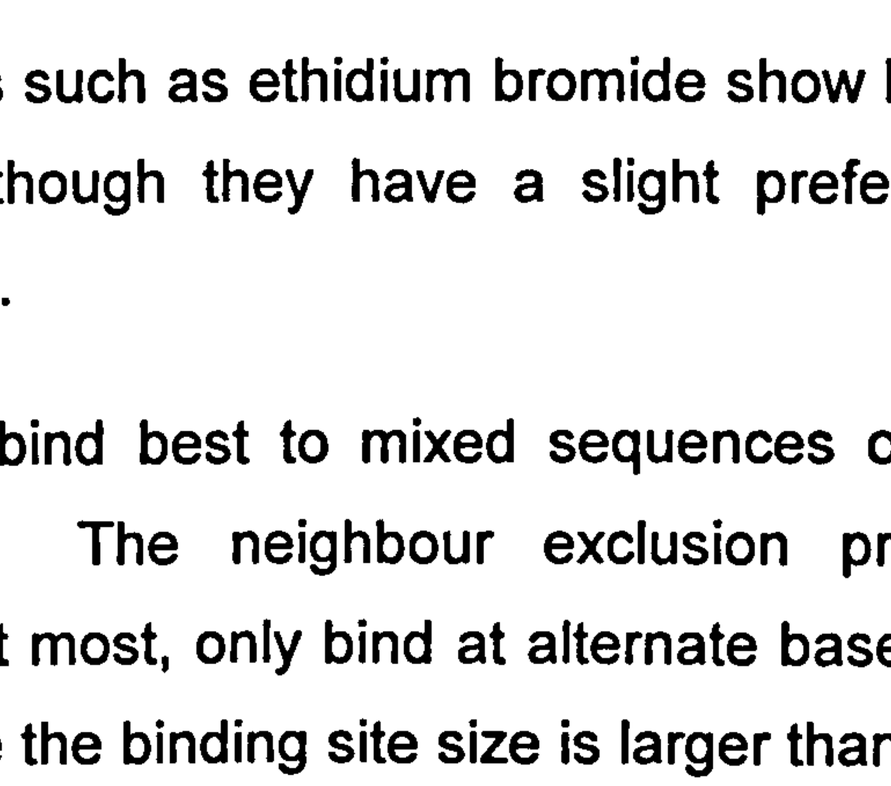

Ethidium bomide

Intercalators have proved to be particularly useful in the inhibition of polymerase activity because the duplex is stabilized and therefore harder to unwind. In addition the enzyme is unable to bind to the disrupted regions of DNA, which in turn results in the inhibition of replication, transcription, endonuclease activity or any other enzyme involved in DNA modification. There are a number of commercial anti-tumour drugs such as amasacrine that act by inhibiting topoisomerase II, which, as described earlier, is involved in winding and unwinding (super coiling) of DNA during transcription and replication.

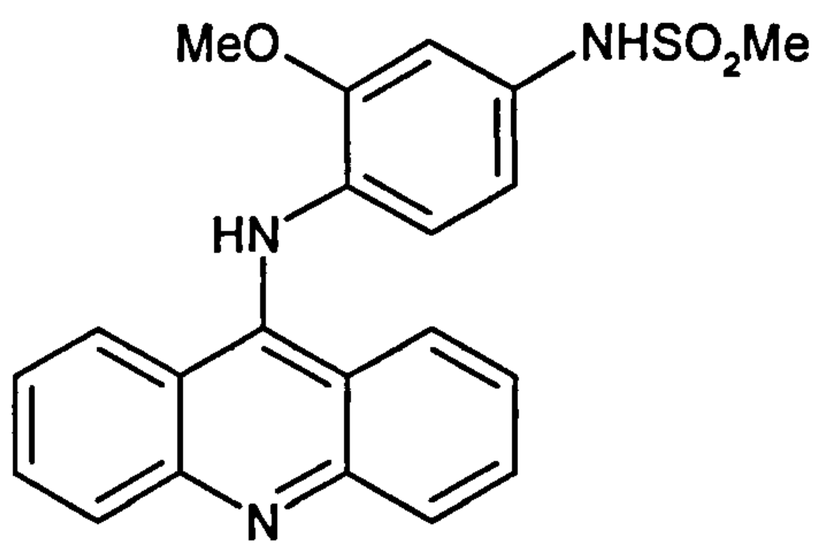

Amsacrine (m-AMSA)

Amsacrine has been shown to bind selectively to alternating purine-pyrimidine sequences[3].

1.5 Metal complexes as DNA binding ligands

Up until the late 1970s most of the synthetic and natural DNA binding molecules had been organic in nature. As researchers delineate on a molecular level how genetic information is expressed, a more complete understanding of how to target DNA sites with specificity is being developed. This in turn is leading to possible new chemotherapeutic

agents and probes such as transition metal complexes. The complexes of d^6 transition metals have been found to be very suitable as DNA binding agents due to their inertness and stability under physiological conditions. Coupling this with their well-defined and tunable molecular architecture and their high solubility in aqueous media, there is huge potential for developing these molecules as site-specific DNA binding agents.

The primary mode of binding for these transition metal complexes is intercalation and they have become known as metallointercalators. All the complexes studied contain an extended aromatic ligand, which protrudes away from the metal centre and is ideally set up for intercalation. It has also been shown that the nature of the ancillary ligands has a marked effect on the binding affinity and selectivity of these DNA binding molecules. By systematically changing the nature of these ancillary ligands it is possible to tune the DNA binding properties and the photo-reactive properties of the molecules. Moreover by taking advantage of the rich photophysical handles that these complexes poses it is easy to monitor and quantify their binding to DNA. Once the exact mode, strength and site-specificity of the binding has been determined it is possible (due to the rich photochemical and redox properties of these molecules) to perform chemistry on the DNA bases themselves.

1.5.1 Early complexes incorporating phenanthroline and bipyridine ligands

Lippard and co workers were the first to establish that a square planar metal complex containing an aromatic heterocyclic ligand could bind to DNA through intercalation[10]. Barton and co workers soon extended the complexes to three dimensions, when they started using octahedral metal

centres. The early studies focused on the tris(phenanthroline) complexes of zinc, cobalt and ruthenium (Figure 1.11)[11,12].

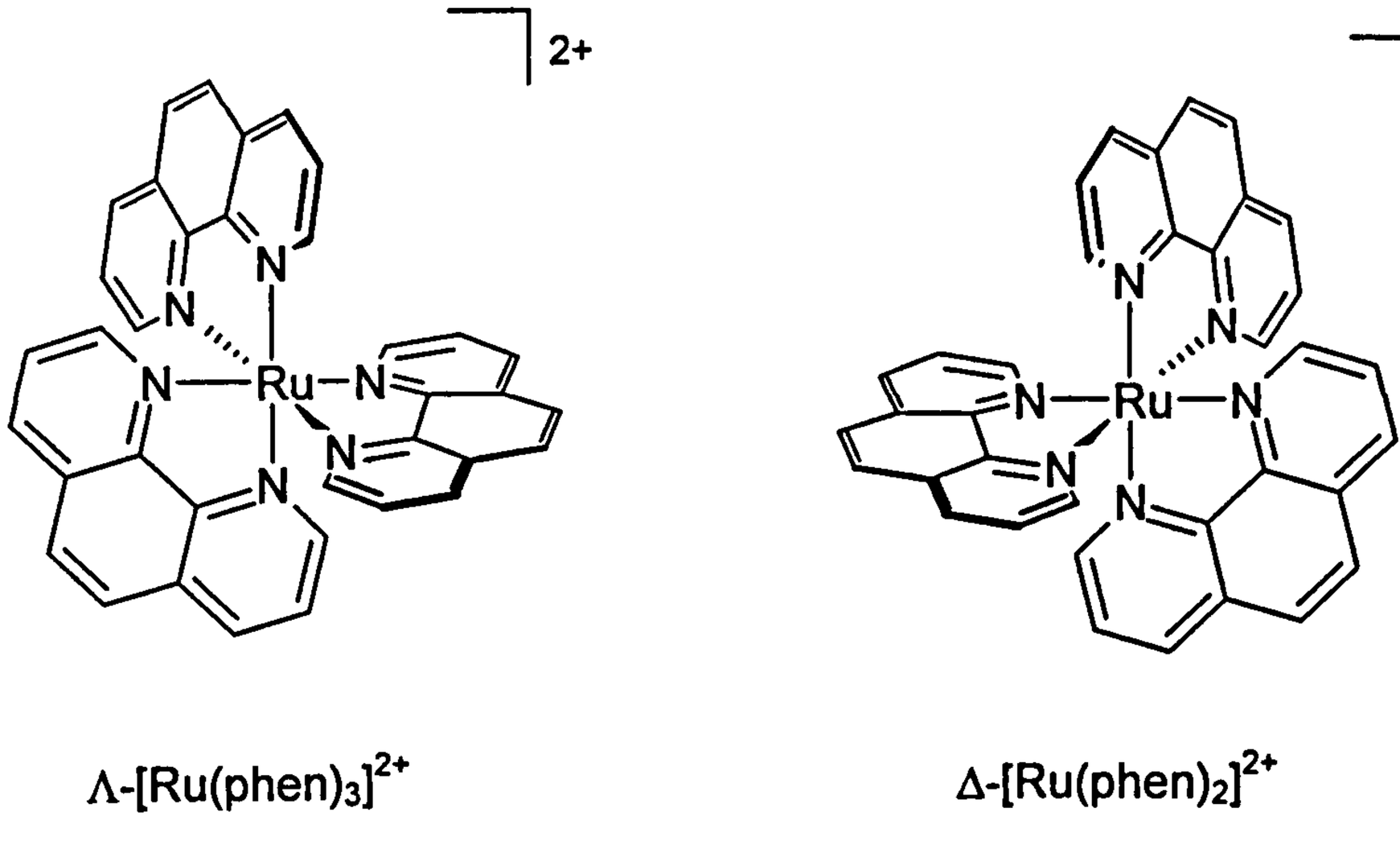

Λ-$[Ru(phen)_3]^{2+}$ Δ-$[Ru(phen)_2]^{2+}$

Figure 1.11:- *The Λ&Δ-enantiomers of trisphen Ruthenium(II)*

Through NMR[13] and photophysical studies[12,14]. They suggested that the cationic tris-(phenanthroline) complexes bound to DNA through all three of the noncovalent modes discussed earlier. One important observation to come from these early studies was that there was a small but significant preference for the right-handed Δ-isomer when bound to right-handed B-form DNA. However the binding modes and exact orientation of these tris-(phenanthroline) ruthenium(II) complexes have been open to much debate.

In the early papers to emerge from Barton's laboratory the mode of interaction of $[(phen)_3Ru]^{2+}$ with B-form DNA was deemed to be electrostatic and hydrophobic contacts with the DNA in the major groove, with partial intercalation of one of the phenanthroline ligands into the DNA base stack. Equilibrium dialysis experiments showed that the intrinsic binding constant was small ca. 10^{-3} mol^{-1} dm^3 and highly dependent upon salt concentration, which indicates a large electrostatic component to the

binding free energy[12]. Luminescence quenching experiments revealed a bi-exponential decay indicating two emitting species were present, one of which is quenched more readily than the other[15]. Barton proposed that the species which was more readily quenched was bound in a groove binding interaction, and was therefore more accessible to the quenching agent, where as the other species was intercalated deep within the major groove of DNA and was much less accessible to the quenching agent. The chiral discrimination of the binding event was rationalised by assuming propeller twist of Δ-$[(phen)_3Ru]^{2+}$ was symmetry matched to the right handed helix found in B-form DNA allowing it to bind preferentially over Λ-$[(phen)_3Ru]^{2+}$. Barton also reported sequence selectivity based upon steady-state polarisation of excited states, which show that the preference for the Δ-$[(phen)_3Ru]^{2+}$ increases upon increasing GC content of the DNA although no change in binding affinity is observed. This has been rationalised by the fact that the major groove becomes narrower with increasing GC content and therefore closer in width to the diameter of $[(phen)_3Ru]^{2+}$ thus amplifying the important steric contacts between the complex and the sides of the groove needed for chiral discrimination.

Chiral discrimination of this type is clearly dependent upon matching the symmetry of the metal complex with that of the DNA double helix. However the debate is still raging as to whether the tris-phenanthroline ruthenium(II) complexes are able to intercalate into the base stack of DNA at all.

In 1992 Norden and co-workers published the results of an NMR study[16] they had undertaken, seemingly contradicting all of the structural elucidations proposed by Barton. They show NOE data which shows that both Δ- and Λ-$[(phen)_3Ru]^{2+}$ bind to the AT region of the self complementary oligonucleotide $[d(CGCGATCGCG)_2]$ in the minor groove. The cross peaks observed between protons on the metal complex and the oligonucleotide show they are at distances of less that 5 Å apart. The

H2 of adenine located at the bottom of the minor groove is shown to interact with protons on one of the phenanthroline rings and sugar protons H1' and H4' both facing the minor groove interact with the phenanthroline protons. Both enantiomers exhibit similar cross peaks, however more were observed with the Λ-enantiomer but higher concentrations of drug were needed to see them. The oligonucleotide cross peaks are not affected in any way upon binding of the drug indicating no change in conformation on interaction with the drug, indicating no intercalation is taking place. The binding kinetics are rapid and the complex is in fast exchange resulting in sharp signals, which again is an indication of no intercalation taking place. In summary both Λ and Δ-$[(phen)_3Ru]^{2+}$ binds to the AT region of $[d(CGCGATCGCG)_2]$ through electrostatic and groove binding interaction within the minor groove. The issue of intercalation was disproved once-and-for-all when Chaires *et al.* published viscosity data showing only a very small increase in viscosity upon binding of tris-phenanthroline ruthenium(II) to DNA indicating a non-intercalative mode of interaction[17].

Finally, a detailed spectroscopic and modelling account by Rodger *et al.* showed that the equilibrium binding constant was dependent upon the degree of saturation of the DNA by the drug complex[18]. They also report two modes of interaction. Λ-$[(phen)_3Ru]^{2+}$ was shown by CD and LD studies to orientate in the major groove through partial insertion of one of the phen moieties into the major groove (Figure 1.12). The phen moiety orientates itself within the major groove in plane with the base pairs although phen does not protrude far enough away from the metal centre to facilitate full intercalation. The Δ-$[(phen)_3Ru]^{2+}$ species binds exclusively in the minor groove by slotting a phen moiety vertically into the groove nearly perpendicular to the plane of the base pairs (Figure 1.12). This mode results in considerable widening of the minor groove to maximise interactions between the backbone and the other two phen

ligands on the complex. Again strong preferences were seen for AT regions of DNA over GC regions.

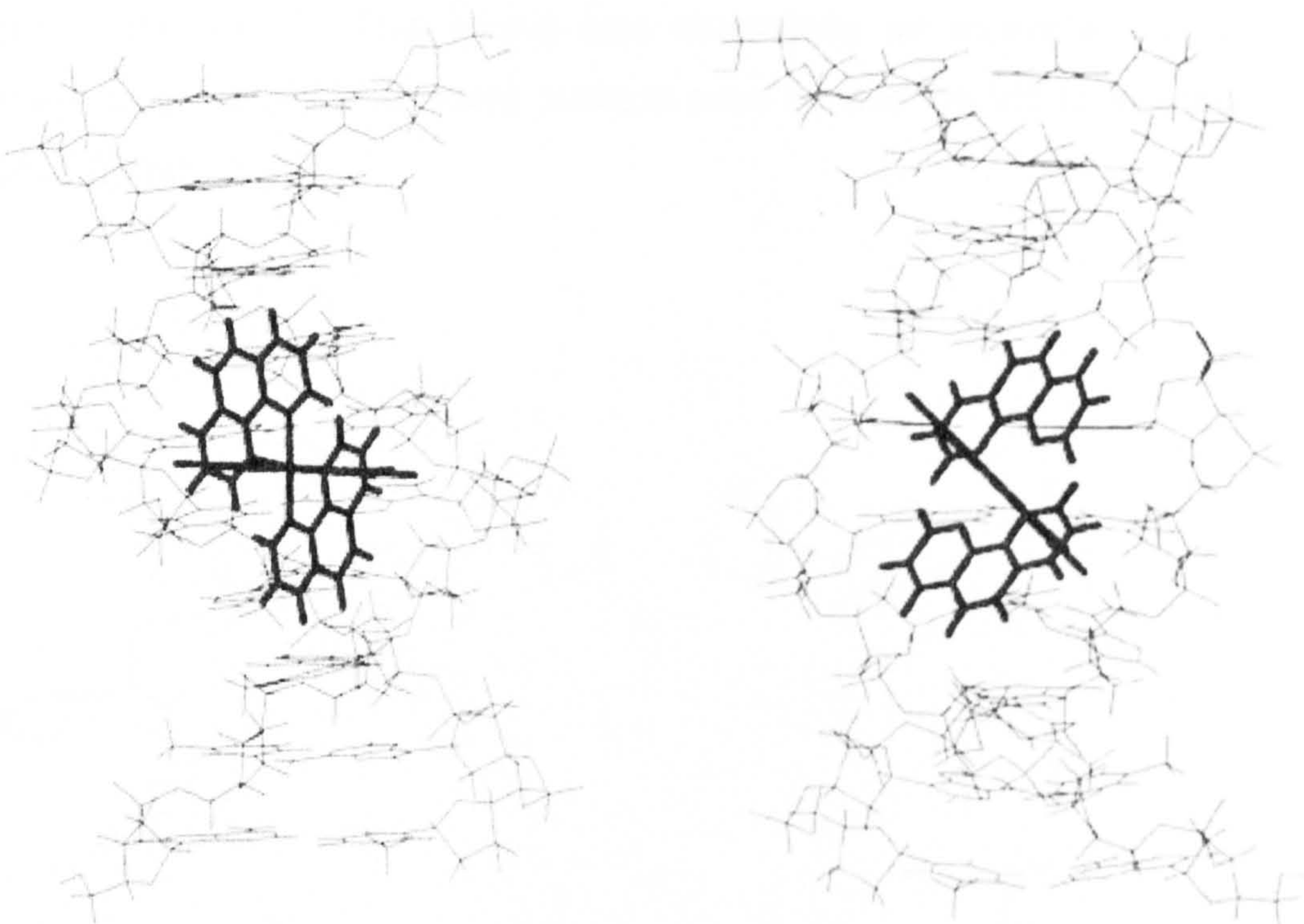

Figure 1.12:- *Energy minimised binding modes of Λ-$[(phen)_3Ru]^{2+}$ left and Δ-$[(phen)_3Ru]^{2+}$ right.*

Although tris-phenanthroline ruthenium(II) complexes were shown to bind to DNA and show a degree of symmetry recognition, the binding affinities for DNA were unimpressive, and were highly dependent upon sequence, salt and temperature. In order for these metallointercalators to become useful in chemotherapeutics all of these problems needed to be addressed.

1.5.2 dpphen complexes of ruthenium(II)

Increasing the surface area of the intercalating ligand in these complexes

should serve to maximise the stacking interaction, and thereby increasing the binding affinity. In 1984 Barton and co-workers reported the ruthenium(II) complexes of dpphen (dpphen = 4,7-diphenyl-1,10-phenanthroline)[19]. This ligand was essentially an extended version of phen, which could offer more surface area on the ligands to interact with DNA (Figure 1.13).

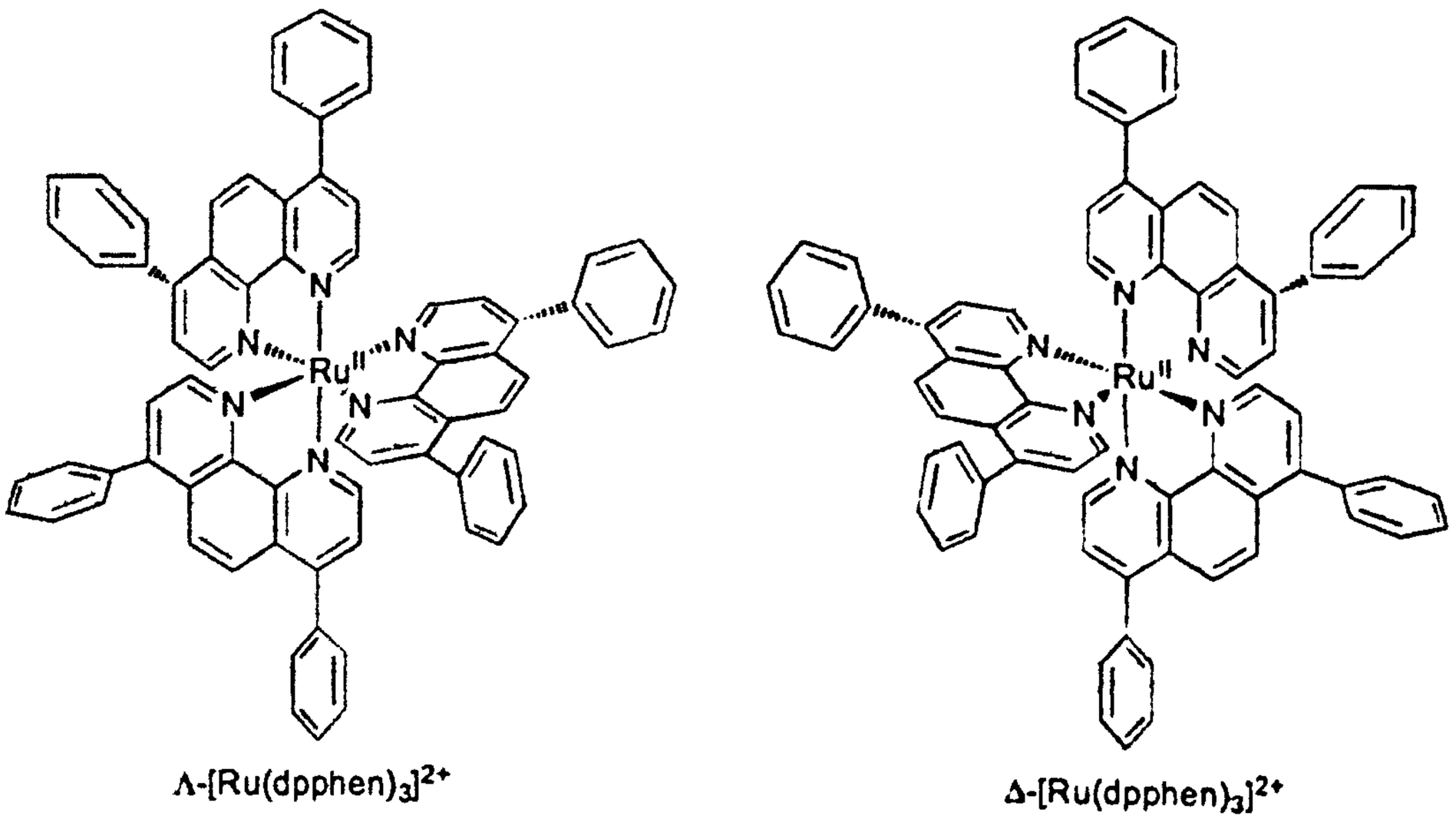

Λ-[Ru(dpphen)$_3$]$^{2+}$ Δ-[Ru(dpphen)$_3$]$^{2+}$

Figure 1.13:- *dpphen complexes of ruthenium(II)*

Barton suggested that the extended surface area of the ligands served to enhance the chiral recognition already observed in [(phen)$_3$Ru]$^{2+}$. Luminescence quenching experiments seemed to show that Λ-[(dpphen)$_3$]$^{2+}$ bound to B-form DNA exclusively through an electrostatic interaction whereas Δ-[(dpphen)$_3$Ru]$^{2+}$ interacts with B-form DNA by intercalation of one of the dpphen ligands and subsequent threading of a pendant phenyl from the major groove to the minor groove.

Again the growing number of researchers investigating metal complex DNA interactions disputed these initial claims and in 1997 a communication was published by Norden showing the absence of any

chiral discrimination whatsoever between Λ- and Δ-$[(dpphen)_3Ru]^{2+}$ and B-form DNA[20]. UV studies (Figure 1.14) on each of the enantiomers showed that the observed hypochromisity is identical in each case indicating similar interactions of both enantiomers.

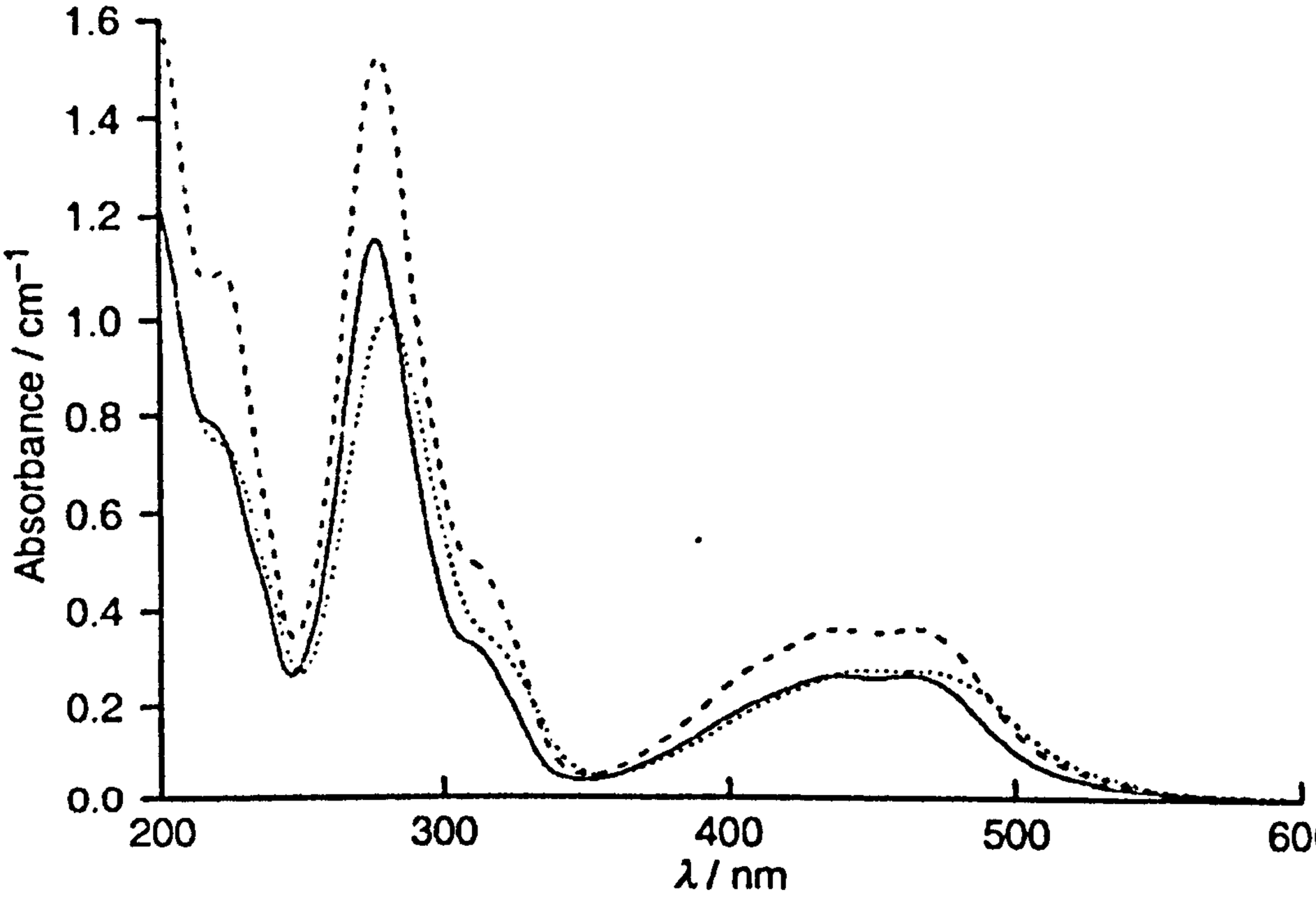

Figure 1.14:- *UV spectrum of Δ-$[(dpphen)_3Ru]^{2+}$ (—), Λ-$[(dpphen)_3Ru]^{2+}$ (....) and 50% ethanol (----) in the presence of CT-DNA.*

Furthermore, the induced CD spectrum of the Δ-enantiomer is equal in magnitude but opposite in sign to that of the Λ-enantiomer (Figure 1.15) again indicating both enantiomers interact with B-form DNA in a similar manner.

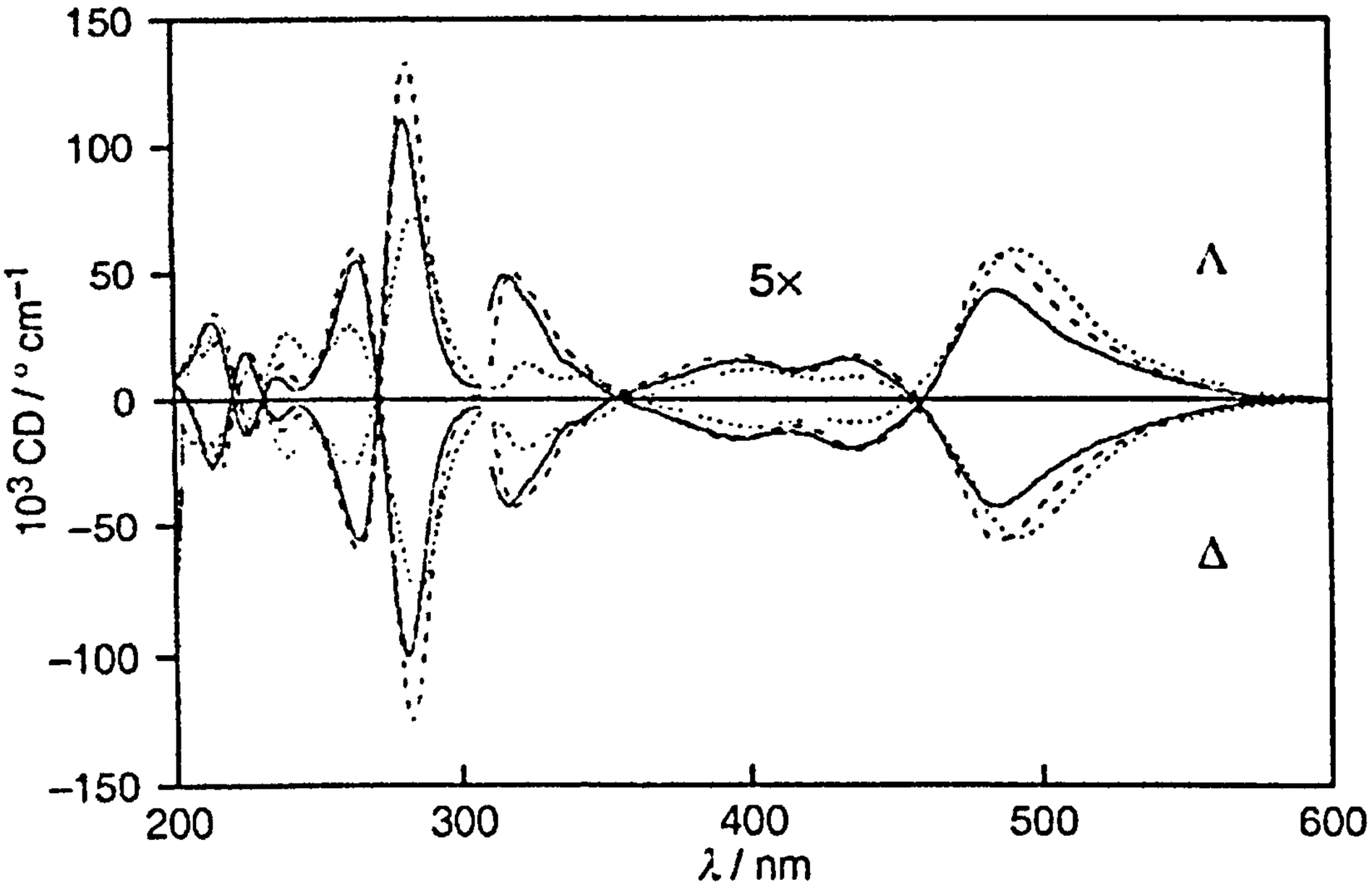

Figure 1.15:- *CD spectra of $[(dpphen)_3Ru]^{2+}$ in acetate buffer (—), 50% ethanol (---) and CT-DNA (.....)*

LD studies indicated a number of random orientations of both enantiomers of $[(dpphen)_3Ru]^{3+}$ with respect to the DNA axis, indicating a non-rigid non-intercalative mode of interaction. One possible reason for this discrepancy in binding behaviour may be the poor solubility and general hydrophobic nature of $[(dpphen)_3Ru]^{2+}$. In the initial studies Barton and co-workers used the dichloride and perchlorate salts of the complex which needed 10% DMSO in the buffer to ensure solubility. The presence of DMSO could possibly alter the conformational properties of B-form DNA and falsely induce chiral discrimination. Norden and co-workers worked on the di-acetate salt of the complex, which showed greater solubility allowed them to carry out the binding studies in a pure aqueous medium.

By now it was clear that in order to design sequence-specific DNA binding drugs a system needed to be developed that formed a well-defined predictable anchor either in the major or minor groove around which

further functionality can be built.

1.5.3 Ruthenium(II) dppz complexes

Barton and Sauvage were the first to take this lead by preparing the bisphen ruthenium(II) complex of dipyrido[3,2-a:2',3'-c]phenazine (dppz)[21].

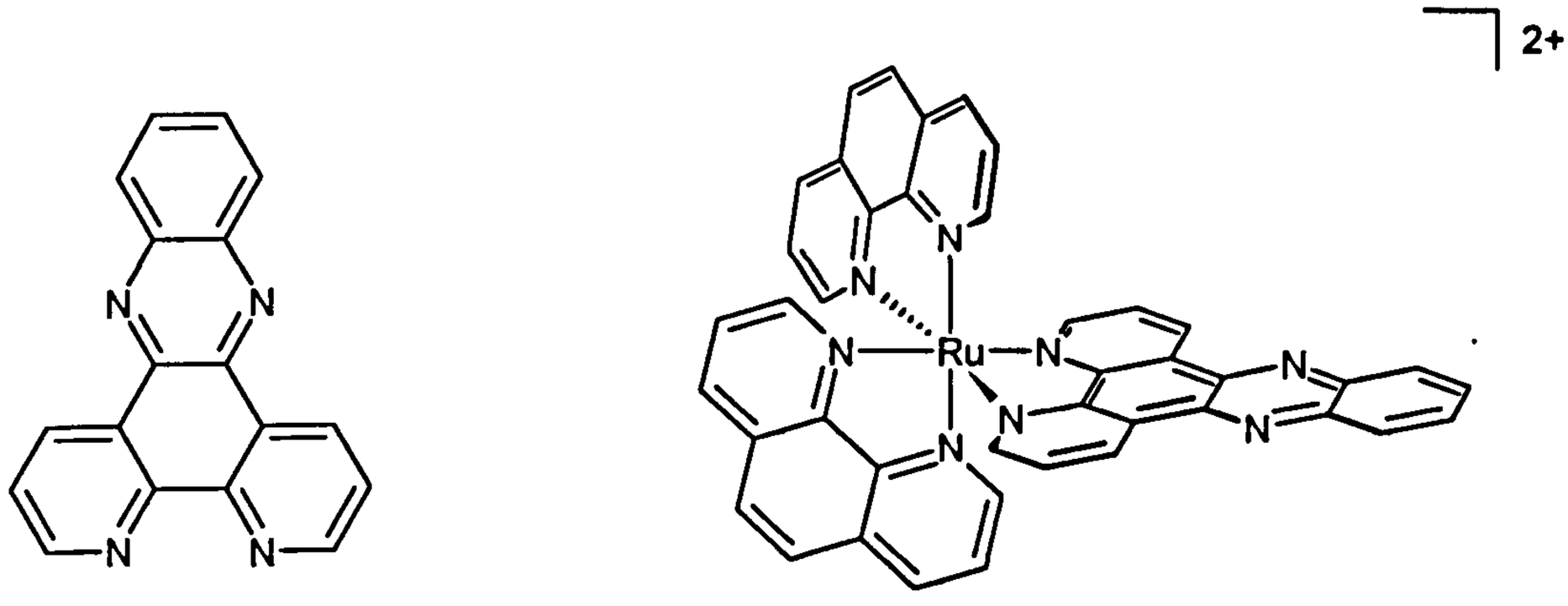

Figure 1.16:- *dppz and its associated ruthenium(II) complex*

1.5.4 The molecular light switch effect

$[(phen)_2Rudppz]^{2+}$ has been shown to have an atypical electronic structure compared to other tris-diimine complexes of ruthenium(II)[22-24]. Electrochemical and photophysical measurements in both the ground and excited states show that the charge transfer is directed from the metal centre to the phenazine ring of the dppz ligand. The major non-radiative deactivation pathway of this excited state is likely to be the protonation of one or both of the nitrogen atoms in the phenazine ring. This makes the excited state of this complex extremely dependent upon its

microenvironment. The complex shows a strong metal to ligand charge transfer luminescence in hydrophobic solvents such as acetonitrile, or dichloromethane. In aqueous or protic solvents, however, this excited state is completely quenched and no emissions are observed because protons are available to protonate the ring nitrogens and facilitate non-radiative decay. Upon titration of DNA into aqueous solution of the complex this luminescence returns, indicating that the ring nitrogens of the dppz ligands are being shielded from the solvent.[25]

This suggests that the dppz ligand is intercalated deep within the π system and behaving as though it is in a hydrophobic solvent. This phenomenon has been termed the "molecular light switch effect" and has proved a very useful handle through which the binding can be monitored.

Although the mode of interaction of $[(phen)_2Rudppz]^{2+}$ with B-form DNA has been established as intercalation of the phenazine ligand into the base pair stack, luminescence lifetime studies showed bi-exponential decay indicating the presence of two emitting species, one with a considerably longer lifetime than the other.

The two species have been identified as perpendicular and side-on modes of intercalation (Figure 1.17).

In the side on mode, one of the ring nitrogens on the phenazine ligand is still accessible by water as it points out into the major groove, resulting in quenching of the excited state, albeit much slower than if it were free in solution. In the perpendicular mode both of the phenazine ring nitrogens are fully intercalated into the base pair stack, rendering them inaccessible by water, which results in a greatly enhanced and longer lived excited state.

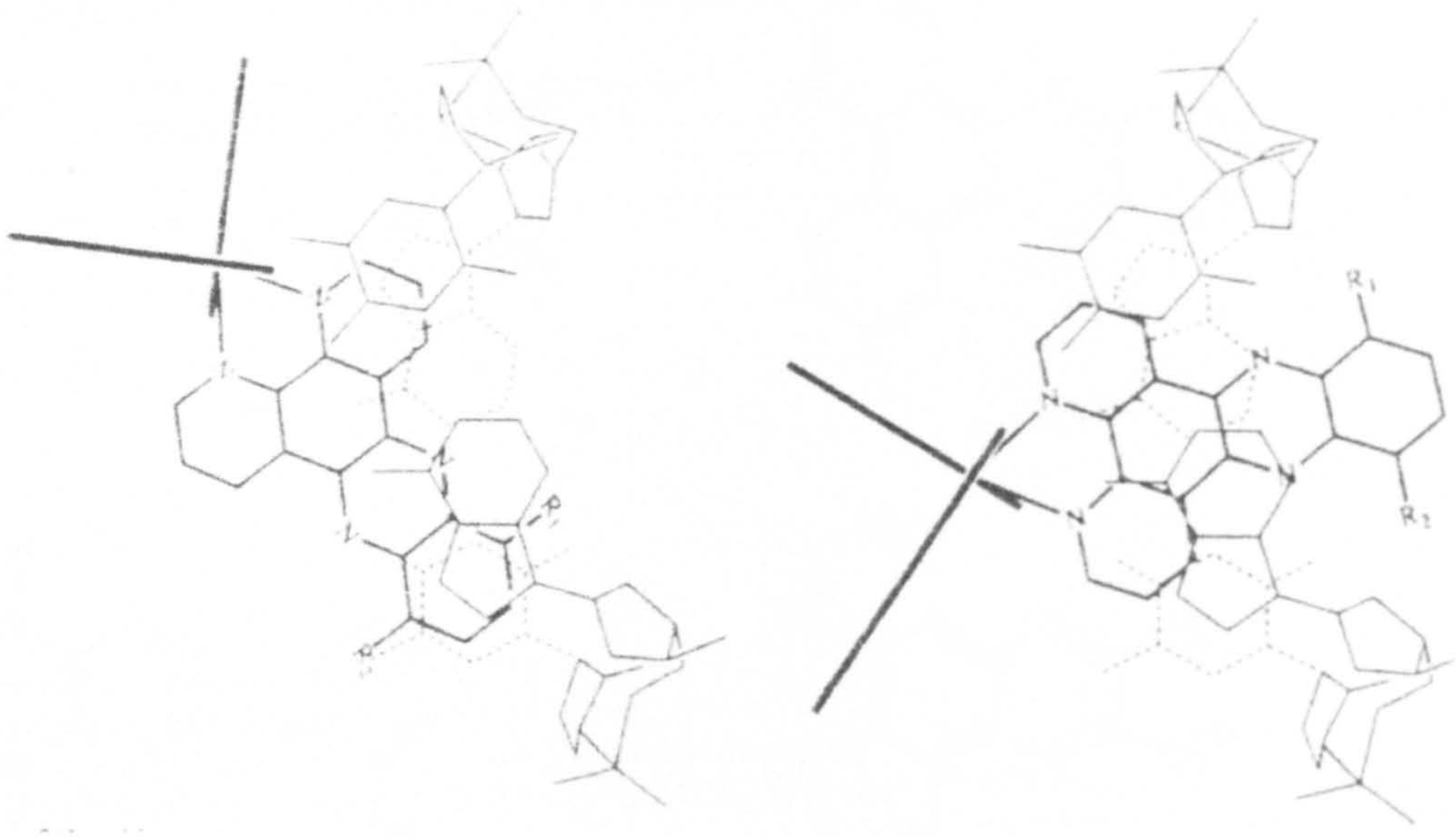

Figure 1.17:- *Side on (left) and perpendicular (right) modes of intercalation of dppz into B-form DNA*

The preparation of a series of substituted derivatives of $[(phen)_2Rudppz]^{2+}$ (Figure 1.18) served to strengthen this hypothesis. None of the derivatives can be called molecular light switches as they all showed some luminescence in aqueous solution[26]. However upon titration of CT-DNA they all showed differing degrees of enhancement of the luminescence and of the excited state lifetimes. Complexes of DPPM, DPPM2 and DPPA all show significant enhancement of luminescence upon titration with CT-DNA indicating the kind of protection from solvent upon intercalation seen in the parent complex $[(phen)_2Rudppz]^{2+}$. The excited state decay observed for $[(phen)_2RuDPPM2]^{2+}$ is another good indicator towards of two modes of intercalation as it shows a tri-exponential decay. As DPPM2 is asymmetric, the methyl group on the terminal phenyl ring can either point into the groove or into the base pair stack upon intercalation.

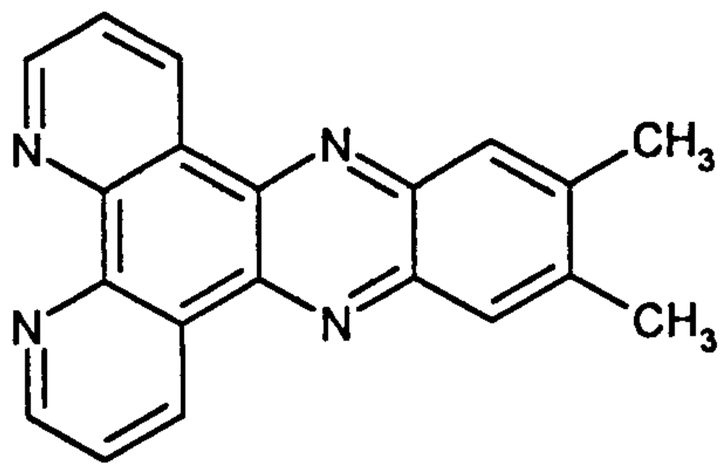

DPPX

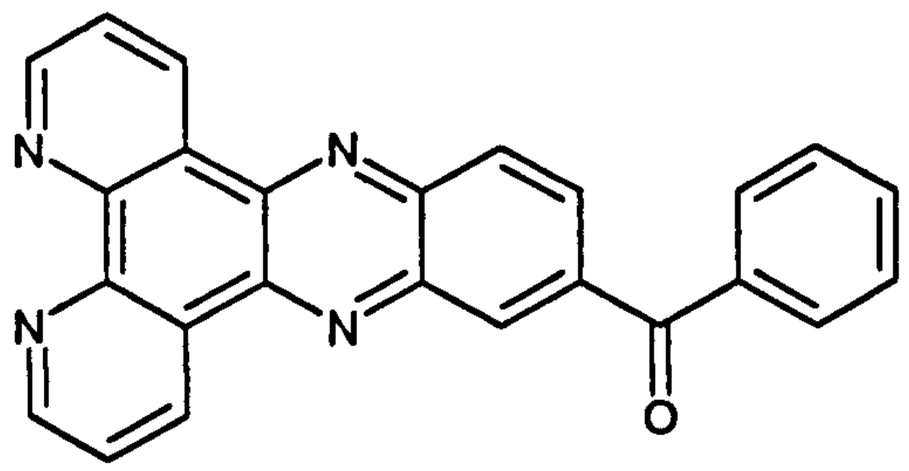

DPPB

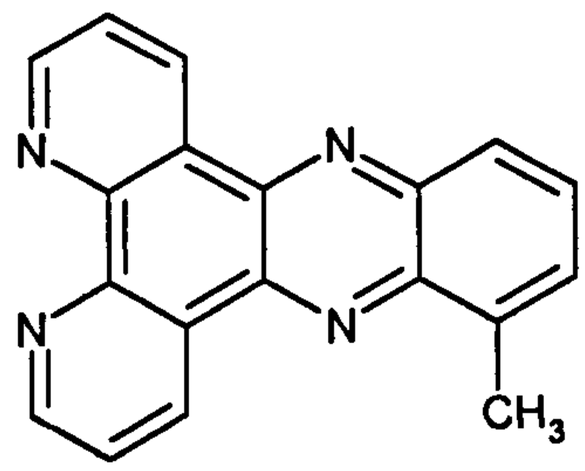

DPPM2

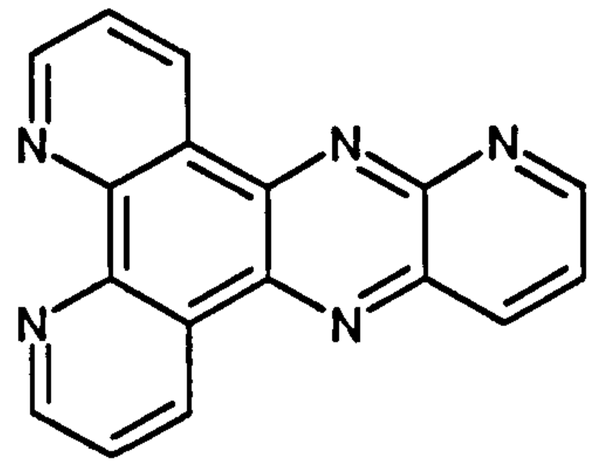

DPPP2

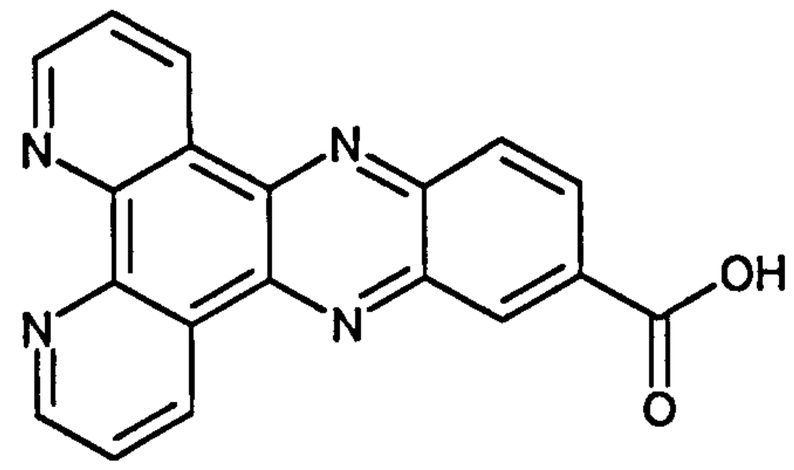

DPPA

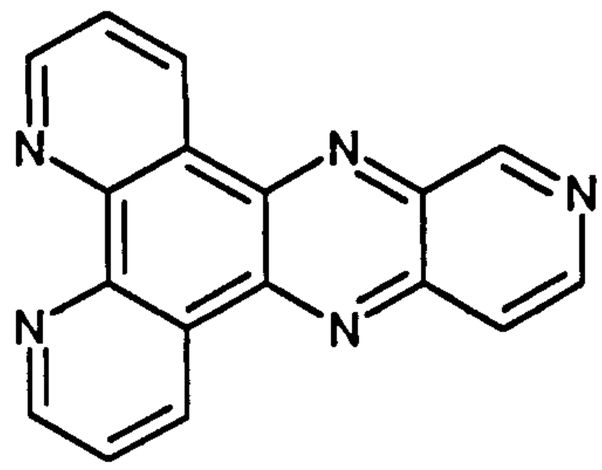

DPPP3

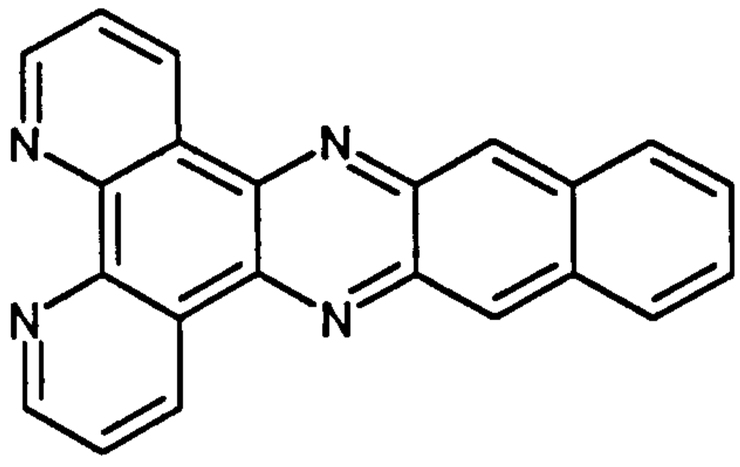

DPPN

Figure 1.18:- *Substituted dppz derivatives*

The positioning of the methyl group on the terminal phenyl ring of DPPM2 partially shields the phenazine nitrogen from water, different degrees of

quenching can be expected at the free nitrogen and the shielded nitrogen sites resulting in the tri-exponential decay.

In1993 Norden *et al.* published new data on the resolved enantiomers of $[(phen)_2Rudppz]^{2+}$. They showed by flow LD, CD and luminescence titrations that both the Δ- and Λ- forms of the complex bind to B-form DNA with similar binding affinities *ca.* 10^8 mol^{-1} dm^3 [27]. However they observed the relative quantum yield of the Δ-enantiomer was some 60-80 times higher than for the Λ- enantiomer. They proposed that this was due to the existence of two binding modes originating from a ligand distribution effect. They report a higher fraction of the shorter lifetime species at low [Ru]/[DNA] ratios and suggest this is because isolated ligands in the lattice are more accessible to solvent than closely packed ligands at the saturation point. In 1997 Norden and co-workers extended this theory by presenting evidence suggesting that the intercalation takes place from within the minor groove. If this were the case then there would be no room within the minor groove to accommodate the second binding orientation proposed by Barton *et al.*[28]. They report that binding of both Δ- and Λ-$[(phen)_2Rudppz]^{2+}$ to T-4 DNA is not hindered in any way. T-4 DNA is 100% glycosylated at the cytosine 5-CH_2-OH position in the major groove which would provide a significant steric obstacle for the complex to overcome. Additionally, there were no significant difference between the lifetimes observed with poly(dA).poly(dT) and poly(dC).poly(dC) ruling out preferential binding to the AT regions of T-4 DNA free from glycosylation.

In 1998 Barton *et al.* published a study based upon competitive binding experiments with well-known well characterised major and minor groove binding agents[29]. Δ-α-$[Rh[(R,R)\text{-}Me_2trien]phi]^{3+}$ has been shown to bind in the major groove of [d(5'-GAG**TGCA**CTC-3')] at the highlighted residues. When rac-$[(phen)_2Rudppz]^{2+}$ was mixed with the duplex at relatively low mixing ratios and then Δ-α-$[Rh[(R,R)\text{-}Me_2trien]phi]^{3+}$ was

titrated into the complex, the luminescence intensity observed from the ruthenium complex at 617nm decreased until a molar ratio of 1:1 Rh / duplex was reached. The intense absorption at 375nm assigned to the phenazine $\pi \rightarrow \pi^*$ transition of the ruthenium complex, increases to a maximum at 1:1 Rh / duplex. This showed that the rhodium complex directly displaces the intercalated ruthenium complex. Competitive binding of rac-$[(phen)_2Rudppz]^{2+}$ with Distamycin shows no decrease in the ruthenium emission but in fact the intensity of the emission is increased. This is due to stiffening of the duplex by Distamycin resulting in greater protection of the ruthenium complex from solvent. Binding of rac-$[(phen)_2Rudppz]^{2+}$ with a 1:1 mixture of [poly(dA).poly(dT)] and [poly(dG).poly(dC)] DNA shows that the luminescence decay is a linear combination of the decay profiles in the presence of [poly(dA).poly(dT)] and [poly(dG).poly(dC)] independently. This shows that although binding affinities are high for each DNA polymer, in direct competition ~85% of the complexes are bound preferentially to [poly(dA).poly(dT)]. As CT-DNA (42% GC) and T-4 DNA (34% GC) are rich in A-T regions, and the decay profiles of rac-$[(phen)_2Rudppz]^{2+}$ binding to both samples are so similar even with T-4DNA being 100% glycosylated in the major groove. This seems to indicate that rac-$[(phen)_2Rudppz]^{2+}$ binds preferentially to AT sites on both the natural DNA sequences and the binding would be unperturbed glycosylation within the major groove of GC sites.

In the same year Collins and Aldrich-Wright published data showing that bis-phen ruthenium(II) complexes of dpq and dpqc (dpq = dipyrido-[3,2-d:2',3'-f]-quinoxaline and dpqc = dipyrido-[3,2-a:2',3'-c]-(6,7,8,9-tetrahydro)-phenazine) (Figure 1.19), two ligands related to dppz, bind DNA oligonucleotides through intercalation from the minor groove[30]. This demonstrates how small structural perturbations can dramatically alter the binding characteristics of a system.

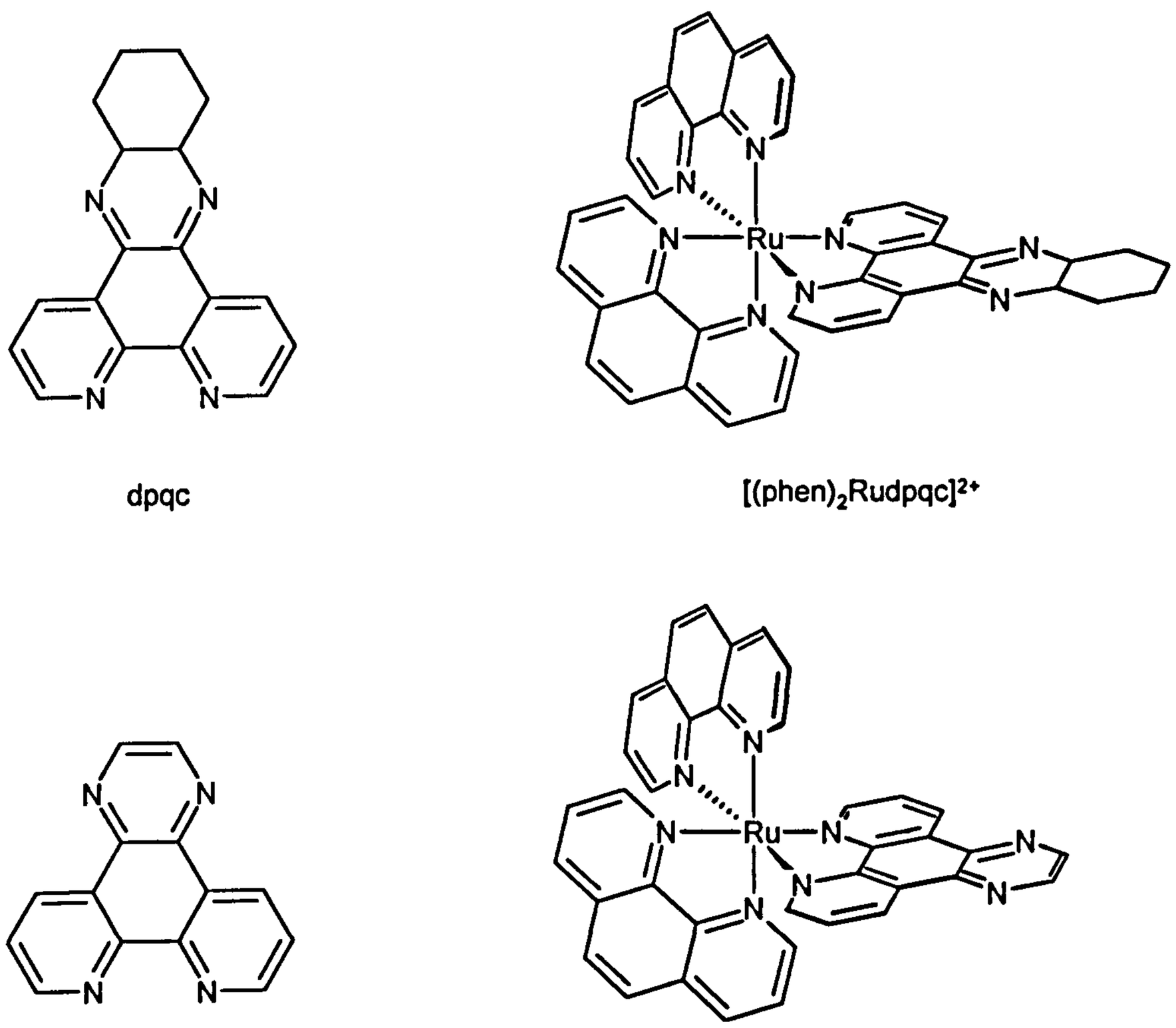

Figure 1.19:- *dpq and dpqc complexes of ruthenium(II)*

1.5.5 PHEHAT complexes as metallointercalators

Kirsch de-Mesmaeker *et al.* extended the area of the intercalating ligand even further when his group prepared the bisphen ruthenium(II) complex of 1,10-phenanthroline[5,6-b]-1,4,5,8,9,12-hexaazatriphenylene (PHEHAT) (Figure 1.20)[31].

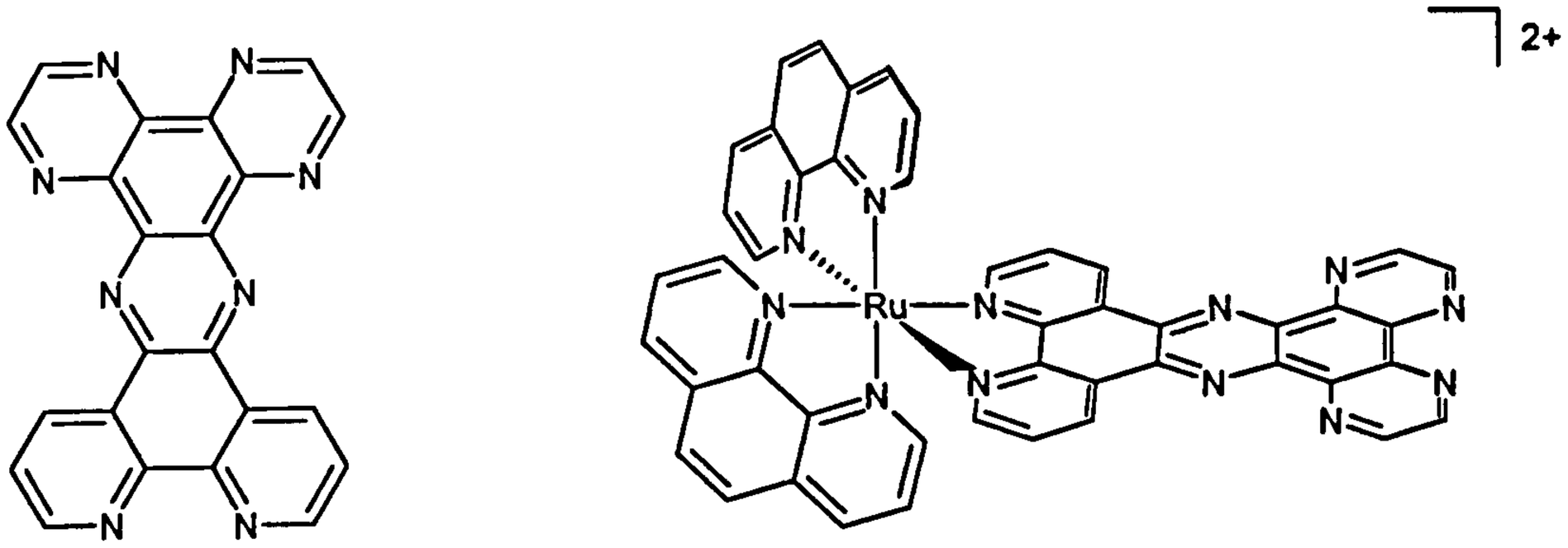

PHEHAT [(phen)$_2$RuPHEHAT]$^{2+}$

Figure 1.20:- *The structure of PHEHAT and its ruthenium(II) complex*

PHEHAT complexes display the light switch effect of the dppz complexes and binding affinities to are comparable to those of the dppz complex.

The metal to ligand charge transfer (MLCT) excited state in PHEHAT complexes is very oxidising[32-34], and is thus able to photo-cleave the phosphate backbone of DNA forming photo-adducts. The primary process that initiates DNA cleavage corresponds to a photo-induced electron transfer, generally from a guanine base to the excited state complex. Barton and co-workers has shown that this electron transfer process is long range and can take place over a distance of some 40 base pairs. An informative review of DNA charge transport chemistry has been presented by Barton *et al.*[35]

1.5.6 Designing a ligand as a base pair mimic

In contrast to the dppz ligands, the 9,10-phenanthrenequinone ligand (phi) was designed to provide an expanse of aromatic structure across the base pair rather than along the diad axis[36]. The phi ligand projects far from the metal centre due to the use of imines as the coordinating chelaters, as can be seen in the parent complex [(phen)$_2$Rhphi]$^{3+}$ (Figure

1.20).

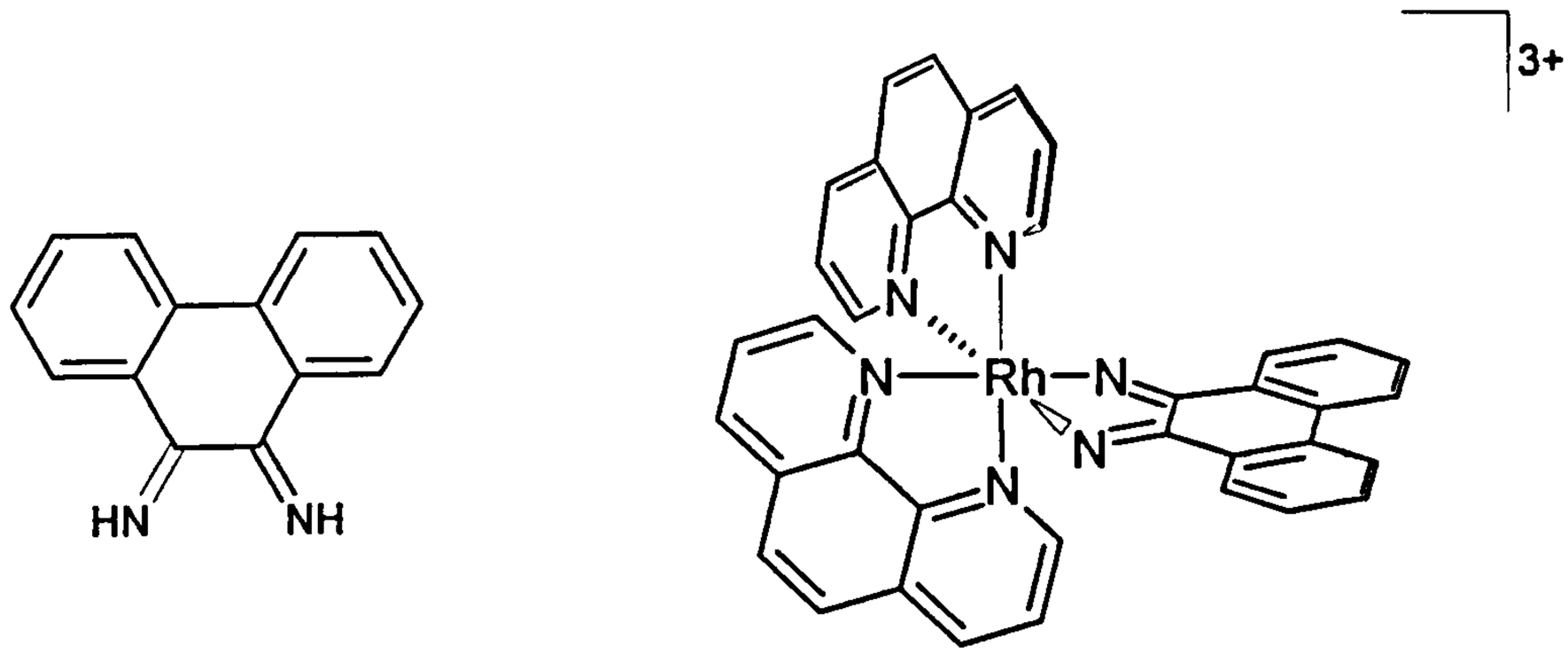

9,10-phenanthrenequinone diimine $[(phen)_2Rhphi]^{3+}$

Figure 1.20:- *9,10-phenanthrenequinone di-imine and its complex*

The phi ligand was first designed in an attempt to match the positioning of aromatic rings with those of the base pairs. The phi complex also differs from the dppz complexes in terms of the photochemistry and, therefore in terms of their utilisation. Phi complexes of both ruthenium(II) and rhodium(III) show no detectable photoinduced emission and therefore the will be no photochemical signature to exploit upon DNA binding. However, phi complexes of rhodium have been continually exploited as they have the ability to cleave DNA at the site of intercalation when they are irradiated with high-energy light (310 - 320 nm). The DNA cleavage pattern is non-specific and cleavage takes place wherever the complex intercalated. The ability of rhodium phi complexes to site-specifically cleave DNA has been invaluable in characterising how metallocomplexes bind to DNA with specificity, as well as high affinity.

1.5.6 Designing a ligand to detect base pair mismatches

The rhodium complex of the ligand chrysi (chrysi = 5,6-chrysinequinone diimine) (Figure 1.21) shows preferential binding to base pair mismatches over normal base pairs within B-form DNA[37,38]. As the chrysi ligand is an extension of the phi ligand, the reason for the preferential binding is due to sterics. The chrysi ligand is too big to intercalate between a normal base pair, but a base pair mismatch results in significant perturbation of the DNA structure around the mismatch allowing the chrysi ligand to be easily accommodated. This is reflected in the fact that, on binding to double helical DNA, the binding constant for the chrysi complex is over two orders of magnitude lower than of the phi complex.

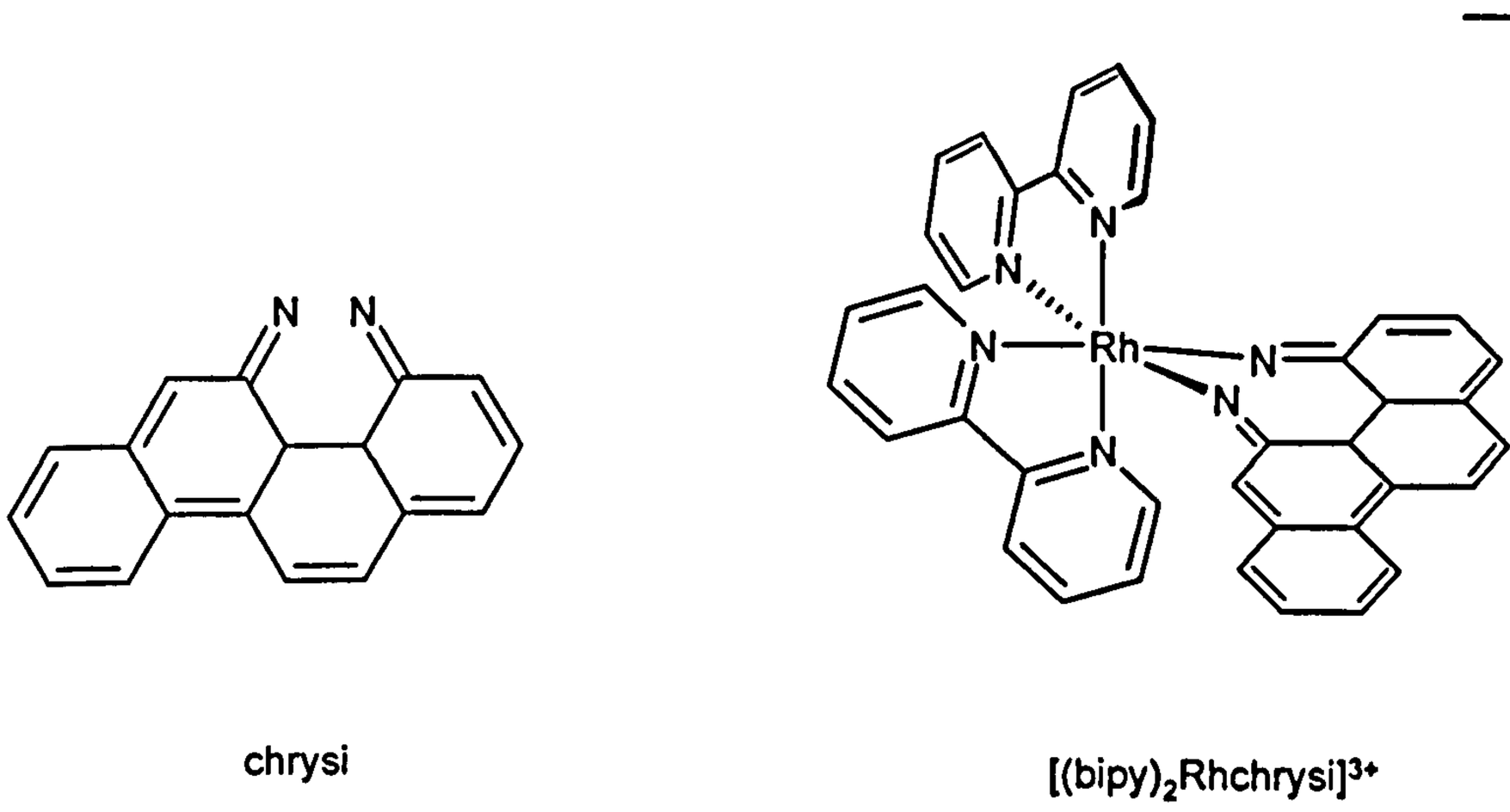

chrysi

$[(bipy)_2Rhchrysi]^{3+}$

Figure 1.21:- *chrysi and its corresponding rhodium(III) complex*

Once bound to the site of the mismatch, the complex can photochemicaly cleave the DNA at the adjacent 3' base on each strand. Many diseases such as hereditary nonpolyposis colorectal cancer are due to the failure of mismatch repair (MMR) systems within the diseased cells which then leads to an accumulation of base pair mismatches. The ability of these complexes to selectively target these mismatch sites within diseased cells

shows their enormous potential as future diagnosis or site-specific chemotherapeutic agents.

1.5.7 Cyclometalated rhodium(III) intercalators

Replacement of the bipy ligand with ppy (ppy = 2-phenylpyridine) in the two rhodium complexes $[(bipy)_2Rhphi]^{3+}$ and $[(bipy)_2Rhchrysi]^{3+}$ results in the formation of $[(ppy)_2Rhphi]^{+}$ and $[(ppy)_2Rhchrysi]^{+}$ (Figure 1.22).

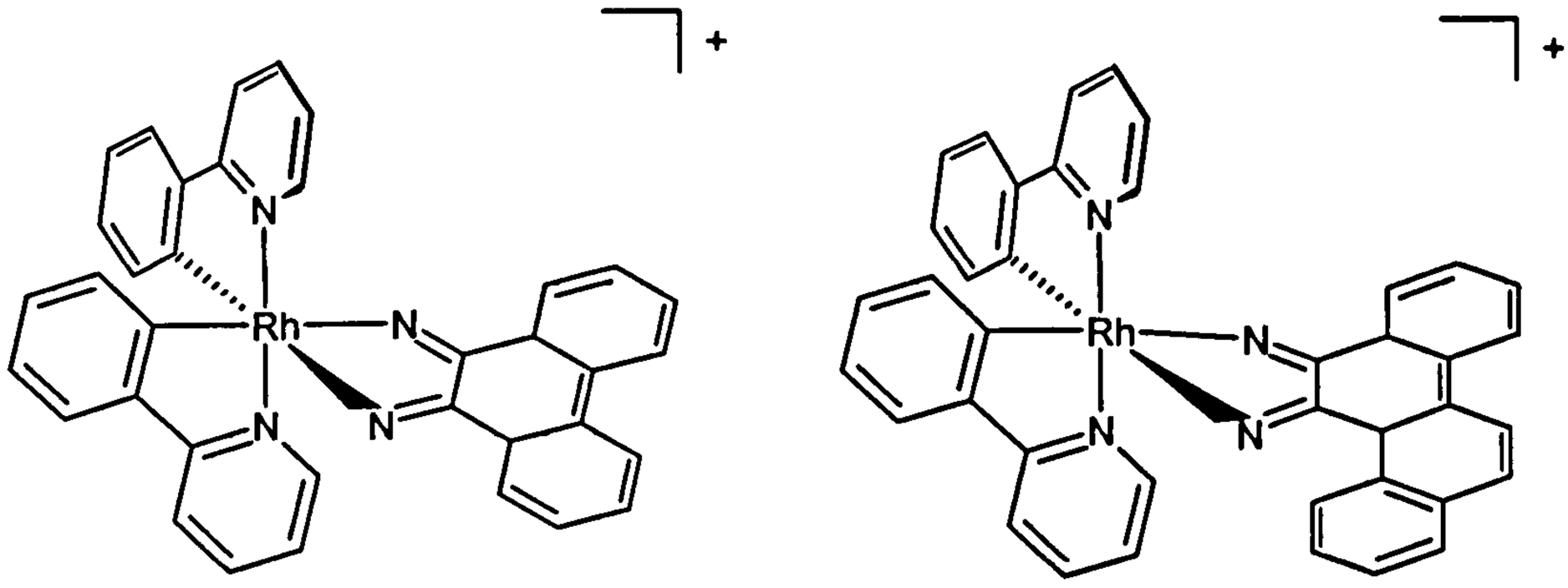

$[(ppy)_2Rhphi]^{+}$ $[(ppy)_2Rhchrysi]^{+}$

Figure 1.22:- *Cyclometalated rhodium complexes of phi and chrysi*

These cyclometalated complexes have extremely similar geometries and shapes as their bipy counterparts but they are mono-cations. This reduction in charge should allow easier passage of these complexes across cellular membranes etc. However, binding and photo-cleavage studies show a decrease in binding affinity of two orders of magnitude due to reduced electrostatic contributions and a 14-fold decrease in the efficiency of $[(ppy)_2Rhphi]^{+}$ to photo-cleave DNA over its tri-cationic $[(bipy)_2Rhphi]^{3+}$ sister complex[39]. The metal-carbon bonds present in the cyclometalated species results in an induction of electron density from the ligand to the metal centre. As photo-cleavage occurs by the abstraction

of a hydrogen atom from the sugar backbone by the intercalating ligand, the shift in electron density results in a higher energy MLCT transitions and reduced ability to abstract the proton, hence a decrease in efficiency. Nonetheless these complexes are worth pursuing as the orientation, due to the *trans-effect* of the nitrogen donor in each of the ppy ligands is axial. This will significantly reduce the number of structural isomers formed if an asymmetric substituted form of the ppy ligand is used, resulting in increased product yields and easier purification procedures.

1.5.8 Rhenium intercalators

The diversity of bidentate di-imine ligands means that they can be co-ordinated easily to other metal centres. Rhenium(I) complexes incorporating di-imine ligands have been shown to have all the necessary spectroscopic characteristics needed to be useful nucleic acid probes. Also complexes with the general formula $[(CO)_3PyReL_2]^+$ have had extensive structural characterisation and are known to have an octahedral geometry with the three carbonyls occupying a facial arrangement.

In 1995 two papers were published simultaneously by Wing-Wah Yam *et al.*, and Schanze *et al.* reporting the synthesis and DNA binding studies on three structurally similar rhenium(I) complexes of dppz and dppn (dppn = benzo[I]dipyrido-[3,2-a:2',3'-c]phenazine) (Figure 1.23)[40,41].

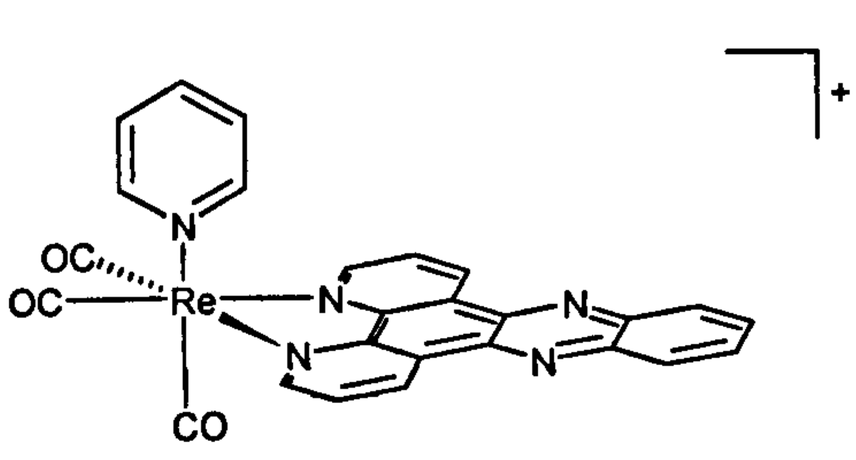

$[(CO)_3PyRedppz]^+$

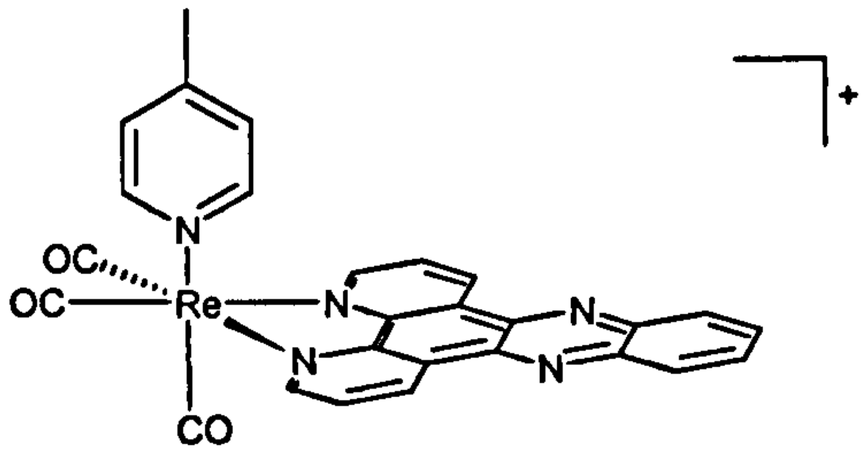

$[(CO)_3Me\text{-}PyRedppz]^+$

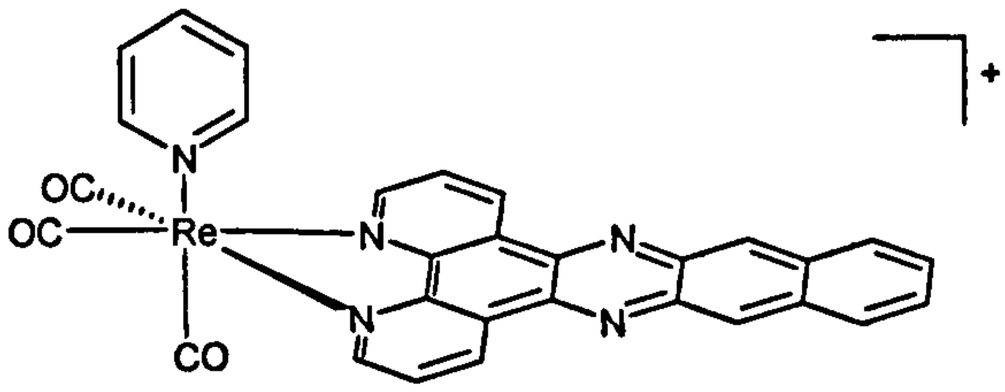

$[(CO)_3PyRedppn]^+$

Figure 1.23:- *Rhenium(I) intercalators based upon dppz*

All three complexes showed hypochromicity in all of their absorption bands when titrated with CT-DNA. The luminescence titration studies turned out to be far more interesting. The dppz derivative showed a 13-fold increase in emission intensity upon titration with CT-DNA as opposed to only a 1.3-fold increase from the dppn derivative. This anomaly was credited to the greater extension of the aromatic ligand in dppn resulted in aggregation in aqueous solution and inhibited binding to DNA. Analysis of the emission data for the dppz complex titrated with CT-DNA with the McGhee-von Hippel model revealed a binding constant of $4.2x10^4$ mol^{-1} dm^3 and a binding site size of 2. Analysis of the UV-Visible titration data for the dppn complex revealed a binding constant of $6.4x10^4$ mol^{-1} dm^3 with CT-DNA[42].

The binding of both complexes was also studied with poly(dA).poly(dT) and poly(dG).poly(dC) shoed a greatly enhanced preference of both the dppz, and dppn complexes for AT sites. The binding data shows an

affinity for DNA approximately 10 fold lower than that of the ruthenium(II) analogues which can presumably accredited to there being less charge on the rhenium(I) complexes.

1.5.9 Iridium based systems

Recently Barton *et al.* have reported the synthesis and DNA binding studies of the tris-heteroleptic complex $[Ir(bipy)(Phen)(phi)]^{3+}$ (Figure 1.24)[43].

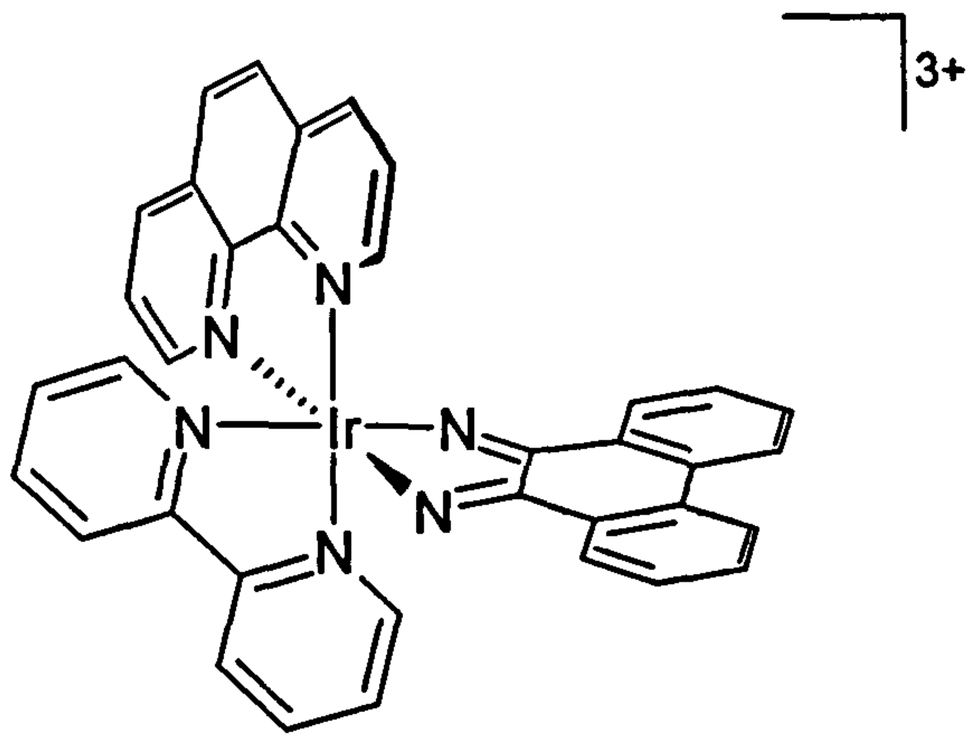

$[Ir(bipy)(phen)phi]^{3+}$

Figure 1.24:- *The tris-heteroleptic $[Ir(bipy)(Phen)(phi)]^{3+}$ complex*

UV-visible titrations with CT-DNA show strong hypochromicity in the $\pi \rightarrow \pi^*$ transition of the phi ligand, indicating that it is deeply intercalated in the DNA helix analogous to its rhodium(III) counterpart. Unlike the rhodium(III) complex, the iridium(III) complex shows a chemically reversible reduction centred on the phi ligand. This reduction has been used to probe its interaction with DNA and coulometric titrations reveal a binding affinity $k = 1.1 \times 10^6$ mol^{-1} dm^3 which is an order of magnitude lower than its rhodium counterpart.

Electrochemistry is becoming an increasingly useful tool for probing both the interactions of metallointercalators with DNA and the charge transport properties of the DNA π-stack.

1.5.10 DNA recognition based on shape selection[44,45]

Due to their shape and polarity, different intercalating ligands stack with different orientations within the DNA double helix and, as such, provide somewhat different strategies for the specific recognition of sites on DNA. This phenomenon is emphasised by the fact that two complexes of dppz $[(CO)_3PyRedppz]^+$ and $[(phen)_2Rudppz\}^{2+}$ show small but significant preferences for A-T rich sequences of DNA over their G-C rich counterpart.

As the extended heterocyclic ligands of dppz and phi complexes intercalate between the base pairs of the DNA, the other ancillary ligands on the complexes are brought into close proximity with the DNA base pairs and, as a result, specific noncovalent interactions between the ancillary ligand functionalities and functionality in the DNA groove can be made.

A good example of how secondary interactions are important in recognising distinct binding sites is the sequence specificity between the two rhodium phi complexes $[(phen)_2Rhphi]^{3+}$ and $[(phi)_2Rhbipy]^{3+}$. $[(phen)_2Rhphi]^{3+}$ shows a moderate preference for sites with high propeller twisting towards the major groove. This means $[(phen)_2Rhphi]^{3+}$ preferentially cleaves at 5'-YYR-3' (where Y is pyrimidine and R is purine) sites. Comparison of the crystal structures of DNA oligonucleotides with the photo-cleavage patterns for $[(phen)_2Rhphi]^{3+}$ enabled the determination of the critical structural features for recognition. It was proposed that the propeller twisting allows shape selection by opening up the B form DNA purines in 5'-YYR-3' dramatically, thus permitting facile

intercalation of the phi ligand. In contrast, 5'-RRY-3' not only closes the major groove, but also places the pyrimidines in highly unfavourable positions with respect to the phenanthroline rings. $[(phi)_2Rhbipy]^{3+}$ shows almost no sequence or structure specificity. Inspection of the geometry of this metal complex shows that the non-intercalating phi ligands are positioned away from possible steric clashes with the helix. Therefore, a simple comparison of the shapes between these two metal complexes highlights the idea that steric clashes or their avoidance can dominate site selectivity Figure 1.25).

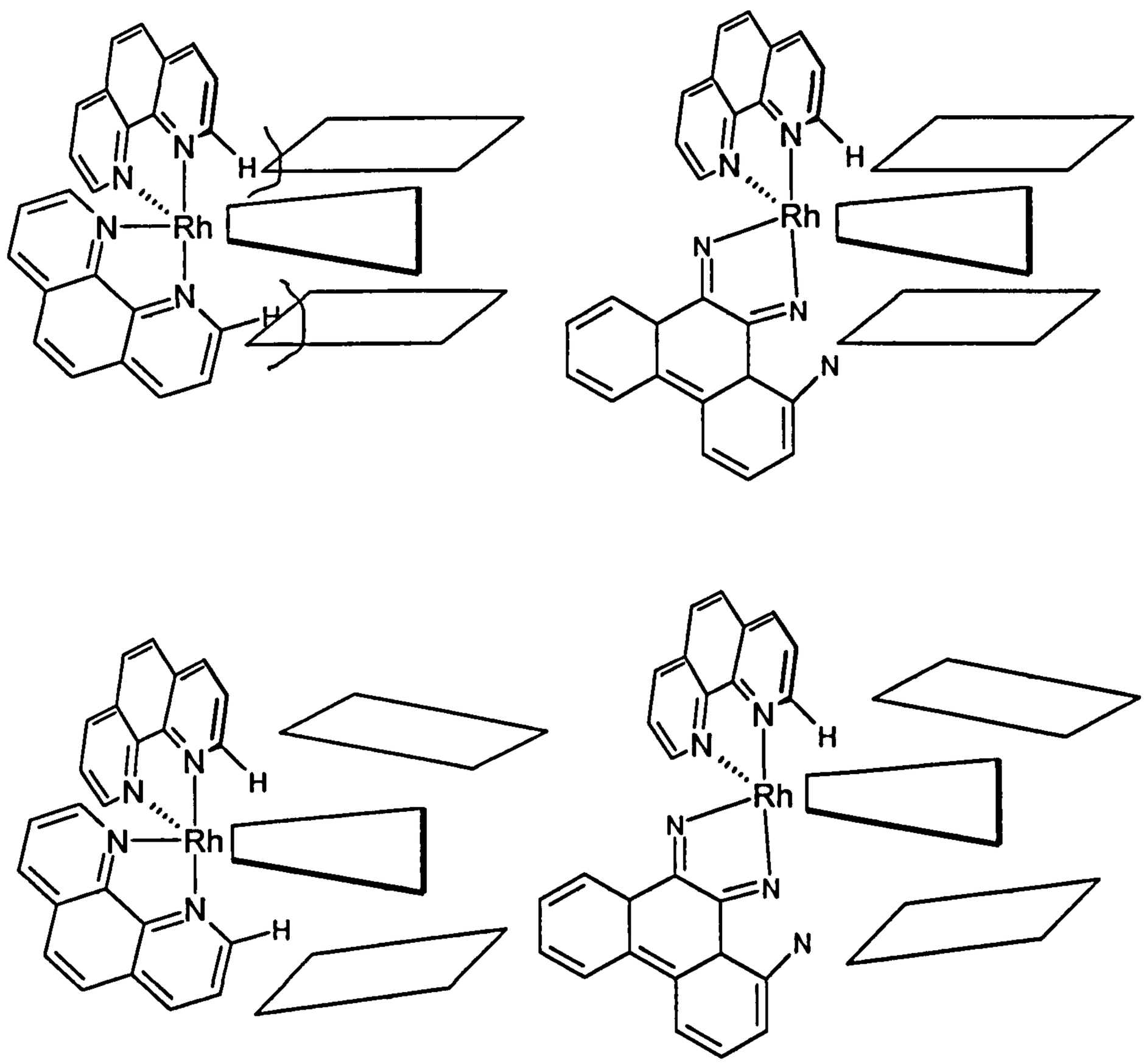

Figure 1.25:- *Rhodium(III) phi complexes showing steric interactions important in sequence recognition.*

1.5.11 Direct readout of recognition sites within the grooves of DNA

Another strategy for site-specific recognition of DNA is the utilisation of direct hydrogen bonding or van der Waals' interactions between functionality on the ancillary ligands of the intercalator and sites within the DNA grooves. By incorporating complementary functionality into the ancillary ligands, the desired specificity can be achieved. A family of rhodium amine complexes, based around the phi ligand, have been synthesised and the selectivity for a four base pair site has been tested[46,47]. It is found that $[(NH_3)_4Rhphi]^{3+}$, $[en_2Rhphi]^{3+}$ and $[[12]andN_4Rhphi]^{3+}$ cleave specifically at 5'- G C-3' sites. The well-defined structural geometry of these complexes indicated the possibility of hydrogen bond formation between axial amines of the metal complexes and the O-6 of guanine. A control complex incorporating a thiocrown $[[12]aneS_4Rhphi]^{3+}$, which lacks hydrogen bonding capability was tested in parallel experiments and was seen to bind with no specificity.

The introduction of an O-6 methyl guanine in place of guanine on the targeted oligonucleotides disrupts binding to this site, indicating a hydrogen bonding interaction is present. In contrast, replacement of guanine with 7-deazaguanine did not disrupt recognition, suggesting that hydrogen bonding to the N7 of the guanine is not an important factor in the binding and recognition of these metal complexes.

Barton and co-workers designed and synthesised a complex specifically to bind into a 5'-TGCA-3' site[48]. The targeting of the site was based upon hydrogen bonding contacts between axial amines and the O-6 of guanine, as well as van der Waals' contacts between the pendant methyl groups on the metal complexes and the methyl groups on the flanking thymines[46]. Photo-cleavage data indicated that the complex binds to the target 5'-TGCA-3' site and the binding constant is 9×10^7 mol^{-1} dm^3 [49]. A high resolution NMR structure[49,50] and, recently, a crystal structure[51] of

the metal complex intercalated into the major groove confirm that this complex targets the sequence in the major groove and, remarkably, each of the predicted contacts are present (Figure 1.26).

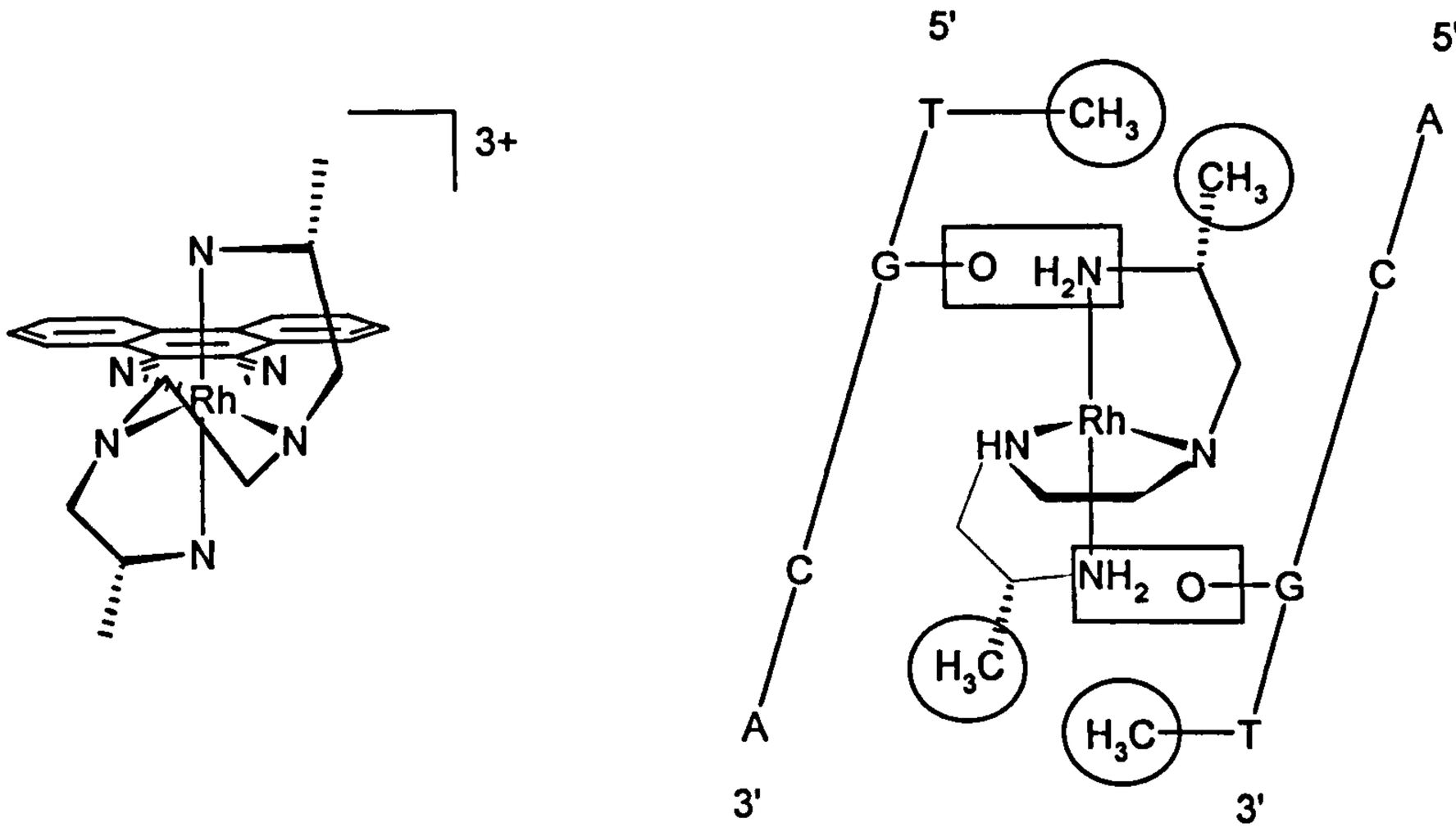

Figure 1.26:- *Δ-[(R,R)Me$_2$trienRhphi]$^{3+}$ (left) and its non-covalent interactions with 5'-TGCA-3'.*

The crystal structure of the rhodium intercalator bound specifically to the central 5'-TGCA-3' site at eight base pair oligonucleotide is solved at 2Å resolution and it is the first crystallographically characterised metallointercalator bound to a DNA duplex (Figure 1.27). The structure shows that the base pairs are well stacked, and the phi ligand is deeply intercalated between them. The conformation of the deoxyribose sugars at the intercalation site is B-form which shows that metallo intercalation causes minimal structural perturbation to the DNA, and that the intercalated ligand resembles an inserted base pair.

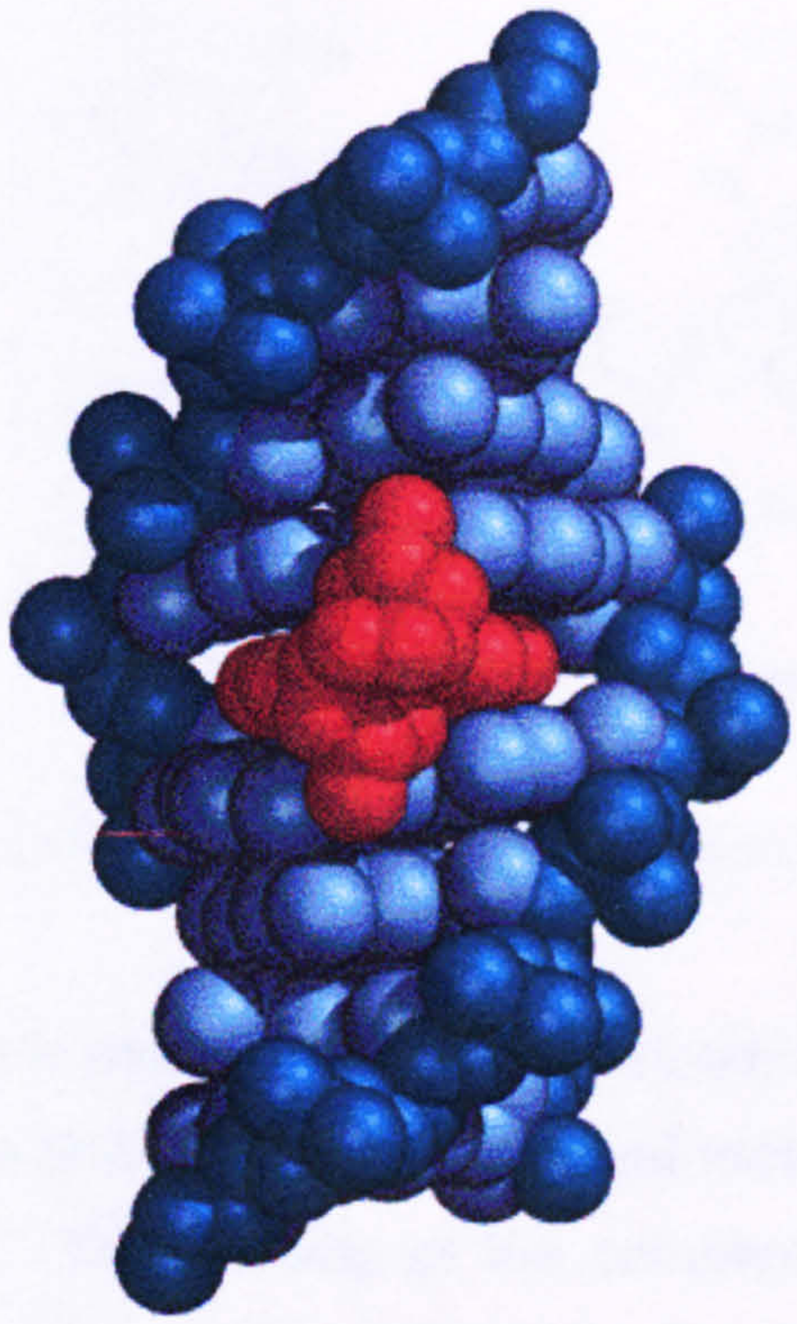

Figure 1.27:- *X-ray crystal structure of Δ-[(R,R)Me$_2$trienRhphi]$^{3+}$ intercalated into a DNA duplex*

1.5.12 Cationic lanthanide complexes as DNA binding agents

IDavid Parker *et al*. have assembled a series of cationic lanthanide complexes with a pendant *N*-methylphenanthridinium chromophore[52,53] (Figure 1.28). These are some of the first lanthanide complexes, which have a well-defined structure and are kinetically stable towards racemisation in solution.

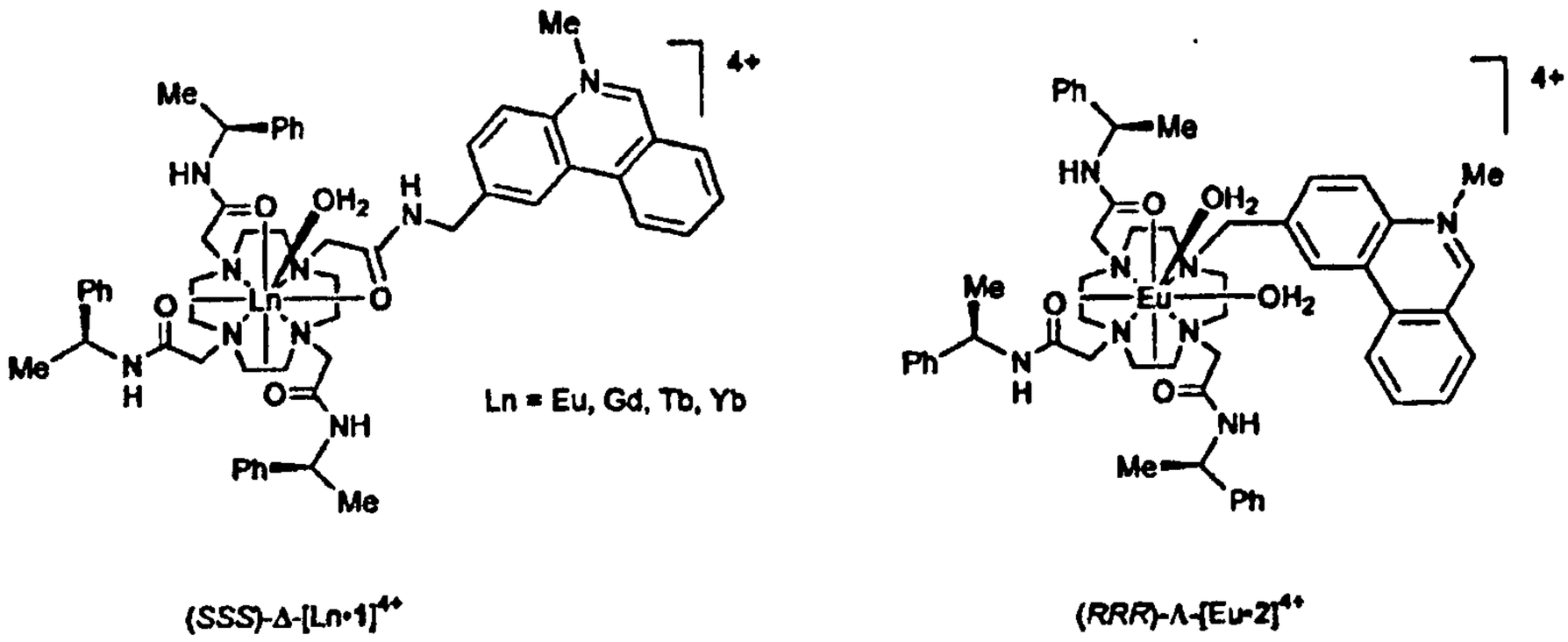

Figure 1.28:- *Cationic lanthanide complexes developed by Parker et al.*

In these complexes the pendant *N*-methylphenanthridinium moiety serves to intercalate into the DNA helix and the chiral metal complex sits in the groove of the DNA. The chirality of the complexes is defined by the configuration of the remote carbon stereogenic centre. The complexes showed good affinity for DNA with the Δ-enantiomer binding stronger than the Λ-enantiomer. There is also a preference for GC sequences of DNA (for the Δ-enantiomer k = 8.7×10^{-6} mol^{-1} dm^3 $duplex^{-1}$ for $[(GC)_6]_2$ and 1.6×10^{-5} mol^{-1} dm^3 $duplex^{-1}$ $[(AT)_6]_2$)[53]. The complexes also showed extremely good affinity for circular Plasmid DNA[52]. The coordinatively unsaturated complexes [Ln.2] which contain two coordinated water molecules have been shown to bind reversibly to hydrogen phosphate anions offering scope for hydrolytic activity with the phosphate backbone of DNA[54].

1.6 Bimetallic DNA binding complexes

1.6.1 Modulation of DNA binding properties by ancillary ligands

One of the first bimetallic DNA binding complexes was assembled around the bis chelating ligand dpb (dpb= 2,3-bis(2-pyridyl)benzo[g]quinoxaline). The ligand has two bidentate chelating sites and is therefore capable of binding to two metal centres simultaneously[55,56]. When the two metal centres are $(phen)_2Ru^{2+}$ the complex shows very little affinity for DNA, as the steric bulk of the four phenanthroline ligands prevents efficient intercalation of the extended aromatic ligand into the DNA double helix. When the two metal centres are $(NH_3)_4Ru^{2+}$ the steric bulk of the ancillary ligands is dramatically reduced and the complex is free to interact with DNA (Figure 1.29).

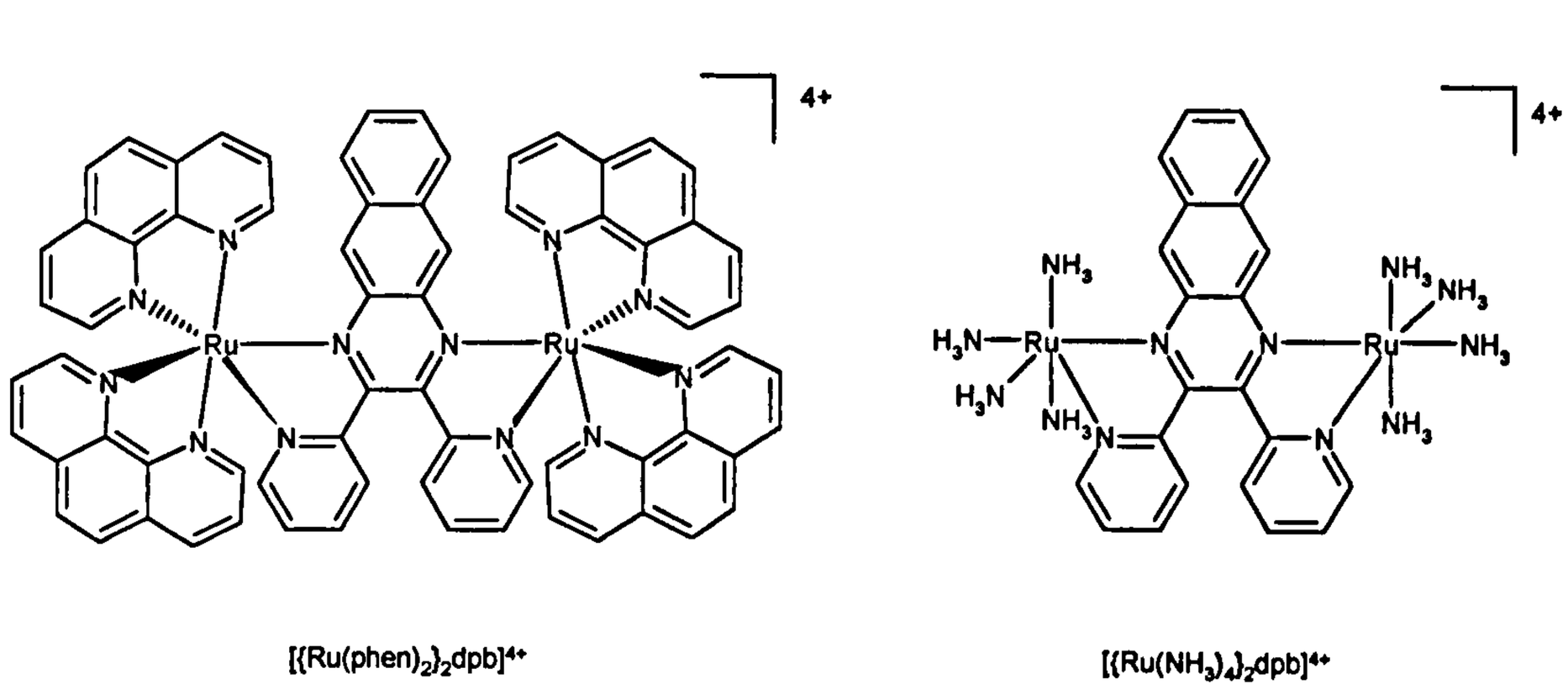

Figure 1.29:- *Phen and NH_3 complexes of dpb*

Analysis of the binding with a model related to the McGhee-von Hippel model developed by Bard *et al.* returned a binding constant of $8.3x10^5$ mol^{-1} dm^3 and a site size of 6 base pairs reflecting the bulkiness of the complex.

1.6.2 Linking two DNA binders together

In order to further increase the affinity of metallointercalators for DNA the first series of bimetallic bis-intercalators have begun to emerge. Kelly *et al.* developed the first of these systems. They simply took the relatively poor DNA binding complex $[(bipy)_3Ru]^{2+}$ and linked two of them together with an aliphatic chain (Figure 1.30) [57,58]

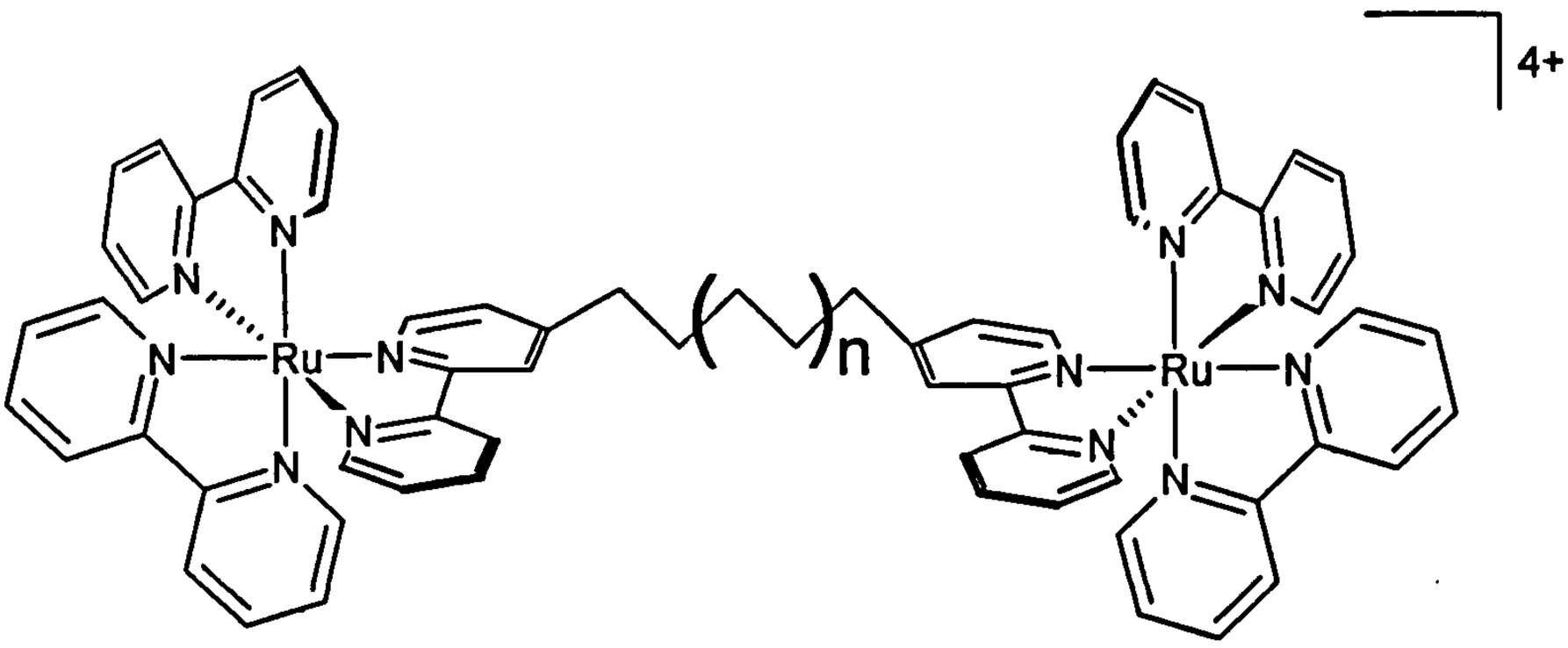

n=3, 5 or 7

Figure 1.30:- *Bimetallic DNA binding complex developed by Kelly et al.*

The binding affinity is improved by two orders of magnitude in the bimetallic species over the monometallic species, with the optimum linker length reported to be seven carbons in length. Also, the salt dependency of the bimetallic species was drastically reduced compared to the monomer with significant amounts of bimetallic species bound even at salt concentrations in excess of 500 mM.

1.6.3 Covalently joining two dppz moieties together

In 1996 Norden and his group published DNA binding data on a novel bimetallic system bridged by head to head dppz ligands (Figure 1.31) [59]

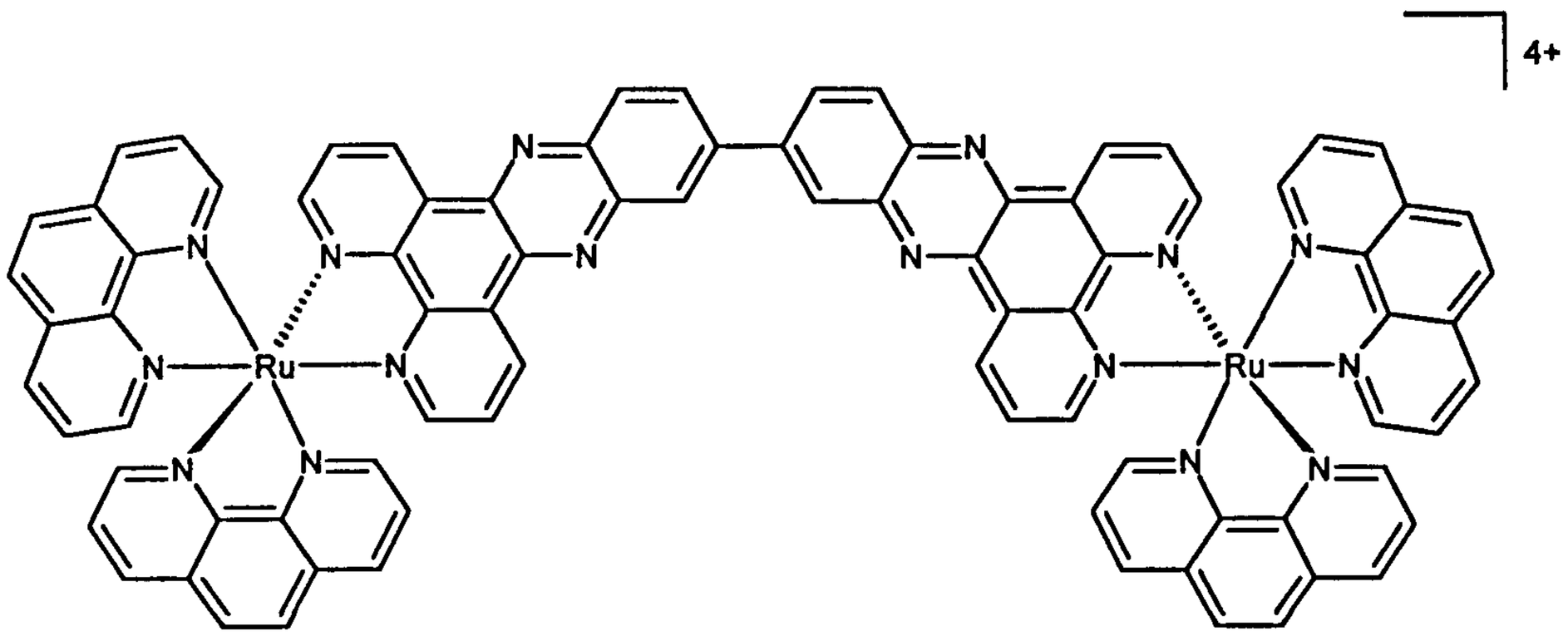

Figure 1.31:- *Bis-dppz bimetallic ruthenium(II) complex*

This system incorporates two chiral ruthenium centres and the DNA binding characteristics differ between all three isomers ΔΔ, ΛΛ and ΔΛ. For the ΛΛ-complex, stopped flow linear dichroism and circular dichroism spectra suggest a binding confirmation in which the concave face of the bis-dppz ligand envelops the sugar phosphate backbone, thus placing one RuL_2 moiety in each groove. However, the ΔΔ- complex binds in a distinctly different way, possibly with both metal centres in the same groove. The complexes are non-luminescent in aqueous solution, as well as in the presence of DNA, so competitive binding studies with the well characterised Δ-$[(phen)_2Rudppz]^{2+}$ were used to determine binding affinities. The order of binding strength was found to be ΔΔ > ΛΛ *ca.*≈ $5x10^{11}$ mol^{-1} dm^3.

1.6.4 A DNA staple

Norden *et al.* took this system one stage further by synthesising the bimetallic species of the $[(phen)_2Rudppz]^{2+}$ complex (Figure 1.32)[60].

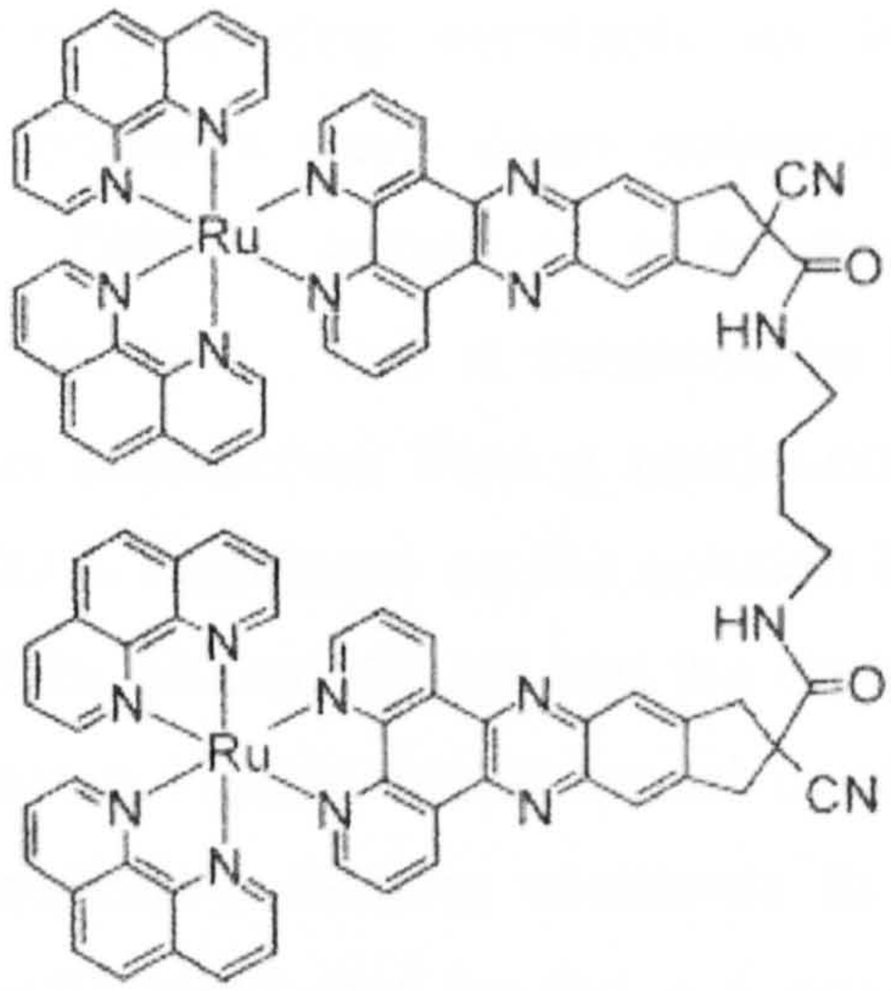

Figure 1.32:- *DNA staple developed by Norden and his group*

They have named this a DNA staple, as both of the bisphen ruthenium(II) units pass directly through the core of the DNA into the groove on the opposite side of the DNA (Figure 1.33).

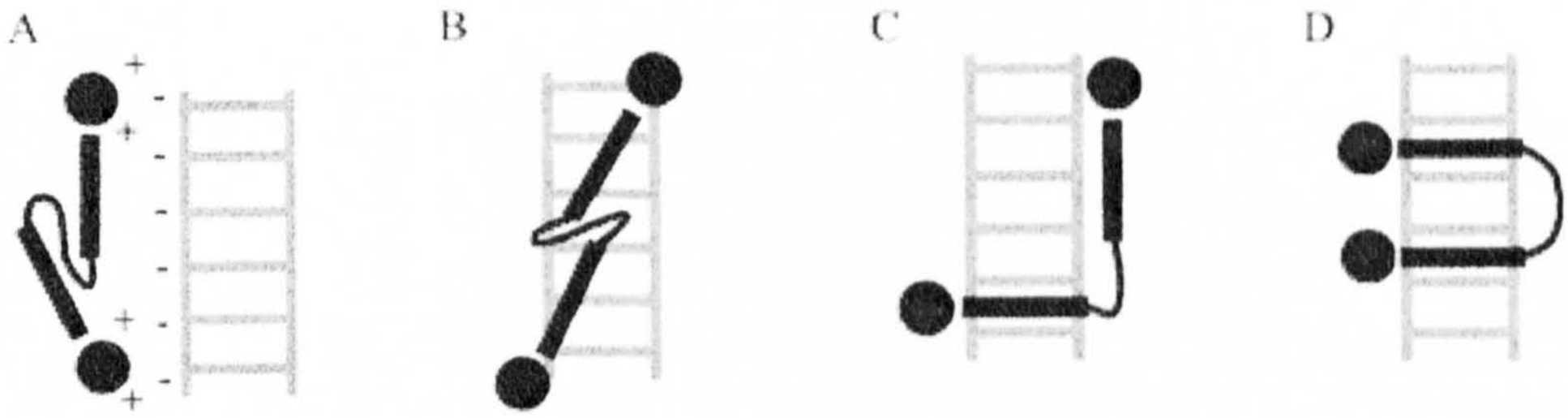

Figure 1.33:- *Schematic DNA-interaction modes of the DNA staple. (A)* Electrostatic external binding. *(B)* Groove binding. *The subunits positioned in either minor or major groove of DNA. (C)* Mono-intercalation. *One subunit intercalated the other one, either in a groove or freely dangling (D)* Bis-intercalation. *Both subunits intercalated, either in the minor or the major groove, the bridging chain residing in the opposite groove.*

This gives very high binding affinities and extremely slow dissociation rates. According to Norden, normal emission and absorption were not

appropriate for obtaining binding constants for this system[61]. The equilibrium binding constants have been determined by an emission dilution experiment. DNA is added to a solution of the drug until saturation binding is reached. This is assumed to be 4:1 ratio of DNA phosphate to drug as determined from a continuous variation analysis. The emission intensity is monitored as the solution is diluted with buffer. The data is corrected for dilution effects and the data is fitted to a revised form of the McGhee-von Hippel model based upon a site size of four base pairs. The equilibrium binding constants to CT DNA has been determined to be $3x10^{-8}$ mol^{-1} dm^3 for the Δ-Δ enantiomer at 110mmol NaCl. This value has been adjusted to $1.7x10^{-10}$ $mol^{-1}dm^3$ for binding at 50mmol NaCl[61]. The association kinetics were determined by conventional stop flow kinetic analysis.

1.6.5 A bipyrimidine bridged system

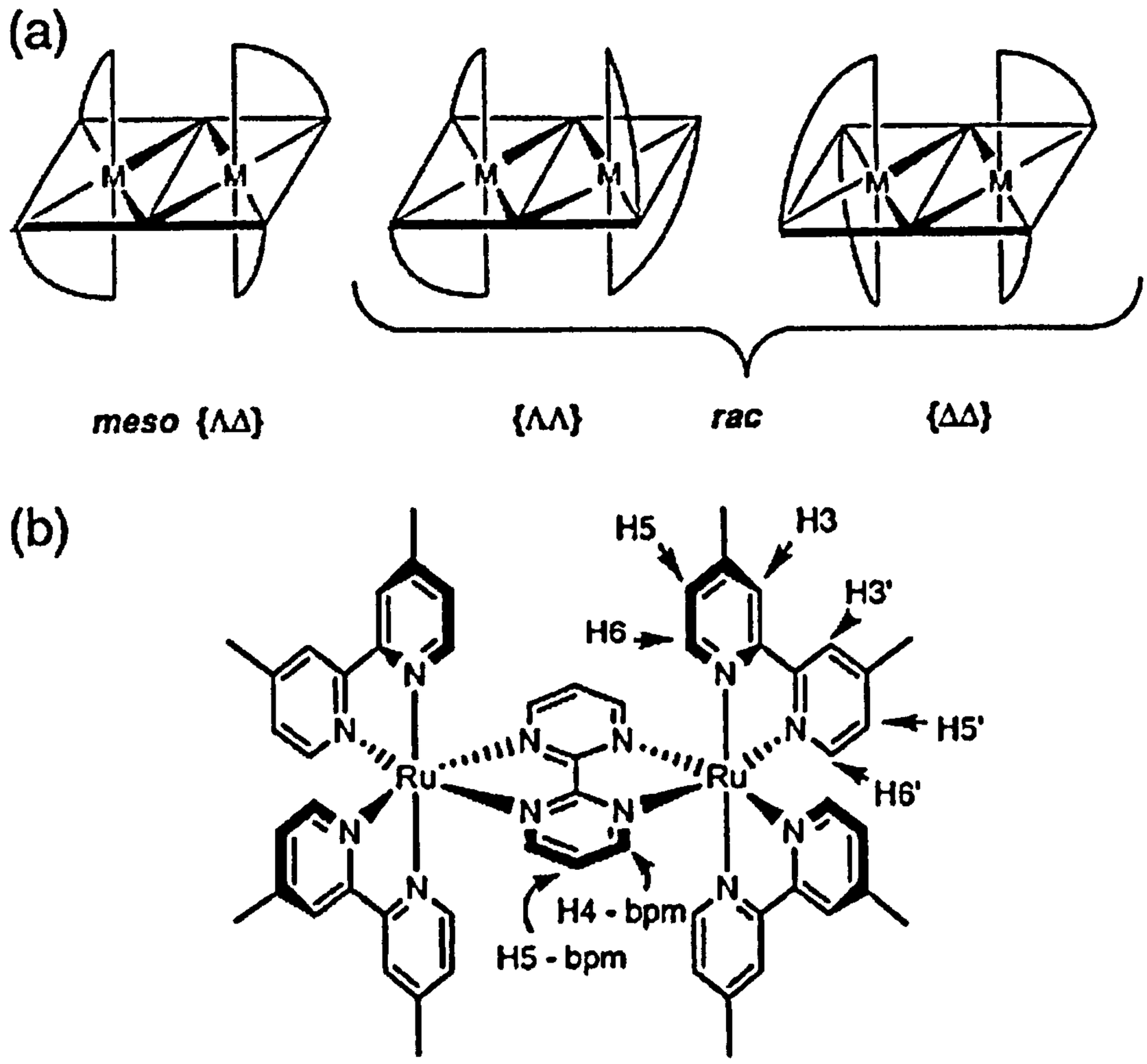

Figure 1.34:- *bis-ruthenium(II) bpm bridged complex and schematic representation of the three diasterioisomers*

The Australian group of Keene *et al.* have synthesised and published data on the bipyrimidine bridged bis-ruthenium(II) species $[\{Ru(Me_2bipy)_2\}_2(\mu\text{-bpm})]^{4+}$ (where Me_2bipy = 4,4'-dimethyl-2,2'-bipyridine; bpm = 2,2'-bipyrimidine) (Figure 1.34)[62].

The binding of the ΛΔ, ΔΔ and ΛΛ isomers to the synthetic oligonucleotide d(3'-CAATCCGGATTG-5')$_2$ was characterised by ^{1}H NMR spectroscopy. Titration of the complexes with the dodecamer induced significant shifts in the proton resonances of the sugar residues and the aromatic proton resonances of the metal complexes. The resonances corresponding to the H3' and H3 on the metal complexes shifts systematically throughout

the titrations and were used to estimate the binding constants. Binding constants ca. $3x10^3$ and $2x10^3$ mol^{-1} dm^3 were calculated for the ΛΛ- and ΔΔ- isomers, respectively.

NOESY experiments were performed to try to determine the mode of interaction of the complexes. The complexes were found to reside in the minor groove with one of the bidentate Me_2phen ligands from each metal centre slotting into the groove (Figure 1.35).

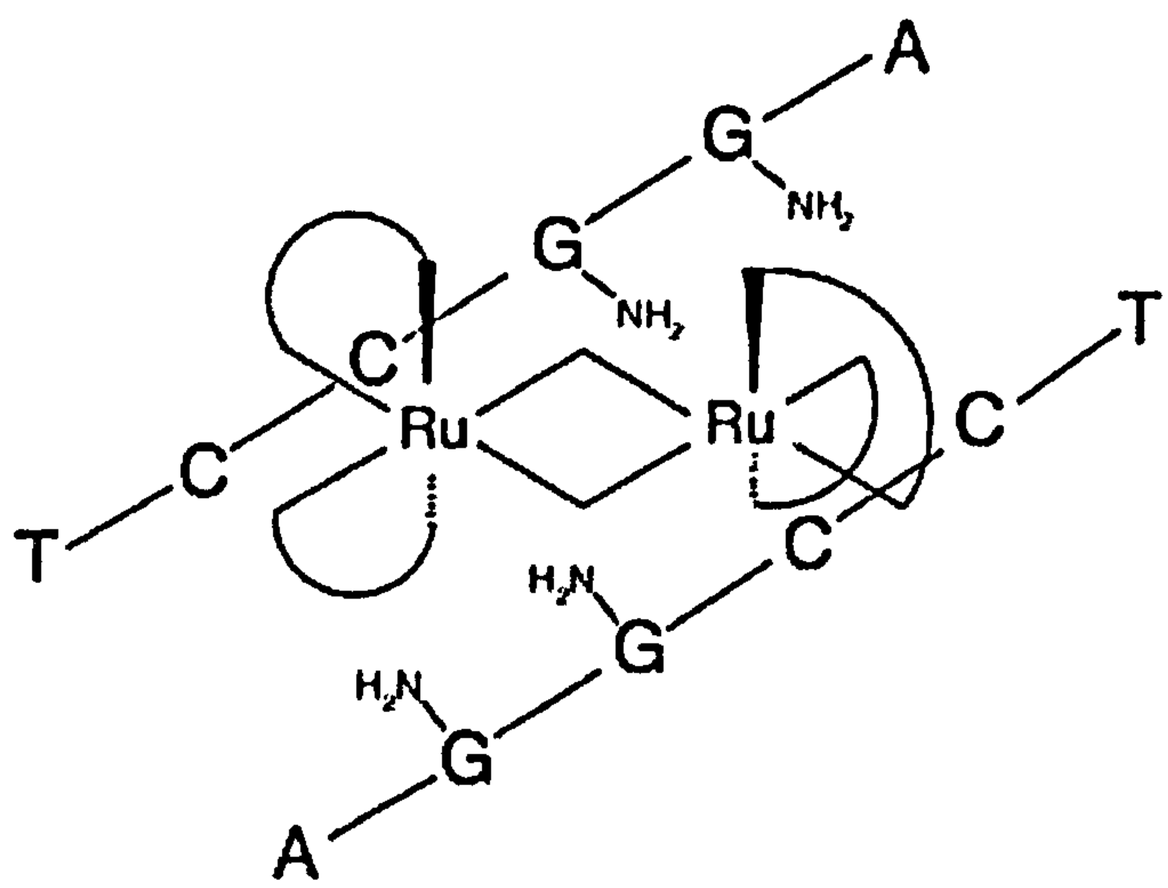

Figure 1.35:- *A schematic showing the ΛΛ-stereo isomer of [{Ru(Me2bpy)2}2(μ-bpm)]4+ binding to the central CCGG region of the dodecanucleotide d(CAATCCGGATTG)2. The metal complex is bound across the minor groove in a manner that positions only one bidentate ligand from each ruthenium into the groove and close to the cytosine residues and away from the guanine amino groups. If the central C and G residues on each strand were interchanged (i.e. C to G and G to C) the guanine amino groups would sterically hinder the metal complex binding.*

1.6.6 A supramolecular cylinder as a major groove binder

Hannon *et al.* have demonstrated the use of a supramolecular cylinder as a major groove DNA binding agent[63]. The cylinders that are formed from the spontaneous self-assembly of three imine-based ligands around two divalent iron centres to form a triple helical structure (Figure 1.36).

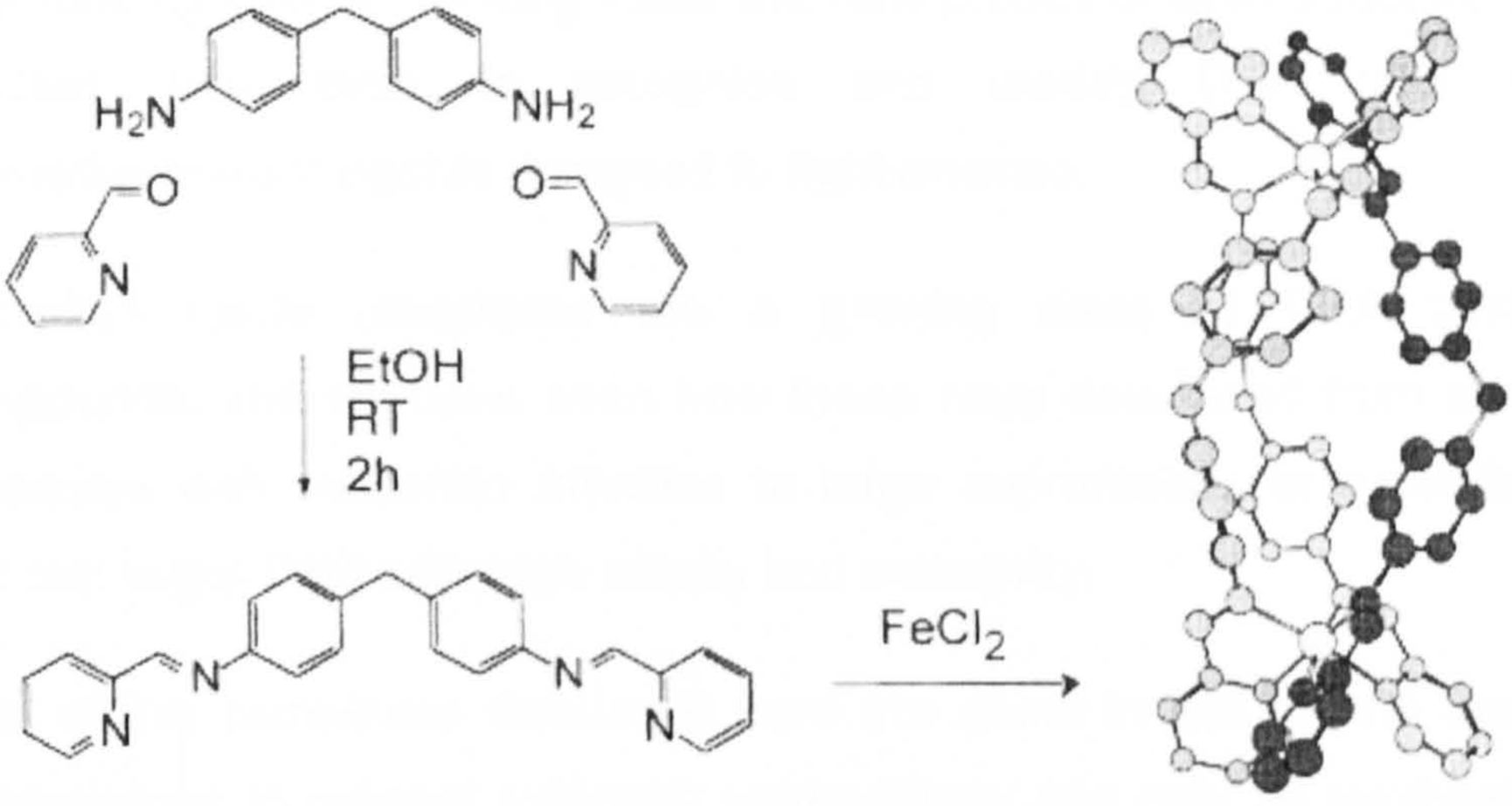

Figure 1.36:- *The molecular structure of the ligand and the tetracationic triple helical supramolecular cylinder* $[Fe_2(C_{25}H_{20}N_4)_3]Cl_4$

Once assembled, these cylinders have a size and shape that is comparable to those of zinc finger proteins and bind in the major groove of the DNA spanning five base pairs. Once bound, they proceed to wrap up the duplex in a intramolecular fashion which can be observed by CD, NMR and AFM imaging techniques.

This is a good example of the way in which supramolecular assemblies allow chemists to bridge the size gap between traditional small molecule and larger biomolecule DNA-recognition motifs.

1.7 Conclusions

We have seen in this introduction that DNA is essential to life and that any modifications to the information stored within it can be catastrophic for the organism it resides in. Many of the secrets of its structure and function have now been unearthed leading to the development of new DNA binding agents. Among these are new probes of DNA structure and function, new tools to recognise and modify DNA and new chemotherapeutic agents designed to fight disease.

Transition metal complexes are a growing class of DNA binding compounds, and we have seen how these have developed from simple molecules with moderate affinities to large supramolecular assemblies that can target DNA with high affinity and selectivity.

Most of the complexes discussed here are chiral in nature and due to shortcomings in present synthetic methodology can only be synthesised as racemic mixtures which require difficult and time consuming chiral separations. This problem is amplified when the system is extended to contain more than one chiral metal centre.

Having seen the potential of the bimetallic systems for increasing the binding affinity and selectivity of metal complexes for DNA we have undertaken a study to try to develop a series of achiral monometallic complexes with high affinity and selectivity for DNA and then extend this to achiral bimetallic complexes. This approach greatly simplifies the synthetic procedures required to build large well-defined complexes designed to interact with DNA

Chapter 2

Extended terpyridine complexes of ruthenium(II) and rhenium(I)

2.1 Introduction

For many years now ruthenium(II) and rhenium(I) complexes containing polypyridyl chelating ligands have been extensively studied. The rich photophysical and redox properties associated with these complexes makes them potentially useful in light harvesting[64-66], electron transfer[67-69], non-linear optics[70-72], catalytic water splitting[73], self-assembly[74] and recently probes for biological systems[75].

This chapter is concerned with the synthesis and characterisation of a series of ruthenium(II) and rhenium(I) complexes incorporating 4'-extended terpyridine ligands with a view to producing a series of novel complexes with favourable DNA binding properties.

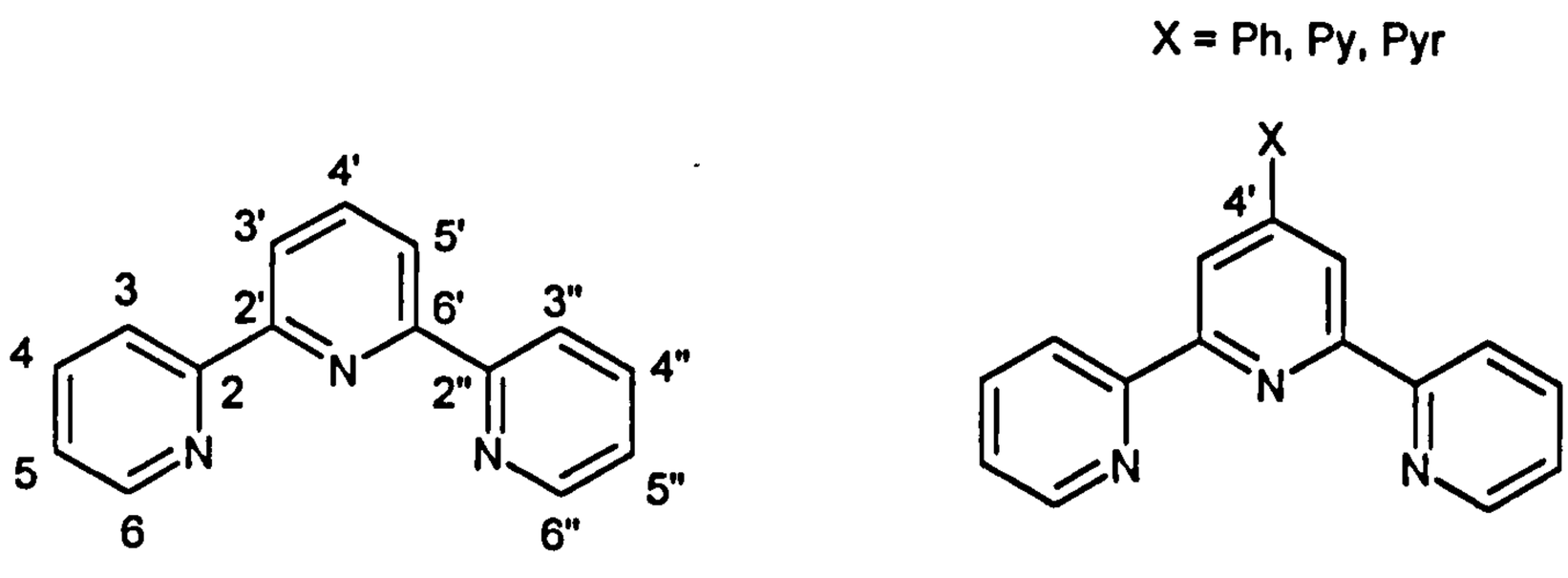

Figure 2.1:- *Terpyridine and 4'-extended terpyridines showing the atom numbering Scheme.*

A series of transition metal complexes incorporating 4'-extended terpyridine ligands have been synthesised, which are expected to bind to DNA through intercalation of the extended terpyridine moiety into the base stack of DNA. The system allows variation of numerous characteristics of the molecules such as charge, chirality and hydrogen-bonding ability without changing the overall shape of the complex (Figure 2.2).

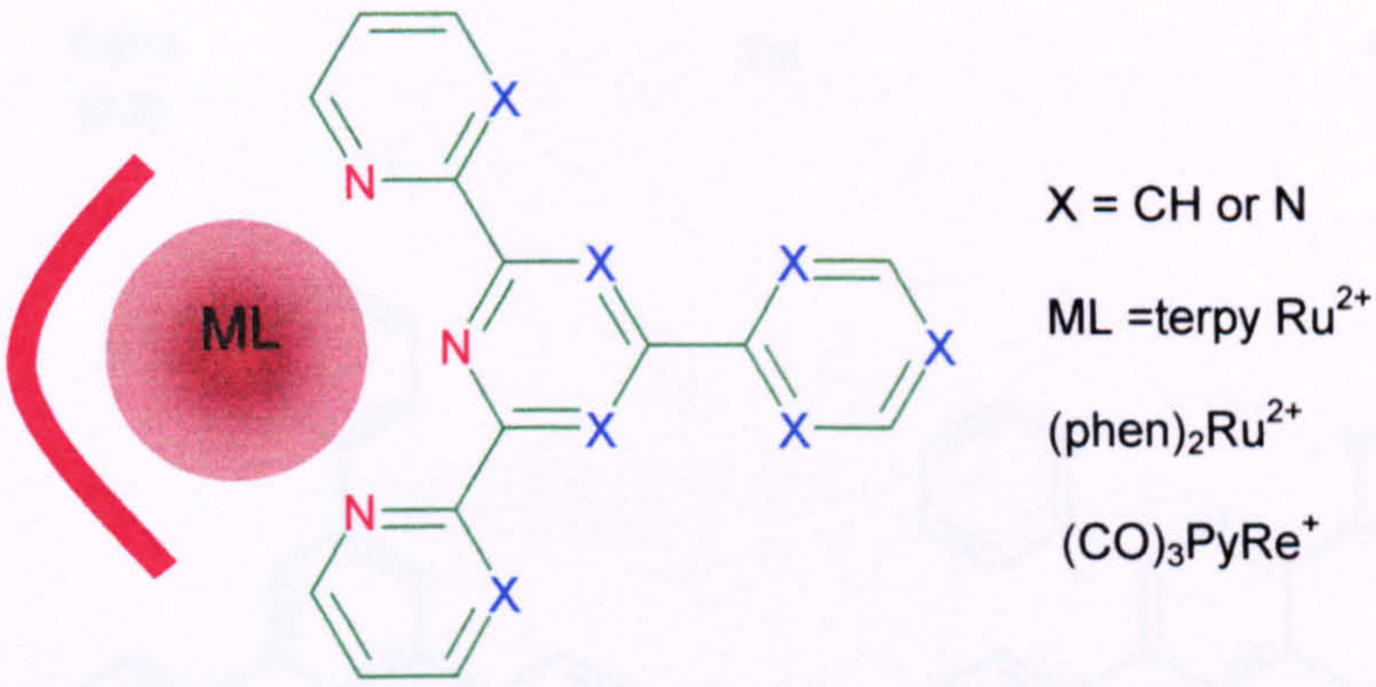

Figure 2.2:- *Schematic of the extended terpyridine systems designed for DNA binding*

The complexes can be achiral (ML = $terpyRu^{2+}$) or chiral (ML = $(phen)_2Ru^{2+}$. The overall charge on the complexes varies from +1 in the rhenium complexes to +2 in the ruthenium complexes.

The DNA binding characteristics of each of these complexes has been carried out, to determine what effects these changes have and this aspect will be discussed in detail in Chapters five and six.

The five ligands chosen as the intercalating domains for this study are 2,4,6-tris(2-pyrimidyl)1,3,5-triazine **(2.2)** (Tpymt), 2,4,6-tris(2-pyridyl)1,3,5-triazine (Tpt), 2,2':4,4'':6,2''-quaterpyridine **(2.5)** (Qtpy), 4'-phenyl-2,2':6',2''-terpyridine **(2.6)** (P-terpy) and tetra-2-pyridyl-1,4-pyrazine **(2.7)**

(Tpp), shown in Figure 2.3. These ligands are all flat polyaromatic structures, which should be ideally set up for intercalation into the DNA base stack.

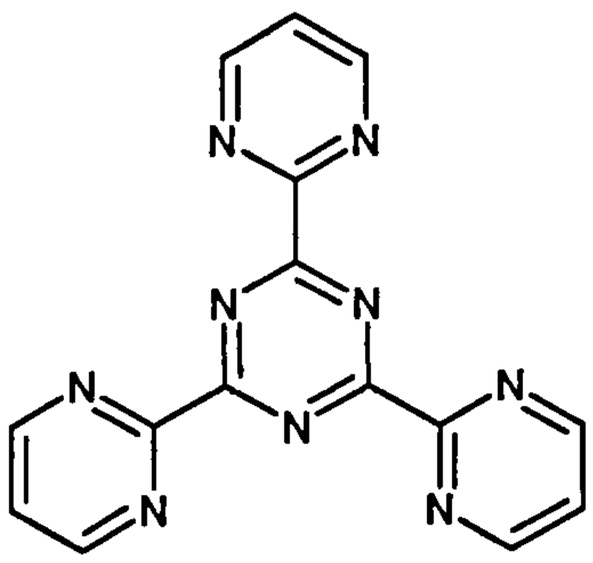

Tpymt
(2.2)

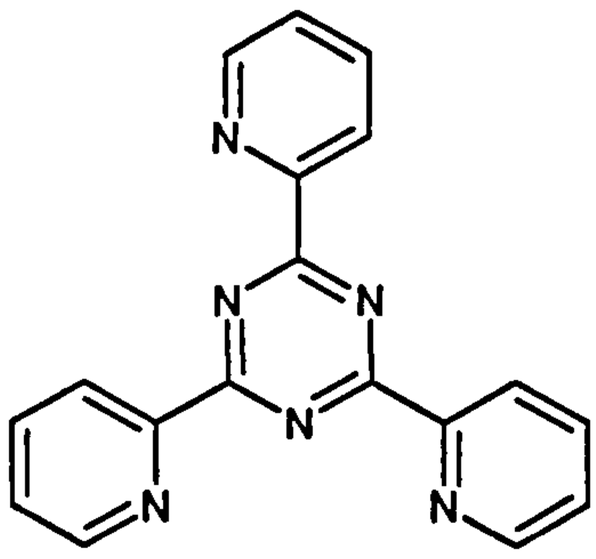

Tpt

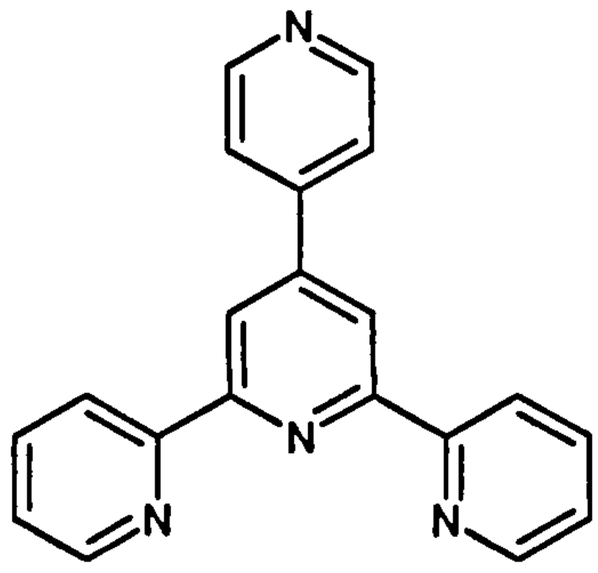

Qtpy
(2.6)

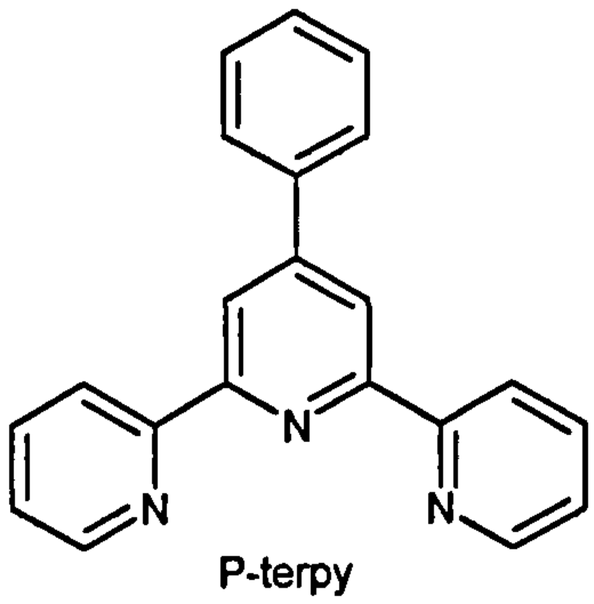

P-terpy
(2.5)

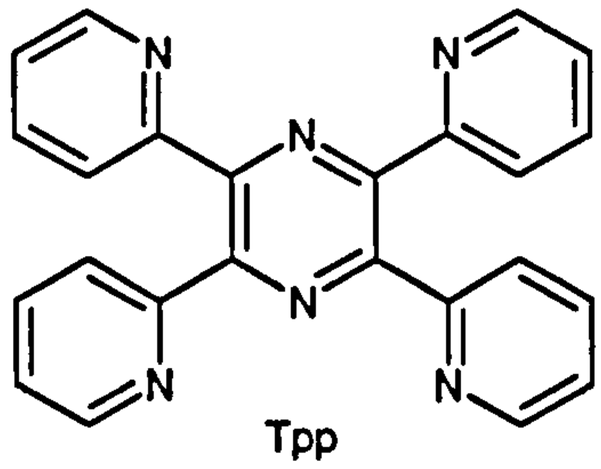

Tpp
(2.7)

Figure 2.3:- The extended terpyridine ligands used in this study

The four ligands Tpymt, Tpt, Qtpy and P-terpy all have the same general shape, however, they differ in the number and position of nitrogens in the aromatic system. Tpp is a slightly different shape to the other four ligands and it contains an extra aromatic ring, which increases the surface area available for intercalation.

2.1.1 Terpyridine coordination modes

Terpyridine and 4'-extended terpyridines are multidentate ligands meaning they can coordinate to a metal through one, two or three of their

basic ring nitrogens. This is termed η^1, η^2 or η^3 coordination (Figure 2.4), however, more common names are mono-dentate, bidentate and tridentate.

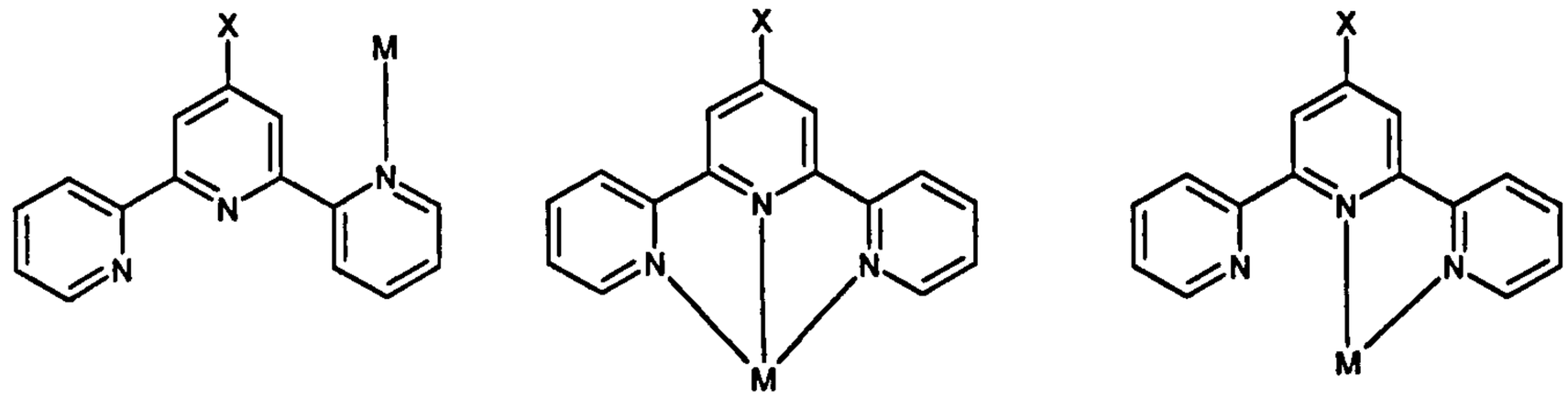

n^1coordination mode n^3 coordination mode n^2 coordination mode

Figure 2.4:- *η^1, η^2 and η^3 coordination of terpyridine derivatives to transition metals*

2.1.2 Ruthenium polypyridyl chemistry

Ruthenium complexes of general formulae $[RuL_6]^{2+}$, $[Ru(L_2)_3]^{2+}$ and $[Ru(L_3)_2]^{2+}$, (L = py; L_2 = phen; L_3 = terpy, etc.) can be prepared by a variety of methods. The chemistry of ruthenium has been extensively reviewed by Seddon *et al.*[76] and Shröeder *et al.*[77].

A convenient starting material for the preparation of tris di-imine ruthenium(II) complexes is $(phen)_2RuCl_2.2H_2O$. This is prepared from $RuCl_3.3H_2O$ and phenanthroline in dry DMF as described by Sullivan *et al.*[78]. LiCl is added to ensure there are Cl^- ions present to prevent tri-substitution.

$(phen)_2RuCl_2.2H_2O$ can be reacted with a third bidentate ligand to form tris-chelate compounds. A review by Balzani *et al.* not only describes modern synthetic procedures towards ruthenium tris chelate complexes, but extends this to polynuclear systems[79]. These reactions are normally carried out in water or water/alcohol solvent systems, with moderate to

high yields (30-90%) for the mononuclear systems. Purification of the complexes can be achieved with chromatography on alumina, silica or ion exchange columns. Generally the main impurity results from ligand scrambling to form tris-phenanthroline ruthenium(II). Keeping reaction times and temperatures to a minimum can reduce this.

The reaction of the related compound $(bipy)_2RuCl_2.2H_2O$ with terpyridine to form $[(bipy)_2RuN,N\text{-}terpy]^{2+}$ has been reported previously by Constable *et al.* (Scheme 2.1)[80]. This synthesis was achieved by refluxing $(bipy)_2RuCl_2.2H_2O$ with terpyridine in methanol. ^1H NMR and crystal structures show that the desired six-coordinate octahedral complex is formed, with the terpyridine acting as a bidentate ligand.

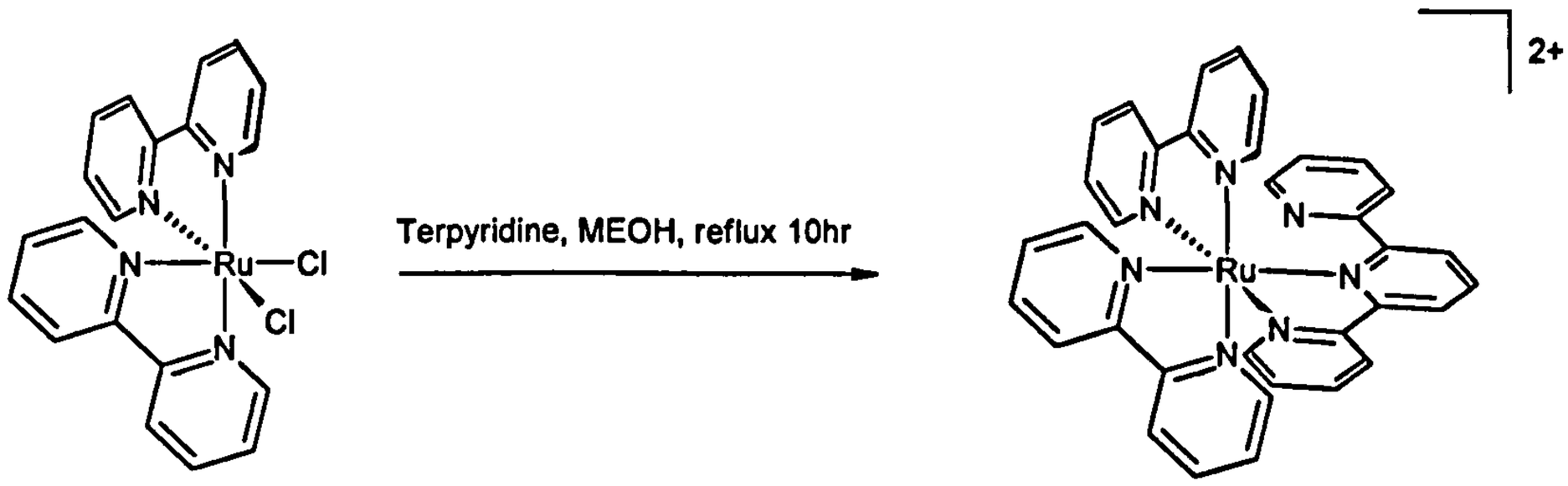

Scheme 2.1:- *Synthesis of $[(bipy)_2RuN,N\text{-}terpy]^{2+}$*

The coordination chemistry of η^3-bound terpyridine and higher oligopyridines with ruthenium(II) has been subject to a number of reviews,[81-84] particularly with respect to their use in light harvesting and energy transfer complexes.

The convenient starting material $terpyRuCl_3.3H_2O$ **(2.8)** can be prepared from the reaction of terpy with $RuCl_3.3H_2O$ in ethanol at reflux for 3 hours[85].

Further reaction of $terpyRuCl_3.3H_2O$ with a second terpyridine or oligopyridine (L^3) results in the formation of a complex of general formula

[terpyRuL^3]$^{3+}$. A range of solvents have been used for this reaction including methanol, ethanol, or water ethanol mixtures. The solvent system that the ligand is most soluble in is usually chosen as the solvent, as extended terpyridine and oligopyridines tend to be quite insoluble. The application of a reducing agent such as *N*-methylmorpholine or triethylamine helps the reduction of ruthenium(III) to ruthenium(II). The reactions are typically high yielding 70-90% with chromatographic purification achieved with acetonitrile toluene mixtures on alumina[81-84] or ion-exchange resin.

2.1.3 Rhenium(I) polypyridyl chemistry

Two recent reviews on the photophysical properties of rhenium(I) complexes of phenanthroline[86] and one on the self-assembly of rhenium(I) boxes etc.[87] cover all of the relevant rhenium(I) coordination chemistry required for this study.

If $(CO)_5ReCl$ is heated to reflux in toluene in the presence of a bidentate di-imine ligand such as 1,10-phenanthroline, compounds of general formula $(CO)_3ClRe(phen)$ are produced. The complexes have an octahedral geometry with the three carbonyls occupying one face of the octahedron (Scheme 2.2) this is due to the trans effect. The carbonyl ligands, which are strong π acceptors exert a greater trans directing effect than the chloride ligand, so the di-imine ligand substitutes two carbonyl ligands in the equatorial plane *trans* to two other carbonyls[88].

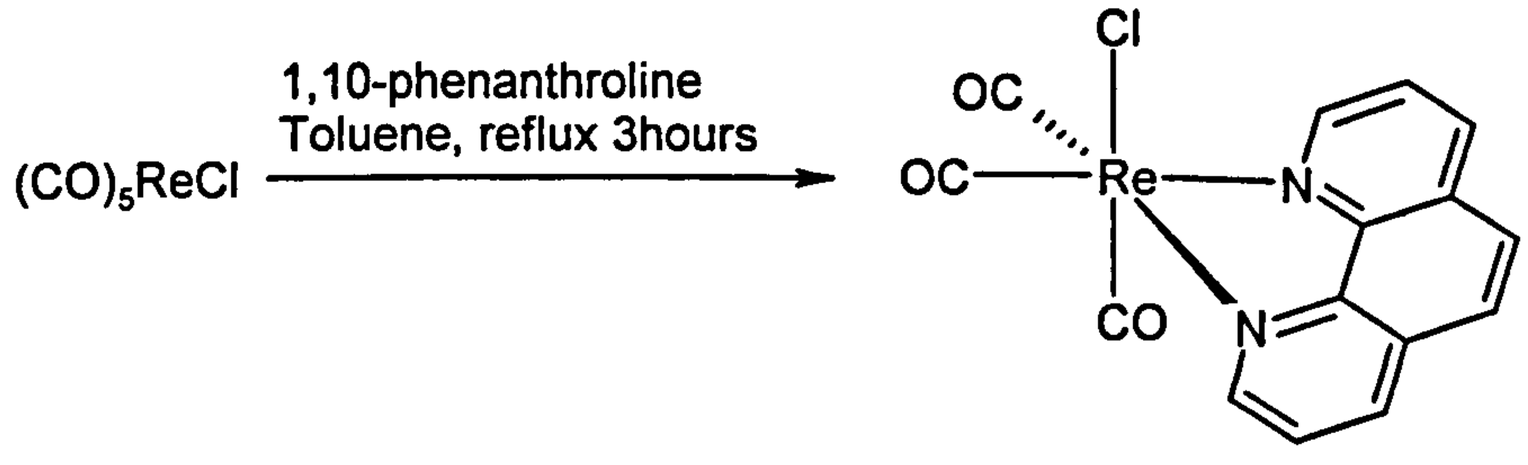

Scheme 2.2:- *Synthesis of rhenium(I) di-imine complexes*

The axial chloride can now be substituted with an organic nitrile ligand such as acetonitrile. This has been achieved in a number of ways, but the simplest seems to be the reaction of the rhenium(I) chloride with silver triflate in acetonitrile. This reaction is virtually quantitative and the only side product, insoluble silver chloride, can be easily filtered off.

There are a number of examples of $(CO)_3ReX$ coordinated to terpyridine type ligands (X= Cl, Br, I). In all cases the terpyridine acts as a bidentate ligand.

P-terpy and Qtpy have been coordinated to the $(CO)_3ReBr$ centre by Orrell *et al.* and dynamic NMR studies have been reported[89-92]. Variable temperature studies show that the rhenium centre flips between the two available bidentate coordination sites of the terpyridine moiety.

In all cases the synthesis of $(CO)_3XReL_3$ (L_3 = terpyridine moiety) is archived by refluxing a 1:1 mixture of $(CO)_5ReX$ and L_3 in a high boiling point solvent such as toluene, benzene or heptane. Yellow orange microcrystalline solids are obtained upon prolonged cooling.

2.2 Synthetic studies

2.2.1 Ligand synthesis

Tpymt **(2.2)** was synthesised from the high temperature trimerisation or 2-cyanopyrimidine. The crude Tpymt was purified by acidic extraction from the melt followed by charcoal decolourisation treatment. The resulting hydrochloride salt was deprotonated with ammonia solution giving analytically pure Tpymt in 40% yield (Scheme 2.3)[93].

Synthesis of 2-cyanopyrimidine **(2.1)** was achieved as published by Gohring *et al.* with a DABCO catalysed substitution of 2-chloropyrimidine with sodium cyanide in DMSO[94] (Scheme 2.3).

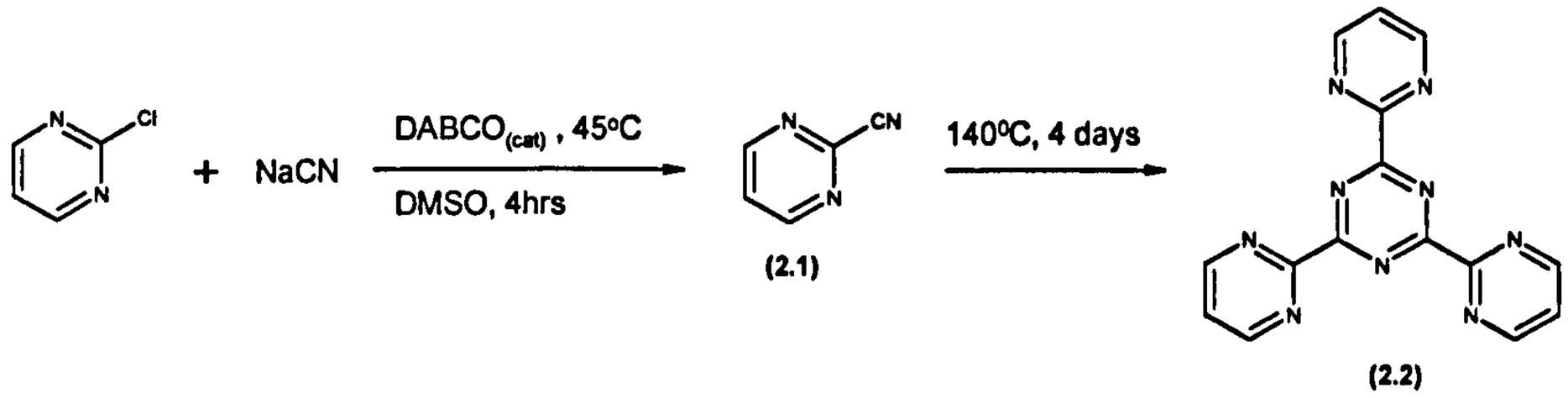

Scheme 2.3:- *Synthesis of Tpymt* ***(2.2)*** *from 2-chloropyrimidine* ***(2.1)***

P-Terpy[95] **(2.5)** and Qtpy[96] **(2.6)** were synthesised by modifications to literature procedures. The procedures consisted of two consecutive condensations. Firstly 2-acetylpyridine and either benzaldehyde or 4-pyridinecarboxaldehyde were reacted with NaOH in ethanol/water. This produced the 1,5-bis(2-pyridyl)-3-phenyl-pentan-1,5-dione or the 1,5-bis(2-pyridyl)-3-(4-pyridyl)-pentan-1,5-dione, respectively. This was further condensed with ammonium acetate in ethanol to produce the appropriately 4-substituted terpyridine (Scheme 2.4).

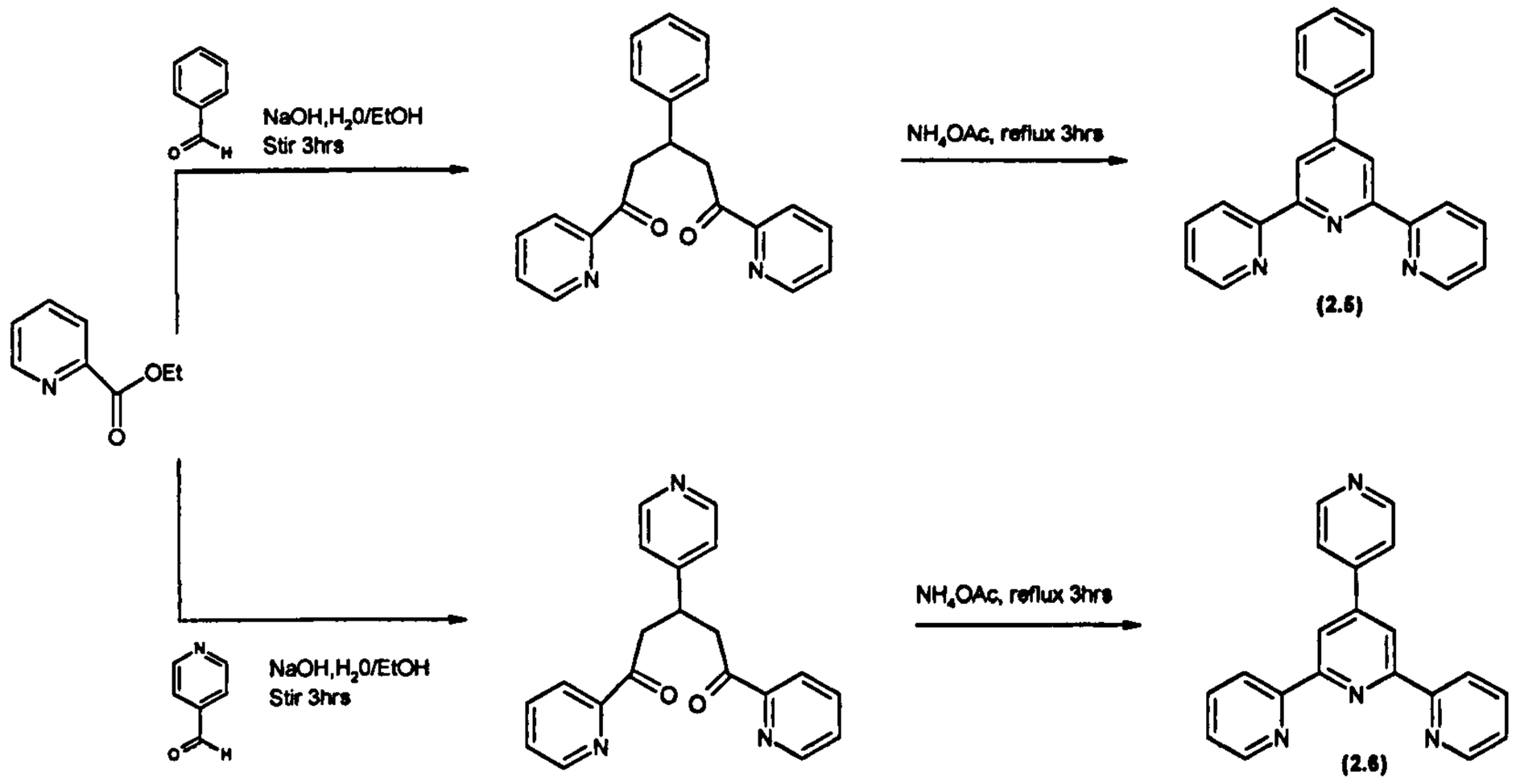

Scheme 2.4:- *Synthesis of P-terpy* ***(2.5)*** *and Qtpy* ***(2.6)***

Tpp **(2.7)** was synthesised as reported by Goodwin *et al.* from the high temperature condensation of pyridoin and ammonium acetate[97].

2.2.2 Extended terpyridine complexes with the Terpy Ru(II) domain

The complexes [TerpyRuTpt]$^{2+}$[98] **(2.9)**, [TerpyRuP-terpy]$^{2+}$[85] **(2.10)** and [TerpyRuTpp]$^{2+}$[99] **(2.11)** (Figure 2.5) had been previously reported and similar procedures were employed in their synthesis.

In all cases except Qtpy a slight excess of the appropriate ligand was refluxed in methanol with terpyRuCl_3.2H_2O **(2.8)** for 10 minutes. A small amount of the reducing agent *N*-methylmorpholine was then added and the solution was refluxed for a further 1-3 hours then cooled to 0°C.

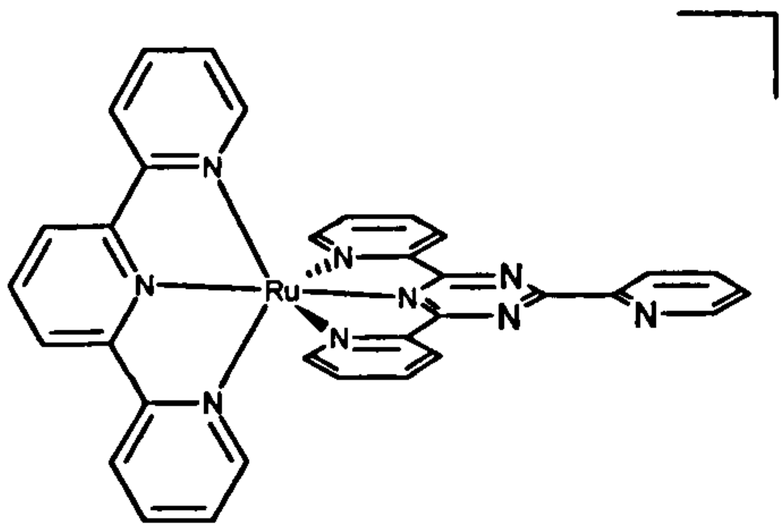

(2.9)

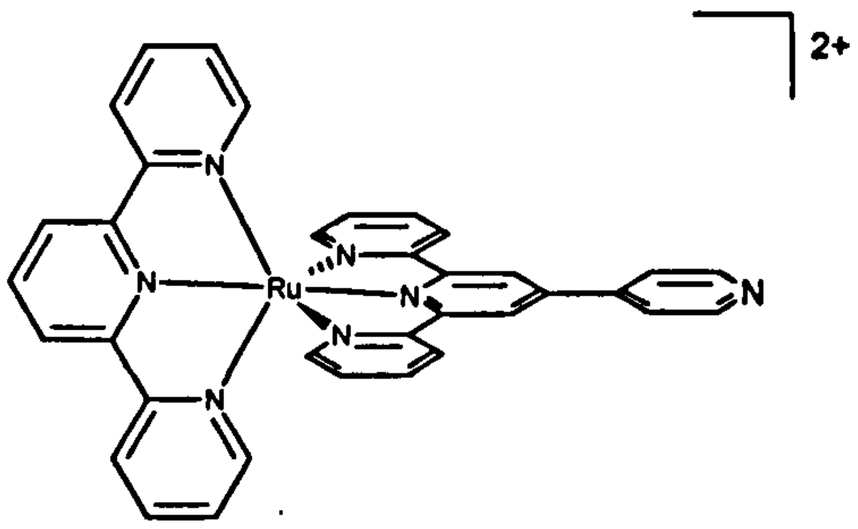

(2.12)

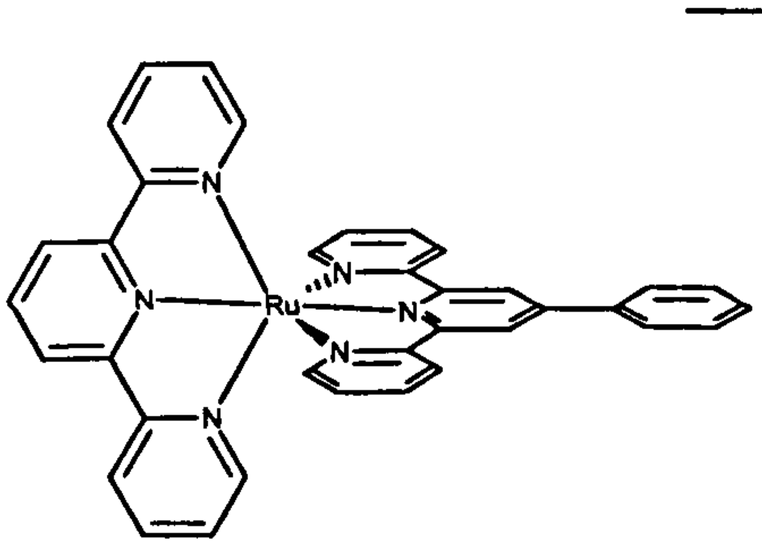

(2.10)

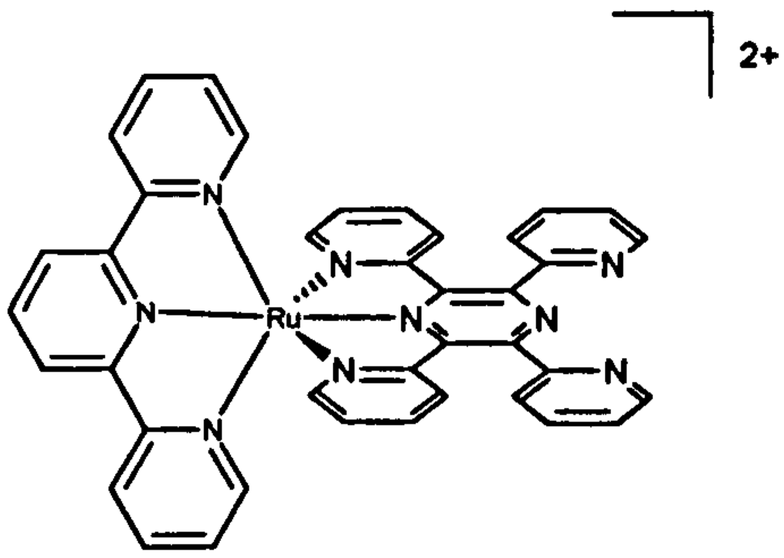

(2.11)

Figure 2.5:- Extended terpyridine complexes of TerpyRu(II)

The purple or red solution was filtered through celite and the methanol was reduced to 1ml. NH_4PF_6 was added, followed by water, which induced the precipitation of the complexes as their PF_6^- salts.

Purification was achieved on silica chromatography columns with 5% KNO_3(aq) in acetonitrile as the eluent. All 1H NMR, MS and microanalysis data was in agreement with previously published reports[98, 85, 99].

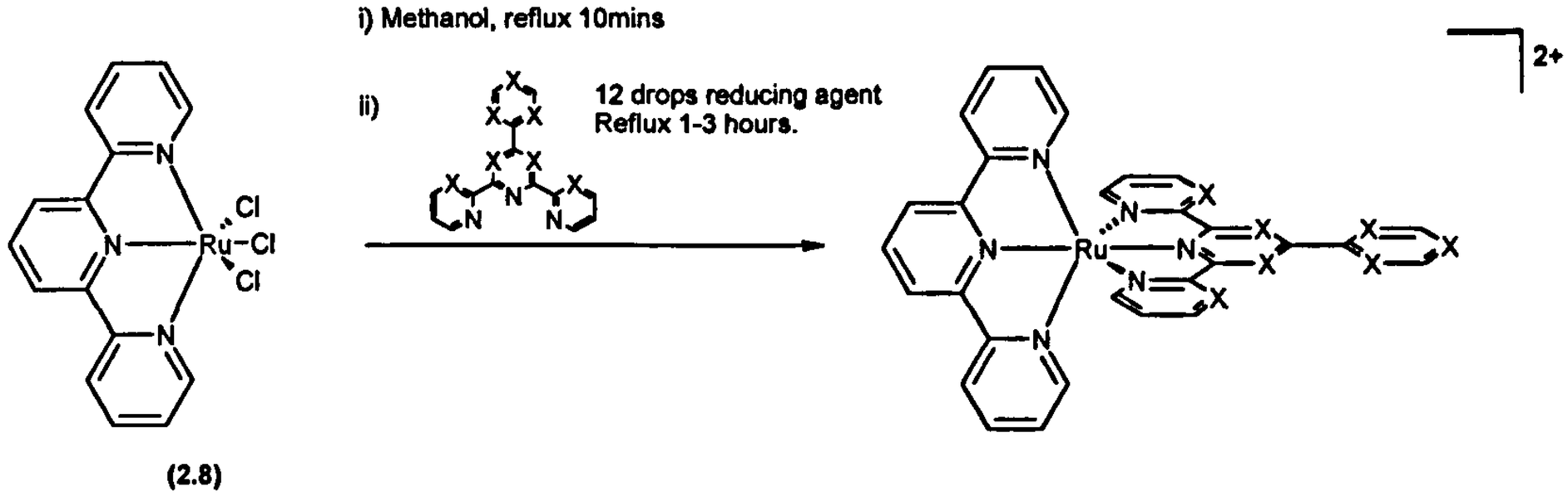

(2.8)

Scheme 2.5:- *Synthesis of 4'-extended terpy complexes using methanol as the solvent*

The synthesis of $[TerpyRuQtpy]^{2+}$ **(2.12)** was successful with the methanol method described above for the other complexes but in an extremely low yield. It was found that if the synthesis was performed at an elevated temperature of 180°C using freshly distilled ethylene glycol as the solvent the yield of **(2.12)** was increased from 15% to 50%. Work up and purification was as for the other complexes. The low yield is presumably due to other species formed from the coordination of the 4'-pyridyl moiety.

Since Tpymt was first synthesised in large quantities in 1976[93], there have been very few reports of transition metal complexes of Tpymt as it hydrolyses to a bis(2-pyrimidyl)carboxamidato complex upon coordination to an electron withdrawing metal centre, such as copper(II)[93] (Figure 2.6).

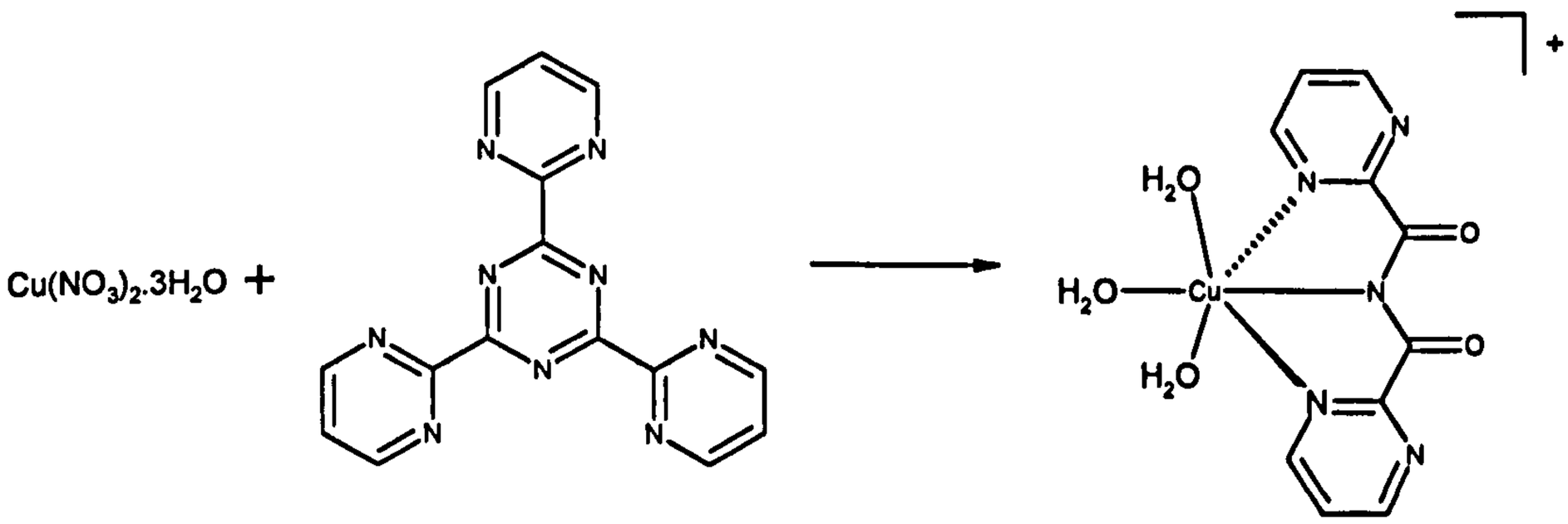

Figure 2.6:- Copper assisted hydrolysis of Tpymt

In order to reduce the risk of hydrolysis in the formation of [Terpy Ru Tpymt]$^{2+}$ the synthesis was designed around a short reaction time and dry degassed solvents. Several solvent systems were tried such as methanol, ethanol, and nitromethane, however, in each case no reaction occurred even when silver was used to remove the chlorides from the terpy$RuCl_3$. The probable reason for the failure of these reactions is the insolubility of the Tpymt ligand in these solvents.

In order to ensure enough ligand dissolved in the reaction mixture there needed to be a large excess of ligand, at least 10-fold and high temperatures were needed to aid the solubility of Tpymt. Dry ethylene glycol was deemed to meet these criteria and, treatment of terpy$RuCl_3$ **(2.8)** and 10 equivalents of Tpymt in N_2-saturated ethylene glycol at 180°C for 30 minutes resulted in the formation of a deep purple solution.

After the solution had slowly cooled to room temperature, the product was treated with saturated aqueous NH_4PF_6, which resulted in the precipitation of a purple solid **(2.13)**. The solid was collected, washed with ice-cold water, ice-cold diethylether and air dried (Scheme 2.6).

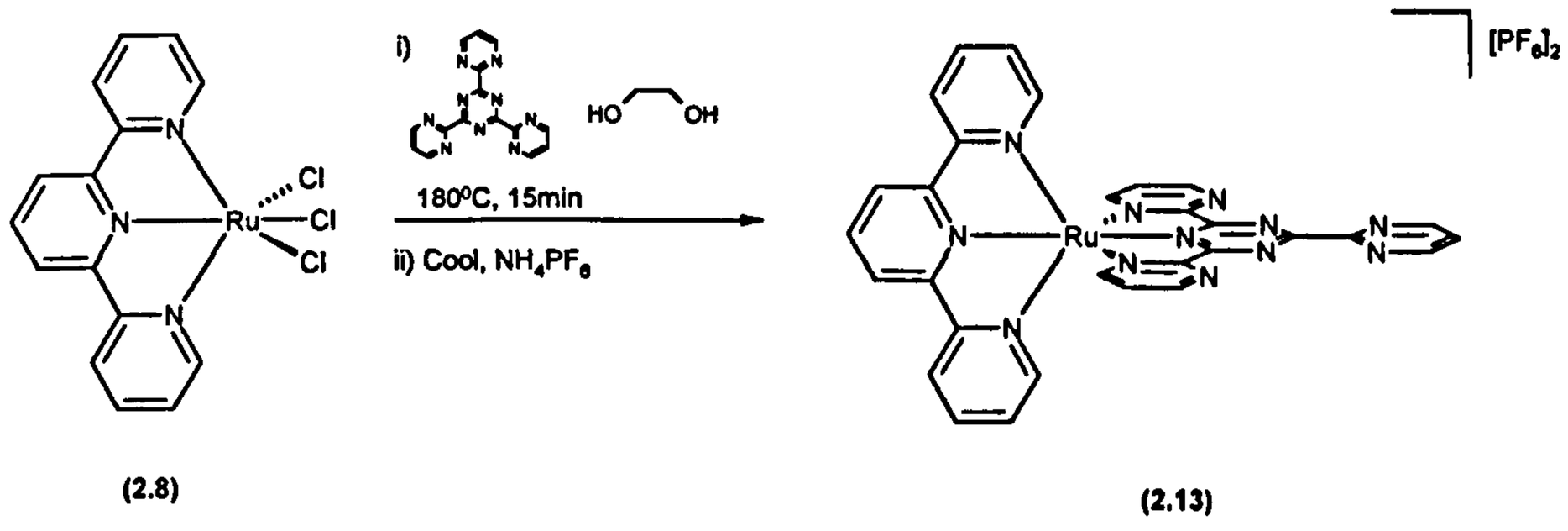

(2.8) (2.13)

Scheme 2.6:- *Synthesis of [TerpyRuTpymt]$^{2+}$* ***(2.13)***

Purification of **(2.13)** was achieved with ion exchange chromatography using Sephadex CM-C25 ion exchange resin. The deep purple band

removed from the column was shown to exclusively contain $[TerpyRuTpymt]^{2+}$ **(2.13)**. The product was obtained in 70% yield and ^1H NMR, FAB-MS, elemental microanalysis and a single crystal X-ray structure are all in agreement with the desired structure. This is the first reported octahedral transition metal complex of Tpymt that is stable to hydroysis. Once synthesised **(2.13)** has been shown to be air and moisture stable with no detectable hydrolysis even after 24 hours in aqueous solution at 30°C.

2.2.3 Extended terpyridine complexes with the $(phen)_2Ru(II)$ domain

When $(phen)_2RuCl_2.2H_2O$ **(2.14)** was refluxed in methanol with two equivalents of the appropriate extended terpyridine ligand, a colour change from black to red-orange occurred between 1 and 4 days (Scheme 2.7). After cooling and filtration, the methanol was removed and the crude product was purified by silica chromatography. After removal of considerable amounts of $[(phen)_3Ru]^{2+}$ the product of general formula $[(phen)_2RuL]^{2+}$ (L = extended terpy) was obtained in 30-70% yield (Figure 2.7).

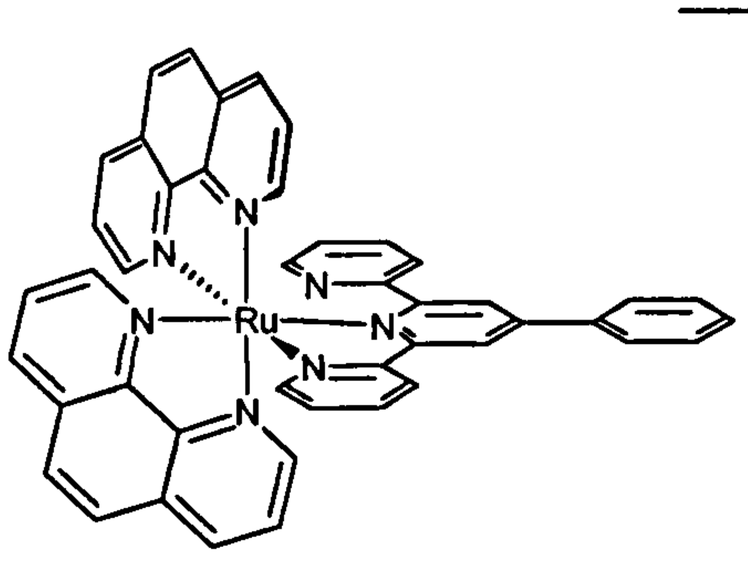

(2.17)

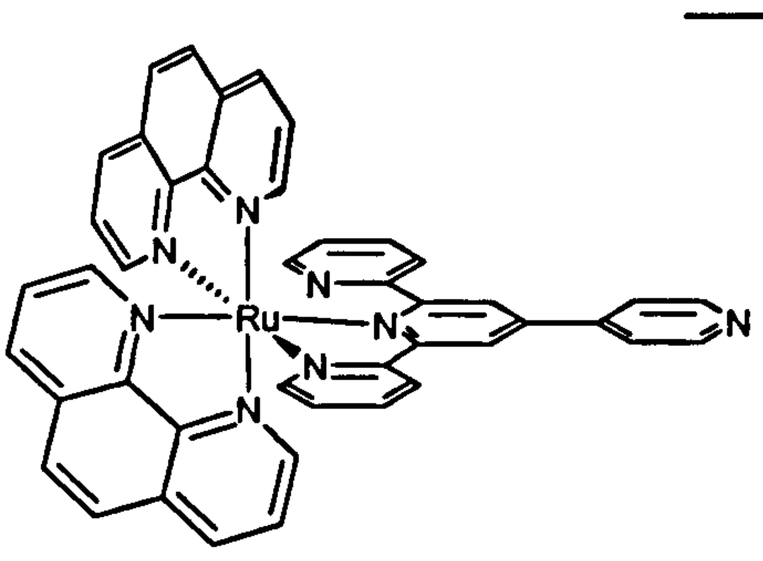

(2.16)

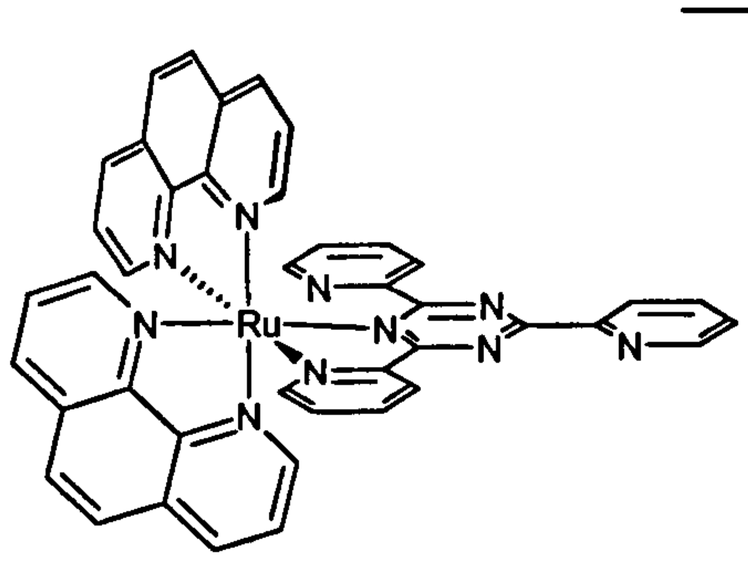

(2.15)

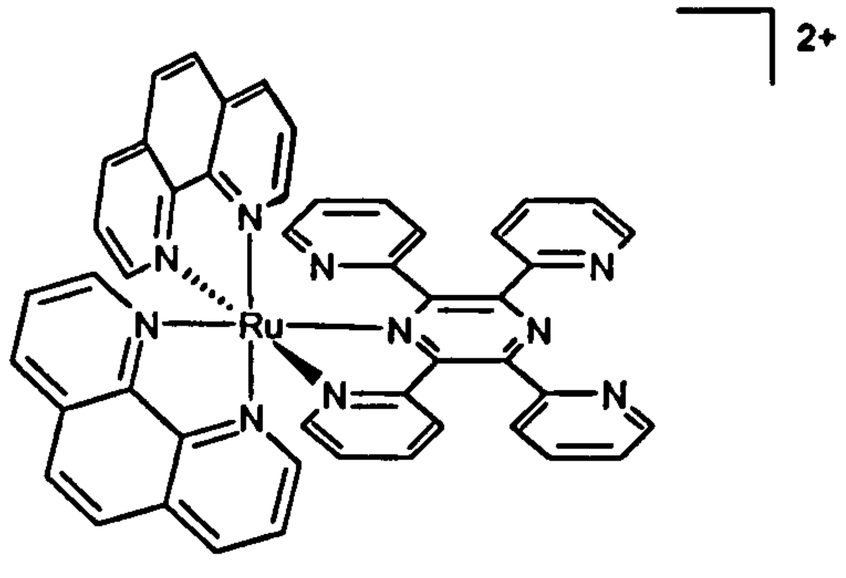

(2.18)

Figure 2.7:- *Extended terpyridine complexes of* $(phen)_2Ru^{2+}$

All attempts to synthesise the Tpymt complex in this series failed due to the hydrolysis of the ligand to the above mentioned bis(2-pyrimidyl)carboximidato species, along with a pyridine-2-carboxylic acid amide species (Figure 2.8). These products proved difficult to separate but they were easily identified by FAB-MS.

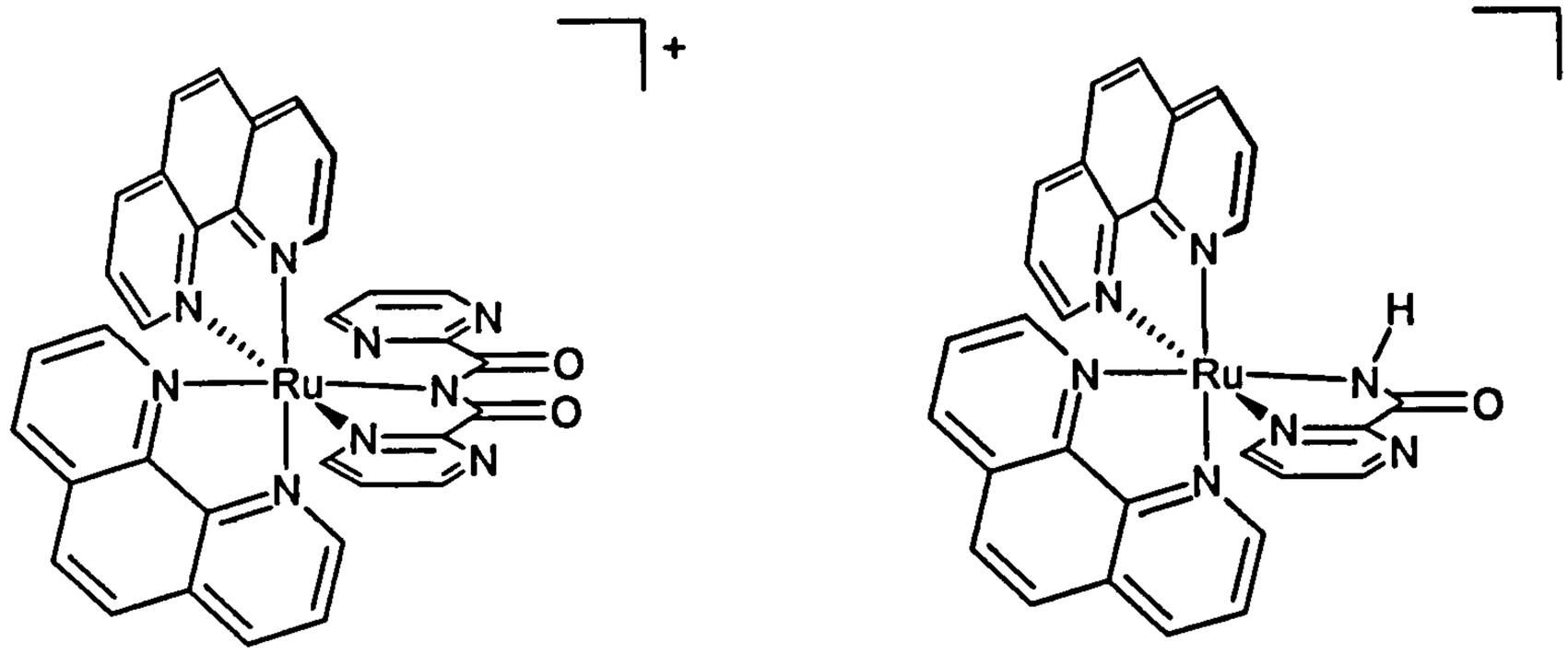

Figure 2.8:- *Hydrolysis products from the attempted synthesis of* $[(phen)_2RuTpymt]^{2+}$

2.2.4 Extended terpyridine complexes with the $(CO)_3LRe^+$ domain.

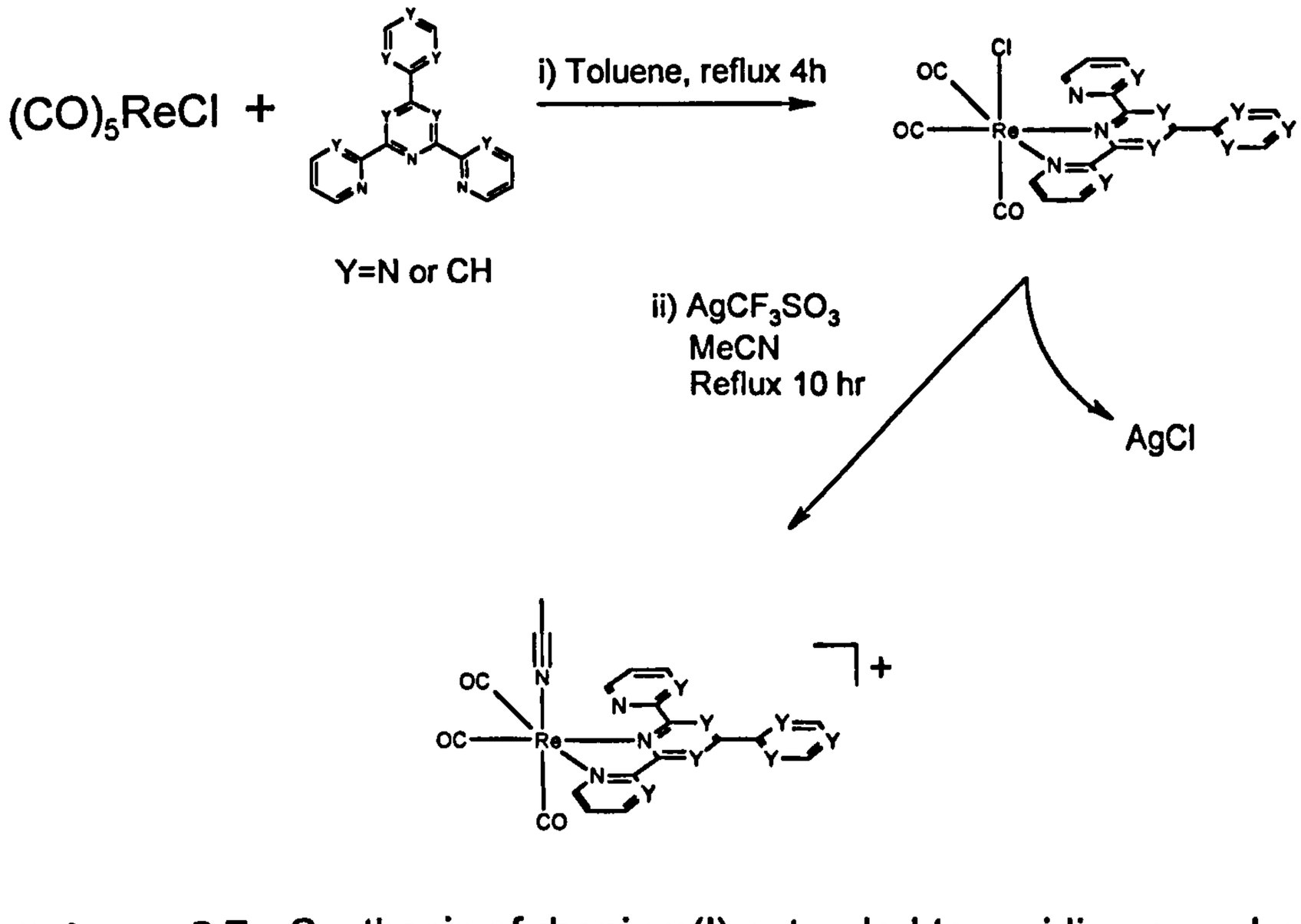

Scheme 2.7:- Synthesis of rhenium(I) extended terpyridine complexes

Building on methodology developed by various groups in the 1980's and 1990's for bipy type complexes of rhenium(I) we have synthesised a

number of extended terpyridine complexes with rhenium(I) as the central metal ion. The general Scheme for the synthesis is outlined below (Scheme 2.7).

Reaction of $(CO)_5ReCl$ the desired extended terpyridine ligand in refluxing toluene for four hours then cooling resulted in the precipitation of the brightly coloured $(CO)_3ClReTerpy$ complex **(2.19-2.22)**. After washing with chloroform to remove the excess ligand the complexes were isolated in 90 – 95% yield. The complexes are very insoluble and only weak broad ^1H NMR spectra could be obtained in d^6-DMSO. However the expected number of signals and their relative integrations were consistent with the expected structures (Figure 2.9). Furthermore, MS and accurate mass data were consistent with the formation of the desired complexes.

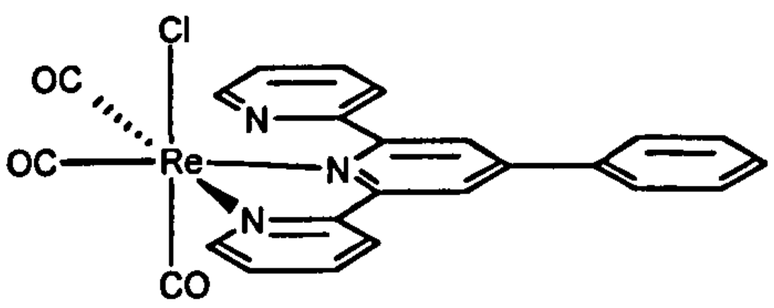

(2.21)

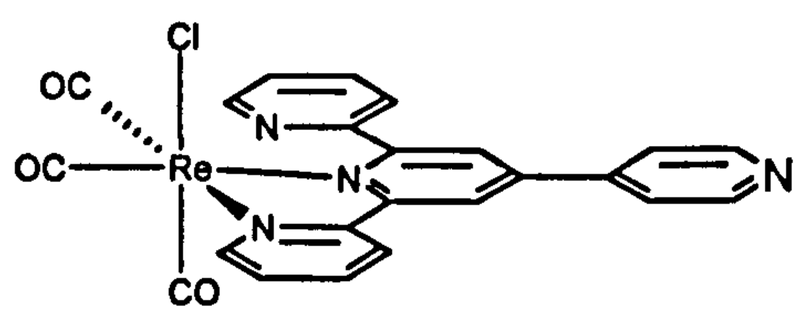

(2.20)

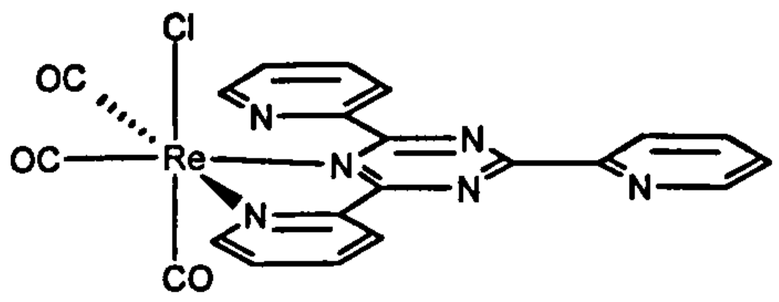

(2.19)

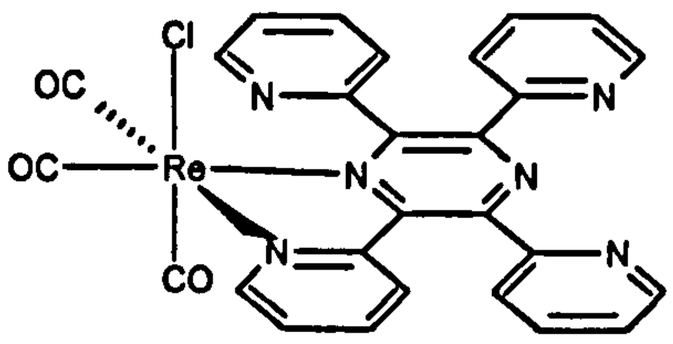

(2.22)

Figure 2.9:- Extended terpyridine complexes of $(CO)_3ClRe(I)$ **(2.19-2.22)**

It was clear that in order to render the complexes soluble the chloride had to be substituted with a neutral ligand such as acetonitrile. This would induce a +1 charge on the complexes making them soluble in aqueous media.

The chloride complexes **(2.19-2.22)** were reacted with $AgCF_3SO_3$ in refluxing distilled acetonitrile for 10 hours resulting in the substitution of the chloride with acetonitrile. The silver chloride produced from the reaction was removed by filtration through celite and the acetonitrile complex **(2.23-2.26)** was recovered from solution by precipitation as triflate salts (Figure 2.10) with excess diethylether. All ^1H NMR spectra, FAB-MS and elemental microanalysis were consistent with the formation of the desired complexes.

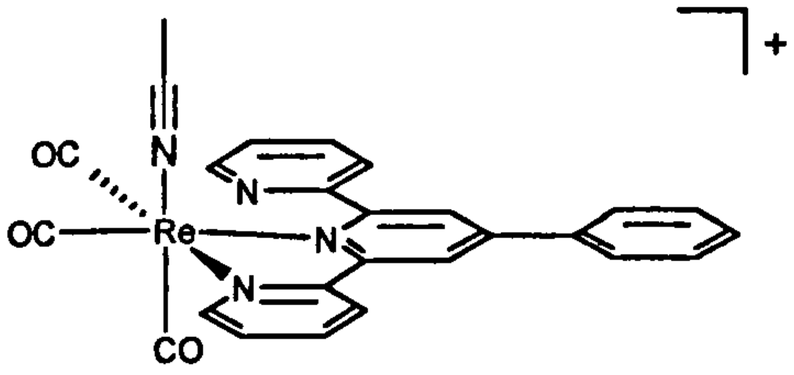

(2.25)

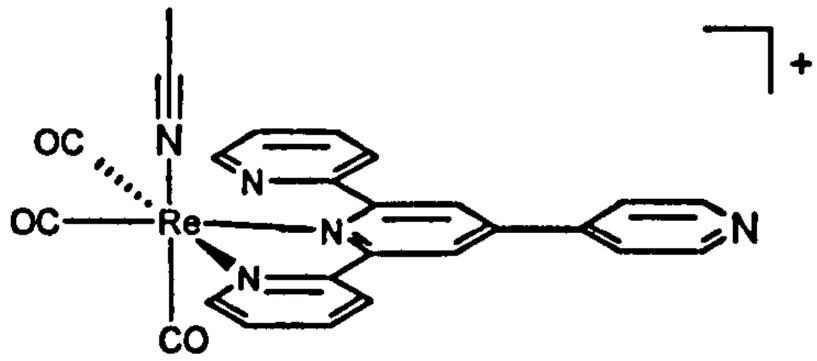

(2.24)

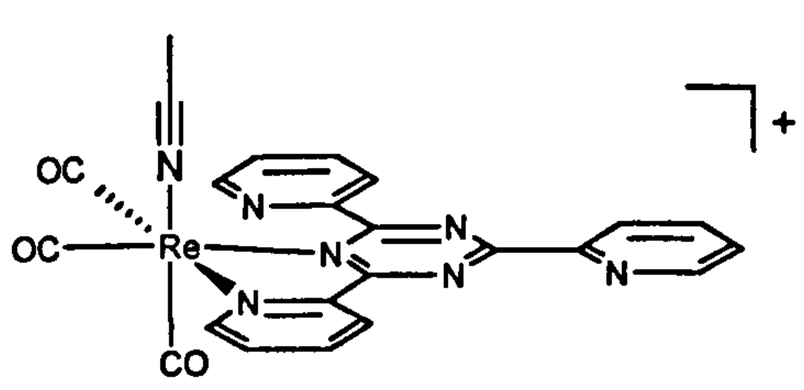

(2.23)

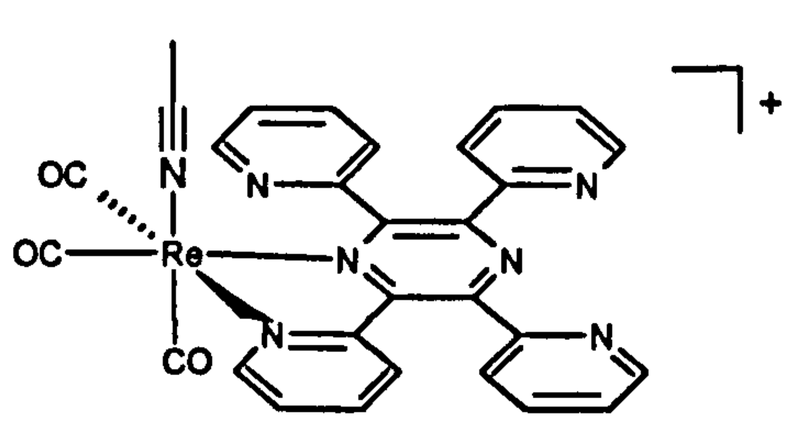

(2.26)

Figure 2.10:- *Rhenium(I) acetonitrile complexes* ***(2.23-2.26)*** *of the extended terpyridine ligands*

2.3 ^1H NMR spectroscopic studies

The 400 MHz ^1H NMR spectrum of **(2.13)** in d^3-nitromethane showed only the signals associated with the complex and no impurities. The downfield

aromatic region is shown below (Figure 2.11).

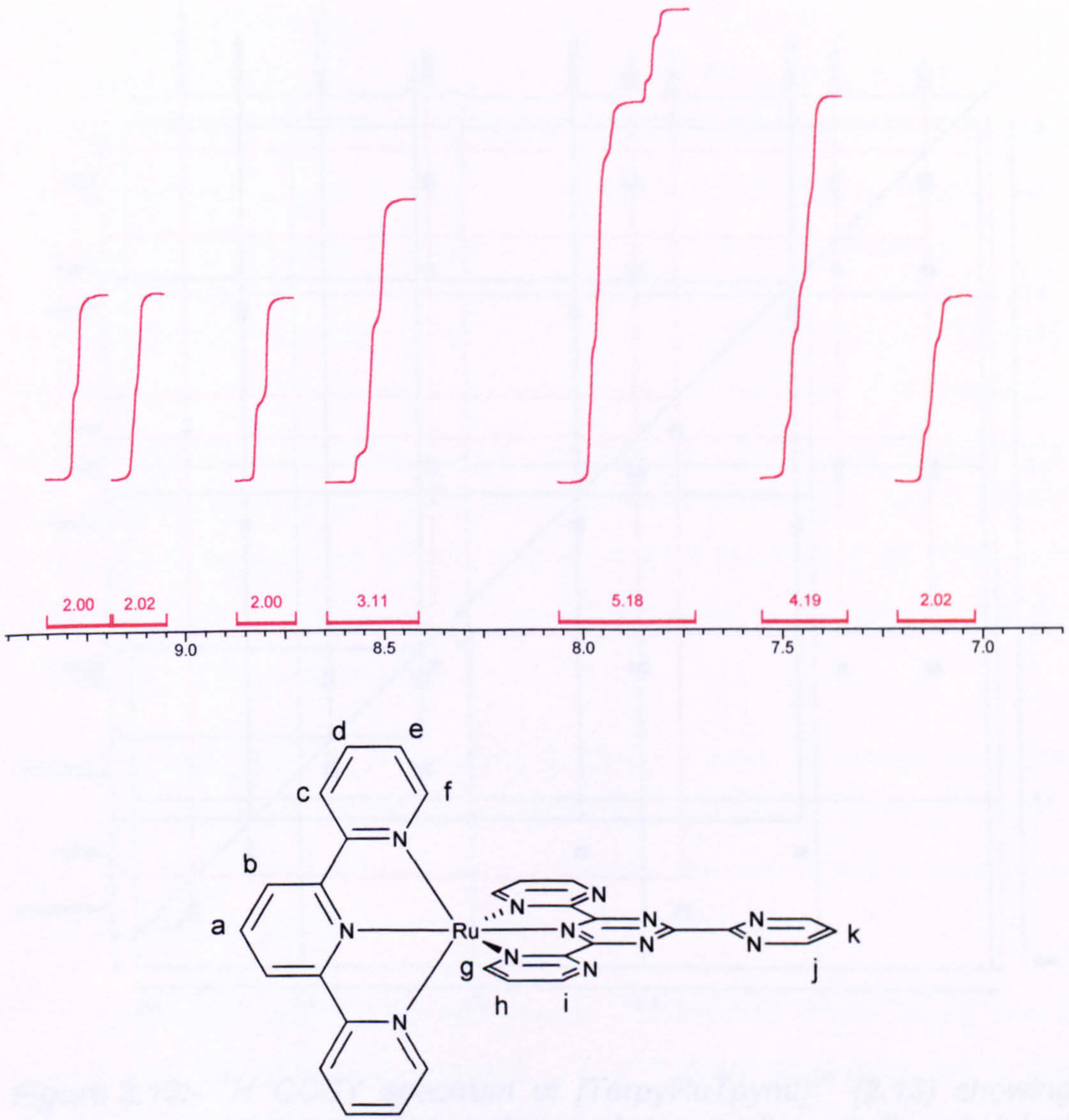

Figure 2.11:- *Downfield region of the 400 Mhz ^1H NMR (d^3-nitromethane) spectrum of $[TerpyRuTpymt]^{2+}$* ***(2.13)*** *with the proton labelling Scheme*

The spectrum is well defined and integrates to 20 protons in total, which is the number of protons expected in the complex (2.5). Although the complex shows two-fold symmetry, the exact assignments of the protons is still not obvious. The proton assignments were made with the help of the COSY spectrum shown in Figure 2.12. Protons residing on each

ligand set can easily be identified, Terpy (red) and Tpymt (blue).

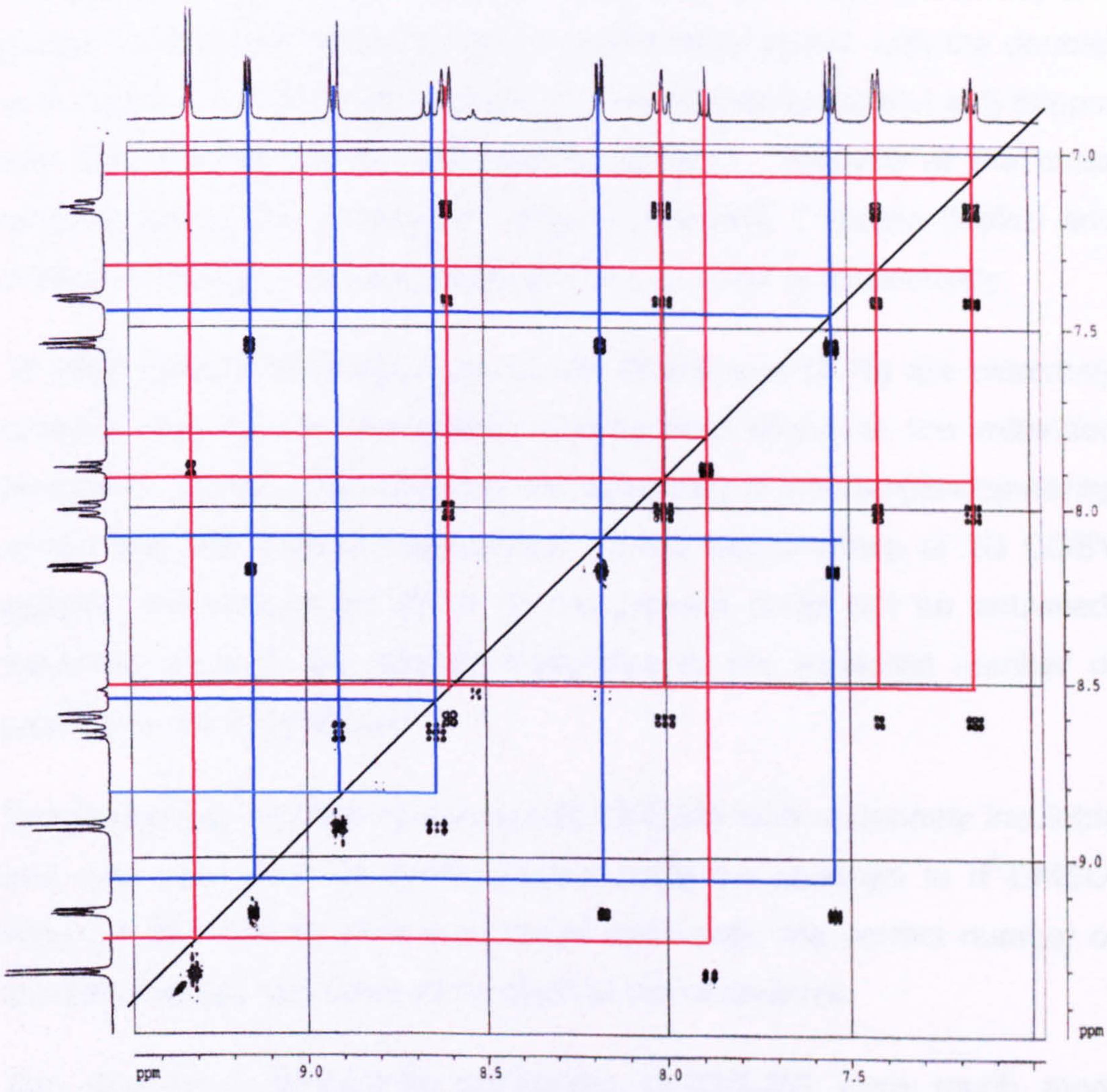

Figure 2.12:- *^{1}H COSY spectrum of [TerpyRuTpymt]$^{2+}$* ***(2.13)*** *showing cross coupling between terpy (red) and Tpymt (blue) protons*

The four doublets residing at 9.15ppm, 8.91ppm, 8.60ppm and 8.16ppm all have large coupling constants of around 9Hz indicating they are adjacent to ring nitrogens. The doublet at 8.91ppm is cross-coupled to the triplet at 8.64ppm, which integrates to one proton, and they are j and k respectively on the free pyrimidine ring of tpymt. As protons g and i are rendered inequivalent due to coordination to ruthenium they can be assigned to the double doublets at 9.15ppm and 8.16ppm. Both of these

protons cross couple to the triplet at 7.54ppm, which can therefore be assigned to proton h. The triplet at 7.88ppm which integrates to only one proton must be the central proton a on the terpy ligand, with the doublet at 9.30ppm (j = 5Hz) being protons b. The remaining doublet at 8.60ppm with 9Hz splitting can be assigned to proton f. Analysis of the cross coupling allows the protons at 7.41ppm (doublet), 7.15ppm (triplet) and 8.00ppm (triplet) to be assigned to protons c, d and e, respectively.

^{1}H NMR spectra of compounds **(2.15), (2.16),** and **(2.18)** are extremely complex due to the asymmetric coordination mode of the extended terpyridine ligands. This destroys any symmetry in the complex rendering all the aromatic protons inequivalent. Even with the help of 2D COSY spectra, full assignment of all of the protons could not be achieved. However, each of the spectra integrates to the expected number of protons for each compound.

The rhenium(I) chloride complexes **(2.19-2.22)** were extremely insoluble and only very poor ^{1}H NMR spectra could be obtained in d^6-DMSO. Although the spectra were very broad and weak, the correct number or aromatic signals can be seen for each of the complexes.

The rhenium(I) acetonitrile complexes **(2.23-2.26)** were much more soluble and therefore well resolved. All of the spectra integrated to the correct number of protons for each of the complexes but as in the bis-phen complexes, the spectra were more complicated than the free ligands themselves. This indicates the extended terpyridine ligands are coordinated in a η^2-mode. This η^2-coordination mode removes the plane of symmetry found in the free ligand and renders all of the protons inequivalent and therefore difficult to assign. In each complex the coordinated acetonitrile ligand appeared as a singlet, integrating to three protons around 2.2ppm. This showed a downfield shift of around 0.5-1ppm for the acetonitrile upon coordination to the metal, which is comparable to values reported elsewhere[100].

2.4 Mass spectrometry studies

The mass spectra of all the complexes were determined by the mass spectrometry service within the Department of Chemistry. The spectra were collected by either FAB or positive ion electrospray techniques. The data are summarised in Table 2.1 and each M/z value is consistent with the desired structure of each complex. Typically, the spectra show the sequential loss of any counter ions followed by loss of any other monodentate ligands such as pyridine or carbonyl. In general ligands coordinated in a bidentate or tri-dentate fashion are not removed from the metal centre upon ionisation.

Table 2.1:- Mass spectrometric data for the extended terpyridine complexes

Complex	M / Z	%	Assignment
[TerpyRuTpymt][PF_6]$_2$	795	25	[TerpyRuTpymt][PF_6]$^+$
	650	100	[TerpyRuTpymt]$^+$
[TerpyRuTpt][PF_6]$_2$	791	100	[TerpyRuTpt][PF_6]$^+$
	646	10	[TerpyRuTpt]$^+$
[TerpyRuQtpy][PF_6]$_2$)	791	70	[TerpyRuQtpy][PF_6]$^+$
	646	50	[TerpyRuQtpy]$^+$
[TerpyRuP-terpy][PF_6]$_2$	788	100	[TerpyRuTpymt][PF_6]$^+$
[TerpyRuTpp][PF_6]$_2$	867	80	[TerpyRuTpymt][PF_6]$^+$
	145	30	[TerpyRuTpymt]$^+$
[(phen)$_2$RuTpt][PF_6]$_2$	919	40	[(phen)$_2$RuTpt][PF_6]$^+$
	774	40	[phen)$_2$RuTpt]$^+$
[(phen)$_2$RuQtpy][PF_6]$_2$	916	25	[(phen)$_2$RuQtpy][PF_6]$^+$
	772	40	[(phen)$_2$RuQtpy]$^+$
[(phen)$_2$RuP-Terpy][PF_6]$_2$	915	70	[(phen)$_2$RuP-Terpy][PF_6]$^+$
	771	15	[(phen)$_2$RuP-Terpy]$^+$
[(phen)$_2$RuTpp][PF_6]$_2$	850	60	[(phen)$_2$RuTpp]$^+$
	670	80	[(phen)RuTpp]$^+$
	688	60	[(phen)RuTpp]F$^+$
	707	80	[(phen)RuTpp]F_2^+
(CO)$_3$ClReTpt	618	35	[(CO)$_3$ClReTpt]$^+$
	590	75	[(CO)$_2$ClReTpt]$^+$

	582	75	$[(CO)_3ReTpt]^+$
	562	30	$[(CO)ClReTpt]^+$
	534	25	$[ClReTpt]^+$
	555	80	$[(CO)_2ReTpt]^+$
$(CO)_3ClReQtpy$	618	50	$[(CO)_3ClReQtpy]^+$
	590	55	$[(CO)_2ClReQtpy]^+$
	582	90	$[(CO)_3ReQtpy]^+$
	554	70	$[(CO)_2ReQtpy]^+$
$(CO)_3ClReP\text{-}terpy$	615	30	$[(CO)_3ClReP\text{-}terpy]^+$
	587	80	$[(CO)_2ClReP\text{-}terpy]^+$
	879	100	$[(CO)_3ReP\text{-}terpy]^+$
	552	30	$[(CO)_2ReP\text{-}terpy]^+$
$(CO)_3ClReTpp$	694	5	$[(CO)_3ClReTpp]^+$
	666	10	$[(CO)_2ClReTpp]^+$
	638	10	$[(CO)\ ClReTpp]^+$
	610	15	$[ClReTpp]^+$
$[(CO)_3MeCNReTpt][CF_3SO_3]$	624	10	$[(CO)_3MeCNReTpt]^+$
	583	60	$[(CO)_3ReTpt]^+$
	555	30	$[(CO)_2ReTpt]^+$
	532	10	$[(CO)ReTpt]^+$
$[(CO)_3MeCNReQtpy][CF_3SO_3]$	582	40	$[(CO)_3ReQtpy]^+$
	554	50	$[(CO)_2ReQtpy]^+$
	525	30	$[(CO)\ ReQtpy]^+$
$[(CO)_3MeCNReP\text{-}terpy][CF_3SO_3]$	702	30	$[(CO)_2ReP\text{-}terpy][CF_3SO_3]^+$
	674	100	$[(CO)ReP\text{-}terpy][CF_3SO_3]^+$
	552	80	$[(CO)_2ReP\text{-}terpy]^+$

2.5 X-ray diffraction studies

X-ray quality crystals of $[TerpyRuTpymt][PF_6]_2$, **(2.13)** $[(phen)_2RuP\text{-}terpy][PF_6]_2$ **(2.17)** and $[(phen)_2RuTpp][PF_6]_2$ **(2.18)** were grown from the vapour diffusion of diethylether into an acetonitrile or nitromethane

solution of the complex and the structures were solved by Harry Adams and Sharon Spey in the X-ray structure determination service of this Chemistry Department.

The projection of the asymmetric unit cell of [TerpyRuTpymt][PF_6]$_2$ is shown in Figure 2.13.

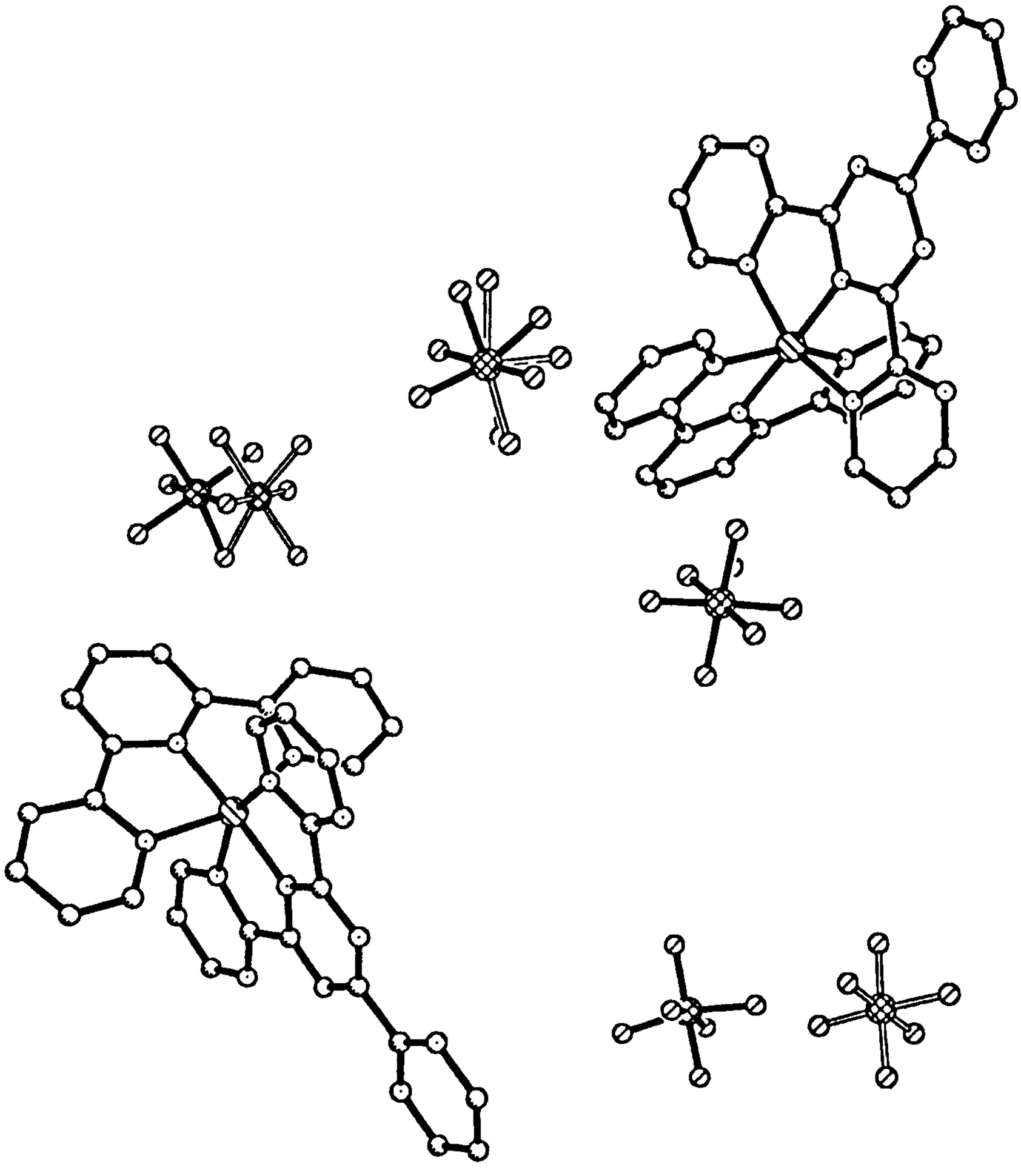

Figure 2.13:- *Projection of the asymmetric unit cell showing the two orientations of the cation and disorder of the anions in the crystal structure of [TerpyRuTpymt][PF_6]$_2$*

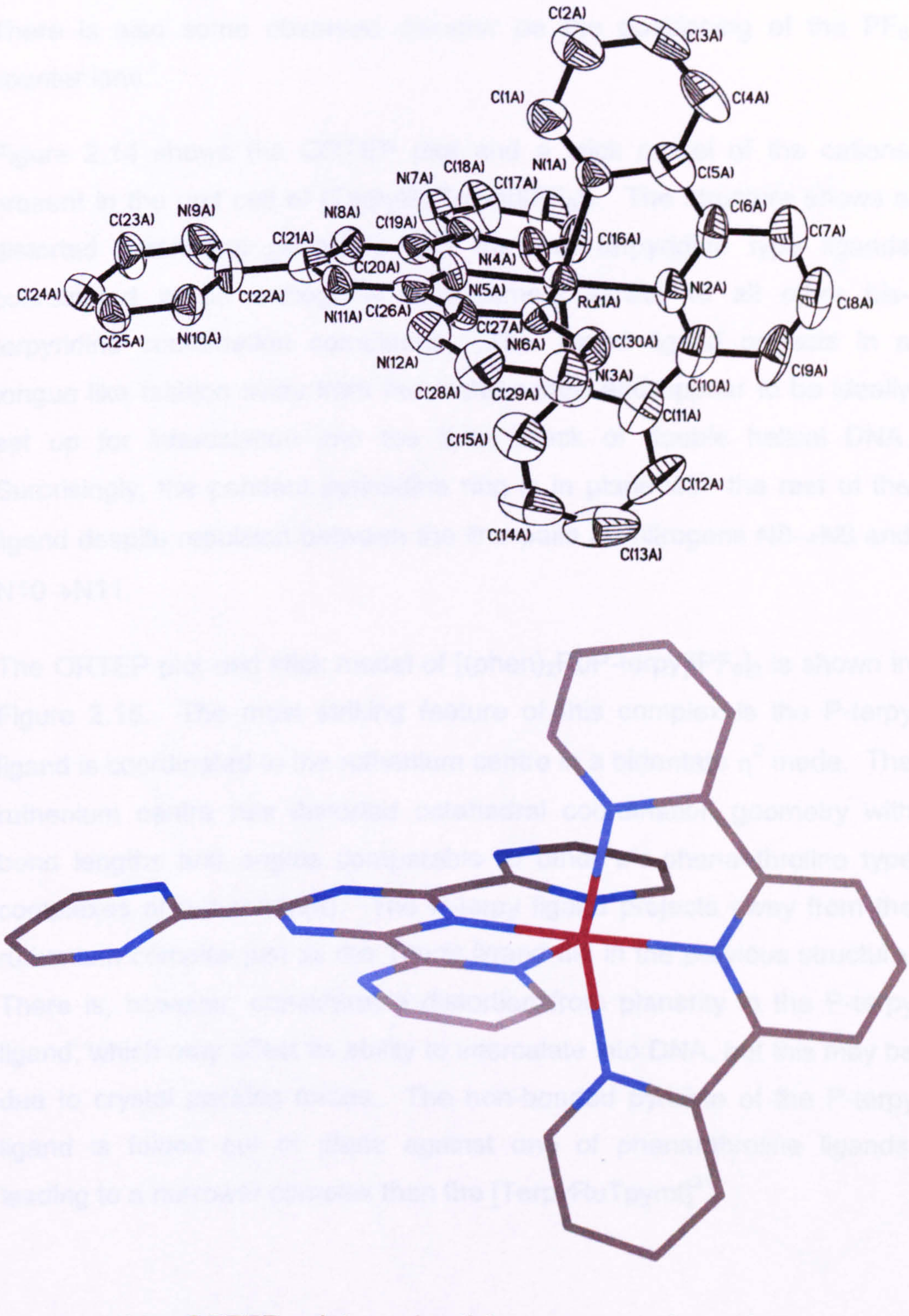

Figure 2.14:- *ORTEP plot and stick representation of the crystal structure one of $[TerpyRuTpymt]^{2+}$ cations present in the unit cell. Hydrogens and lone pairs are removed for clarity*

The unit cell contains two different orientations of [TerpyRuTpymt][PF_6]$_2$. There is also some observed disorder on the positioning of the PF_6 counter ions.

Figure 2.14 shows the ORTEP plot and a stick model of the cations present in the unit cell of [TerpyRuTpymt][PF_6]$_2$. The structure shows a distorted octahedral geometry with the two terpyridine type ligands coordinated in an orthogonal arrangement similar to all other bis-terpyridine coordination complexes. The Tpymt ligand projects in a tongue like fashion away from the metal centre and appear to be ideally set up for intercalation into the base stack of double helical DNA. Surprisingly, the pendant pyrimidine ring is in plane with the rest of the ligand despite repulsion between the line pairs on nitrogens N8→N9 and N10→N11.

The ORTEP plot and stick model of [(phen)$_2$RuP-terpy][PF_6]$_2$ is shown in Figure 2.15. The most striking feature of this complex is the P-terpy ligand is coordinated to the ruthenium centre in a bidentate η^2 mode. The ruthenium centre has distorted octahedral coordination geometry with bond lengths and angles comparable to other tris-phenanthroline type complexes of ruthenium(II). The P-terpy ligand projects away from the ruthenium complex just as the Tpymt ligand did in the previous structure. There is, however, considerable distortion from planarity in the P-terpy ligand, which may affect its ability to intercalate into DNA, but this may be due to crystal packing forces. The non-bonded pyridine of the P-terpy ligand is folded out of plane against one of phenanthroline ligands, leading to a narrower complex than the $[TerpyRuTpymt]^{2+}$.

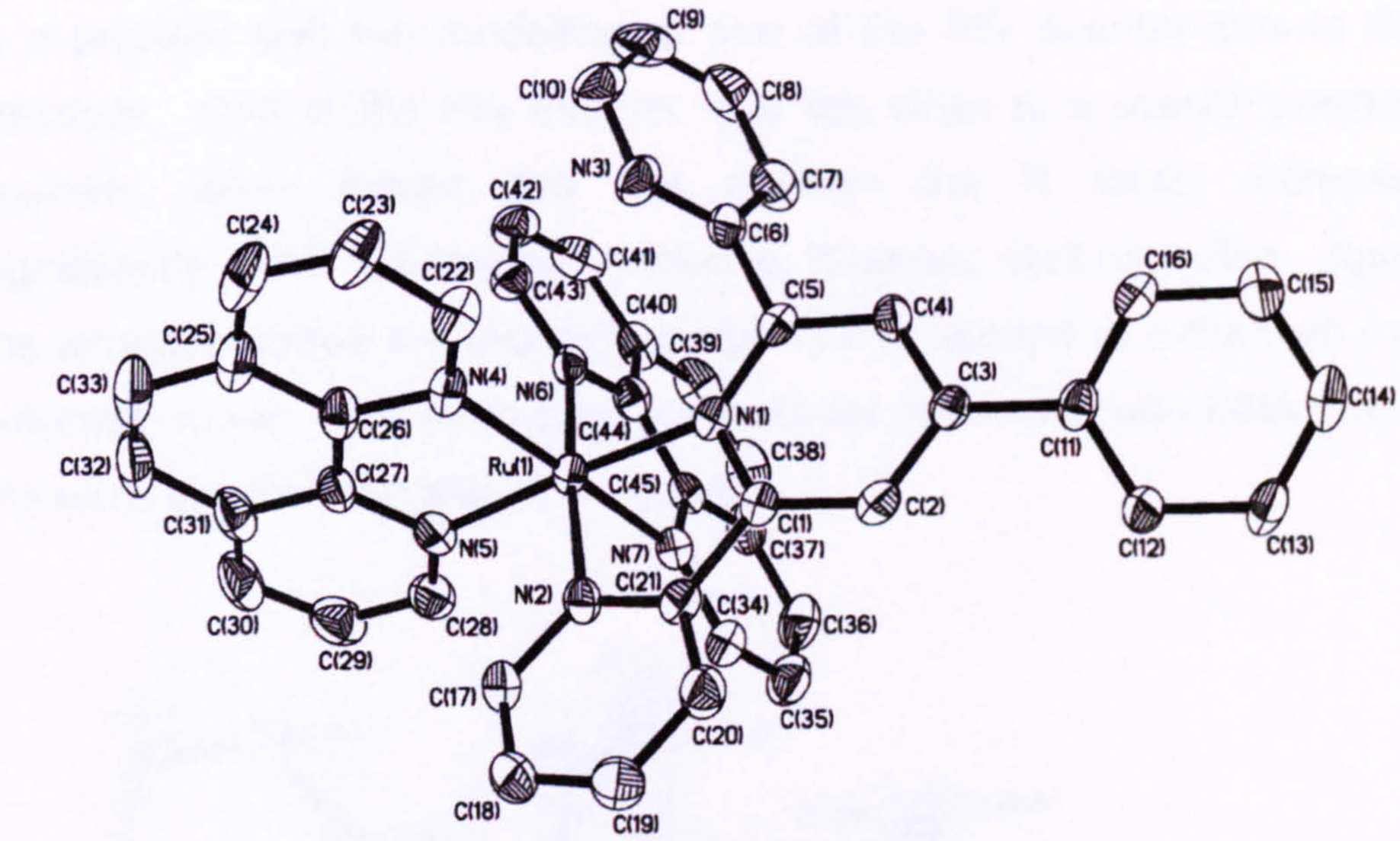

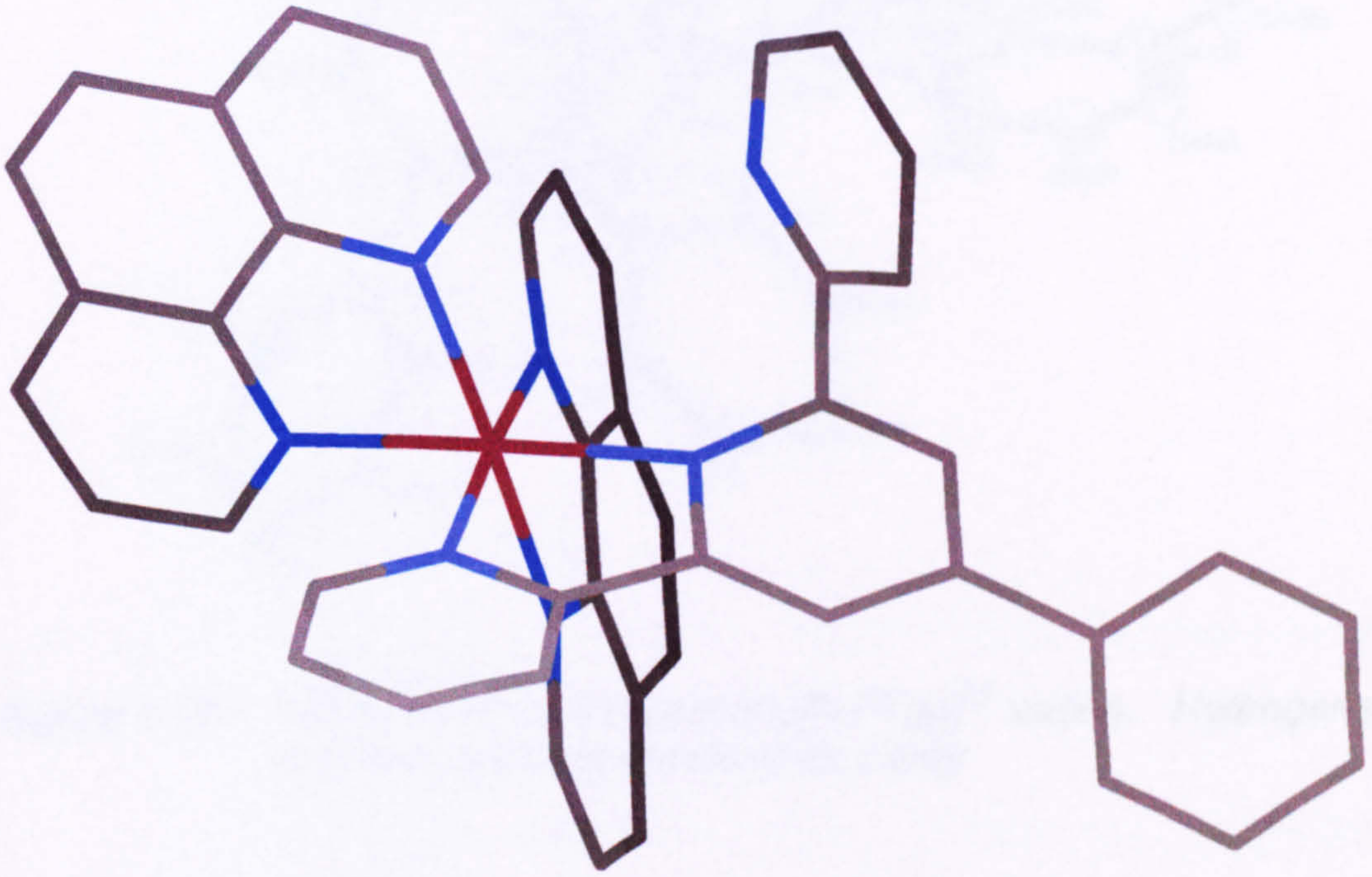

Figure 2.15:- *ORTEP plot and stick model of the $[(phen)_2RuP\text{-}terpy]^{2+}$ cation. Hydrogens and lone pairs are removed for clarity*

The ORTEP plot of $[(phen)_2RuTpp][PF_6]_2$ is shown in Figure 2.16. There is a problem with the modelling of one of the PF_6 counter ions in this structure. One of the PF_6 counter ions lies close to a special position, however, when forced into this position the R factor increases significantly. The ruthenium(II) cation is, however, well modelled. Again the structure shows the terpyridine type ligand bonded to ruthenium in a bidentate mode. The extra area available for interaction with DNA due to the extra pyridine ring should be noted.

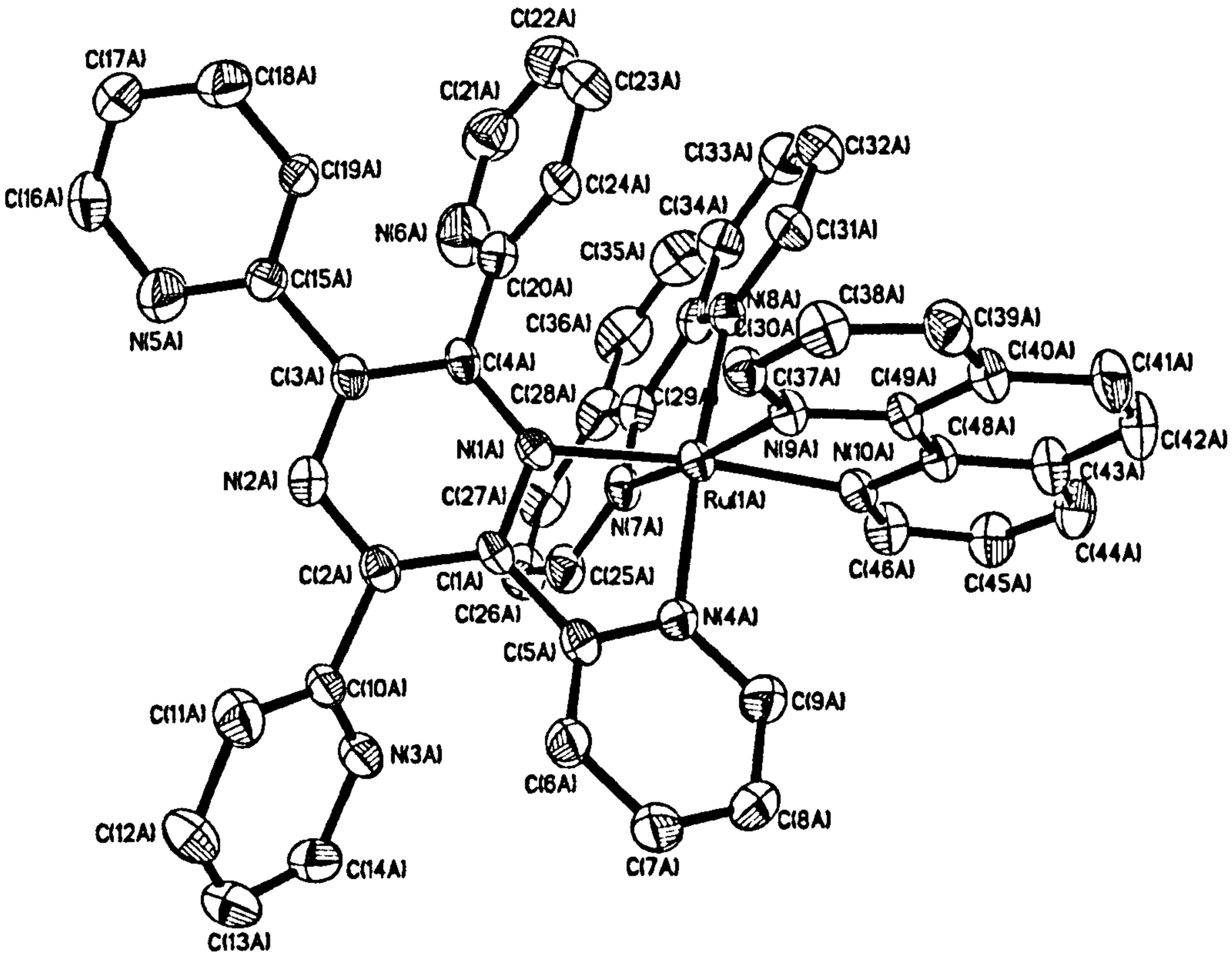

Figure 2.15:- *ORTEP plot of the $[(phen)_2RuPTpp]^{2+}$ cation. Hydrogens and lone pairs are removed for clarity*

2.6 Electrochemistry studies

The cyclic voltammogram of $[TerpyRuTpymt]^{2+}$ is shown in Figure 2.17. The CV was recorded in acetonitrile solution with 0.1M Bu_4NPF_6 as the supporting electrolyte. The CV's were recorded at $150mvs^{-1}$ and showed good reversibility with $\Delta E_p < 100mV$ and $|E_{pc} / E_{pa}| = 1$, unless otherwise stated. All the data were corrected for internal resistance using the AG&G electrochemistry power suite software package based upon normalization of the ferrocene oxidation couple. Table 2.2 shows the CV data for all of the other extended terpyridine complexes.

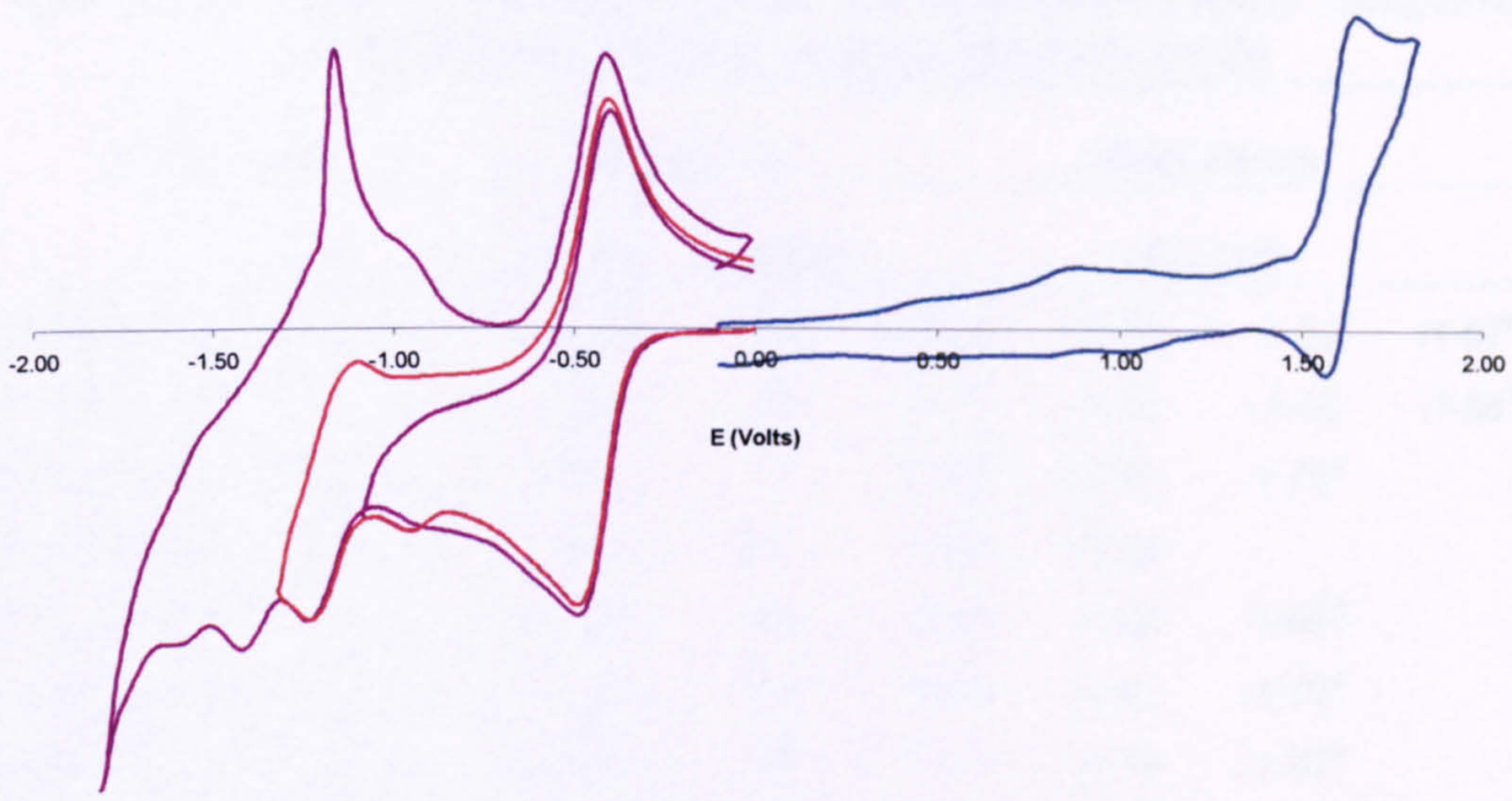

Figure 2.17:- *CV (current vs. Volts) for $[TerpyRuTpymt]^{2+}$ in acetonitrile Vs. $Ag^{+}/AgCl$*

All of the ruthenium complexes show characteristic reversible ruthenium$^{III/II}$ redox couples. The position of these couples is dependant upon the nature of the extended terpyridine ligand in the complex. In both the $TerpyRu^{2+}$ and $(phen)_2Ru^{2+}$ series, the more nitrogen atoms present in the ligand the more anodic the oxidation becomes. The series

is as follows; Tpymt>Tpp≈Tpt>Qtpy>P-terpy with the ligands containing 9, 6, 6, 4 and 3 nitrogens respectively. The inclusion of nitrogens in the terpy ligands serves to reduce the π-electron density on the ligand resulting in reduced π-back bonding to the ruthenium centre. This means that the Ru(III) oxidation state will not be stabilised as well and therefore a higher potential has to be applied to oxidise the ruthenium(II) complex.

Contrary to this trend, the ligand based reductions become easier as the number of nitrogens increase; P-terpy≈Qtpy>Tpt≈Tpp>Tpymt. As the ligands become more electronegative it becomes easier to reduce them and the $L^{0/-I}$ couple appears at a lower negative potential.

Table 2.2:- *Electrochemistry data for the 4'-extended terpy complexes in acetonitrile solution vs a Ag/AgCl electrode*

Compound	Oxidations		Reductions			
	$E_{1/2}$ (V)	Δ_p (mV)	$E_{1/2}$ (V)[a]			
[TerpyRuTpymt]$^{2+}$	+1.62	89	-0.44	-1.18	-1.39	-1.57[b]
[TerpyRuTpt]$^{2+}$	+1.48	74	-0.71	-1.35	-1.59	-1.88[b]
[TerpyRuQtpy]$^{2+}$	+1.37	77	-1.10	-1.41	-1.78[b]	
[TerpyRuP-terpy]$^{2+}$	+0.91	81	-1.07	-1.94		
[TerpyRuTpp]$^{2+}$	+1.50	69	-0.95	-1.40	-1.60[b]	
[(phen)$_2$RuTpt]$^{2+}$	+1.49	92	-0.96	-1.41	-1.72[b]	
[(phen)$_2$RuQtpy]$^{2+}$	+1.34	85	-1.13	-1.39	-1.67[b]	
[(phen)$_2$RuP-terpy]$^{2+}$	+1.28	86	-1.25	-1.37	-1.45[b]	
[(phen)$_2$RuTpp]$^{2+}$	+1.43	92	-0.87	-1.37	-1.59[b]	-1.71[b]
[(CO)$_3$MeCNReTpt]$^{+}$	+1.66[b]	-	-0.57	-1.02[b]	-1.28[b]	
[(CO)$_3$MeCNReQtpy]$^{+}$	+1.41[b]	-	-1.11	-1.28[b]	-1.60[b]	
[(CO)$_3$MeCNReP-terpy]$^{+}$	+1.36[b]	-	-1.15	-1.36[b]	-1.55[b]	

[a] Δ_p < 100 mV for all reversible reductions

[b] event was chemically irreversible, therefore only E_p values are quoted

The corresponding rhenium$^{II/I}$ oxidation is characteristically irreversible but the same trend in oxidation potential is observed.

2.7 Spectroscopic studies

The UV-Visible absorption spectra and luminescence emission spectra were recorded for all the extended terpyridine complexes. Unless otherwise stated, the spectra were recorded in acetonitrile solution at room temperature. As the spectra were used to monitor the binding of the complexes to DNA in an oxygenated aqueous media and no attempt was made to eliminate oxygen from the samples.

An example of the spectra obtained is shown in Figure 2.18, which shows the UV-Visible absorbance spectra for the $phen_2Ru(II)$ complexes.

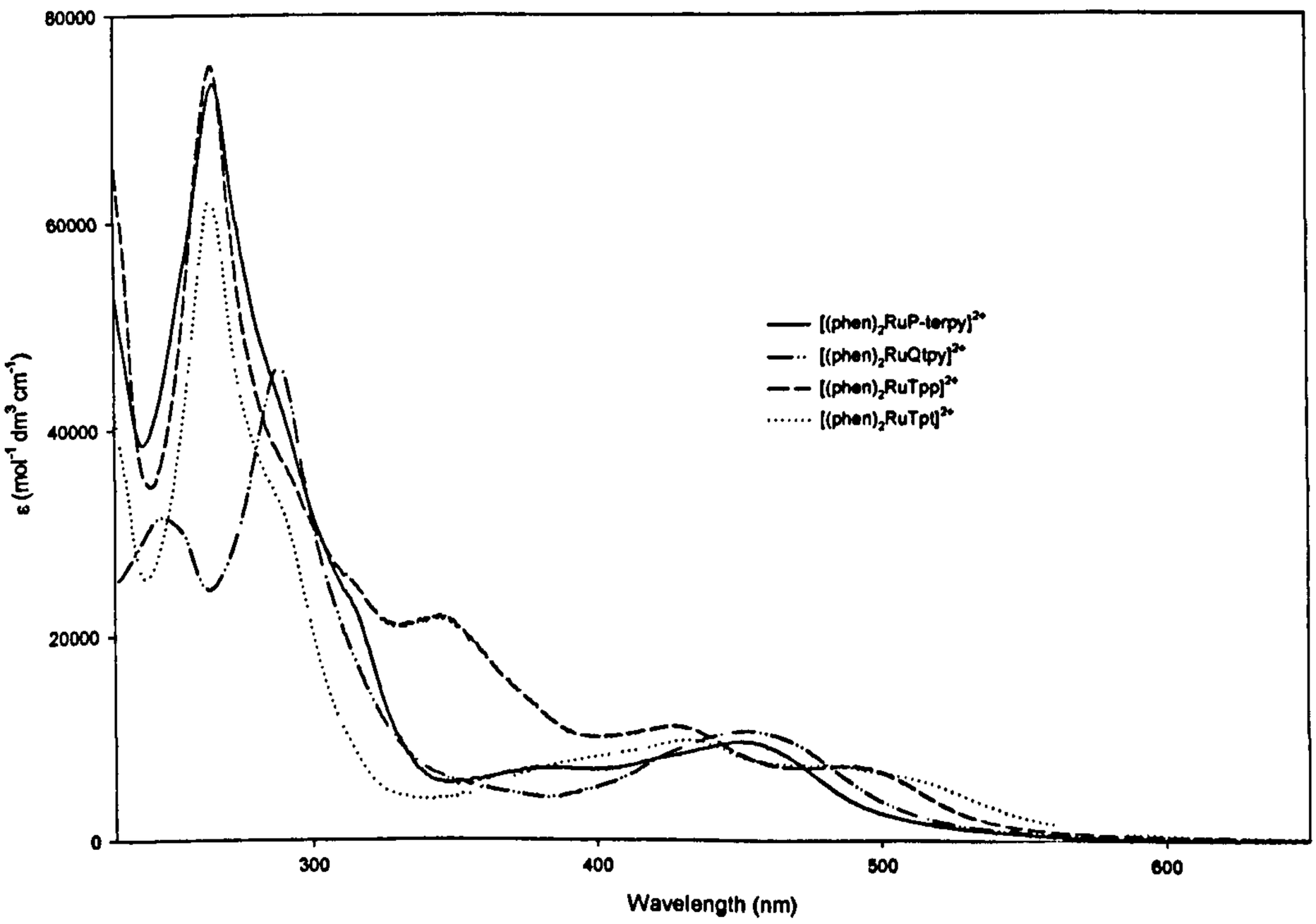

Figure 2.18:- *UV-Visible spectra of the $(phen)_2Ru$ extended terpyridine complexes recorded in acetonitrile solution*

The low energy bands (350-550nm) present in all of the ruthenium(II) complexes are characteristic of MLCT transitions from the ruthenium(II) centre to the various pyridyl components of the coordinated ligands.

These low energy transitions are similar in both energy and intensity (5,000 – 20,000 mol^{-1} dm^3 cm^{-1}) to those observed in the numerous tris-phenanthroline and bis-terpyridine type complexes present in the literature, giving rise to their intense red through purple colours. The intense higher energy bands, typically <300nm can be assigned to ligand centered $\pi \rightarrow \pi^*$ and $n \rightarrow \pi^*$ transitions.

The rhenium(I) complexes show much simpler UV-Visible spectra typically consisting of a sharp MLCT transition appearing around 300-320nm with a tail extending to around 450nm in the visible region. The ligand centered $\pi \rightarrow \pi^*$ and $n \rightarrow \pi^*$ transitions appeared as either two bands or one broad band in the 230 – 300nm region of the spectrum. Again these values are typical of other rhenium(I) polypyridyl complexes found in the literature.

Table 2.3:- *Spectroscopic data for the 4'-extended terpyridine complexes recorded in acetonitrile solution*

Complex	Absorption			Emission	
	λ_{max} (nm)	ε ($mol^{-1}dm^3$ cm^{-1})	Assignmen	λ_{ex} (nm)	λ_{em} (nm)
[TerpyRuTpymt][PF_6]$_2$	269	35,121	LC $\pi \rightarrow \pi^*$	-	-
	296	20, 531	LC $\pi \rightarrow \pi^*$		
	316	14,572	LC $\pi \rightarrow \pi^*$		
	330	18,346	LC $\pi \rightarrow \pi^*$		
	474	13,796	MLCT		
[TerpyRuTpt][PF_6]$_2$ (2.1)	271	Sh		-	-
	280	37,183	LC $\pi \rightarrow \pi^*$		
	299	34,933	LC $\pi \rightarrow \pi^*$		
	326	sh	LC $\pi \rightarrow \pi^*$		
	479	14,350	LC $\pi \rightarrow \pi^*$		
			MLCT		
[TerpyRuQtpy][PF_6]$_2$ (2.2)	229	Sh		-	-
	238	25,584	LC $\pi \rightarrow \pi^*$		
	273	36,438	LC $\pi \rightarrow \pi^*$		
	309	35,498	LC $\pi \rightarrow \pi^*$		
	324	sh	LC $\pi \rightarrow \pi^*$		
	485	15,204	MLCT		
[TerpyRuP-terpy][PF_6]$_2$ (2.3)	239	32,867	LC $\pi \rightarrow \pi^*$	-	-
	272	49,327	LC $\pi \rightarrow \pi^*$		
	279	48,267			

	307	61,000	LC $\pi\rightarrow\pi^*$		
	481	23,806	LC $\pi\rightarrow\pi^*$		
			MLCT		
[TerpyRuTpp][PF_6]$_2$ (2.4)	194	10,800	LC $\pi\rightarrow\pi^*$	-	-
	224	13,300	LC $\pi\rightarrow\pi^*$		
	274	10,000	LC $\pi\rightarrow\pi^*$		
	283	sh	LC $\pi\rightarrow\pi^*$		
	310	10,600	MLCT		
[(phen)$_2$RuTpt][PF_6]$_2$	264	62239	LC $\pi\rightarrow\pi^*$	450	725
	284	sh	LC $\pi\rightarrow\pi^*$		
	402	sh	MLCT		
	432	9912	MLCT		
	470	7519	MLCT		
[(phen)$_2$RuQtpy][PF_6]$_2$	244	31138	LC $\pi\rightarrow\pi^*$	450	674
	287	45977	LC $\pi\rightarrow\pi^*$		
	450	10428	MLCT		
[(phen)$_2$RuP-terpy][PF_6]$_2$	220	60272	LC $\pi\rightarrow\pi^*$	450	595
	264	72782	LC $\pi\rightarrow\pi^*$		
	310	sh	LC $\pi\rightarrow\pi^*$		
	385	7134	MLCT		
	450	9775	MLCT		
[(phen)$_2$RuTpp][PF_6]$_2$	264	75751	LC $\pi\rightarrow\pi^*$	430	715
	344	21820	LC $\pi\rightarrow\pi^*$		
	427	11308	MLCT		
	488	7306	MLCT		
[$(CO)_3$MeCNReTpt]$^+$	251	26604	LC $\pi\rightarrow\pi^*$	-	-
	295	27103	LC $\pi\rightarrow\pi^*$		
	302	25108	LC $\pi\rightarrow\pi^*$		
	377	5171	MLCT		
[$(CO)_3$MeCNReQtpy]$^+$	253	28110	LC $\pi\rightarrow\pi^*$	310	417
	279	sh	LC $\pi\rightarrow\pi^*$		
	330	12727	MLCT		
[$(CO)_3$MeCNReP-terpy]$^+$	251	26207	LC $\pi\rightarrow\pi^*$	310	370
	277	26735	LC $\pi\rightarrow\pi^*$		
	328	17372	MLCT		

As expected, none of the terpy derivatives of the compounds show any room temperature luminescence, which is completely consistent with other published compounds. The lowest lying excited state which is the triplet metal-to-ligand-charge-transfer state ^{3}[MLCT] normally centered on the ligand π^* LUMO, is very low lying in bis-terpyridine type complexes. This undergoes fast non-radiative deactivation <1ns resulting in no room temperature emission[101]. The bis-phen ruthenium compounds show characteristic emission spectra. The complexes were excited at 450nm directly into the MLCT bands. The observed emissions occurred between

595 and 725nm. The more nitrogen atoms that are present in the extended terpyridine ligand, the lower the energy of the emission. This is because the LUMO, The ligand π^* is lowered in energy as the number of nitrogens increase (Figure 2.19).

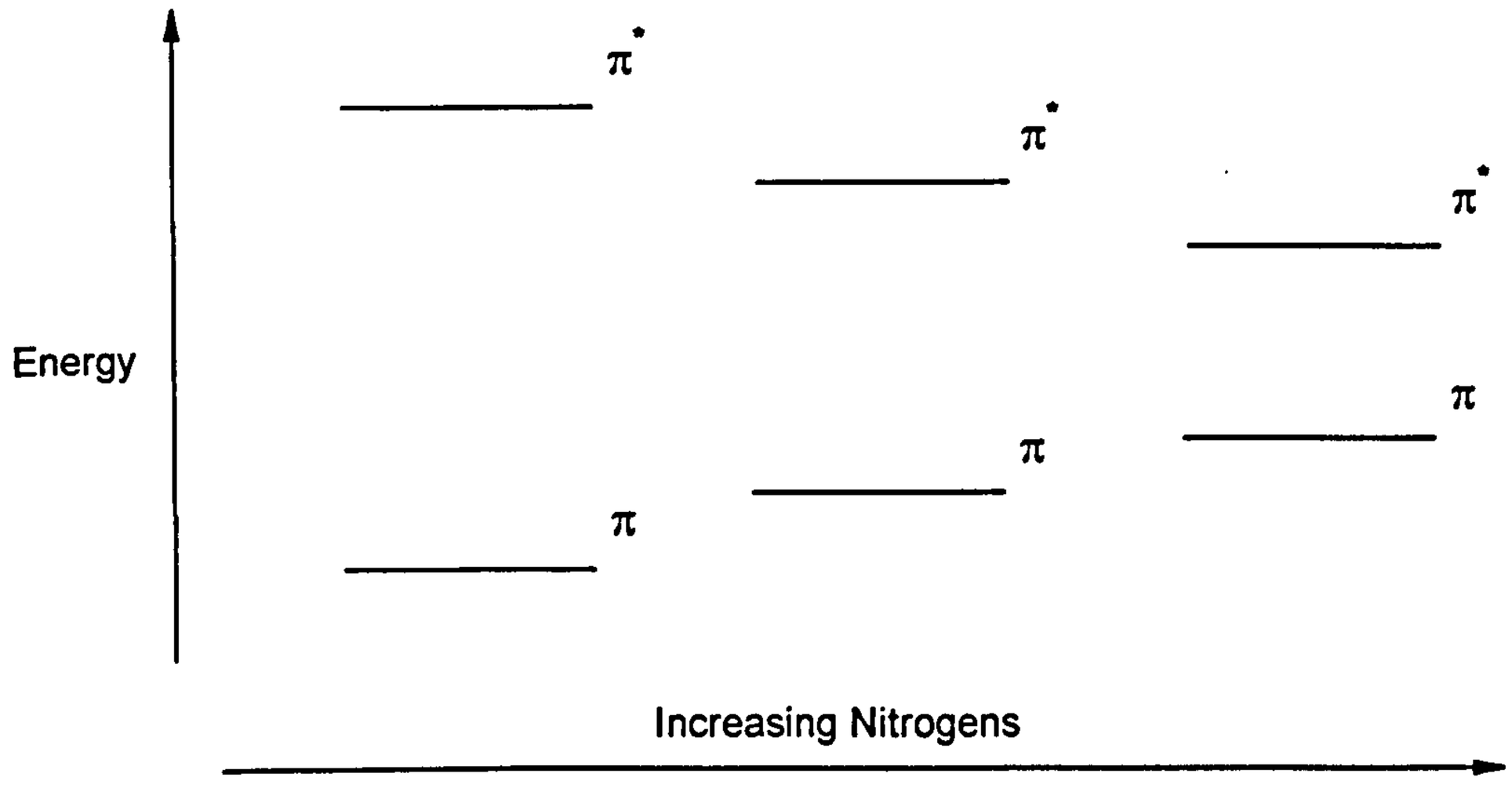

Figure 2.19:- *Schematic of the relative energy of ligand π and π^* orbitals as the number of nitrogens in the aromatic system increase*

The two rhenium complexes $[(CO)_3MeCNReP\text{-}terpy]^+$ and $[(CO)_3MeCNReQtpy]^+$ showed very high energy (380-420nm) structured emissions (Figure 2.20). Both complexes were excited at 310nm and the resulting low energy emission is presumed to be ligand-centered, but at present the exact pathway is not known. Further studies are underway to try and quantify and hence find the origin of these interesting emissions. The Tpt complex showed no emission when excited at a range of different wavelengths. To our knowledge this is the first such rhenium(I) complex containing a triazine moiety and as such we can only postulate that the triazine serves to quench the excited state of the complex.

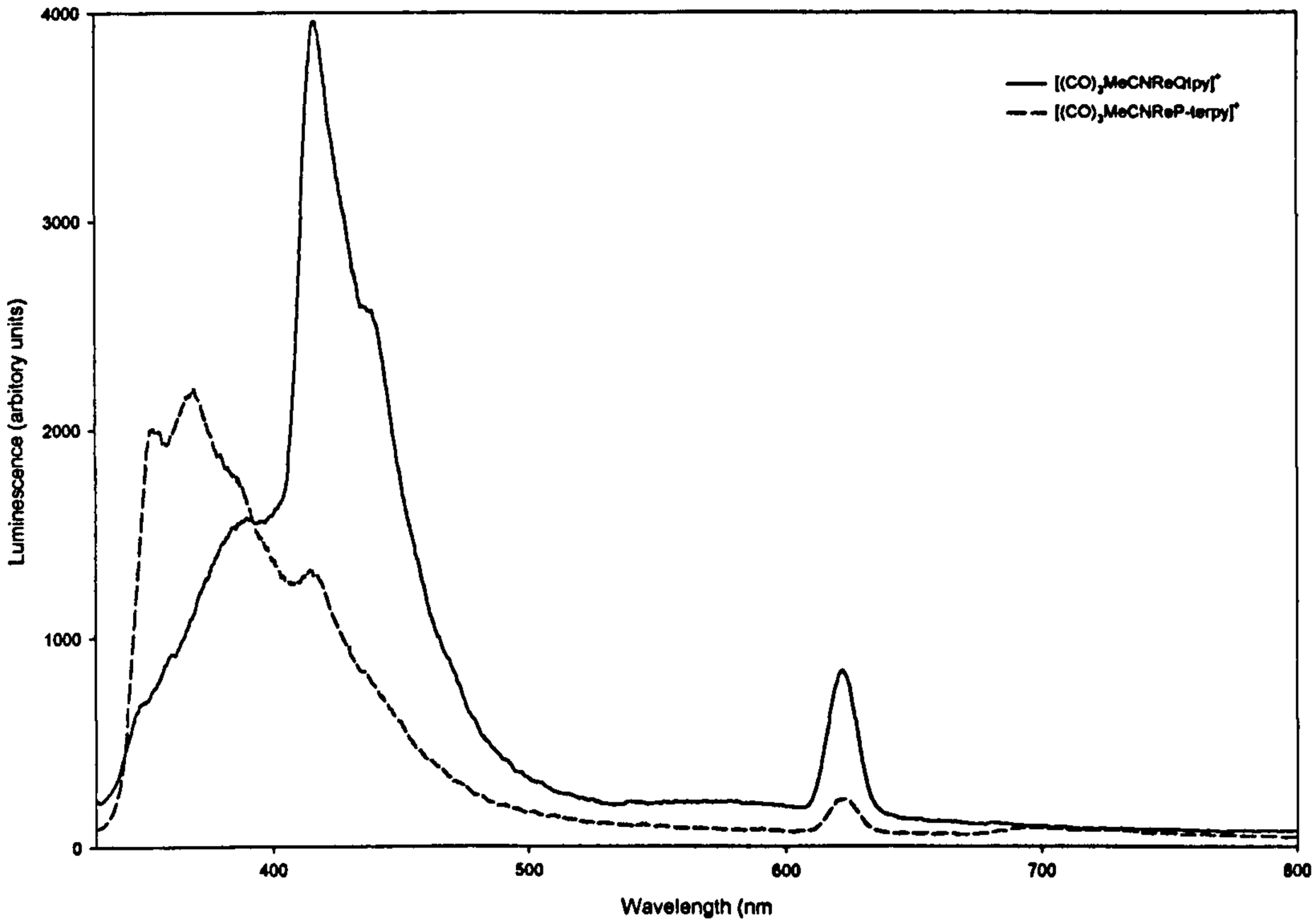

Figure 2.20:- *Emission spectr recorded in acetonitrile solution for* $[(CO)_3MeCNReQtpy]^+$ *and* $[(CO)_3MeCNReP\text{-}terpy]^+$

2.8 Conclusions

A series of ruthenium(II) and rhenium(I) complexes containing 4'-extended terpyridine ligands has been prepared. ^1H NMR, mass spectrum and in some cases X-ray crystal structures have shown the complexes to adopt the required geometry with the extended aromatic ligand projecting away from the metal centre. These complexes are ideally set up for interaction with double helical DNA. Moreover, they have been shown possess rich photophysical signatures that can be used to monitor their binding to DNA. Results from the DNA binding assays are discussed in Chapters 5 and 6.

Chapter 3

Tris-pyrazolyl methane complexes of Ruthenium(II)

3.1 Introduction

Over the past decade or so, metal complexes incorporating the poly-aromatic ligand dppz have been extensively studied with respect to their interactions with DNA[21,102-104]. Particular interest has centred on the ability of ddpz complexes to report the nature of their surroundings[24]. In non-aqueous environments ruthenium dppz complexes show intense luminescence upon excitation with light of a suitable wavelength into the MLCT transition of the complex. In aqueous environments this luminescence is completely quenched through hydrogen bonding of water molecules to the phenazine nitrogens of dppz. When DNA is added to aqueous solutions the luminescence is switched back on[21]. It has been shown by a variety of techniques that the dppz ligand intercalates into the base stack of the DNA, thus protecting the phenazine nitrogens from water quenching, although the exact orientation of the complex with the DNA has been open to much debate[25,27,105,106]. Dppz complexes show good affinity for DNA, and coupled with their rich photochemistry and redox properties, they show great potential as DNA binding agents. There are, however, still many problems to be addressed before they possess the affinity and specificity of other DNA binding agents.

Because of limitations in the synthetic procedures chelate complexes of ruthenium(II) have to be synthesised as a racemic mixture of Λ- and Δ-

forms. As a consequence of the DNA binding properties differing between the two enantiomeric forms, they have to be resolved via long and tedious procedures, often resulting in a significant loss of compound[27]. Furthermore, as the ruthenium(II) centre is coordinately saturated any attempt to extend or modify the geometry of the system involves modification of the aromatic ancillary ligands themselves[59,60] often resulting in wasteful statistical mixtures of compounds[107,108].

In this study we begin to address these two problems, firstly by developing an achiral ruthenium(II) system based around the well-characterised dppz moiety. Secondly, we have introduced a free coordination site, which is available to further extend the system or modulate the charge of the system.

3.1.1 Tripodal facially coordinating ligands

In order to achieve the required geometry for the proposed system we needed to cap one face of the octahedral ruthenium(II) complex. This will leave three more coordination sites available for further substitution. Reaction of the facially capped species with a bidentate ligand such as dppz would result in the formation of a species with all the requirements for binding to DNA. The axial coordination site can then be used to tune the system further (Figure 3.1).

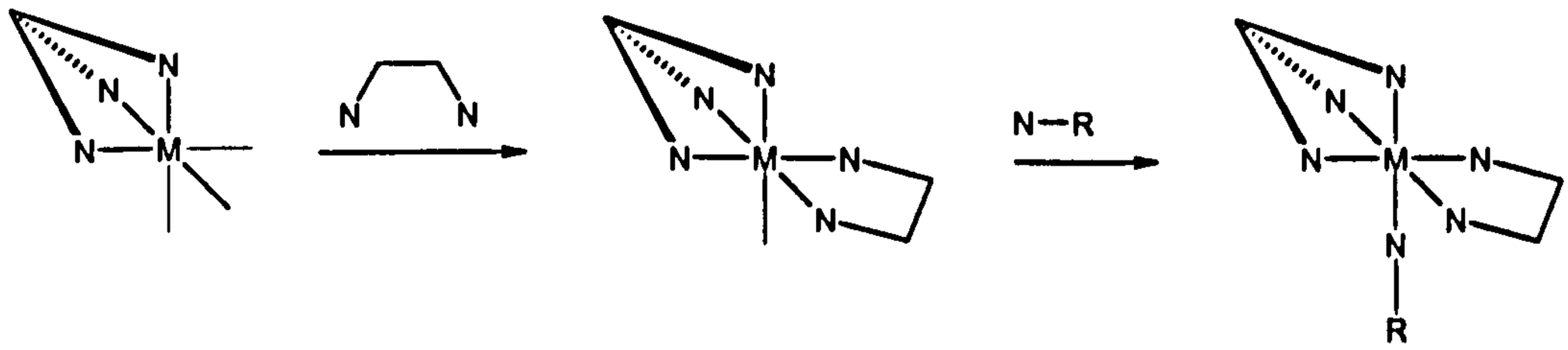

Figure 3.1:- *Proposed route of synthesis*

There were several candidates for use as the facially capping tripodal

ligand such as tris-(1-pyrazolyl)borate, tris-(1-pyridyl)methanol and tris-(1-pyrazolyl)methane (Tpm) (Figure 3.2).

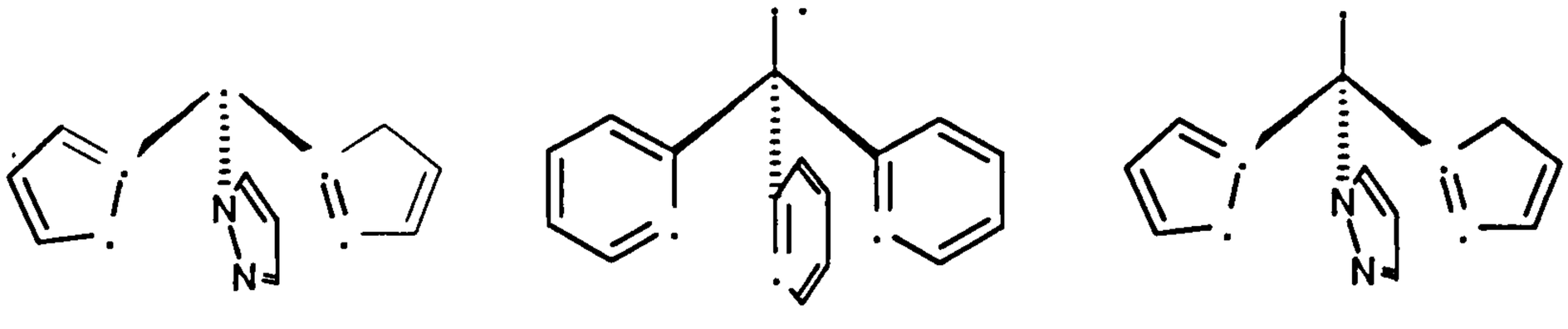

Figure 3.2:- Some tripodal ligands

Tris-(1-pyridyl)methanol[109] requires a complicated synthesis and is difficult to obtain in large quantities. While the chemistry of tris-pyrazolyl borates is well developed, its use was not deemed suitable due to its tendency to hydrolyse in aqueous environments.

Recent advances in synthetic procedures as reported by Reger *et al.* allows tris-(1-pyrazolyl)methane and derivatives to be easily prepared in high yields[110], so this is used as the facially capping tripodal ligand in this study.

In 1988 Mayer *et-al.* reported the synthesis of $TpmRuCl_3 . 3H_2O$ and its reaction with bidentate ligands to produce $[TpmClRuL_2]^+$ (where L_2 = bipy, phen etc.) (Scheme 3.1)[111].

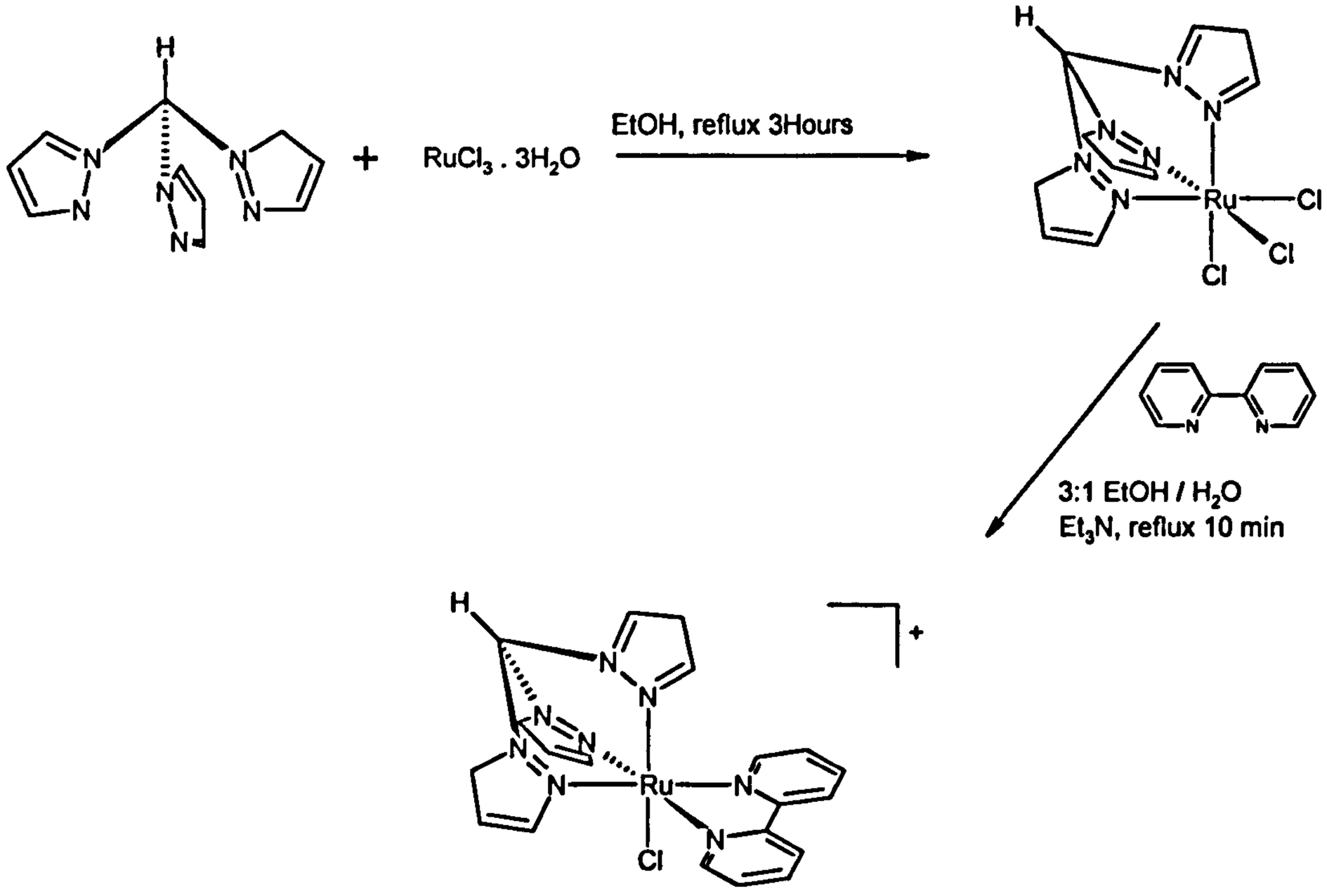

Scheme 3.1:- *Mayers synthesis of Tpm ruthenium(II) complexes*

The axial chloride can be substituted for practically any pyridine or nitrile ligand. First the chloride is removed with silver nitrate in ethanol/water. Addition of the nitrogen donor ligand and further refluxing affords the coordination of the ligand to the axial site. The reaction is almost quantitative and the substituted product requires little or no purification[111].

3.2 Synthetic studies

3.2.1 Ligand synthesis

Tpm **(3.3)** was synthesised as reported by Reger *et al.* from a $CHCl_3$ – H_2O phase transfer reaction[110]. A large excess of Na_2CO_3 base affords the deprotonation of pyrazole and initiates its subsequent reaction with

$CHCl_3$ (Scheme 3.2)

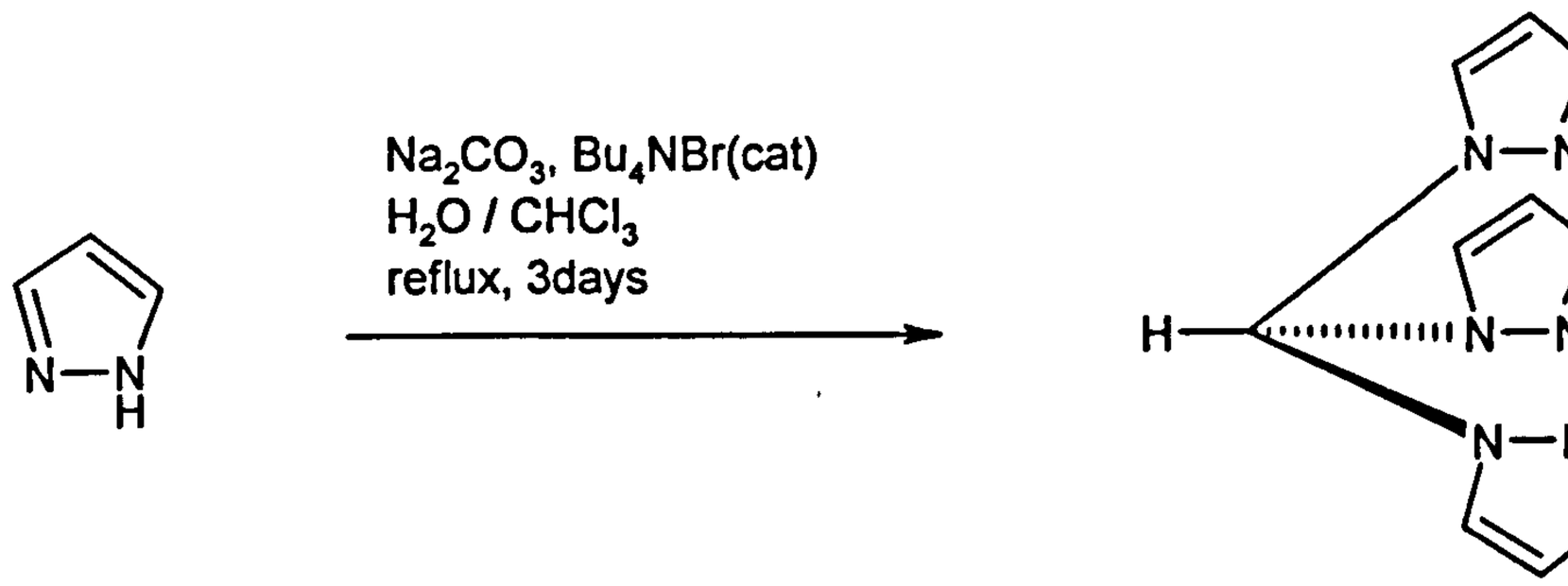

(3.3)

Scheme 3.2:- *Synthesis of Tpm* ***(3.3)***

Dppz **(3.2)** was prepared by literature methods (Scheme 3.3) from the condensation of 1,10-phenanthroline-5,6-dione (dpq) **(3.1)** with o-phenyline-diamine in ethanol[112]. dpq **(3.1)** was prepared from the acidic oxidation of 1,10-phenanthroline with bromine[27].

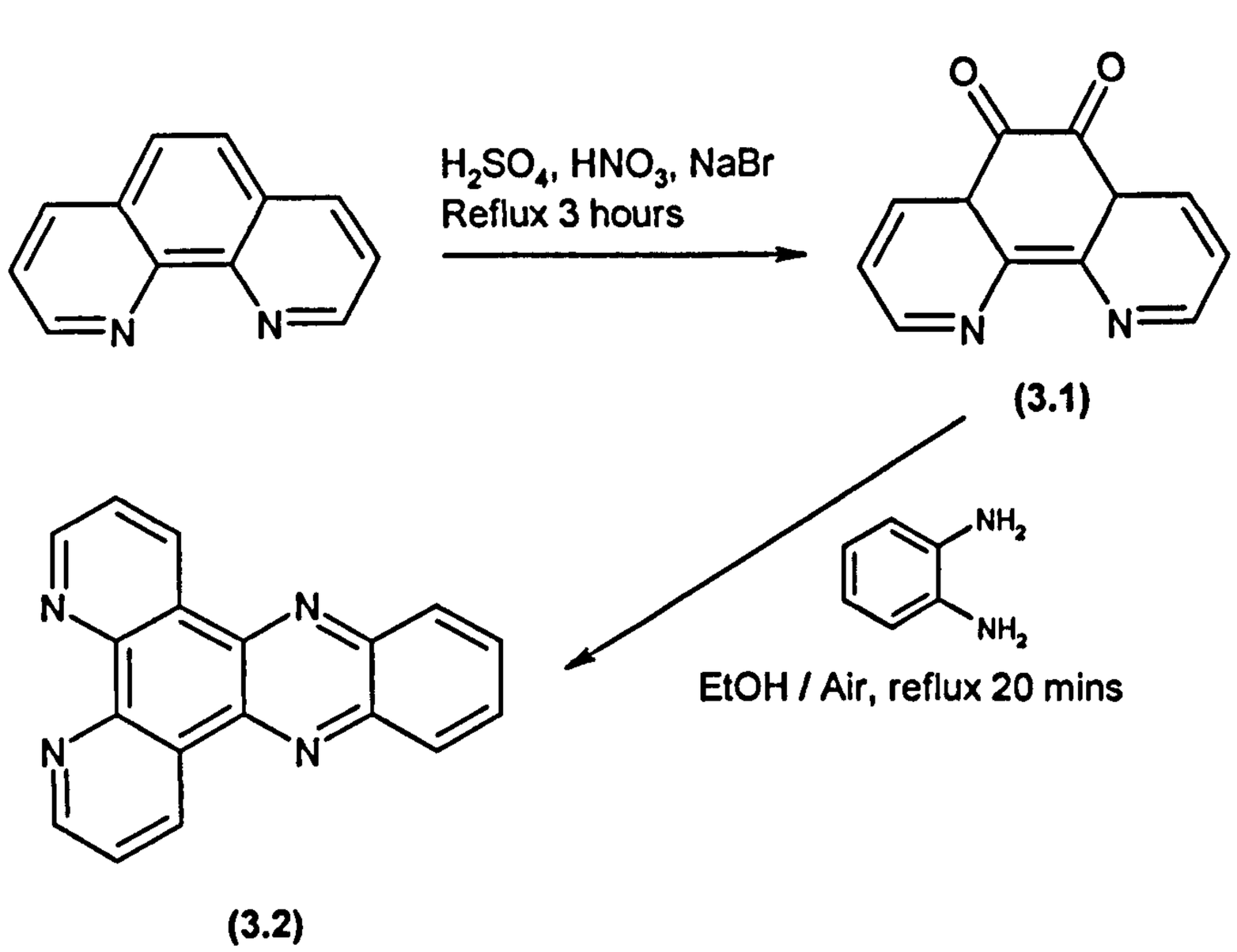

(3.2)

Scheme 3.3:- *Synthesis of dppz* ***(3.2)***

3.2.2 Preparation of $[TpmClRudppz]^+$ (3.5)

The starting material $TpmRuCl_3.xH_2O$ **(3.4)** was prepared by the method reported by Mayer *et al.* by refluxing $RuCl_3.3H_2O$ with a slight excess of Tpm in ethanol for three hours[111].

Refluxing **(3.4)** with a slight excess of dppz in 3:1 ethanol: water along with 1ml of the reducing agent triethylamine for 10 minutes resulted in the formation of the mono cationic complex $[TpmClRudppz]^+$ **(3.5)** (Scheme 3.4). The compound was isolated as a PF_6^- salt by reducing the solvent volume to 5ml and adding a molar excess of NH_4PF_6. The crude compound was purified by column chromatography on neutral alumina with 1: 1 acetonitrile: toluene as the eluent. The single dark red band contained the product **(3.5)**, which was characterised by ^1H NMR, FAB-MS and accurate mass.

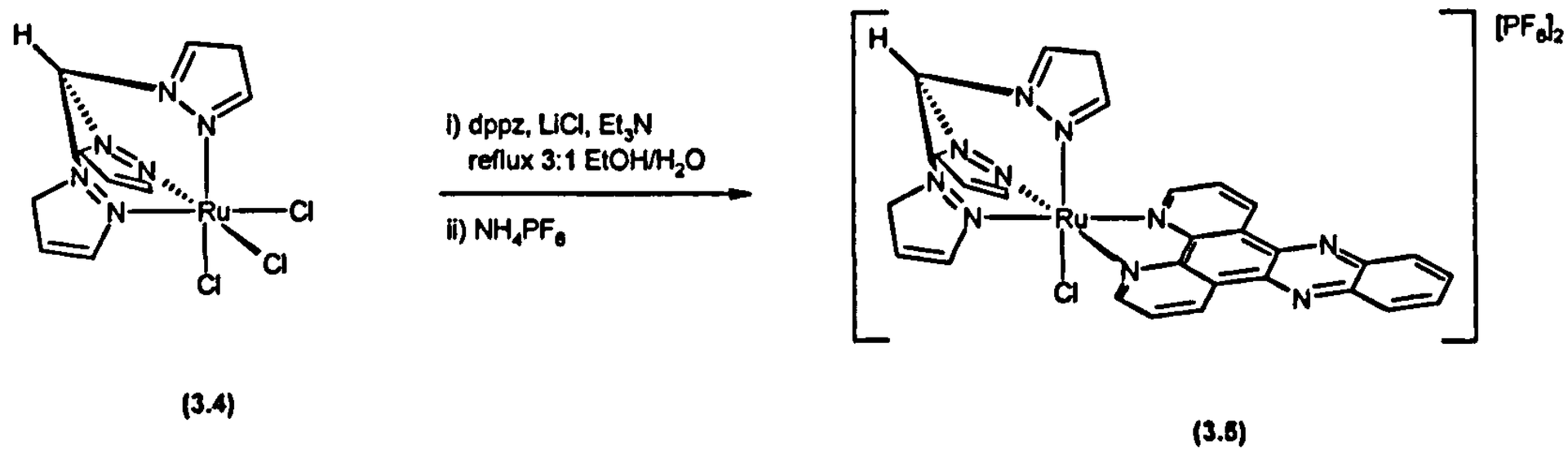

(3.4) (3.5)

Scheme 3.4:- *Preparation of $[TpmClRudppz]^+$ (3.5)*

3.2.3 Preparation of $[TpmPyRudppz]^{2+}$ (3.6)

Conversion of **(3.5)** to its chloride salt by treatment with $^nBu_4NCl$ in acetone rendered it water soluble allowing it to be refluxed with two equivalents of $AgNO_3$ in 1:1 ethanol: water. This resulted in the abstraction of the axial chloride and its subsequent precipitation as

insoluble AgCl, which was removed from the reaction mixture by centrifugation. Addition of excess pyridine and further refluxing for 6 hours leads to the formation of the pyridine substituted complex **(3.6)**. Again the complex was isolated as its PF_6^- salt by reducing the volume of solvent and addition of a molar excess of NH_4PF_6. The product was shown to be pure upon isolation and no further purification was required.

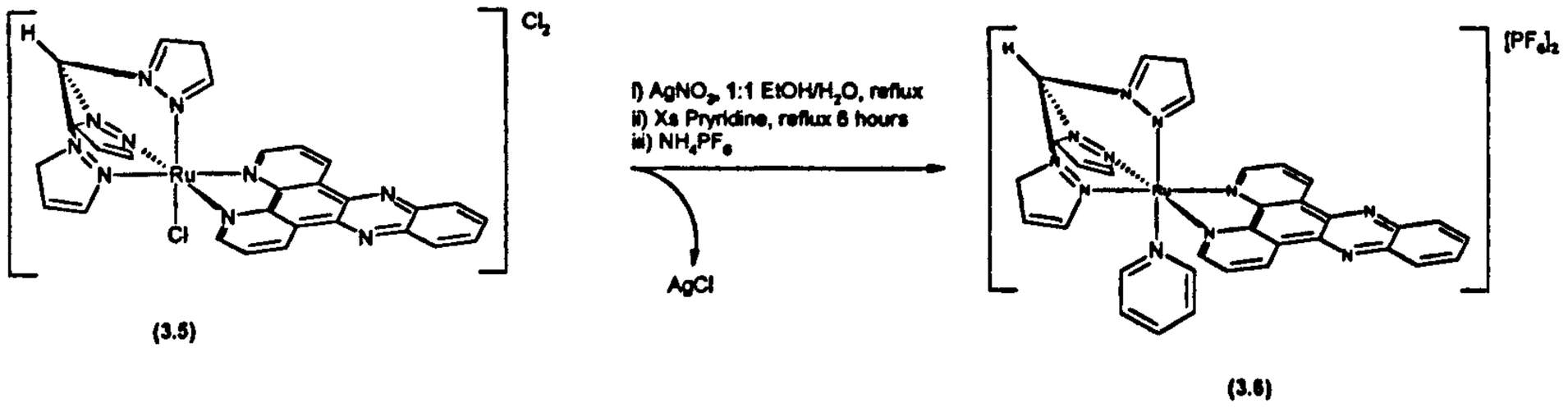

Scheme 3.5:- *Preparation of [TpmPyRudppz]$^{2+}$* ***(3.6)***

3.2.4 Preparation of [TpmMeCNRudppz]$^{2+}$ (3.7)

Refluxing **(3.5)** with $AgCF_3SO_3$ in freshly distilled acetonitrile leads to the abstraction of the axial chloride with precipitation of insoluble AgCl and subsequent substitution with acetonitrile (Scheme 3.6). The AgCl was removed by filtration through celite. To ensure complete metathesis to the PF_6^- salt the acetonitrile was removed and the residue was taken up in 1 ml methanol. A molar excess of NH_4PF_6 was then added followed by 10 ml water, which resulted in precipitation of **(3.7)** as its PF_6^- salt. No further purification was required and the compound was characterised by ^1H NMR, FAB-MS and accurate mass determination.

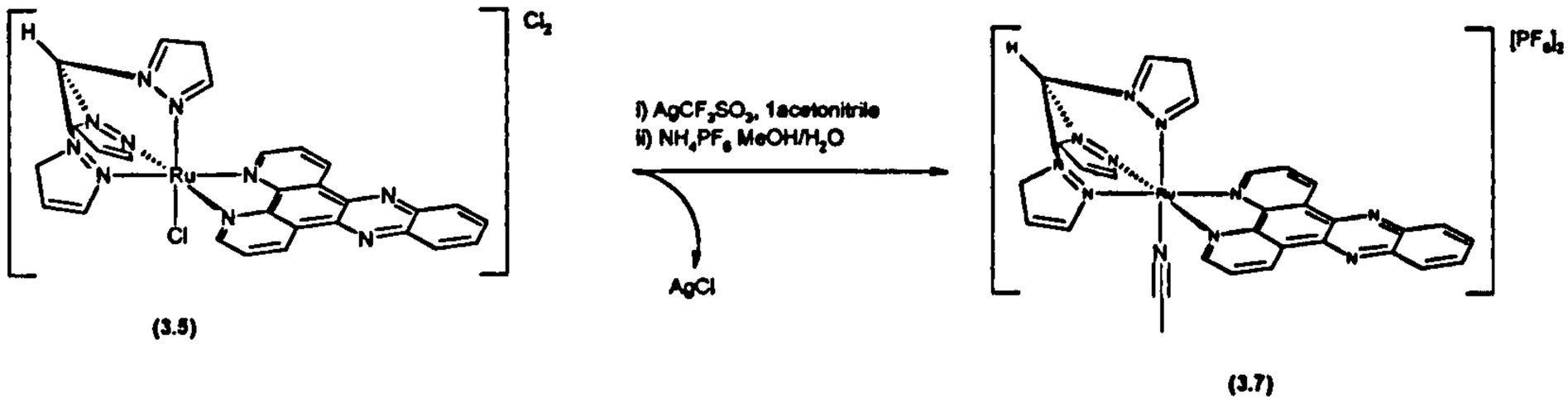

Scheme 3.6:-** preparation of [TpmMeCNRudppz]$^{2+}$ **(3.7)

3.3 ^{1}H NMR spectroscopic studies

All three of the Tpm ruthenium(II) complexes showed well resolved ^{1}H NMR spectra.

Figure 3.3 shows the downfield region of the ^{1}H NMR spectrum of [TpmClRudppz]$^{+}$ recorded at 250MHz in d^{6}-acetone. A 2D COSY spectrum (not shown) recorded at 400MHz in d^{6}-DMSO was used to aid the assignment of the protons although it was quite broad.

The spectrum of complex is fairly simple due to the plane of symmetry running through the molecule. The sharp singlet at 9.63ppm is characteristic of the de-shielded proton on the Tpm methane (a)[111]. The doublet at 9.57ppm has a coupling constant of 9 Hz suggesting it is adjacent to a ring nitrogen. Cross-referencing of this proton on the COSY shows it is coupled to the double doublet at 8.06ppm, and the double doublet at 9.17ppm. All three of these protons integrate to two and can therefore be assigned to protons h, i and j on the phenanthroline section of dppz. The three proton signal at 8.57ppm can be assigned to protons pyrazole protons b and e and analysis of coupling patterns allows two of the protons of the three proton multiplet at 6.87ppm to be assigned to proton f on the two equatorial pyrazoles. The single proton triplet at

6.30ppm is coupled to both protons at 8.47ppm (b) and 6.87ppm and can be assigned to proton (c) with 6.87ppm being assigned to proton (d) of the axial pyrazole. The final two protons 8.52ppm and 8.17ppm each integrating to two protons coupled to each other and are the two phenazine proton k and l.

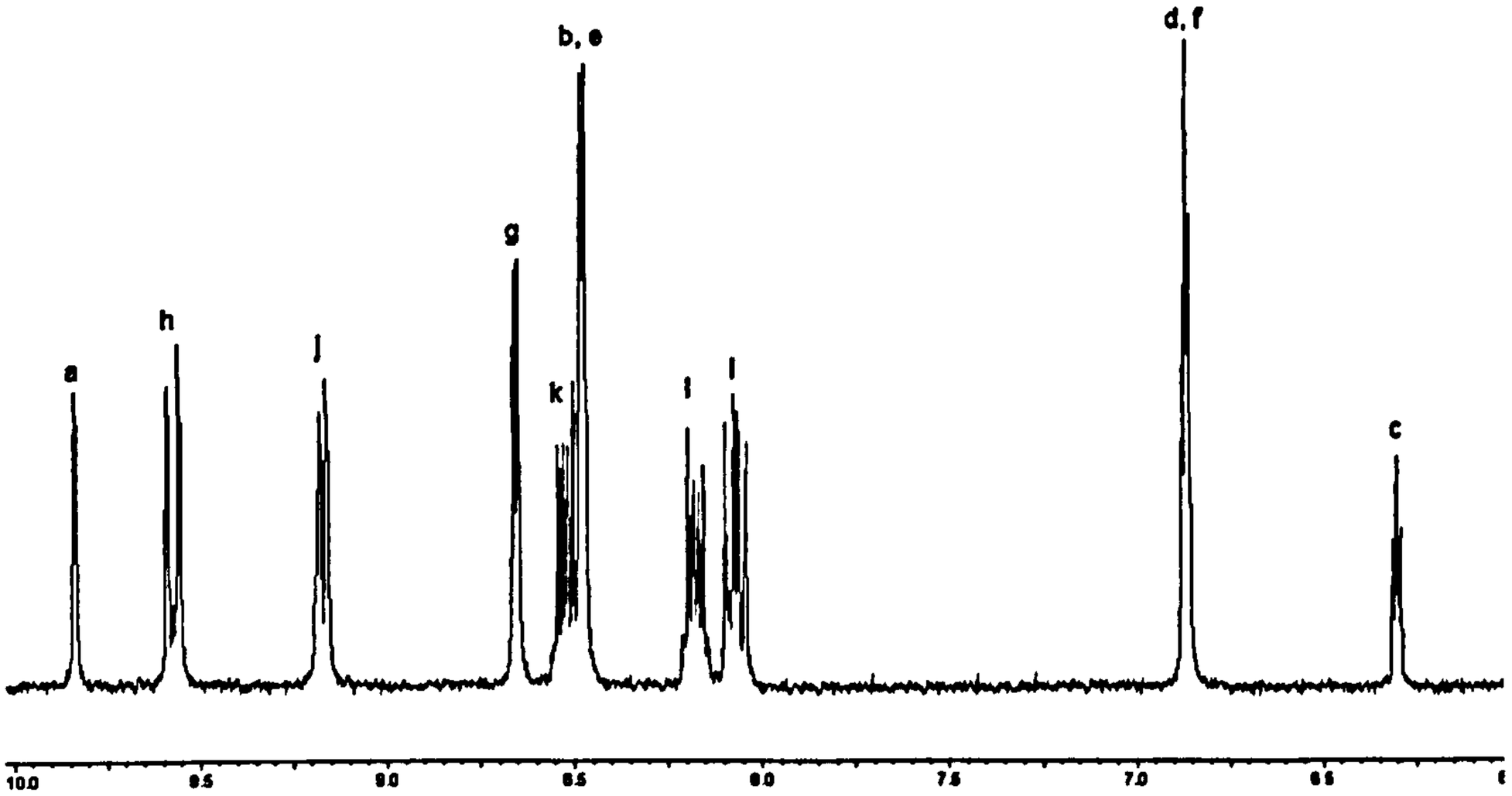

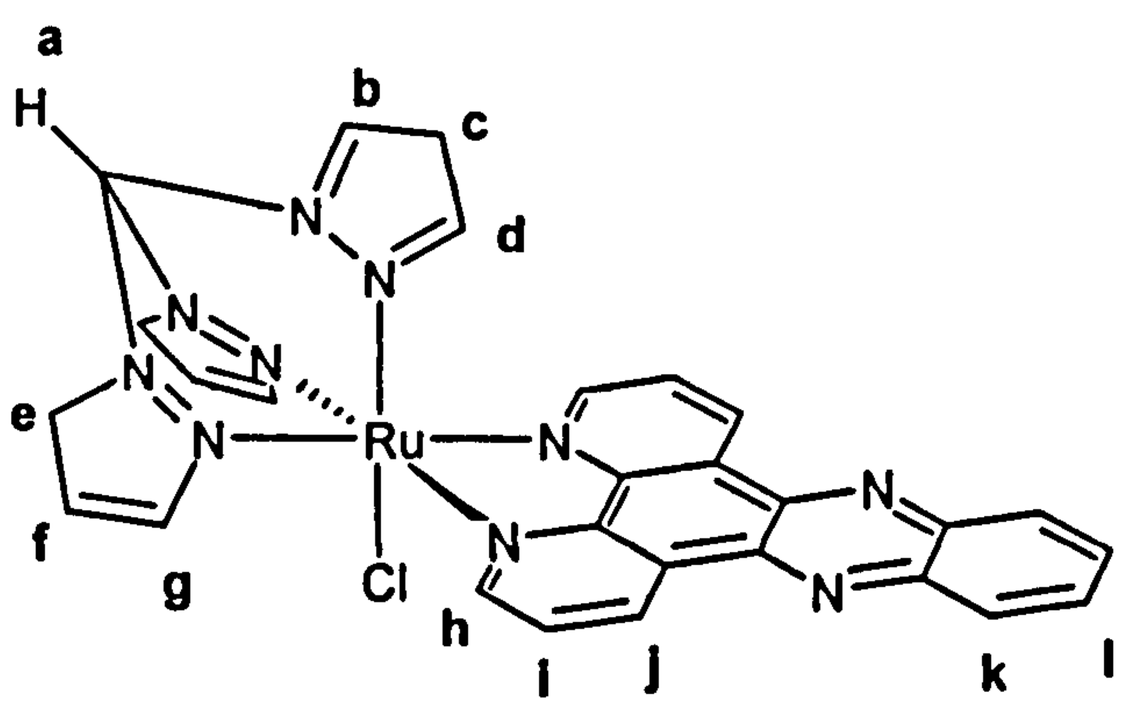

Figure 3.3:- *Downfield region of 250MHz ^1H NMR spectrum of [TpmClRudppz]$^+$ with proton labeling scheme*

The aromatic region of the 400MHz ^1H NMR spectrum in d^6-acetone of $[TpmPyRudppz]^{2+}$ is shown in Figure 3.3 with the proton labelling scheme. The COSY spectrum of the complex is shown in Figure 3.5 with cross coupling between Tpm protons (blue), dppz protons (red) and

pyridine protons (green). Again the spectrum is fairly simple due to a plane of symmetry running through the molecule. With the help of the 2D COSY spectrum the complete assignment of the protons has been achieved.

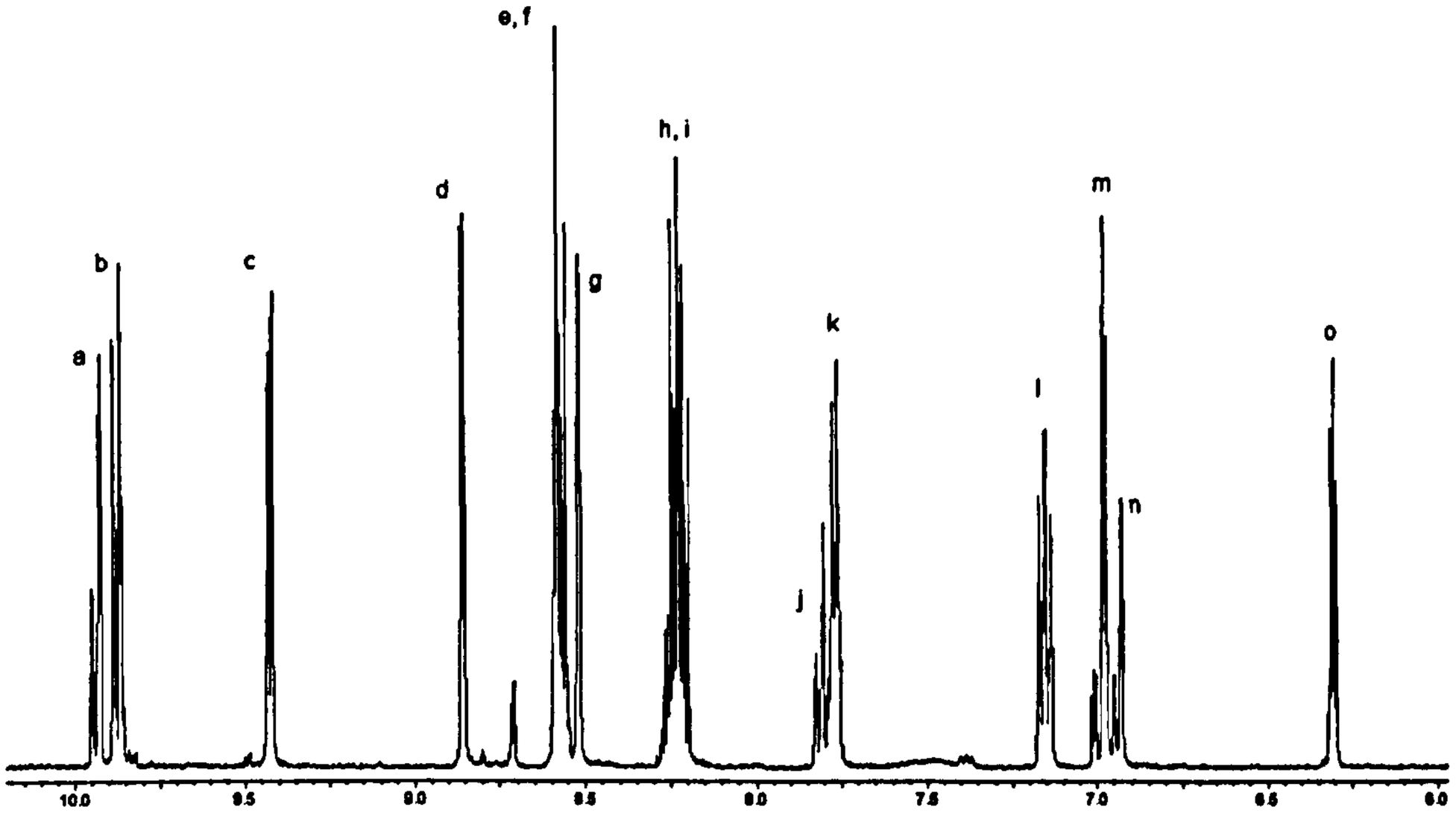

a

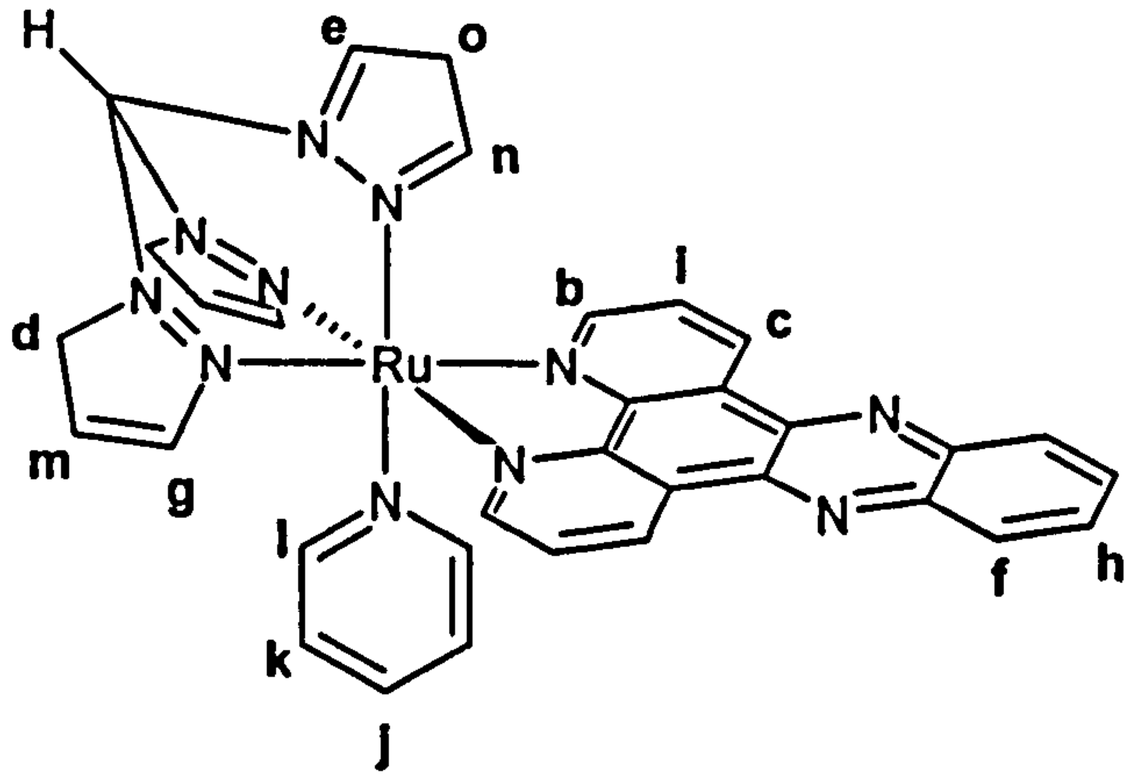

Figure 3.4:- *Downfield region of 400MHz ^1H NMR (d^6 acetone) of $[TpmPyRudppz]^{2+}$ with proton labelling scheme*

The sharp singlet at 9.93ppm can be assigned to the highly shielded methyl proton of Tpm. The six protons of the two equivalent pyrazoles occupying the equatorial positions are seen at 8.85ppm (b), 6.98ppm (c)

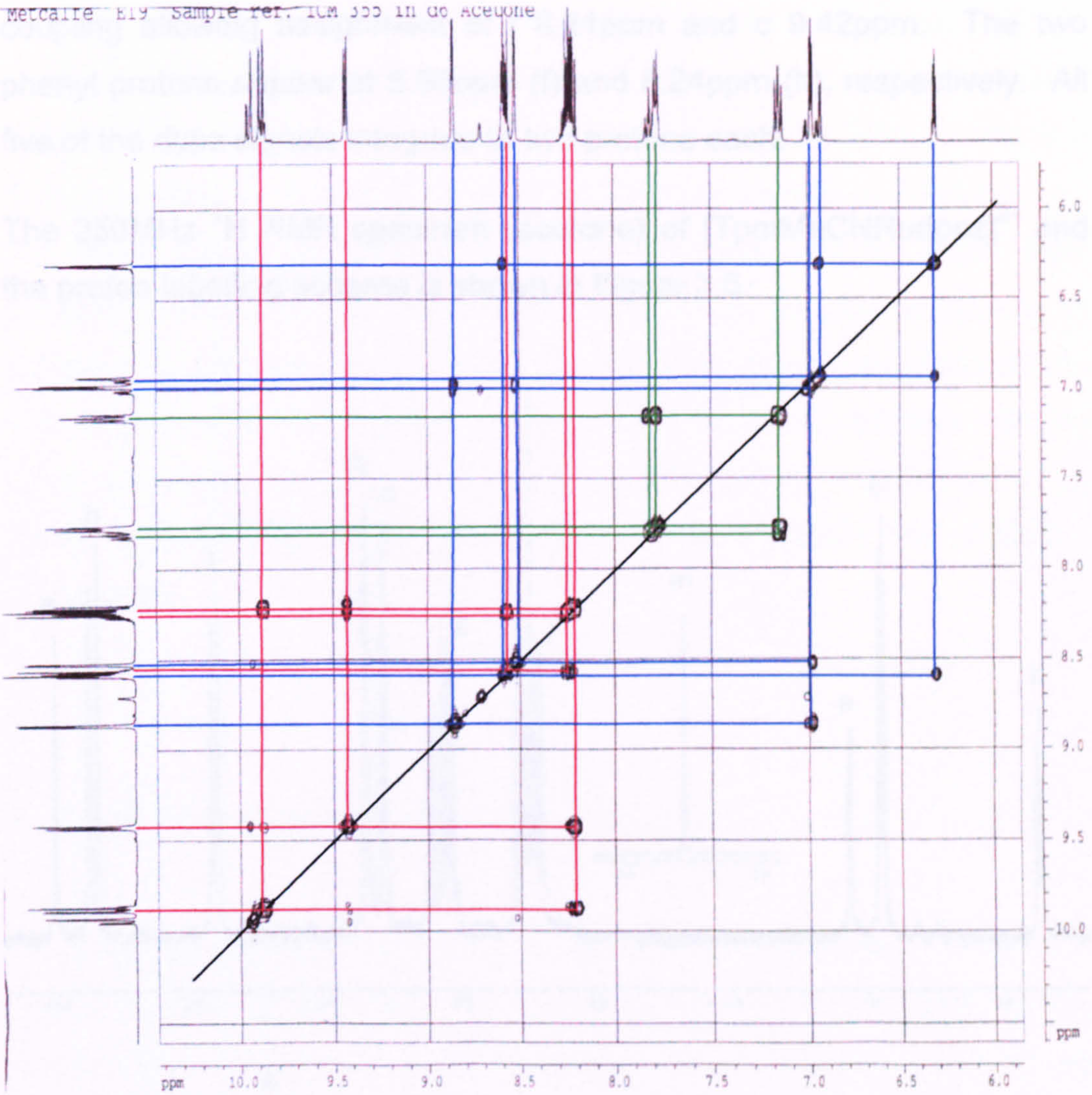

Figure 3.5:- *^{1}H COSY spectrum of [TpmPyRudppz]$^{2+}$ showing protons from Tpm (blue), dppz (red) and pyridine ligands (green)*

and 5.52ppm (d), respectively, with all three integrating to two protons each. The three protons of the pyrazole occupying the axial coordination site integrate to one proton each and appear at 8.58ppm (e), 6.30ppm (f) and 6.93ppm (g), respectively. The characteristic signals of a coordinated pyridine appear at 7.8ppm (triplet) C4 proton, integrating to one proton, 7.15ppm (triplet) C3 proton, integrating to two protons and 7.76ppm (doublet) C2 proton integrating to two protons. The proton at 9.87ppm has a large coupling constant of 9Hz and can be assigned to proton b on the phenanthroline portion of the dppz ligand with cross

coupling allowing assignment of i 8.21ppm and c 9.42ppm. The two phenyl protons appear at 8.56ppm (f) and 8.24ppm (h), respectively. All five of the dppz signals integrate to two protons each.

The 250MHz ^{1}H NMR spectrum (acetone) of $[TpmMeCNRudppz]^{2+}$ and the proton-labelling scheme is shown in Figure 3.6.

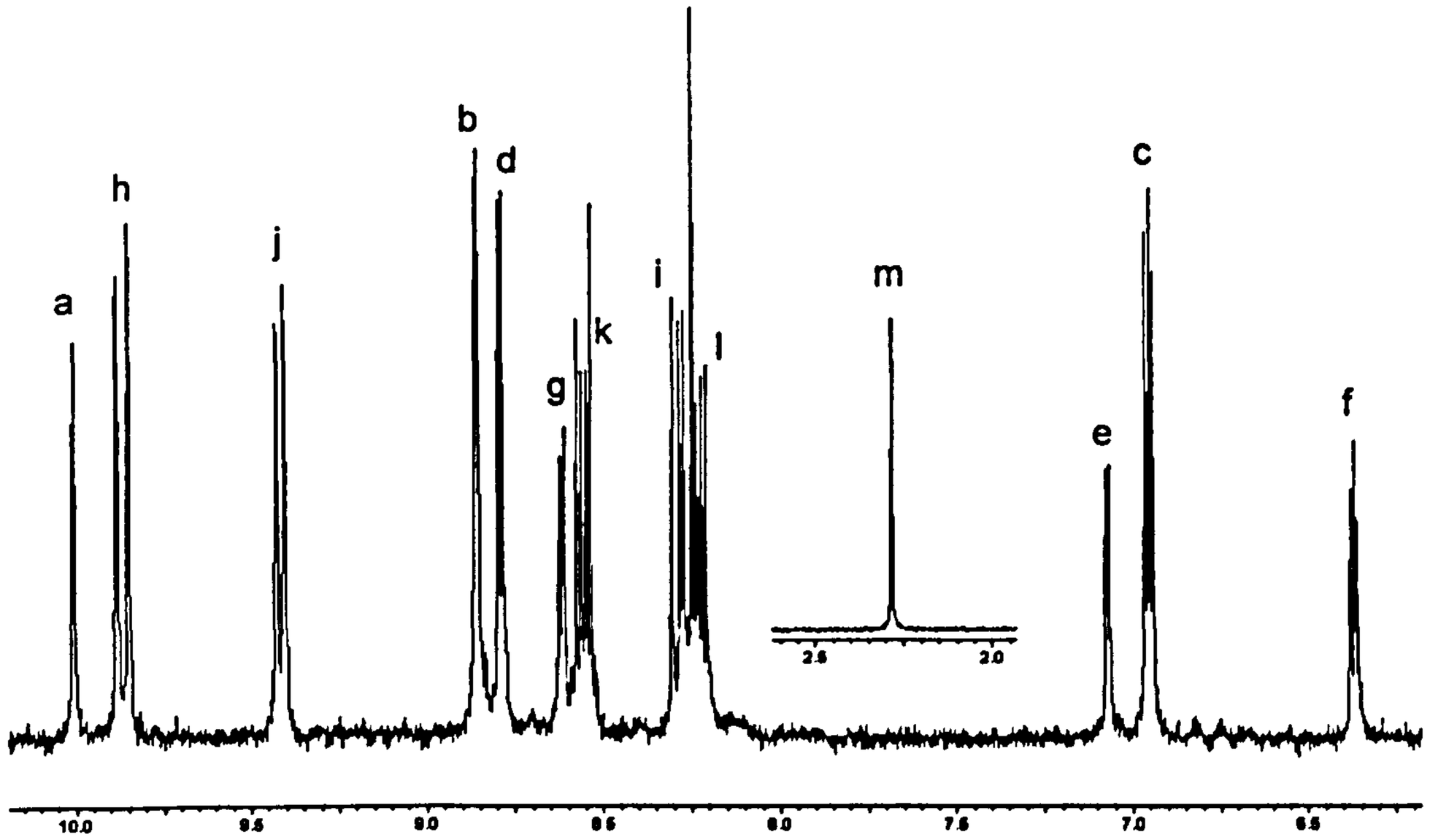

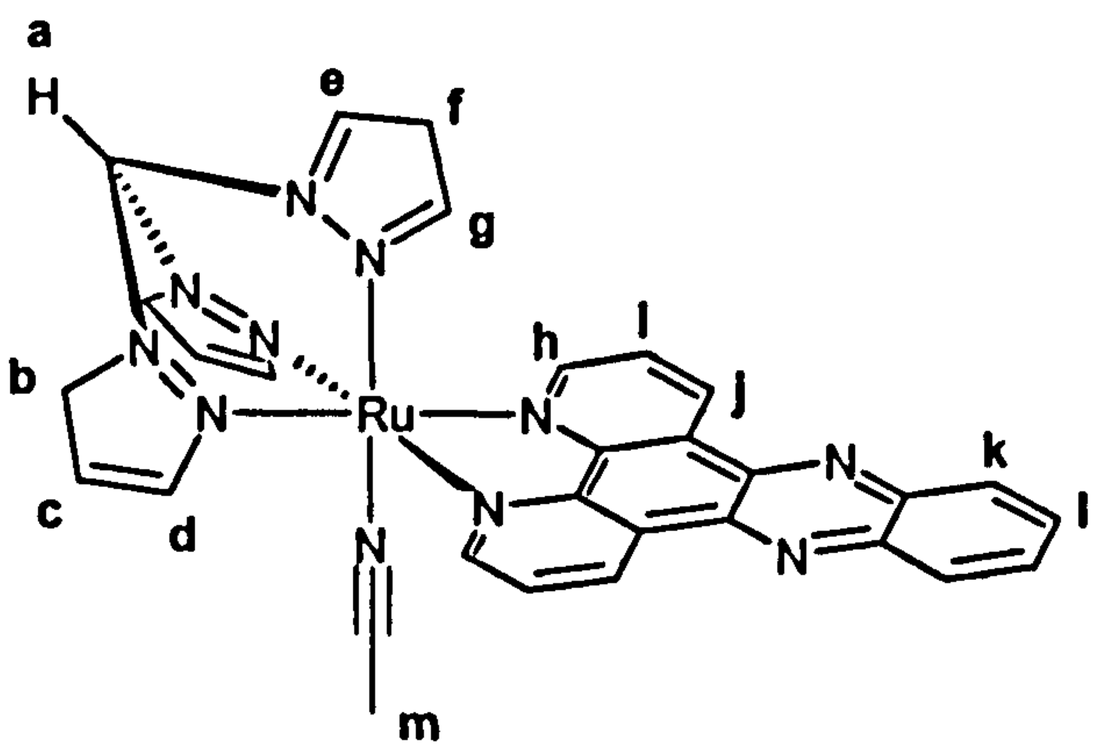

Figure 3.6:- *Downfield region of 250MHz ^{1}H NMR spectrum of $[TpmMeCNRudppz]^{2+}$ with proton labelling scheme*

The sharp singlet at 2.29ppm integrates to three protons and is in the expected position of a coordinated acetonitrile ligand (m). The singlet is

at 10.01ppm, is characteristic of the methyl proton of Tpm (a). COSY cross coupling shows the three equatorial pyrazole protons each integrating to two protons each are the double doublet at 8.80ppm (b), the double doublet at 6.95ppm (c) and the double doublet at 8.86ppm (d). The three signals integrating to one proton each are the three axial pyrazole protons and are the double 7.07ppm (e), the double doublet at 6.37ppm (f) and the double doublet at 8.62ppm (g). The characteristic 9Hz doublet at 9.87ppm is the phenanthroline proton (h) of dppz with the other two being the double doublets at 8.27ppm (i) and 9.42ppm (j). Finally the two-phenazine protons appear at 8.22ppm and 8.56ppm respectively.

3.4 Mass spectrometry data

The FAB-MS data for the Tpm monomers is summarised in Table 3.1. The data back up the structural assignments made by ^{1}H NMR, as the spectra of each of the three complexes show masses that can be assigned to the desired structures. Peaks corresponding to loss of one PF_6^- counter ion and then loss of the axial ligand are seen for each of the complexes.

Table 3.1:- *FAB-MS data for the Tpm monomers*

Compound	M/z	%	Assignment
[TpmClRudppz][PF_6]	633	100	[TpmClRudppz]$^+$
	597	30	[TpmRudppz]$^+$
[TpmPyRudppz][PF_6]$_2$	676	50	[TpmPyRudppz]$^+$
	752	100	[PyRudppz][PF_6]$_2^+$

	598	30	$[TpmRudppz]^+$
$[TpmMeCNRudppz][PF_6]_2$	784	100	$[TpmMeCNRudppz][PF_6]^+$
	638	70	$[TpmMeCNRudppz]^+$
	597	80	$[TpmRudppz]^+$

3.5 Electrochemical studies

Cyclic voltammetry (CV) was carried out on all three of the Tpm monomers. All measurements were carried out in nitrogen-saturated acetonitrile with 0.1M Bu_4NPF_6 as the support electrolyte and a saturated silver-silver chloride reference electrode. All the data were corrected for internal resistance using the AG&G electrochemistry power suite software package based upon normalization of the ferrocene oxidation couple. The CV's were recorded at $150mvs^{-1}$ and showed good reversibility with $\Delta E_p < 100mV$ and $|E_{pc} / E_{pa}| = 1$, unless otherwise stated. The data are summarised in Table 3.2.

Table 3.2:- *Electrochemistry data for the Tpm monomers*

Compound	Oxidations		Reductions		
	$E_{1/2}$ (V)	ΔE_p (mV)	$E_{1/2}$ (V)[b]		
$[TpmClRudppz][PF_6]$	+0.89	97	-0.91		
$[TpmPyRudppz][PF_6]_2$	+1.30	60	-0.87	-1.24a	
$[TpmMeCNRudppz][PF_6]_2$	+1.36	90	-0.86	-1.29a	-1.67a

[a] reductions are not fully chemically reversible, only E_p values are quoted

[b] Δ_p <100 mV for all reduction processes

All three of the Tpm complexes display oxidations associated with the $Ru^{(III)/(II)}$ couple. Figure 3.7 shows that all three of the complexes exhibits one reversible oxidation couple, however, the $E_{½}$ varies by nearly 400mV between the complexes.

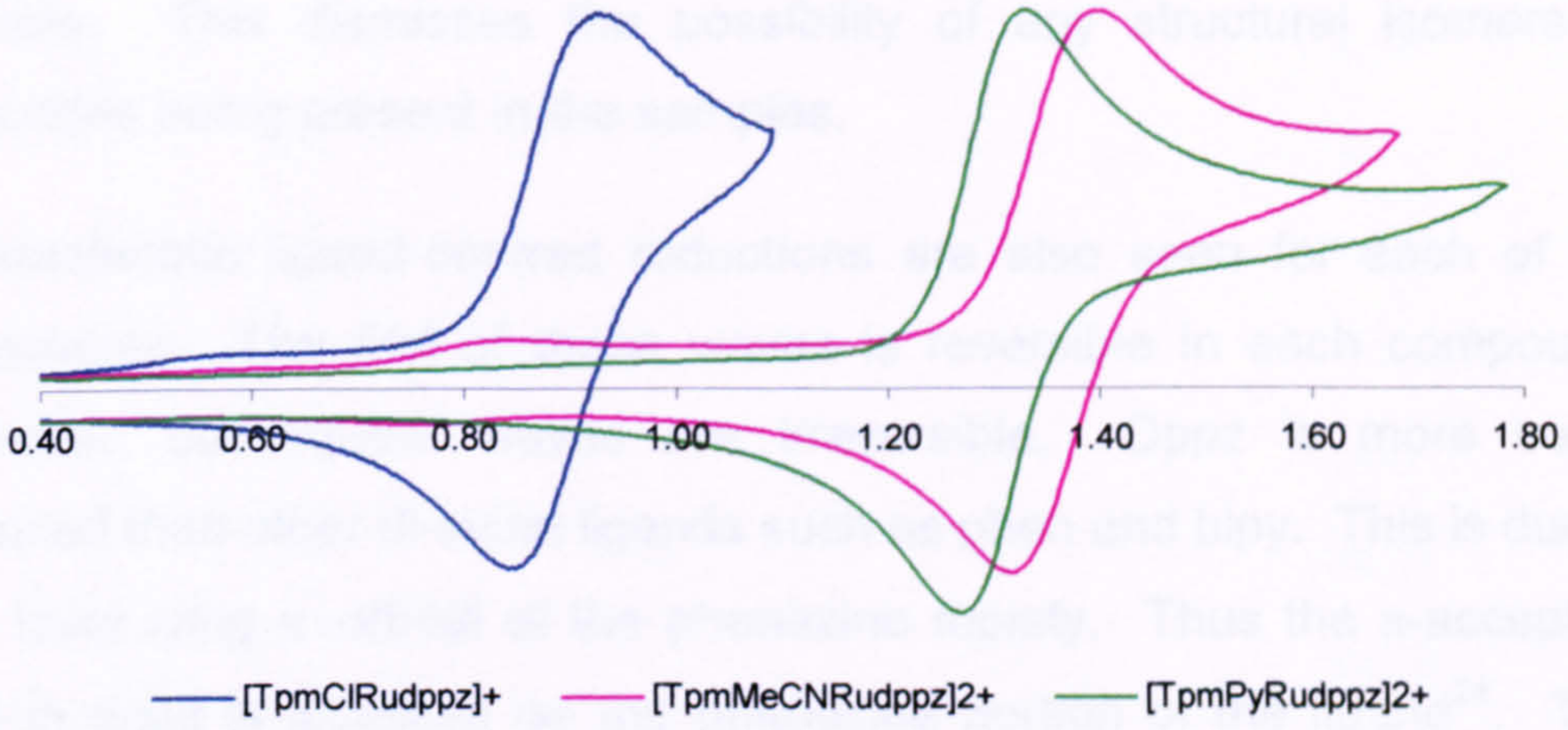

Figure 3.7:- *Electrochemical CV (current vs volts) for the Tpm monomers.*

The position of the $Ru^{(III)/(II)}$ couple is dependent upon the nature of the axial ligand on the complex. When the ligand is chloride the $Ru^{(III)/(II)}$ couple occurs at 0.89V, when it is pyridine the $Ru^{(III)/(II)}$ couple occurs at 1.30V and when the ligand is acetonitrile the $Ru^{(III)/(II)}$ couple occurs at 1.36V. This behaviour can be rationalised by the σ- and π-donor and acceptor characteristics of the axial ligand. Chloride is a good σ-donor and a good π-donor so it effectively has an induction effect pushing electrons onto the metal centre and destabilising the Ru(II) oxidation state, and at the same time stabilising the Ru(III) oxidation state, therefore the complex is relatively easy to oxidize. Pyridine is a good σ-donor ligand but also a good π-acceptor which means there is some delocalisation of the d-electrons off the metal onto the pyridine. This has the effect of stabilising the Ru(II) oxidation state and making the oxidation

more difficult. Nitriles are poorer σ-donors and better π-acceptors than pyridines so the Ru(II) oxidation state is stabilised even more, resulting in the $Ru^{(III)/(II)}$ couple being slightly more anodic than for the pyridine.

Moreover, the oxidation waves show the presence of only one oxidatively active domain, suggesting only one metal environment is present in each sample. This dismisses the possibility of any structural isomers or impurities being present in the samples.

Characteristic ligand-centred reductions are also seen for each of the complexes. The first of these waves is reversible in each compound, however, subsequent waves are irreversible. Dppz is more easily reduced than other di-imine ligands such as phen and bipy. This is due to the lover lying π^*-orbital of the phenazine moiety. Thus the π-accepting site in dppz is localised on the phenazine portion of the ligand[24]. This makes any electrochemical and photochemical processes involving this orbital very sensitive to its surroundings.

3.6 UV-Visible spectroscopic studies of the Tpm monomers

The UV-visible spectra of the complexes were recorded in acetonitrile (Figure 3.8) and the data are summarised in Table 3.3.

Table 3.3:- UV-Visible data for the Tpm monomers

Compound	λ max (nm)	ε (mol^{-1} dm^3 cm^{-1})	Assignment
$[TpmClRudppz]^+$	272	58403	$\pi \rightarrow \pi^*$
	351	14008	$\pi \rightarrow \pi^*$

	367	12534	MLCT
	445	7853	MLCT
	519	sh	MLCT
[TpmPyRudppz]$^{2+}$)	277	62553	$\pi \rightarrow \pi^*$
	312	22315	$\pi \rightarrow \pi^*$
	351	22718	$\pi \rightarrow \pi^*$
	398	9112	MLCT
	484	sh	MLCT
[TpmMeCNRudppz]$^{2+}$	277	55055	$\pi \rightarrow \pi^*$
	356	13664	$\pi \rightarrow \pi^*$
	402	sh	MLCT
	455	3804	MLCT

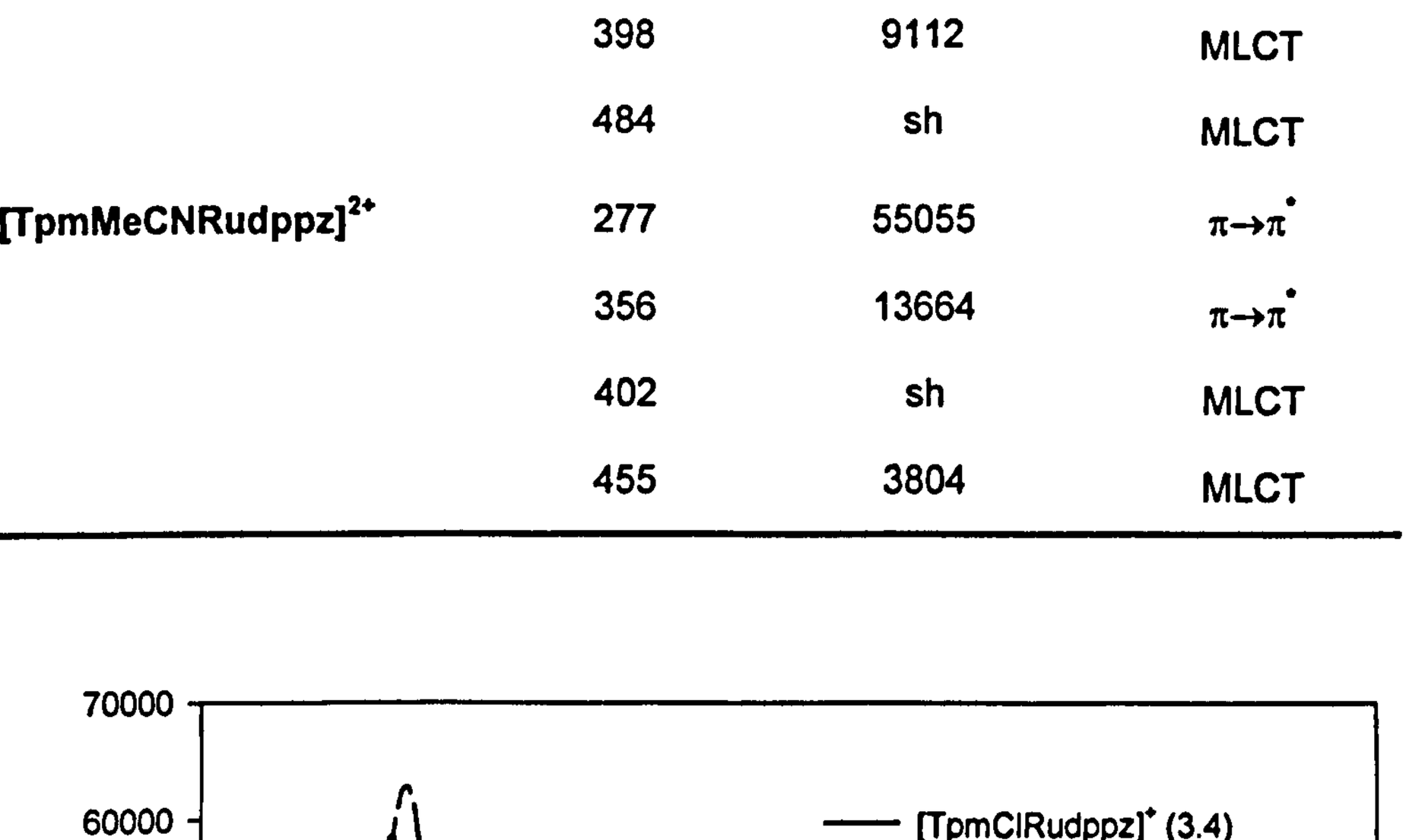

Figure 3.8:- *UV-Visible absorption spectra in acetonitrile for the three Tpm monomers*

All three spectra are dominated by the high-energy band at 270 – 290nm which correspond to the $\pi \rightarrow \pi^*$ transitions of the aromatic nitrogen donor ligands. The absorption spectrum of the free dppz ligand in DMF shows a double absorption in the near UV region with maxima at λ = 358 and 376nm. These have been assigned to $\pi \rightarrow \pi^*$ transitions of the phenazine ring in dppz[24]. Based on this, we can assign the moderately intense bands in the near UV regions of the complexes to this transition, which in the case of $[TpmClRudppz]^+$ has two maxima at 351nm and 367nm, $[TpmPyRudppz]^{2+}$ one broad maxima at 351nm and $[TpmMeCNRudppz]^{2+}$ one broad maxima at 356nm. The MLCT bands all appear in the visible region of the spectrum which is characteristic of Ru(II) complexes with polyimine ligands coordinated. The bands for $[TpmPyRudppz]^{2+}$ and $[TpmMeCNRudppz]^{2+}$, 398nm and 402nm, respectively, are both higher in energy than $[TpmClRudppz]^+$, 455nm. This correlates with the electrochemistry data, in that the HOMO on the metal centre is stabilized with respect to the LUMO which is in turn destabilised resulting in a higher energy $d\pi$ (Ru)$\rightarrow\pi^*$ MLCT transition in $[TpmPyRudppz]^{2+}$ and $[TpmMeCNRudppz]^{2+}$. The inductive effect of the chloride in $[TpmClRudppz]^+$ destabilises the HOMO and stabilises the LUMO resulting in a lower energy $d\pi$ (Ru)$\rightarrow\pi^*$ MLCT transition.

3.7 Emission spectra of the Tpm monomers

The emission spectra for the Tpm complexes $[TpmClRudppz]^+$, $[TpmPyRudppz]^{2+}$ and $[TpmMeCNRudppz]^{2+}$ were recorded in acetonitrile solution and are shown in Figure 3.10. They have been scaled to the same height for clarity.

The chloride complex $[TpmClRudppz]^+$ shows a lower energy emission at λmax_{emm} = 668nm as opposed to the pyridine complex $[TpmPyRudppz]^{2+}$

λmax_{emm} = 616nm and the acetonitrile complex $[TpmMeCNRudppz]^{2+}$ λmax_{emm} = 613nm. Excitation of each of the complexes was into the MLCT band at 446nm $[TpmClRudppz]^{+}$, 432nm $[TpmPyRudppz]^{2+}$ and 448nm $[TpmMeCNRudppz]^{2+}$, respectively. The lower energy emission of the chloride complex can again be attributed to the fact that chloride has an inductive effect. This de-stabilises the metal centred HOMO relative to the ligand centred LUMO

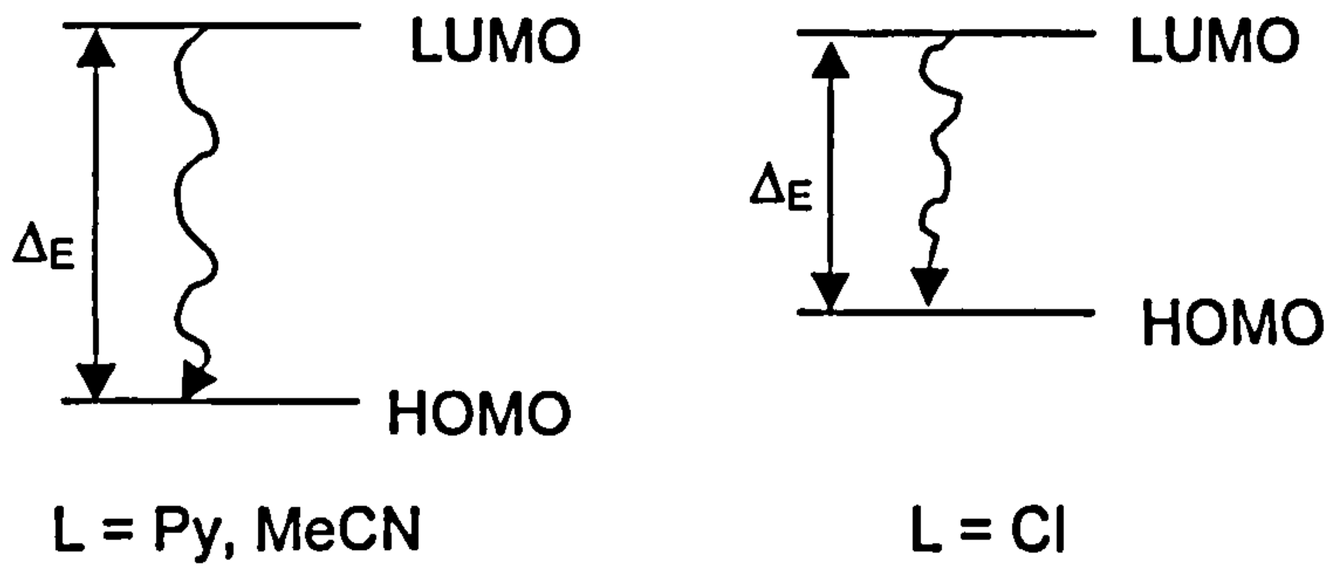

Figure 3.9:- *Schematic showing the effect of the axial ligand L on the relative energy of the metal centred HOMO relative to the ligand centred LUMO.*

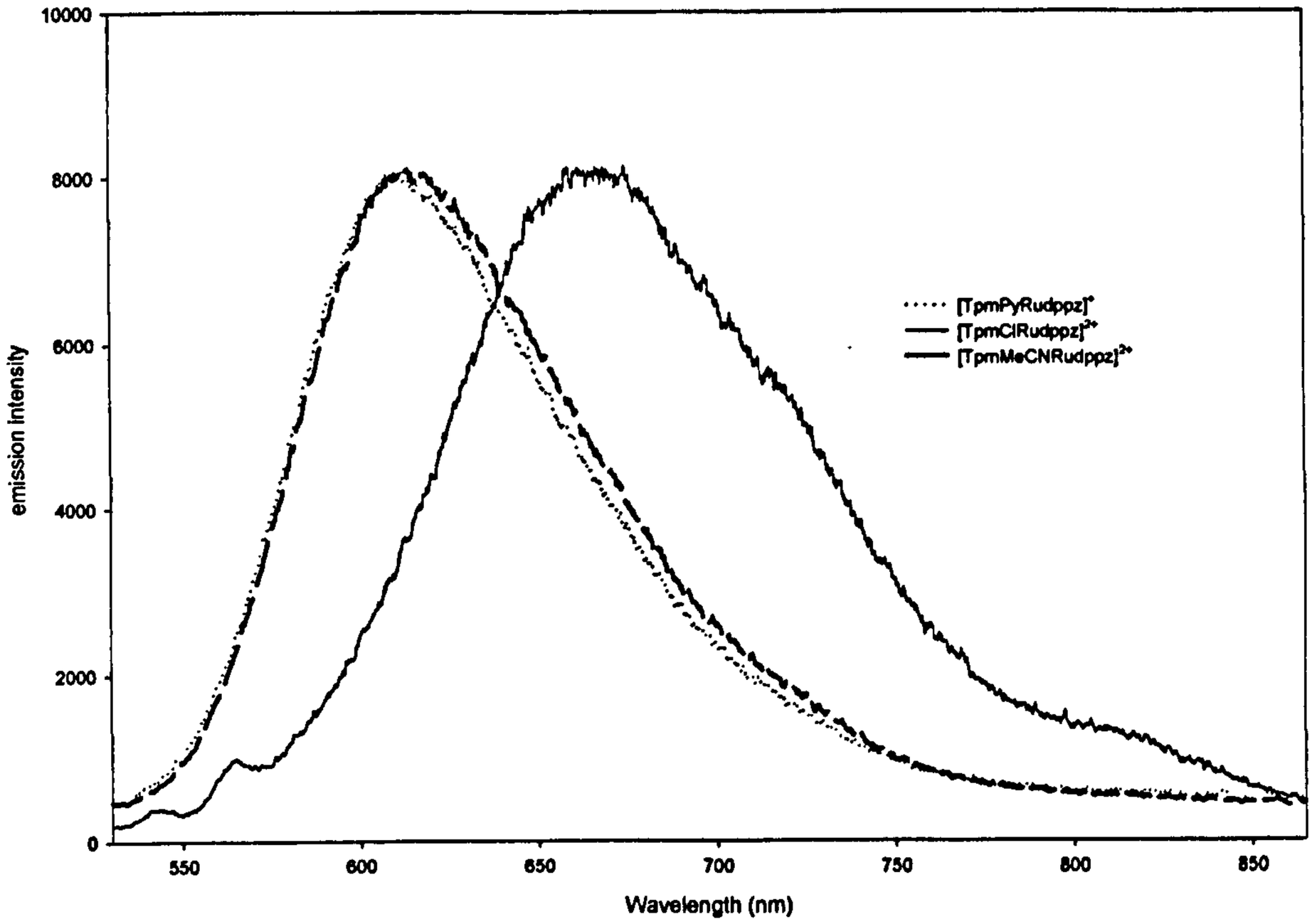

Figure 3.10:- *Luminescence emission spectra for the Tpm complexes recorded in acetonitrile solution*

3.8 Conclusions

In this chapter the synthesis and characterisation of three novel achiral ruthenium(II) complexes based upon the dppz ligand have been discussed in detail. Tpm successfully facially coordinates to the ruthenium centre and the bidentate dppz ligand protrudes away from the metal centre in the axial plane. This results in a geometry, which is ideal for allowing these complexes to interact with DNA in an intercalation mode. With the axial chloride in place the overall charge on the complex is +1, but when the chloride is substituted with either pyridine or acetonitrile the overall charge is increased to +2. This substitution

process yields products that require no further purification. As there is no spectroscopic evidence of any major change of geometry after substitution, a system has been produced which should give a direct insight into the effects of charge on the DNA binding characteristics of these complexes.

Furthermore, spectroscopic studies have revealed rich spectroscopic signatures in the form of characteristic UV-Visible and luminescence spectra, which can be used monitor DNA binding

The DNA binding studies have been undertaken and will be discussed in Chapter 5.

3.9 Further work

Now that the methodology has been developed for quick and high yield substitution of the axial chloride in $[TpmClRudppz]^+$ with pyridines and nitriles, further work could involve incorporation of bulkier ligands into this axial position. This would produce a new series of metallointercalators and would give an insight into the effect of steric bulk on the binding affinity and specificity of this new class of metallointercalators.

The intercalating ligand could also easily be changed allowing fine-tuning of the system to try and target specific DNA sequences.

There is also scope for attaching peptide sequences to this axial position resulting in novel metal peptide conjugate systems. If, as assumed, the mode on interaction of these complexes with DNA is intercalation of the dppz ligand from the major groove, the axial position is ideally orientated for delivering any recognition element or functional domain straight into the major groove itself. Figure 3.11 shows an example of a bifunctional

agent comprising of a ruthenium dppz intercalating domain tethered to a cis-platin type moiety. Compounds of this type can easily be assembled using the "mix n match" methodology developed in this chapter.

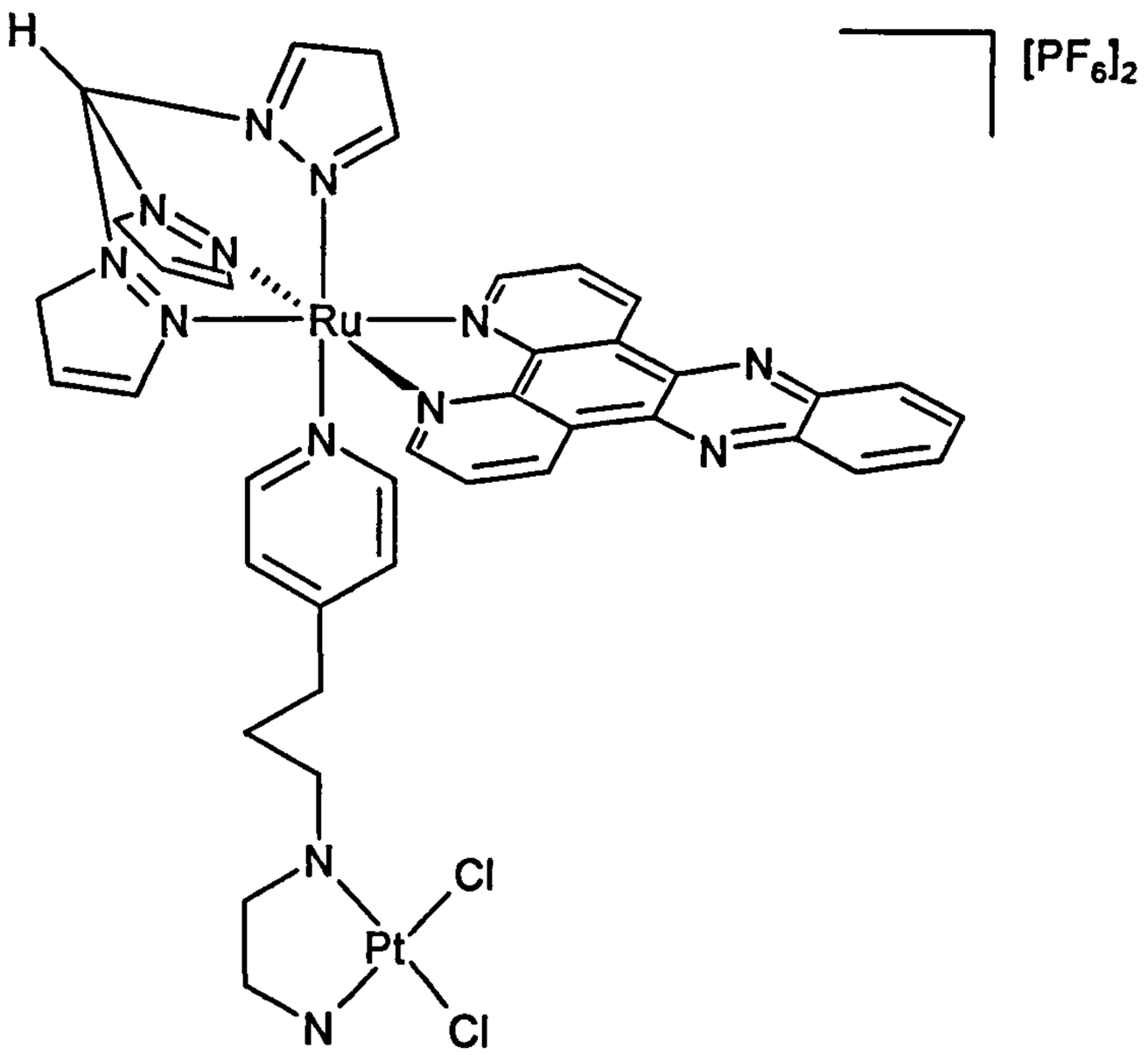

Figure 3.11:- *An example of a bifunctional DNA binding agent*

Chapter 4

Bimetallic complexes as DNA clips

4.1 Introduction

Recently a large amount of research has focused on developing bimetallic systems as DNA binding agents[75]. Kelly *et al.*. has taken the relatively weak binding system of tris phenanthroline ruthenium(II) and linked two of them together[57]. This has increased the binding affinity for DNA by over 100-fold[58]. As both of the ruthenium(II) centres are chiral joining two of them together only serves to increase the problems encountered when these chiral complexes are separated.

In this chapter we report the synthesis and characterisation of a number of bimetallic complexes incorporating the well-characterised DNA intercalating ligand dppz[21,25,113]. Two such systems have been synthesised, one rhenium(I) system and one ruthenium(II) system. Moreover, each of these systems is achiral, alleviating the need for time consuming chromatographic separation of enantiomers.

The mononuclear complex $[(CO)_3PyRedppz]^+$ has previously been shown to bind strongly to DNA[42]. The complex was synthesised with the method developed by Meyer *et al.* (Scheme 4.1)[114].

The starting material $(CO)_5ReCl$ is reacted with the dppz ligand in toluene to give the chloride complex $(CO)_3ClRedppz$. This complex is reacted with silver in acetonitrile to give the acetonitrile substituted complex

$[(CO)_3MeCNRedppz]^+$ which can then be reacted with excess pyridine to give $[(CO)_3PyRedppz]^+$ in almost quantitative yield.

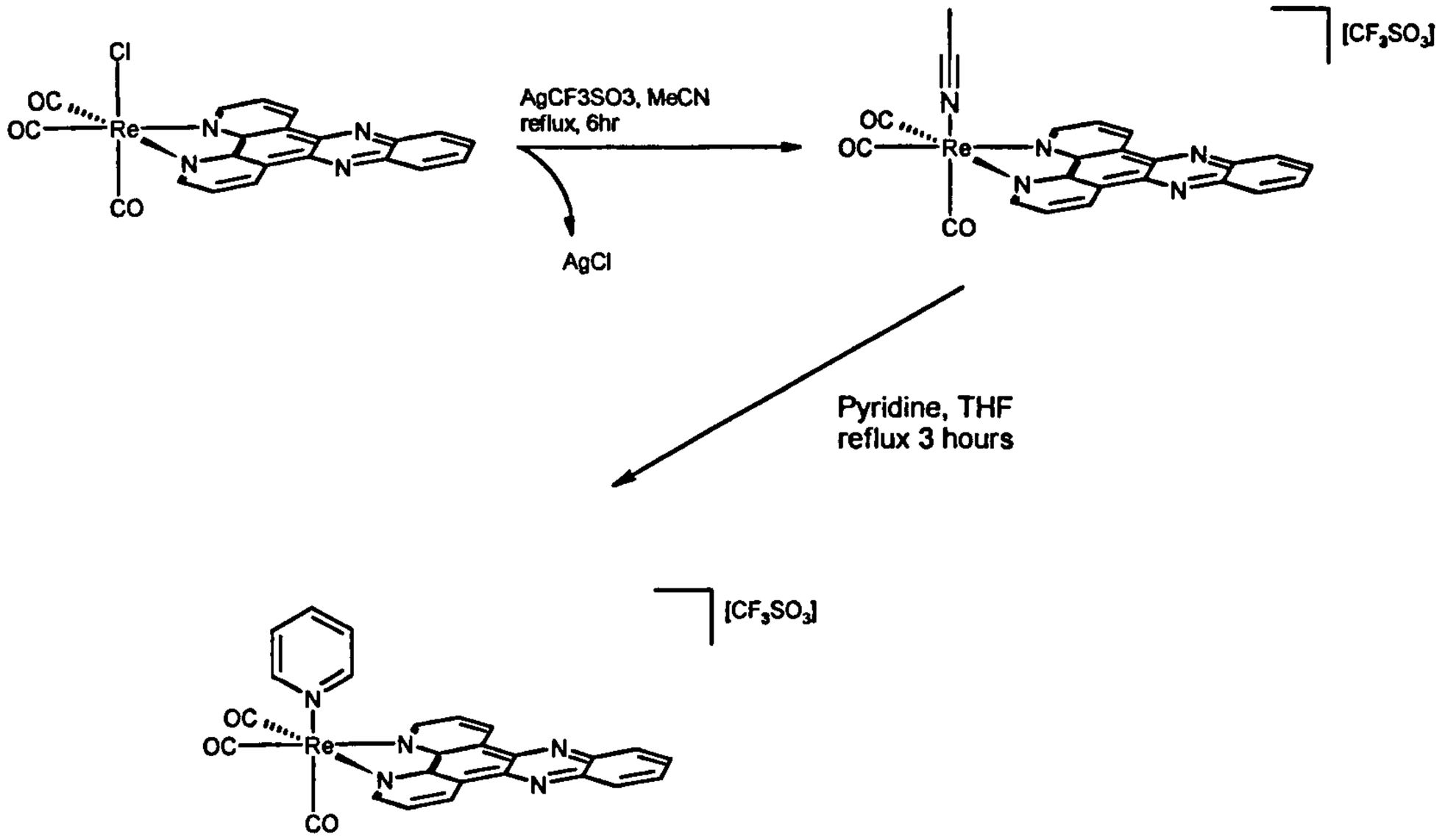

Scheme 4.1:- *Synthesis of the mononuclear dppz complexes of rhenium(I)*

In this study we aim to replace the pyridine ligand with dipyridyl ligands and hence bridge two metal centres thus forming bimetallic rhenium complexes (Figure 4.1). The bridging ligands are 1,2-di(4-pyridyl)-ethane (dpe[2]), 1,3-di(4-pyridyl)-propane (dpp[3]) and 1,5-di(4-pyridyl)-pentane dpp[5]. These ligands have 2, 3 and 5 carbon atoms, respectively, in the alkyl chain bridging the two metal centres.

Furthermore, building on the synthetic methodology developed in Chapter 3 for the synthesis of $[TpmPyRudppz]^{2+}$, we aim to replace the pyridine ligand with the di-pyridyl ligands discussed above which can bridge two metal centres producing a ruthenium DNA clip (Figure 4.1).

These bimetallic complexes should have increased binding affinity to DNA over their monometallic analogues and may bind cooperatively. They offer the possibility of producing synthetic complexes, which have a

binding affinity and specificity comparable to DNA binding protein.

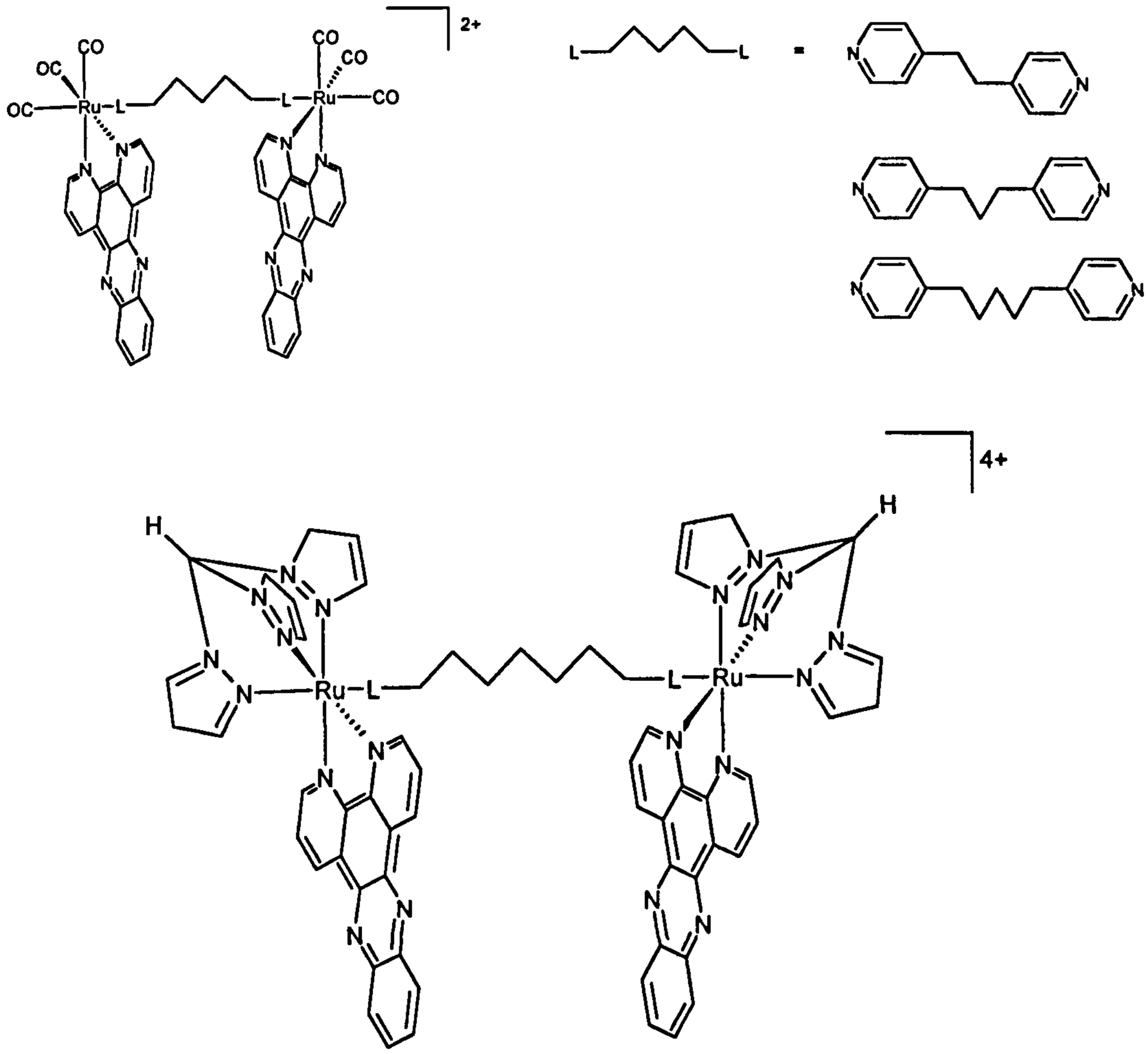

Figure 4.1:- *Bimetallic rhenium and ruthenium complexes proposed in this study*

4.2 Synthetic studies

4.2.1 Ligand synthesis

dppz[112] and Tpm[110] were synthesised as reported in previous chapters. dpe[2] and dpp[3] were obtained from commercial sources, however, dpp[5] was not commercially available.

dpp[5] **(4.1)** was synthesised as described by Jampolsky *et al.*[115] by de-protonation of 4-picoline with potassium amide in liquid ammonia and subsequent reaction with 1,5-dibromopentane (Scheme 4.2).

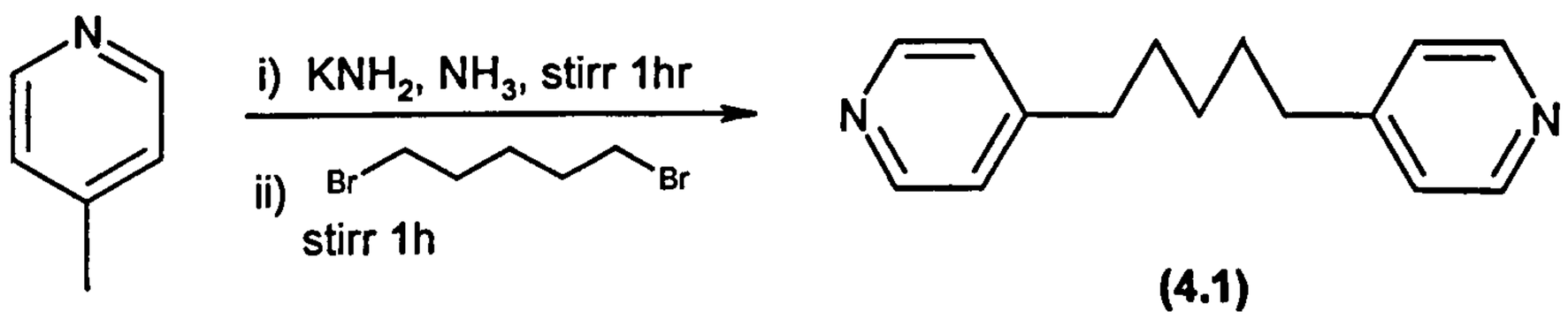

(4.1)

Scheme 4.2:- *Synthesis of 1,5-di(4-pyridyl)-pentane (dpp[5])* ***(4.1)***

4.2.2 Synthesis of the rhenium(I) clips

Initial attempts at the synthesis of the bimetallic rhenium clips were attempted in one step, in an analogous way to the synthesis of $[(CO)_3PyRedppz]^+$ **(4.4)**. The complex $[(CO)_3MeCNRedppz]^+$ **(4.3)** was synthesised as outlined previously[42,114] and then refluxed with half an equivalent of the appropriate di-pyridyl linker in THF (Scheme 4.3). Even after 4 days refluxing no reaction had taken place. Separate studies with the monomer showed that at least a three-fold excess of pyridine was needed for the successful substitution of the acetonitrile ligand.

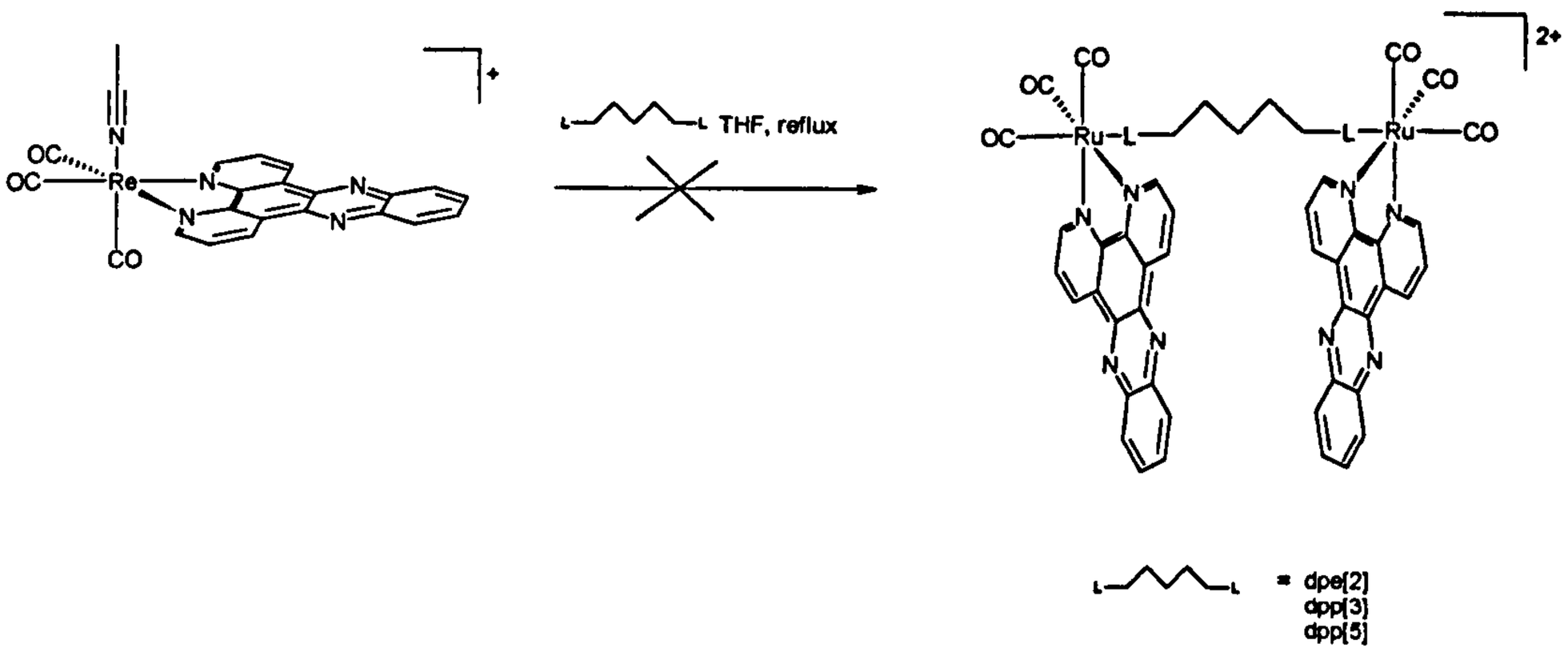

Scheme 4.3:- *Attempted one-step synthesis of rhenium(I) bimetallics*

Searching the literature we found a procedure adopted by Wolfgang *et al.*[116] for bridging two mono-valent metal centres with di-pyridyl type ligands. This method relies on the fact that only mono-cationic species are soluble in dichloromethane solutions. As soon as the ligand bridges the two metal centres, resulting in a di-cationic species, the complex precipitates. This method affords tight control of the stoichiometry and also analytically pure products.

When $(CO)_5ReCl$ is reacted with $AgCF_3SO_3$ in dichloromethane for 3 hours the chloride is removed and precipitated as silver chloride. Upon addition of ½ equivalent of the required dipyridyl linker with stirring at room temperature in the dark for four days the bimetallic species $[\{(CO)_5Re\}_2L\text{-}L]^{2+}$ (L= dpe[2] **(4.5)**, dpp[3] **(4.6)** or dpp[5] **(4.7)**) is precipitated (Scheme 4.4).

These clip precursors were reacted with an excess of dppz in nitromethane at 70°C for 4 days. This resulted in the coordination of a dppz ligand to each of the rhenium centres forming the bimetallic clips **4.8-4.10)** (Scheme 4.5).

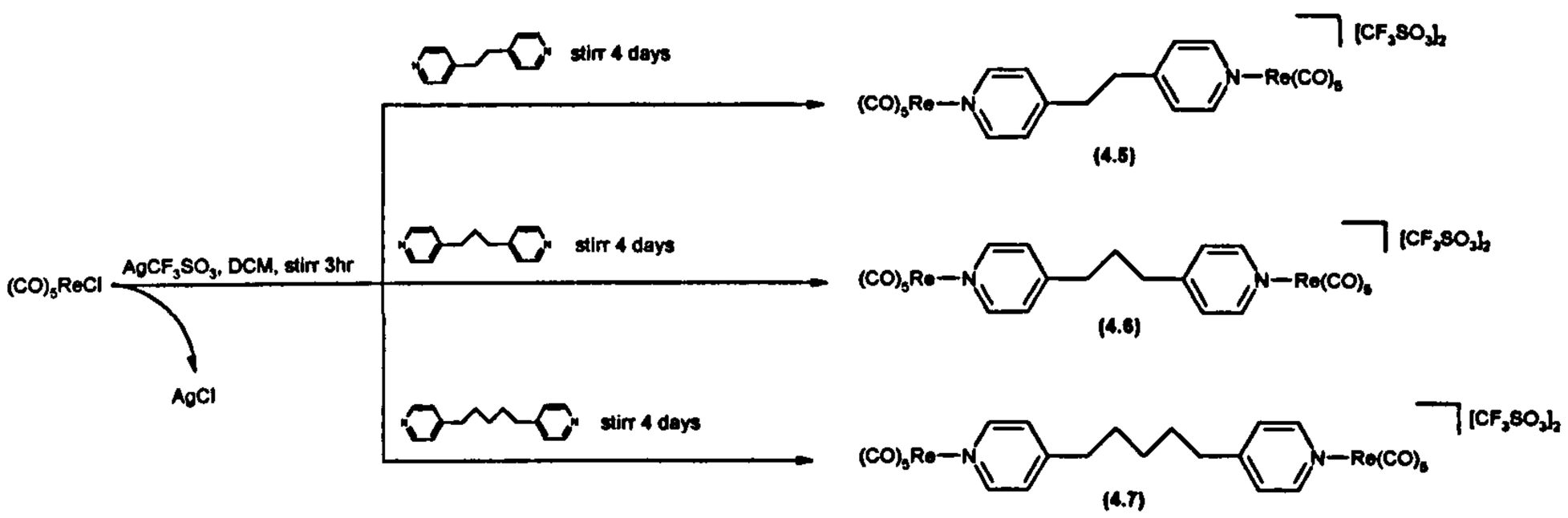

Scheme 4.4:- *Synthesis of the bimetallic clip precursors* ***(4.5-4.7)***

The crude products were collected by reducing the reaction mixture and flash precipitated by addition of diethylether. The clips **(4.8)** and **(4.9)** were purified by size exclusion chromatography on Sephadex LH-20 resin. 3:1 Toluene to acetonitrile was used as the eluent and the first band collected from the column contained the desired product. Clip **(4.10)** would not separate from impurities with size exclusion chromatography so purification was achieved with successive recrystalisations from acetone/water mixtures. All three of the clips were bright yellow solids and were characterised by ^{1}H NMR and electrospray mass spectrometry.

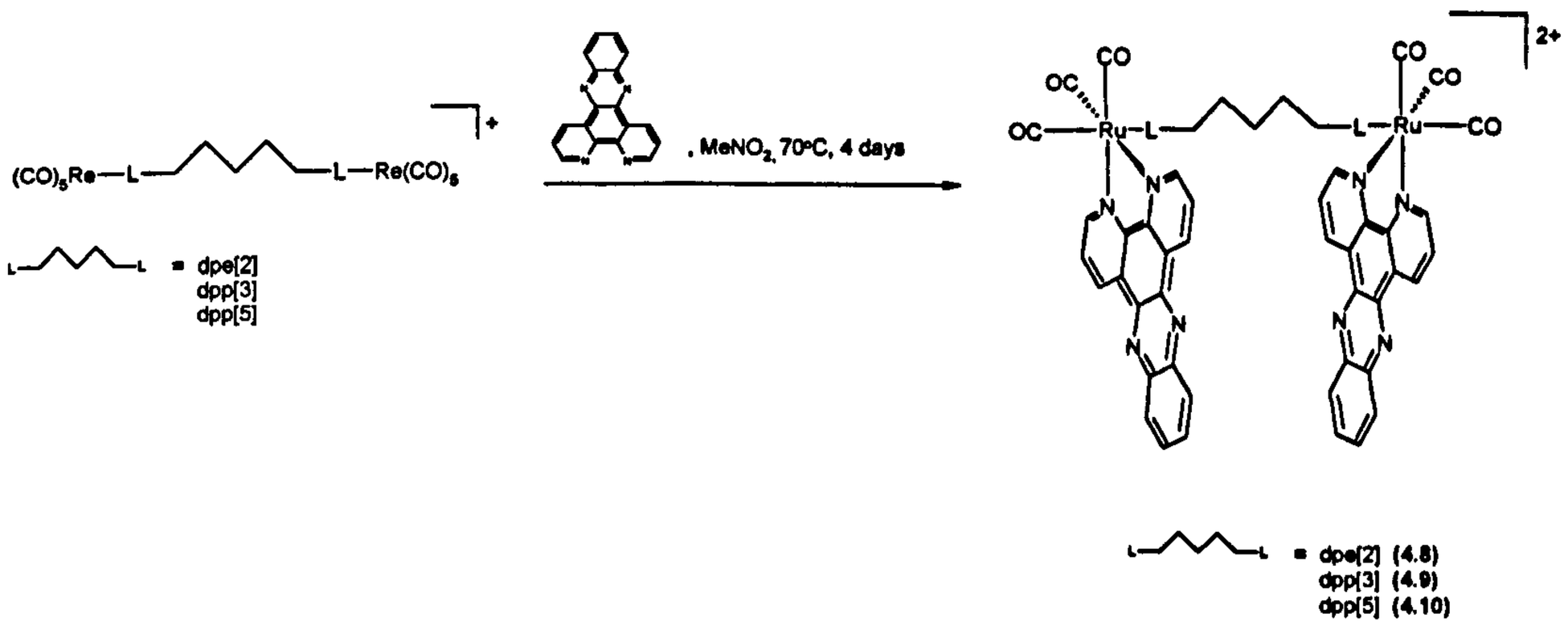

Scheme 4.5:- *Synthesis of the bimetallic rhenium clips* ***(4.8-4.10)***

4.2.3 Synthesis of the ruthenium(II) clips

Using methodology developed in Chapter 3 for the synthesis of $[TpmPyRudppz]^{2+}$ we replaced pyridine with dpp[5] in order to attempt the synthesis of the bimetallic ruthenium complex $[\{TpmRedppz\}_2dpp[5]]^{4+}$ in one step. $[TpmClRudppz]^{+}$ was reacted with silver nitrate in 1:1 $EtOH/H_2O$ for three hours to remove the axial chloride. Half an equivalent of dpp[5] was then added with continued refluxing. However, as in the rhenium case it was found that this reaction only works well when an excess of the pyridine is present and none of the bimetallic product was formed (Scheme 4.6).

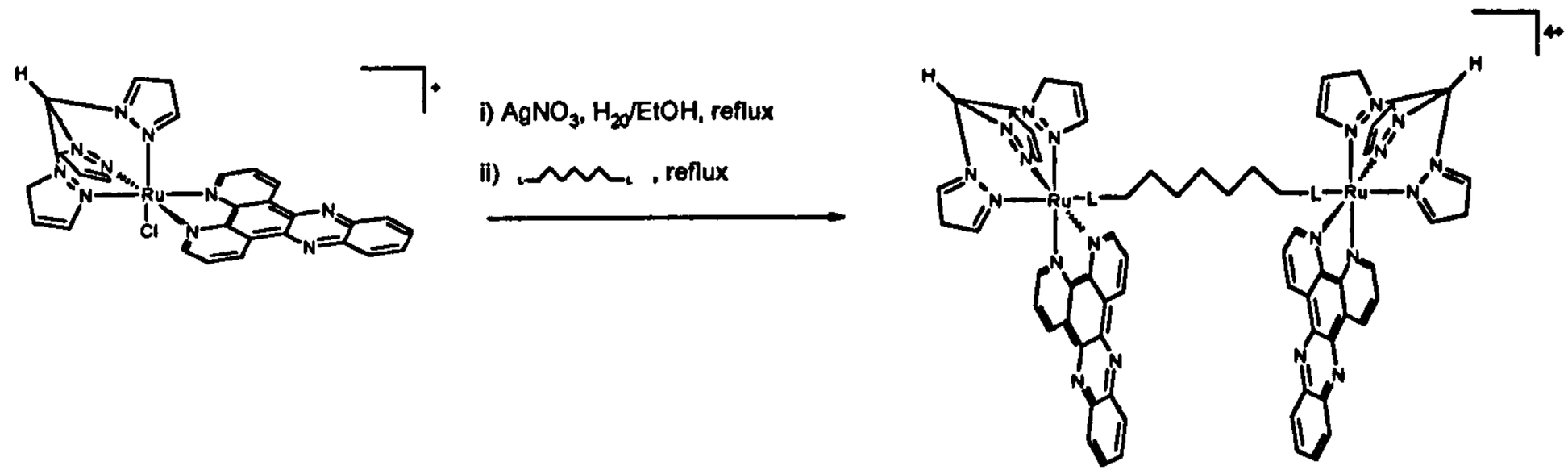

Scheme 4.6:- *The attempted synthesis of ruthenium(II) bimetallics in one step.*

It was clear that as in the case of the rhenium bimetallics the synthesis had to be carried out in two steps.

$[TpmClRudppz]^{+}$ **(3.5)** was reacted with $AgNO_3$ for three hours in refluxing ethanol/water, resulting in removal of the axial chloride precipitation as AgCl. A 10-fold excess of dpp[5] **(4.1)** was added with further refluxing for 10 hours which lead to the mono-coordination of dpp[5] to the axial position (Scheme 4.7) **(4.11)**.

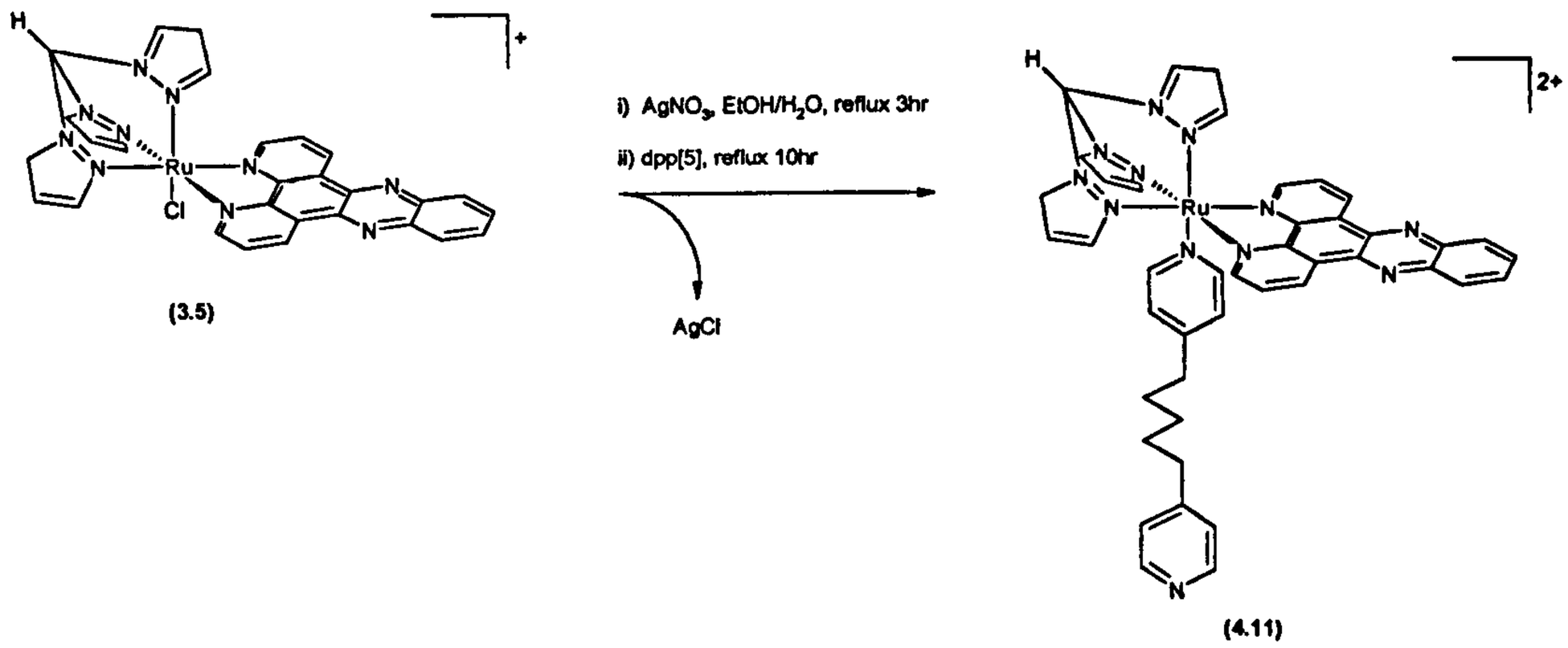

Scheme 4.7:- *Synthesis of [Tpmdpp[5]Rudppz]$^{2+}$* ***(4.11)***

The red orange solution was then concentrated and [Tpmdpp[5]Rudppz]$^{2+}$ **(4.11)** was isolated as a PF_6^- salt by addition of NH_4PF_6. Bu_4NCl was added to a solution of **(4.11)** in acetone, which leads to its precipitation as a chloride salt, allowing the excess ligand to be washed away with acetone. Conversion of **(4.11)** back to the PF_6^- salt and subsequent drying affects a 95% yield of **(4.11)**, which is analytically pure by ^1H NMR, FAB-MS and accurate mass determination.

The final bimetallic was assembled as follows. [TpmClRudppz]$^+$ **(3.5)** was reacted with $AgNO_3$ for three hours in refluxing ethanol/water as before, thus abstracting the axial chloride. The AgCl precipitate was remove by centrifugation and the solution was added dropwise to a two-fold excess of [Tpmdpp[5]Rudppz]$^{2+}$ **(4.11)** which was refluxing in ethanol/water. The dropwise addition coupled with the two-fold excess of [Tpmdpp[5]Rudppz]$^{2+}$ ensured that the pendant pyridine was always in a large excess relative to the other half of the clip allowing the reaction to take place (Scheme 4.8).

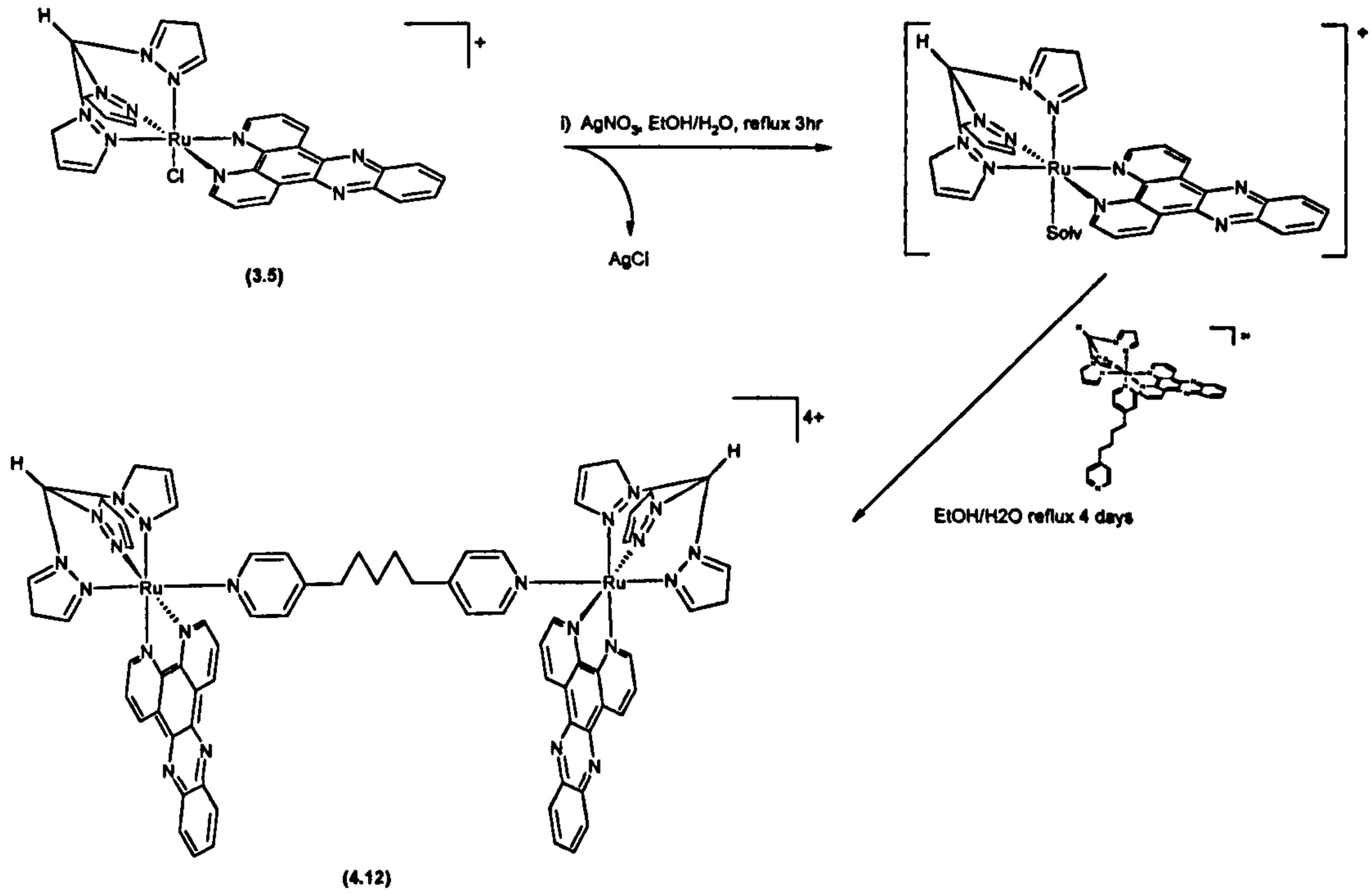

(3.5)

(4.12)

Scheme 4.8:- *Synthesis of the bimetallic ruthenium(II) clip* ***(4.12)***

The burgundy red solution was concentrated and the crude products were isolated as PF_6^- by addition of NH_4PF_6. The products were purified by ion exchange column chromatography on Sephadex CM-C25 ion exchange resin. Several monometallic complexes were eluted off the column with low salt eluents but were not characterised. The product **(4.12)** was eluted off the column with 0.1M NaCl in 5:3 H_2O/acetone and was recovered as a PF_6^- salt in an overall yield of 14%. The reaction was not optimised for yield.

The low yield is probably due to the excessive length of the reaction time. The reaction proved difficult to monitor by TLC as all of the products and reactants ran with very similar R_f values. Reducing the reaction time to a few hours could dramatically improve the yield, as the redox active dppz ligand is prone to decomposition upon prolonged reaction.

4.3 ^{1}H NMR spectroscopic studies

The 250MHz ^{1}H NMR spectra of the di-rhenium clip precursors were recorded in d^6 acetone and the data is shown in Table 4.1. The spectra were well-resolved showing peaks only associated with the complex. The two protons on the pyridine ring were both doublets and the one with the greatest downfield shift and large coupling constant (9Hz) was assigned to proton a adjacent to the ring nitrogen. The first alkyl proton C was in each case a triplet integrating to four protons. The other alkyl protons d and e, where present were multiplets integrating to four and two protons respectively.

Table 4.1:- *^{1}H NMR data for the dirhenium clip precursors*

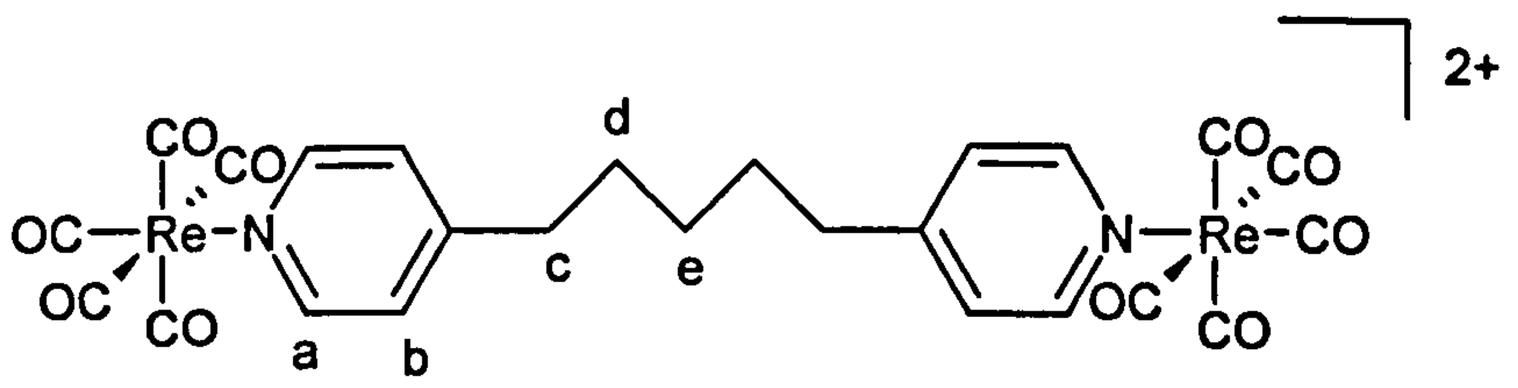

Complex	Chemical shift (ppm)				
	a	b	c	d	e
$[\{(CO)_5Re\}_2dpe[2]]^{2+}$	9.21	7.74	3.25	-	-
$[\{(CO)_5Re\}_2dpp[3]]^{2+}$	9.17	7.67	2.93	2.07	-
$[\{(CO)_5Re\}_2dpp[5]]^{2+}$	9.16	7.62	2.84	1.74	1.49

The rhenium clips themselves were equally well resolved and their spectra recorded again in d^6-acetone essentially showed the characteristic dppz signals as well as the pyridyl signals seen above for the linkers. The full assignment of the signals were made with the help of

a COSY spectrum (not shown), the data are summarised in Table 4.2.

Table 4.2:- *^{1}H NMR data for the rhenium(I) clips recorded in d^6 acetone*

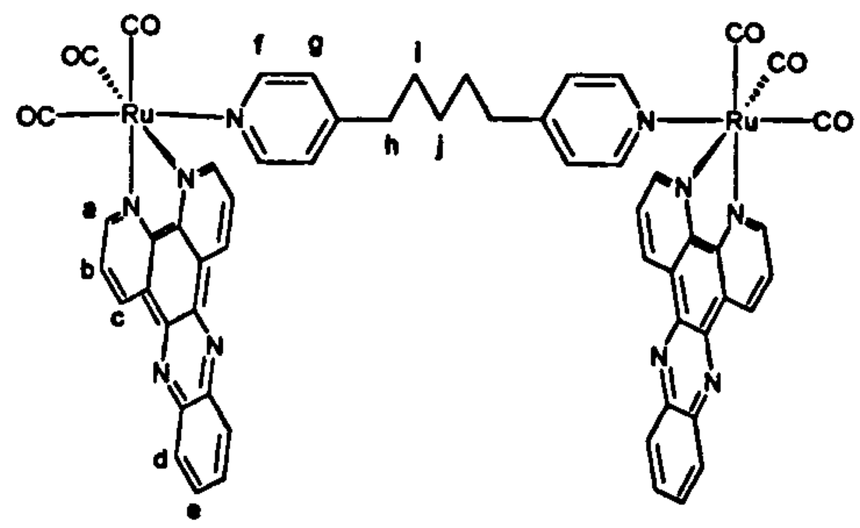

Complex	Chemical shift (ppm)									
	a	b	c	d	e	f	g	h	l	j
[{(CO)$_3$Redppz}dpe[2]]$^{2+a}$	9.85	8.17	9.76	8.50	8.38	8.41	7.17	2.63	-	-
[{(CO)$_3$Redppz}dpp[3]]$^{2+}$	9.71	8.10	9.88	8.39	8.23	8.46	7.13	2.39	1.55	-
[{(CO)$_3$Redppz}dpp[5]]$^{2+}$	9.91	8.16	9.97	8.45	8.40	8.47	7.16	2.37	1.31	1.10

[a] spectrum recorded in d^6-DMSO

The 400MHz ^{1}H NMR spectrum of [Tpmdpp[5]Rudppz]$^{2+}$ is shown in Figure 4.2. The spectrum is well resolved and is fairly simple due to the symmetry of the molecule. The 2D COSY spectrum (Figure 4.3) shows the cross coupling between the different ligand sets, Tpm (blue), dppz (red) and dpp[5] (green).

The characteristic deshielded methane proton of the Tpm moiety is found as a singlet at 9.91ppm. Cross coupling analysis shows the pyrazole protons appearing at 8.53ppm (p), 6.30ppm (o) and 6.92ppm, all one hydrogen for the axial pyrazole and 9.89ppm (d), 6.99ppm (m) and 8.46ppm (f), all two hydrogens for the two equatorial protons. The phenanthroline protons of dppz appear at 9.89ppm (b), 8.23ppm (i) and 9.42ppm (c) all three integrating to two protons each. The two phenazine protons appear at 8.55ppm and 8.25ppm. Due to coordination of one of

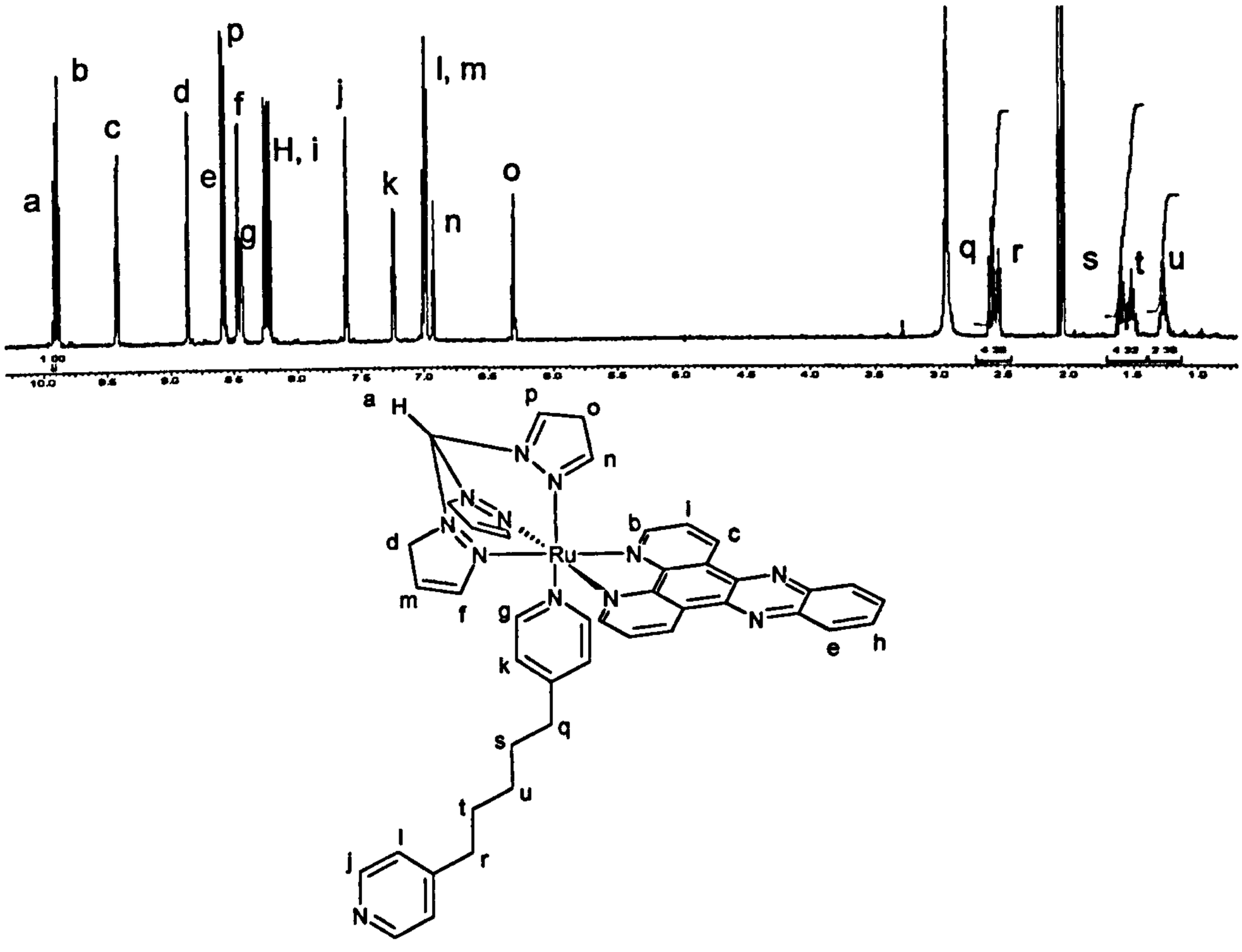

Figure 4.2:- *^1H NMR spectrum (d^6-acetone) of [Tpmdpp[5]Rudppz]$^{2+}$ with proton labelling scheme*

the pyridine moieties of the dpp[5] ligand to the ruthenium centre, all 7 sets of the protons are rendered inequivalent. The four aromatic sets appear at 8.44ppm (g) and 7.61ppm (j). The large coupling constant indicating these protons reside adjacent to ring nitrogens, and the one with the furthest downfield shift was assumed to be coordinated to the ruthenium. The other aromatic protons appear at 7.23ppm (k) and 7.02ppm (l). The two closely positioned triplets at 2.55ppm and 2.60ppm are protons p and q on the alkyl linker. Protons r and s appear as multiplets at 1.59ppm and 1.52ppm. The central alkyl proton t appears as a multiplet at 1.26ppm.

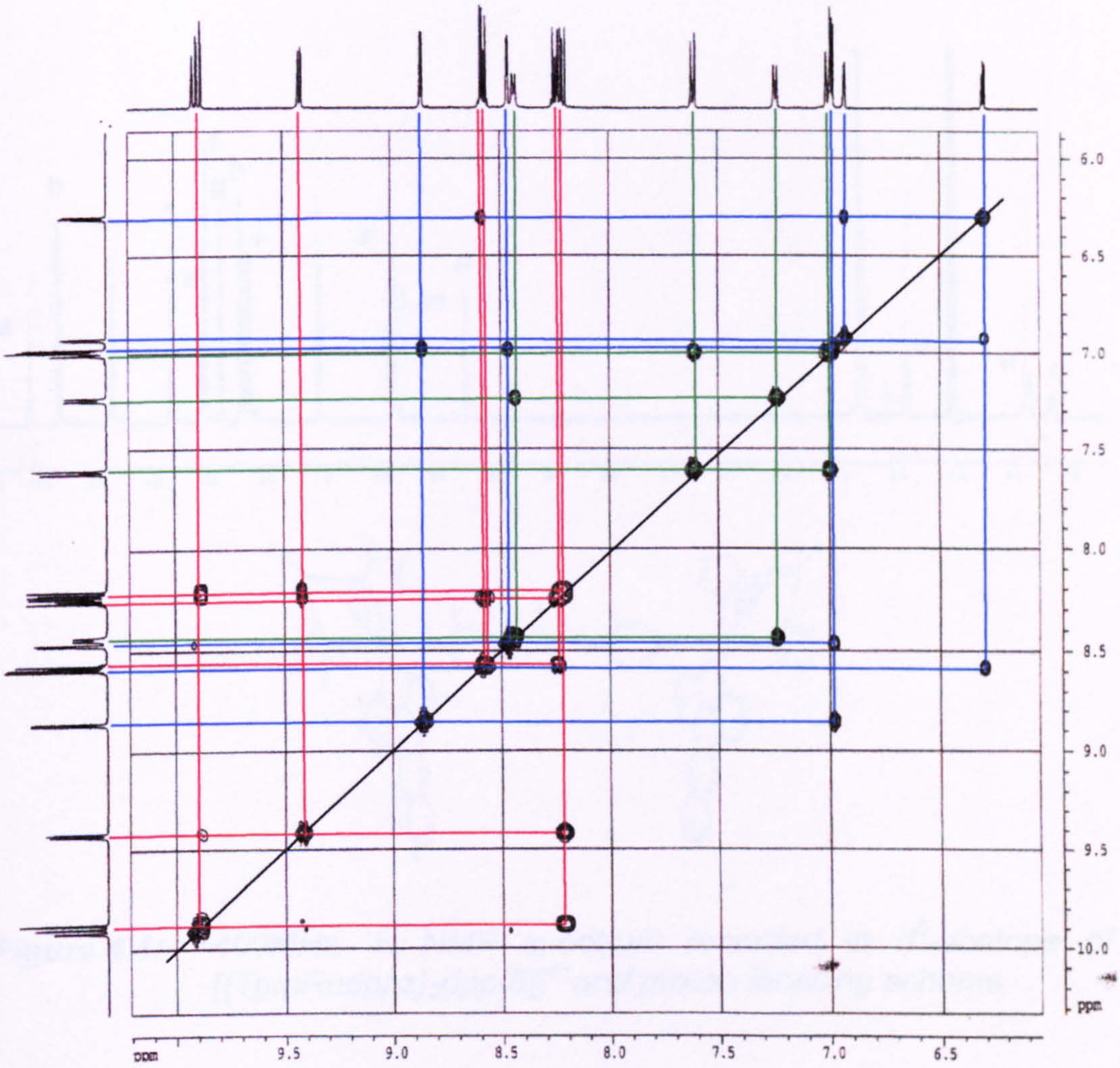

Figure 4.3:- *^1H COSY spectrum of [Tpmdpp[5]Rudppz]$^{2+}$ recorded in d^6-acetone*

The ^1H NMR spectrum recorded in d^6-acetone of the bimetallic ruthenium(II) clip $[\{TpmRudppz\}_2dpp[5]]^{4+}$ is shown in Figure 5.5. The spectrum was fully assigned with the help of a 2D COSY spectrum shown in Figure 5.6. The protons from the Tpm (blue), dppz (red) and dpp[5] (green) ligand sets can easily be seen.

Again the methyl proton of Tpm can be found as a sharp singlet at 10.10ppm. The axial pyrazole protons can be found at 8.60ppm (e), 6.28ppm (n) and 6.89ppm (m) all integrating to two protons each. The equatorial pyrazole protons can be found at 8.86ppm (d), 6.93ppm (l) and

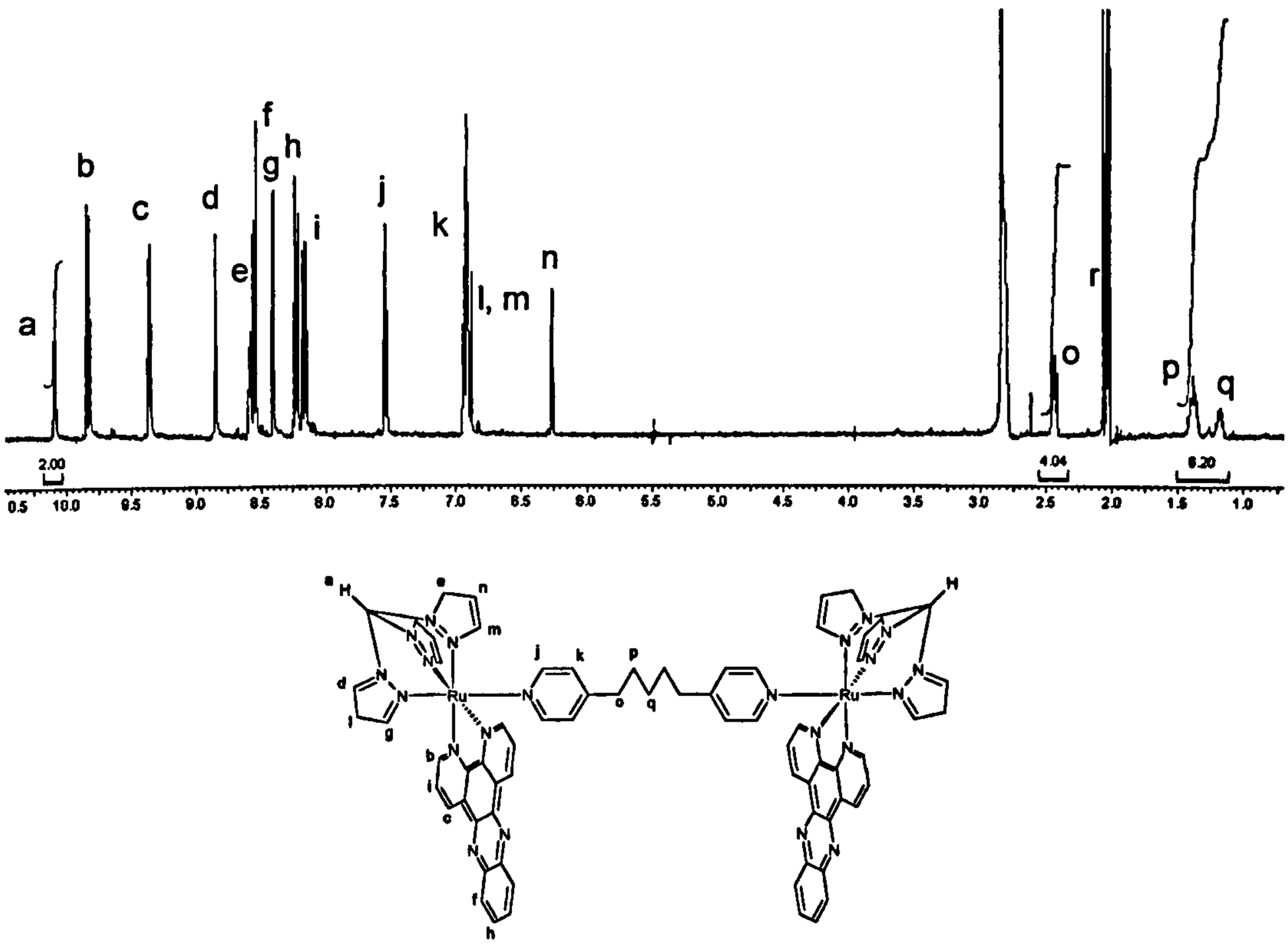

Figure 4.4:- *400MHz ^{1}H NMR spectrum recorded in d^6-acetone of [{TpmRudppz}$_2$dpp[5]]$^{4+}$ and proton labelling scheme*

8.42ppm (g) integrating to four protons each. Analysis of cross coupling shows the phenanthroline dppz protons appear at 9.85ppm (b j=9Hz), 8.17ppm (i) and 9.37ppm (c). The phenazine type protons appear at 8.55ppm (f), which is coupled, to the proton at 8.24ppm (h). The formation of the bimetallic species means that this time the dpp[5] linker ligand is symmetrical with the aromatic protons appearing at 7.55ppm (j, j=9Hz) and 6.93ppm (k). The splitting of the alkyl protons has also disappeared and the three protons appear at 2.44ppm (o, triplet), 1.41ppm (p, multiplet) and 1.18ppm (q, multiplet) with integrals of four, four and two respectively.

As well as complete assignment of all protons and simplification of the spectrum upon formation of the bimetallic complex, further evidence can be drawn from the ratios of integrals.

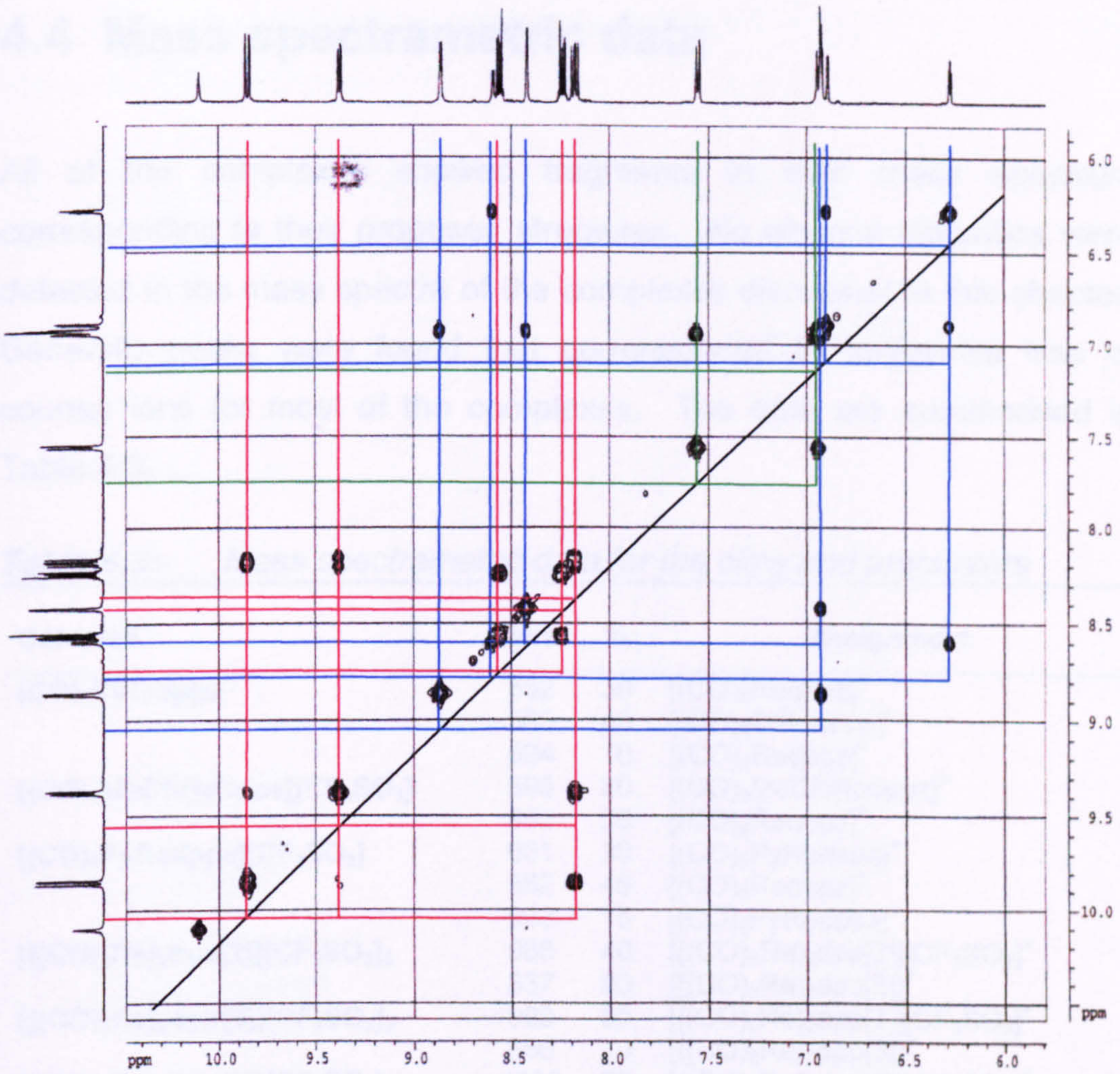

Figure 4.5:- *^1H COSY spectrum of $[\{TpmRudppz\}_2dpp[5]]^{4+}$ recorded in d^6-acetone*

In the monometallic complex $[Tpmdpp[5]Rudppz]^{2+}$ the integral ratio of the methyl proton of Tpm (a) to the central methyl proton (q) of the linker ligand is 1:2. Whereas in the bimetallic complex the ratio is 2:2, indicating two Tpm ligands and thus two ruthenium centres are present for each linker.

4.4 Mass spectrametric data

All of the complexes showed fragments in their mass spectrum corresponding to their proposed structures. No obvious impurities were detected in the mass spectra of the complexes discussed in this chapter. Generally peaks were found that corresponded to sequential loss of counter ions for most of the complexes. The data are summarised in Table 4.3.

Table 4.3:- *Mass spectrametric data for the clips and precursors*

Complex	M/z	%	Assignment
$(CO)_3ClRedppz$	552	30	$[(CO)_3Redppz]^+$
	560	40	$[(CO)_2ClRedppz]^+$
	524	10	$[(CO)_2Redppz]^+$
$[(CO)_3MeCNRedppz][CF_3SO_3]$	593	80	$[(CO)_3MeCNRedppz]^+$
	552	25	$[(CO)_3Redppz]^+$
$[(CO)_3PyRedppz][CF_3SO_3]$	631	30	$[(CO)_3PyRedppz]^+$
	552	45	$[(CO)_3Redppz]^+$
	903	15	$[(CO)_2PyRedppz]^+$
$[\{(CO)_5Re\}_2dpe[2]][CF_3SO_3]_2$	986	40	$[\{(CO)_5Re\}_2dpe[2]][CF_3SO_3]^+$
	837	90	$[\{(CO)_5Re\}_2dpe[2]]^+$
$[\{(CO)_5Re\}_2dpp[3]][CF_3SO_3]_2$	999	50	$[\{(CO)_5Re\}_2dpp[3]][CF_3SO_3]^+$
	850	70	$[\{(CO)_5Re\}_2dpp[3]]^+$
$[\{(CO)_5Re\}_2dpp[5]][CF_3SO_3]_2$	1028	20	$[\{(CO)_5Re\}_2dpp[5]][CF_3SO_3]^+$
	879	80	$[\{(CO)_5Re\}_2dpp[5]]^+$
$[\{(CO)_3Redppz\}_2dpe[2][CF_3SO_3]_2$	1438	20	$[\{(CO)_3Redppz\}_2dpe[2][CF_3SO_3]^+$
	1289	25	$[\{(CO)_3Redppz\}_2dpe[2]]^+$
$[\{(CO)_3Redppz\}_2dpp[3][CF_3SO_3]_2$	1452	40	$[\{(CO)_3Redppz\}_2dpp[3][CF_3SO_3]^+$
	1303	50	$[\{(CO)_3Redppz\}_2dpp[3]]^+$
$[\{(CO)_3Redppz\}_2dpp[5][CF_3SO_3]_2$	1480	15	$[\{(CO)_3Redppz\}_2dpp[5][CF_3SO_3]^+$
	1331	20	$[\{(CO)_3Redppz\}_2dpp[5]]^+$
$[Tpmdpp[5]Rudppz][PF_6]_2$	1113	5	$[Tpmdpp[5]Rudppz][PF_6]_2^+$
	968	40	$[Tpmdpp[5]Rudppz][PF_6]^+$
	823	50	$[Tpmdpp[5]Rudppz]^+$
$[\{TpmRudppz\}_2dpp[5]][PF_6]_4$	1858	10	$[\{TpmRudppz\}_2dpp[5]][PF_6]_3^+$
	857	70	$[\{TpmRudppz\}_2dpp[5]][PF_6]_2^{2+}$

4.5 Spectroscopic studies

The UV-Visible and luminescence studies were recorded in acetonitrile solution for all the complexes except $[Tpmdpp[5]Rudppz][PF_6]_2$ and

[{TpmRudppz}$_2$dpp[5]][PF_6]$_4$ which were recorded in methanol. The data are summarised in Table 4.4.

Table 4.4:- *Spectroscopic data of the mono and bimetallic complexes*

Complex	**Absorption**			**Emission**	
	λ_{max} (nm)	**ε ($mol^{-1}dm^3\ cm^{-1}$)**	**Assignmen**	**λ_{ex} (nm)**	**λ_{em} (nm)**
[(CO)$_3$MeCNRedppz]$^+$	277	41,095	$\pi\rightarrow\pi^*$	-	-
	364	10,343	$\pi\rightarrow\pi^*$		
	282	10,649	MLCT		
[(CO)$_3$PyRedppz]$^+$	278	41,187	$\pi\rightarrow\pi^*$	360	560
	364	9,626	$\pi\rightarrow\pi^*$		
	384	9,608	MLCT		
[{(CO)$_5$Re}$_2$dpe[2]]$^{2+}$	236	Sh	$\pi\rightarrow\pi^*$	-	-
	277	sh	$\pi\rightarrow\pi^*$		
	316	3699	MLCT		
[{(CO)$_5$Re}$_2$dpp[3]]$^{2+}$	233	sh	$\pi\rightarrow\pi^*$	-	-
	276	sh	$\pi\rightarrow\pi^*$		
	316	3,717	MLCT		
[{(CO)$_5$Re}$_2$dpp[5]]$^{2+}$	233	sh	$\pi\rightarrow\pi^*$	-	-
	276	sh	$\pi\rightarrow\pi^*$		
	317	3,710	MLCT		
[{(CO)$_3$Redppz}$_2$dpe[2]]$^{2+}$	281	57,584	$\pi\rightarrow\pi^*$	-	-
	363	12,556	MLCT		
	383	11,866	MLCT		
[{(CO)$_3$Redppz}$_2$dpp[3]]$^{2+}$	280	56,159	$\pi\rightarrow\pi^*$	-	-
	363	12,622	MLCT		
	383	11,779	MLCT		
[{(CO)$_3$Redppz}$_2$dpp[5]]$^{2+}$	281	56,879	$\pi\rightarrow\pi^*$	-	-
	362	12,234	MLCT		
	384	11,992	MLCT		
[Tpmdpp[5]Rudppz]$^{2+}$	279	44,039	$\pi\rightarrow\pi^*$	450	624
	317	16,202	$\pi\rightarrow\pi^*$		
	348	17,559	MLCT		
	397	6,883	MLCT		
	470	2,363	MLCT		
[{TpmRudppz}$_2$dpp[5]]$^{4+}$	279	163,997	$\pi\rightarrow\pi^*$	450	672
	317	50,718	$\pi\rightarrow\pi^*$		
	351	53,251	MLCT		
	399	20,192	MLCT		
	470	6,982	MLCT		

All of the complexes show characteristic absorption spectra for rhenium(I) or ruthenium(II) di-imine complexes[111]. The bisrhenium clip precursors show extremely simple absorption spectra with the only feature being a weak band at around 316nm, which can be assigned to a MLCT transition

to the pyridine linker. The rhenium(I) clips show absorption spectra very similar to their previously reported monometallic analogues[42]. The broad transition at *ca.* 280nm is characteristic of ligand centered $\pi \rightarrow \pi^*$ transitions[24], with the twin transition of moderate intensity being characteristic of MLCT transitions.

The absorption spectra of $[Tpmdpp[5]Rudppz][PF_6]_2$ and $[\{TpmRudppz\}_2dpp[5]][PF_6]_4$ are very similar except that the higher energy $\pi \rightarrow \pi^*$ transitions are much more intense in the bimetallic species than in the monometallic species (ε (279) = 163,997 and 44,039 mol^{-1} dm^3 cm^{-1}, respectively).

The monometallic rhenium(I) complexes show a strong emission in acetonitrile solution at 550-570nm, however, the bimetallic clips show no emissions at all. The excited state is presumably being quenched by the close proximity of the second metal centre. Kelly and others have observed similar phenomena in other bimetallic systems[58].

Both $[Tpmdpp[5]Rudppz][PF_6]_2$ and $[\{TpmRudppz\}_2dpp[5]][PF_6]_4$ show characteristic emissions in methanol solution, however, the emission from the bimetallic is noticeably weaker than the emission from the monometallic species. Again there could be a certain amount of self quenching from the second ruthenium centre taking place resulting in the weaker emission.

4.5 Conclusions

A synthetic strategy has been developed for the assembly of bimetallic systems of both rhenium(I) and ruthenium(II). The methodology demonstrates a "pick n mix " approach to the synthesis. The intercalating domain, linker and even the metal centre can easily be varied at each end

of the clips, by adding the appropriate ligands at different stages of the synthesis. In the future, synthesis of novel hetero-bimetallic clips could result in multifunctional DNA binding agents. For example one metal centre could act as a stable anchor to the helix and the second centre acting as a cleaving agent.

Chapter 5

DNA binding studies

5.1 Introduction

Once a suitable library of potential metal DNA binding agents had been assembled they were assayed with DNA and determine how well they interact with DNA and what structural or electronic characteristic of the compounds affects the nature of this interaction.

In order to quantify the DNA binding properties of the complexes two different assays were employed.

The first of these was a broad spectroscopic assay, in which the entire library was screened against generic calf thymus DNA, with the interaction being observed indirectly through spectral shifts in either the UV-Visible spectra or for those that luminesce, the emission spectrum.

Once this broad assay was complete a selection of the "better" binding agents were subjected to calorimetry studies where they were assayed against more specific sequences of natural DNA such as poly(dG).poly(dC) and poly(dA).Poly(dT) homo-polymers.

5.2 Spectroscopic binding studies

All of the metal complexes in this study exhibit a well-defined UV-Visible

spectrum in both lipophilic and aqueous environments. When a complex binds to DNA it is subjected to a change of local microenvironment from being completely solvated in aqueous solution to being in the hydrophobic environment of the DNA grooves and base stack. This change in local microenvironment can be monitored by perturbations that occur in the UV-Visible spectrum of the complex when the binding event takes place[117]. Binding brings the positive metal centre and the aromatic ligands into close proximity to the poly-anionic backbone of the DNA and the hydrophobic interior of the DNA grooves. This causes perturbations in the metal centred MLCT band and the ligand centred $\pi \rightarrow \pi^*$ bands of the UV-Visible spectrum of the complexes[23,24,117]. These hypochromic shifts in the spectrum are often accompanied by either hypsochromic or bathochromic shifts indicating that the energy of the transition has been altered by stabilisation or destabilisation of the HOMO/LUMO orbitals involved in the transitions upon binding to DNA[117].

As well as perturbations in the UV-Visible spectra of the complexes, the excited state luminescence emission spectra are also sensitive to the microenvironment of the complexes. Polar water molecules can be efficient quenchers of excited states, particularly where they can hydrogen bond to nitrogen donor sites on the complexes. When the complexes bind to DNA they are protected from the aqueous solvent by the hydrophobic interior of the grooves and the base stack. This results in an increased emission upon binding to DNA[21], which can also be used to quantify the interaction with DNA.

5.2.1 Formulating a binding curve[118]

If DNA is titrated into a solution of drug of known concentration the degree of shift in any given band in the UV-Visible spectrum or the luminescence spectrum is proportional to the fraction of drug bound to the

DNA.

For hypochromic shifts in the UV-Visible spectrum the binding curve is constructed as follows. If the absorbance of the free unbound drug is given as A_u, the absorbance of the fully bound drug at saturation is given by A_b and A_{obs} is the observed absorbance of the drug at any given titration point then the fraction of drug bound (χ) to the DNA is given by;

$$\chi = \frac{(A_u - A_{obs})}{(A_u - A_b)} \qquad \textbf{(5.1)}$$

Similarly for luminescence titration where the emission intensity of the drugs increase upon binding to DNA the fraction bound is given by;

$$\chi = \frac{(I_{obs} - I_0)}{(I_b - I_u)} \qquad \textbf{(5.2)}$$

where I_{obs}, I_u and I_b are the emission intensities of the observed, free and fully bound drug respectively.

If χ is plotted against the ratio DNA concentration to drug concentration, also called the mixing ratio (R) then a saturation binding curve can be constructed (Figure 5.1).

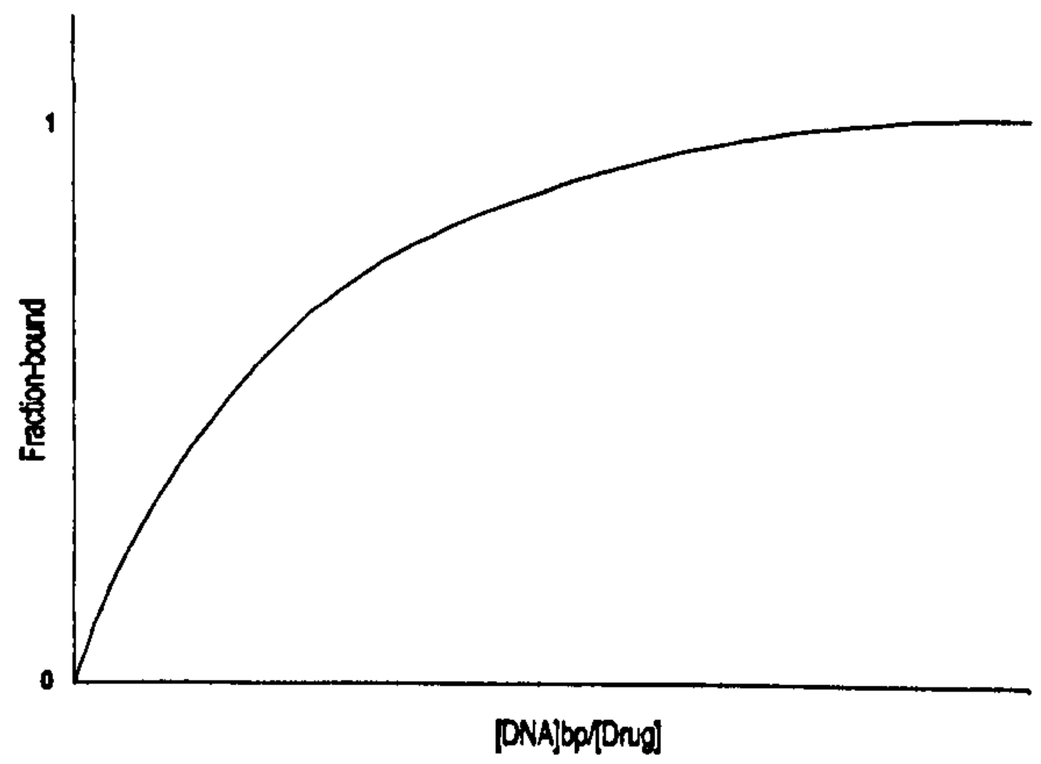

Figure 5.1:- *Schematic of a binding curve showing saturation binding*

5.2.2 Determination of bound and free drug concentrations[118]

If the initial concentration of drug is denoted as Ci it is easy to calculate, from knowing the fraction of drug bound, the concentrations of free (Cf) and bound drug (Cb) at any given titration point.

$$Cb = \chi\ Ci \qquad (5.3)$$

From this as Ci = Cb + Cf

$$Cf = Ci - Cb \qquad (5.4)$$

5.2.3 Scatchard plots[118]

A Scatchard plot (Figure 5.2) was developed as a way of the transforming the hyperbola binding data into a linear binding isotherm, which can be fitted with a least square linear regression analysis to the Scatchard equation (5.5).

$$\frac{r}{Cf} = \frac{B_{max}}{K} - \frac{r}{K} \qquad (5.5)$$

Where r = specific binding

K = equilibrium binding constant

B_{max} = binding density

Scatchard plots are constructed from a plot of specific binding (r) against the ratio of specific binding to free ligand (r/Cf).

$$r = \frac{C_b}{[DNA]} \qquad (5.6)$$

From this the intrinsic equilibrium binding constant (K) can be determined from the reciprocal of the slope, and the binding site size (S) can be determined from the reciprocal of the binding density (B_{max}), which is the X-axis intercept.

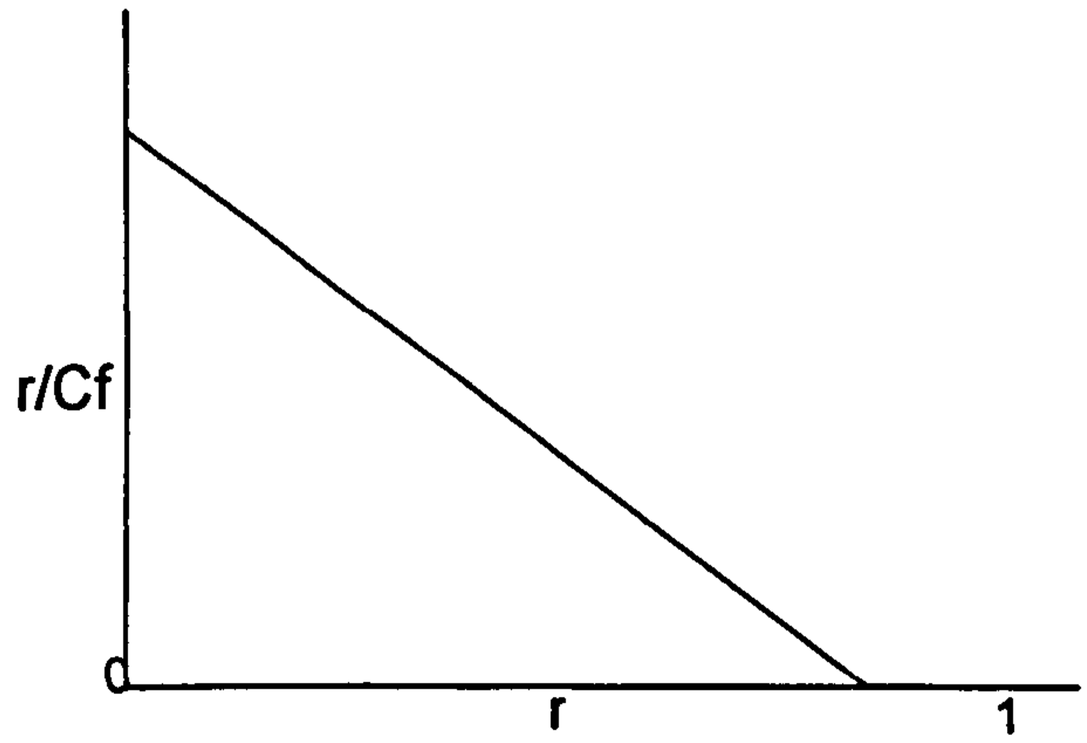

Figure 5.2:- *Schematic of a Scatchard plot*

5.2.4 Development of more accurate models

The Scatchard model was developed for the binding of small ligands to non-interacting isolated binding sites on proteins[118]. Although this simple linear transformation of the binding data works well for 1:1 binding situations, it quickly begins to show weaknesses in more complex systems, as the data are no longer linear. This is the case when calf thymus DNA (CT DNA) is used. CT-DNA is assumed to be an isotropic uniform lattice, with one binding site defined as one base pair. So on any given CT DNA strand there are hundreds if not thousands of potential overlapping binding sites for a drug molecule, hence in our assays the binding isotherm deviated from linearity and a more suitable model was needed to determine the binding parameters K and S.

Since the early 1960's, when this problem first came to ligh,t several papers were published which attempted to solve the inaccuracies caused

by the overlapping of binding sites and co-cooperativity. Latt and Sober (1967) were the first to take into account these problems and developed a highly simplified model for ligand binding to a homogeneous lattice[119]. In 1964 Lifson developed a combinatorial method (which in practice proved to be insoluble) and a method of sequence generating functions[120]. The latter gave rather good estimates for binding constants but was unable to determine site sizes. Crothers (1968) attempted to solve the non-linearity for more complex heterogeneous binding lattices by using a Monte-Carlo method as a limiting case[121]. Zasedatelev *et al.*. (1971) used a combinatorial method accounting both for ligand size and ligand-ligand cooperatively[122]. Shellman (1974) used sequence-generating functions on the heterogeneous lattice problem accounting for both potential binding site overlap and nearest neighbour cooperativity[123]. In addition to these general treatments there have been a number of other solutions to more specific binding problems. Although some of these solutions are very elaborate, none of them are particularly practical allowing them to be easily and universally applied to any general binding problem.

5.2.5 The Mcghee-von Hippel model[124]

It was not until 1974, when the statistical treatment of ligand-lattice interactions was published by Mcghee and von Hippel that a practical model was available for analysing non-linear Scatchard plots and accurately determining binding constants and site sizes.

The aim of Mcghee and von Hippel was to analyse the simplest possible model of ligand-lattice interactions, which allows for the treatment of potential overlap of ligand binding sites.

However, the model does make some large assumptions. First it assumes all of the binding sites on the lattice are isotropic with an equal probability of the drug molecule choosing any given site. There is

assumed to be no cooperativity between the lattice and the drug and in the simple non-cooperative form that we have used there is assumed to be no drug-drug cooperativity. This implies that a drug molecule has no preference for choosing a free binding site over a site adjacent to a bound drug. The non-cooperative form of the model is shown below.

$$\frac{r}{Cf} = K(1-Sr) \bullet \left(\frac{1-Sr}{1-(S-1)r} \right)^{S-1} \qquad \textbf{(5.7)}$$

Where K = Intrinsic binding constant

S = Binding site size in base pairs

Non-linear Scatchard plots are fitted to the Mcghee-von Hippel model using a non-linear least squares approach. As the lattice reaches saturation, the number of free binding sites less than S residues in length increase significantly. An effective concentration of drug up to two orders of magnitude can be needed to increase the occupancy from 90-100%. This has a significant effect on the data and artificially increases the observed binding constant. To minimise these artificial effects the model is fit to experimental data between 30% and 90% bound drug.

5.3 Isothermal titration calorimetry[125,126]

Isothermal titration calorimetry (ITC) is a titration technique used to quantify the thermodynamic binding parameters of a given bimolecular equilibrium. ITC is the only technique available to directly measure the heat of interaction of two or more components, and hence binding constants and other thermodynamic parameters can be obtained without the partitioning of the components and subsequent spectroscopic determination of bound and free drug concentrations.

5.3.1 The ITC experiment

A schematic of a modern micro-calorimeter is shown in Figure 5.3.

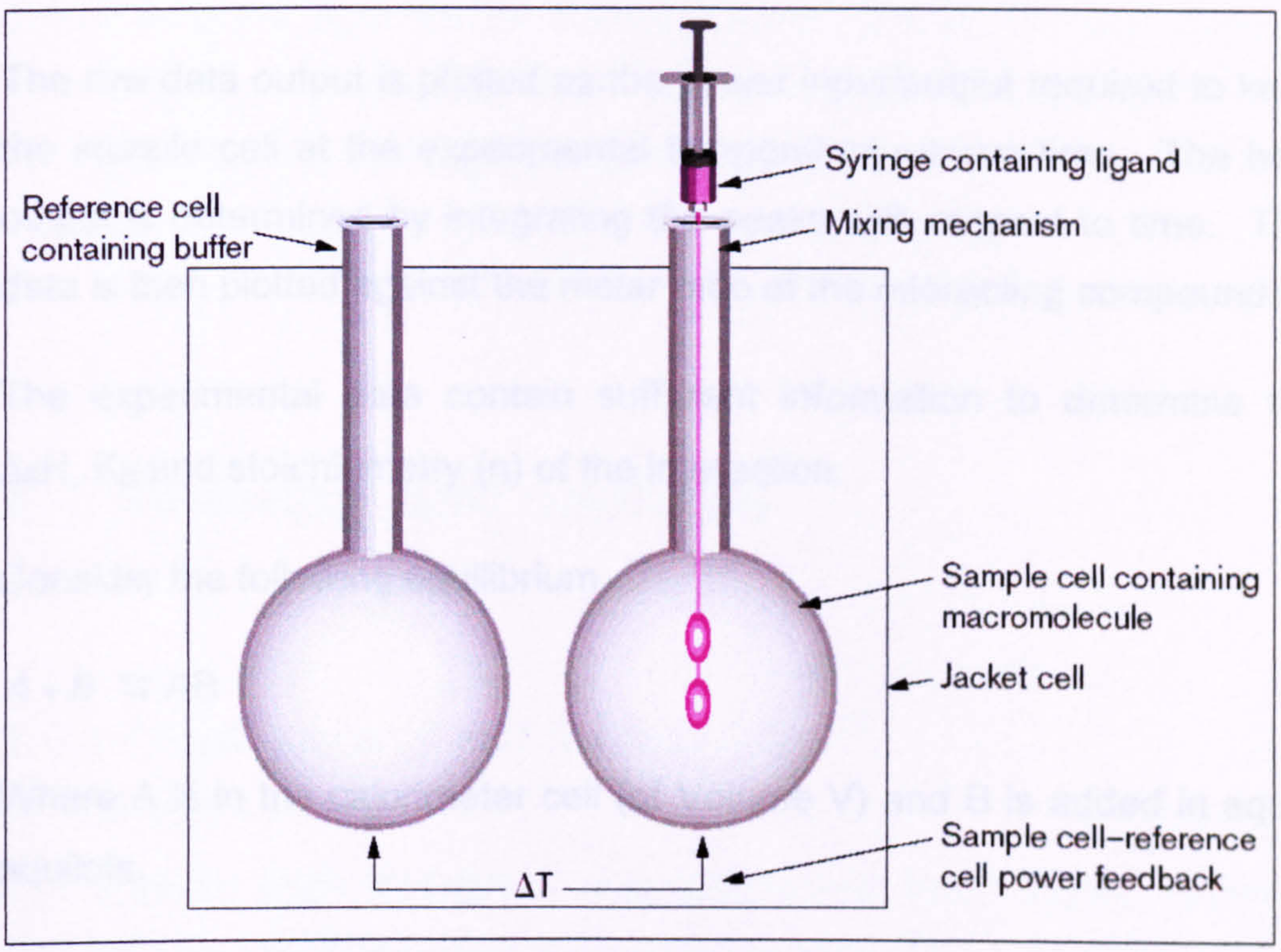

Figure 5.3:- *Schematic of a modern micro-calorimeter*

The instrument consists of two identical cells housed in an isothermal jacket. The jacket is constantly cooled so energy is constantly required to keep the two cells in thermal equilibrium ($\Delta T=0$) at the chosen experimental temperature throughout the duration of the experiment. One cell, the reference cell is filled with buffer solution. The other cell is filled with a solution of the fixed component of the titration in the buffer. A known volume of a solution of the variable component in identical buffer is then titrated at regular intervals into the sample cell. The interaction of the ligand and the drug causes heat to be released or absorbed in the sample cell and the output of the experiment is the heat energy per unit time required to keep the cells in thermal equilibrium. If the interaction is

exothermic, less heat per unit time will be required by the sample cell to keep the two cells in thermal equilibrium. If the interaction in endothermic more heat per unit time will be needed to keep the cells in thermal equilibrium.

The raw data output is plotted as the power input/output required to keep the sample cell at the experimental temperature versus time. The heat output is determined by integrating the peaks with respect to time. This data is then plotted against the molar ratio of the interacting compounds.

The experimental data contain sufficient information to determine the $\Delta_B H$, K_B and stoichiometry (n) of the interaction.

Consider the following equilibrium

$$A + B \leftrightarrows AB$$

Where A is in the calorimeter cell (of Volume V) and B is added in equal aquilots.

The fractional saturation, F, of species A at any point in the titrationcan be determined from the total heat input/output, Q, using the following equation:

$$Q = nFA_T\Delta_B HV \qquad \textbf{(5.8)}$$

Where A_T is the total concentration of A (free and complexed). Since $K_B = F/(1-F)[B]$ and $[B] = B_T - nFA_T$, the following quadratic relationship is obtained:

$$F2 - F\{1+(B_T/nA_T)+(1/nK_BA_T)\}+(B_T/nA_T) = 0 \qquad \textbf{(5.9)}$$

Where B_T is the total concentration of B. Solving equation 5.9 for F and substituting this value into equation 5.8 gives:

$$Q = nA_T\Delta_B H\,(V/2)\,.\,\{X-[X^2-(4B_T/nA_T)^{1/2}\} \qquad \textbf{(5.10)}$$

Where $X = \{1+(B_T/nA_T) + (1/nK_BA_T)\}$. Thus, Q gives a value for the heat content of the interaction after a given injection, which is dependent on the values of the independent variables Δ_BH, K_B, and n.

These data are reported as a least-squares fit with inherent statistical error. There are other algorithms available to fit binding data for more complex interactions involving several independent or interactive binding events.

5.4 Materials and methods

5.4.1 Preparation of calf thymus DNA[127]

Calf thymus DNA (CT-DNA) was purchased from Sigma chemical company as the lyophilised solid sodium salt. A concentrated stock solution of about 5mM was extracted with phenol-chloroform to remove any residual protein. The purity of the sample was determined by UV-visible spectroscopy with A_{260}/A_{280} >1.9 indicating a protein free sample. The DNA pellets obtained from the purification were dissolved in doubly distilled water, with the concentration being determined by ε_{260} = 6600 mol^{-1} dm^3 cm^{-1}. The concentration of the DNA used in the titrations was 3 – 20 mmol in base pairs.

5.4.2 UV-Visible titration protocol

All of the UV-Visible titrations were performed to the following protocol. The buffer used for the titrations was 25mM NaCl, 5mmol Tris, pH 7.0

made with doubly distilled water from a Millipore water purification system. The drug complex was converted to its chloride salt by treating the PF_6^- salt with *n*-Bu_4Cl in acetone, with the chloride salt being collected by centrifugation and copiously washed with acetone. Approximately 10mg of vacuum dried complex was dissolved into 20ml of spectroscopic grade methanol (or buffer if the complex was soluble in buffer alone), and the concentration was determined. This stock solution was then diluted into 5ml of buffer containing 5% methanol (250μl) in total, to give a final drug complex concentration of 15μM. 3000μl of the sample solution was then loaded into a 1cm path length optical glass cuvette and loaded into the spectrometer sample block, which was maintained at 25°C. 3000μl of 5% methanolic buffer was loaded into another identical cuvette and placed in the reference cell of the spectrometer. Both the sample and the reference cells were mixed 30 times with a Gilson P1000 pipette, after which the cells were checked for bubbles. After 30 minutes, to allow the cells to equilibrate, first spectrum was recorded between 650 and 200 nm. 2 - 5μl of DNA solution was then added to both the sample and reference cell, followed by a further 30 times mixing. After checking for bubbles, the spectrum was taken again, this time showing the hypochromic shift indicating the formation of a drug – DNA complex. The titration process was repeated until there was no change in the spectrum for at least four titrations indicating binding saturation had been achieved.

5.4.4 Luminescence titration protocol

All of the luminescence titrations were performed to the following protocol. The buffer used for the titrations was 25mM NaCl, 5mmol Tris, pH 7.0 made with doubly distilled water from a Millipore water purification system. The drug complex was converted to its chloride salt by treating the PF_6^- salt with *n*-Bu_4Cl in acetone, with the chloride salt being collected by centrifugation and copiously washed with acetone. Approximately

10mg of vacuum dried complex was dissolved into 20ml of spectroscopic grade methanol (or buffer if the complex was soluble in buffer alone) and the concentration was determined. This stock solution was then diluted into 5ml of buffer containing 5% methanol (250μl) in total to give a final drug complex concentration of 30-60μM. 3000μl of the sample solution was then loaded into a 1cm path length optical glass cuvette and loaded into the fluorimeter sample block, which was maintained at 25°C. The sample was mixed 30 times with a Gilson P1000 pipette, after which the cell was checked for bubbles. After 30 minutes to allow the cells to equilibrate first spectrum was recorded. 2 - 5μl of DNA solution was then added the sample cell, followed by a further 30 times mixing. After checking for bubbles, the spectrum was taken again, this time showing the increase in emission indicating the formation of a drug – DNA complex. The titration process was repeated until there was no change in the spectrum for at least four titrations indicating binding saturation had been achieved.

5.4.5 Dialysis of the DNA samples for ITC[126]

poly(dA).poly(dT) and poly(dG).poly(dC) homo-polymers were purchased from Pharmacia Botech Ltd and were used as received. Each sample was dissolved in two ml of the buffer (25mmol NaCl, 5mmol Tris.HCl, pH 7.0) and then placed in dialysis tubing. The samples were dialysed for at least 24 hours. The concentration of the DNA was determined by UV spectroscopy using the following molar absorption coefficients (mol^{-1}dm^{3}cm^{-1}) poly(dA).poly(dT), 6000 at 260nm; and poly(dG).poly(dC), 7400 at 253nm.

5.5 Results and discussion

5.3.1 DNA binding studies on the Tpm monometallic and bimetallic complexes

Both UV-Visible and luminescence binding studies were carried out of all of the Tpm ruthenium(II) mono and bimetallic complexes. The raw titration data for the UV-Visible titration of $[TpmPyRudppz]^{2+}$ with CT-DNA is shown in Figure 5.4.

Both the bands at 278nm and 350nm which have be shown to be arising from $\pi \rightarrow \pi^*$ transitions centred on dppz show a high degree of hypochromicity. There is also a significant bathochromic shift as the 278nm band approaches saturation. Both of these phenomena are characteristic of an interaction between the metal complex and the DNA helix[117]. The high percentage hypochromicity also indicates that the interaction is probably intercalative in nature. All of the Tpm ruthenium(II) complexes produced binding data similar to those shown above and the raw data are available on the supplementary data CD.

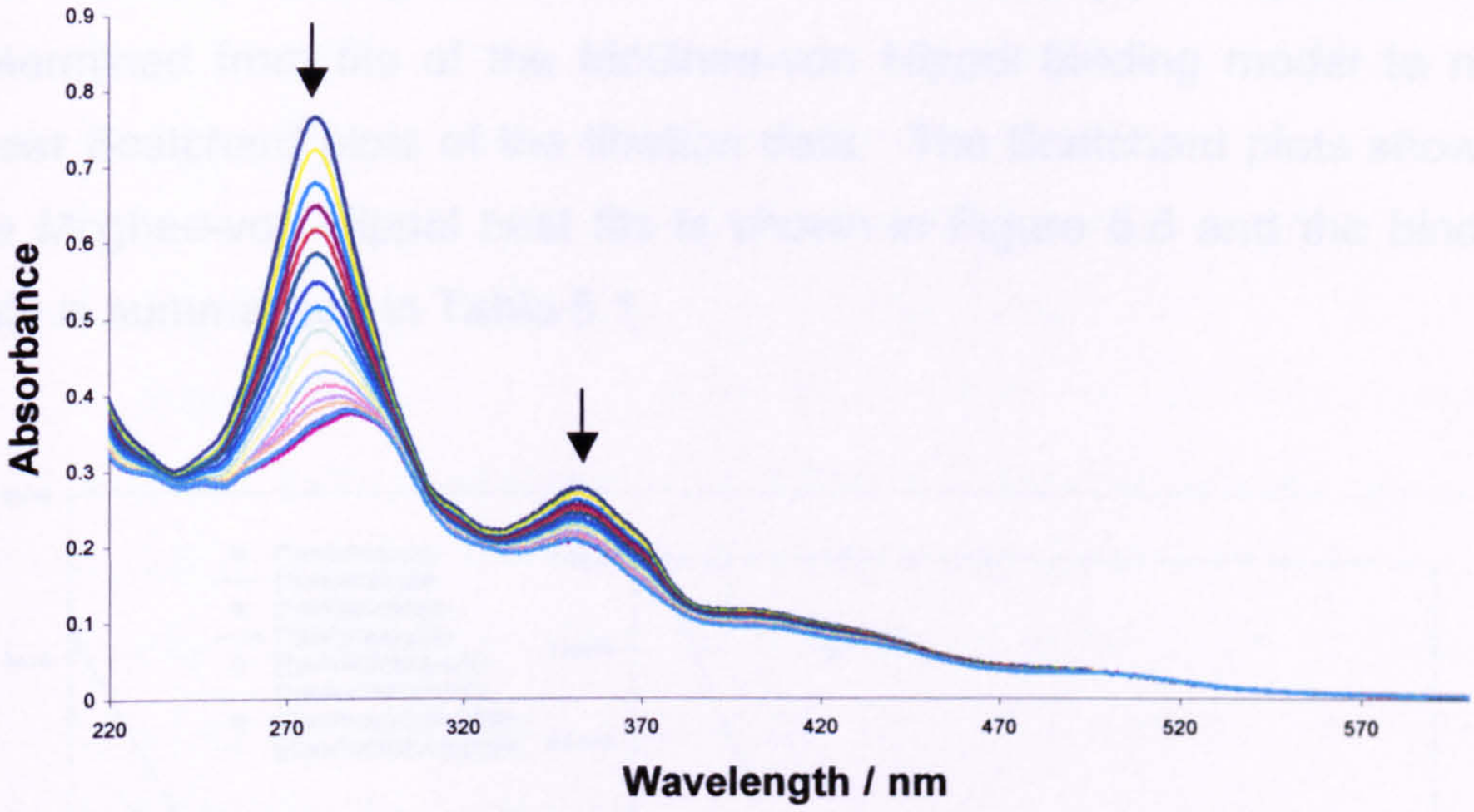

Figure 5.4:- *Raw titration data for $[TpmPyRudppz]^{2+}$ interacting with CT-DNA as moniterd by UV-Visible spectroscopy*

The binding curves for the Tpm ruthenium(II) complexes are shown in Figure 5.5. They all show that saturation binding is taking place.

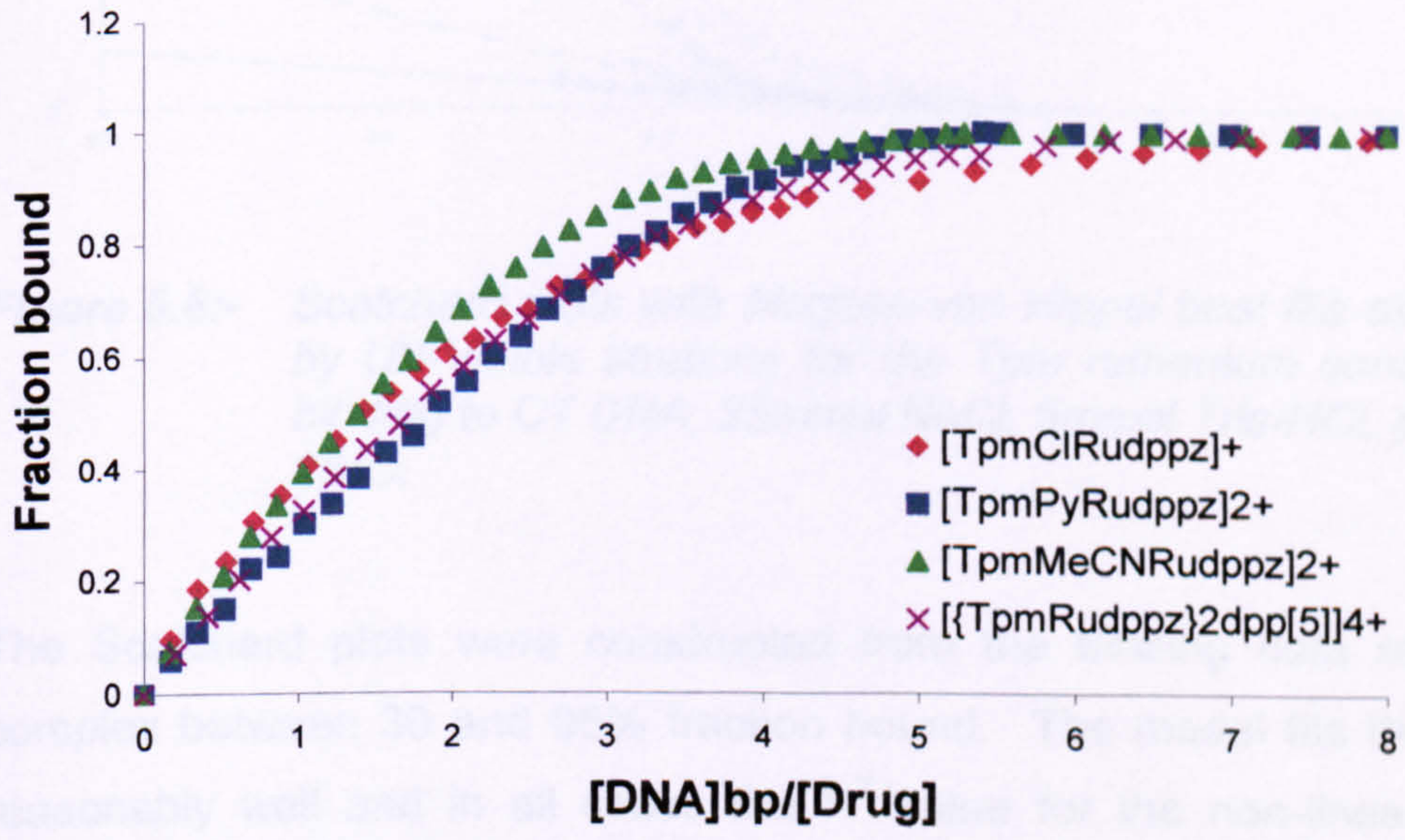

Figure 5.5:- *Binding curves obtained by UV-Visible titrations for the Tpm ruthenium complexes binding to CT DNA, 25mmol NaCl, 5mmol Tris-HCl, pH 7.0, 25°C.*

The intrinsic binding constants for the ruthenium(II) complexes were determined from fits of the McGhee-von Hippel binding model to non-linear Scatchard plots of the titration data. The Scatchard plots showing the Mcghee-von Hippel best fits is shown in Figure 5.6 and the binding data is summarised in Table 5.1.

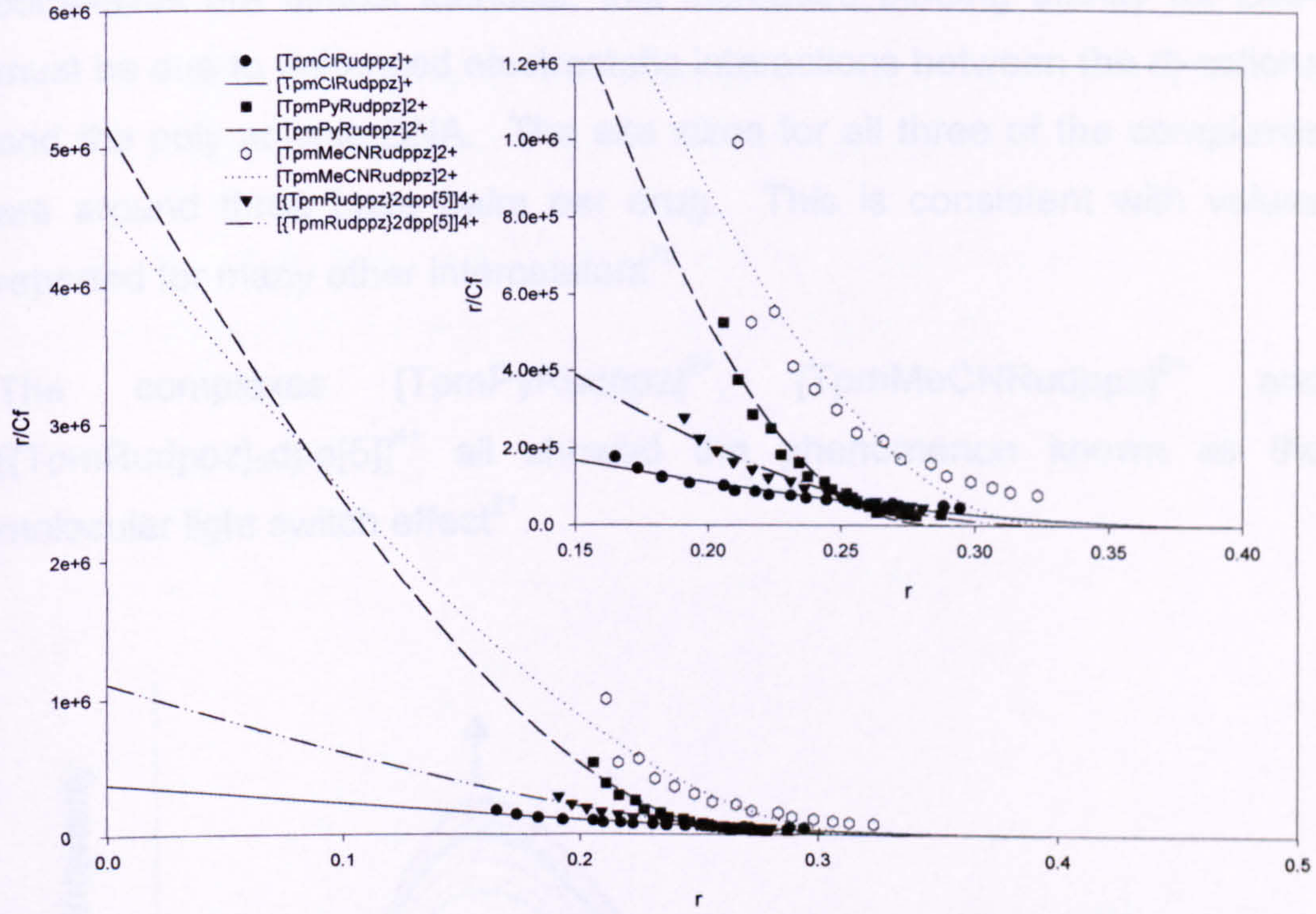

Figure 5.6:- *Scatchard plots with Mcghee-von Hippel best fits obtained by UV-Visible titrations for the Tpm ruthenium complexes binding to CT DNA, 25mmol NaCl, 5mmol Tris-HCl, pH 7.0, 25°C.*

The Scatchard plots were constructed from the binding data of each complex between 30 and 95% fraction bound. The model fits the data reasonably well and in all cases the R^2 value for the non-linear least squares fit was >0.9.

For the three monometallic complexes $[TpmClRudppz]^+$, $[TpmPyRudppz]^{2+}$ and $[TpmMeCNRudppz]^{2+}$, the intrinsic binding

constants were determined as $3.75x10^5$, $5.16x10^6$ and $4.89x10^6$ $mol^{-1}dm^3$, respectively. The ratios of binding constants $[TpmClRudppz]^+$: $[TpmPyRudppz]^{2+}$ and $TpmClRudppz]^+$: $[TpmMeCNRudppz]^{2+}$ are 13.76 and 13.04, respectively. This shows that there is over an order of magnitude increase in binding affinity for the di-cations over the mono-cation. Since the shape and size of all three of the monometallic complexes are almost identical, this increased binding affinity for DNA must be due to enhanced electrostatic interactions between the di-cations and the poly anionic DNA. The site sizes for all three of the complexes are around three base pairs per drug. This is consistent with values reported for many other intercalators[75].

The complexes $[TpmPyRudppz]^{2+}$, $[TpmMeCNRudppz]^{2+}$ and $[\{TpmRudppz\}_2dpp[5]]^{4+}$ all showed the phenomenon known as the molecular light switch effect[21].

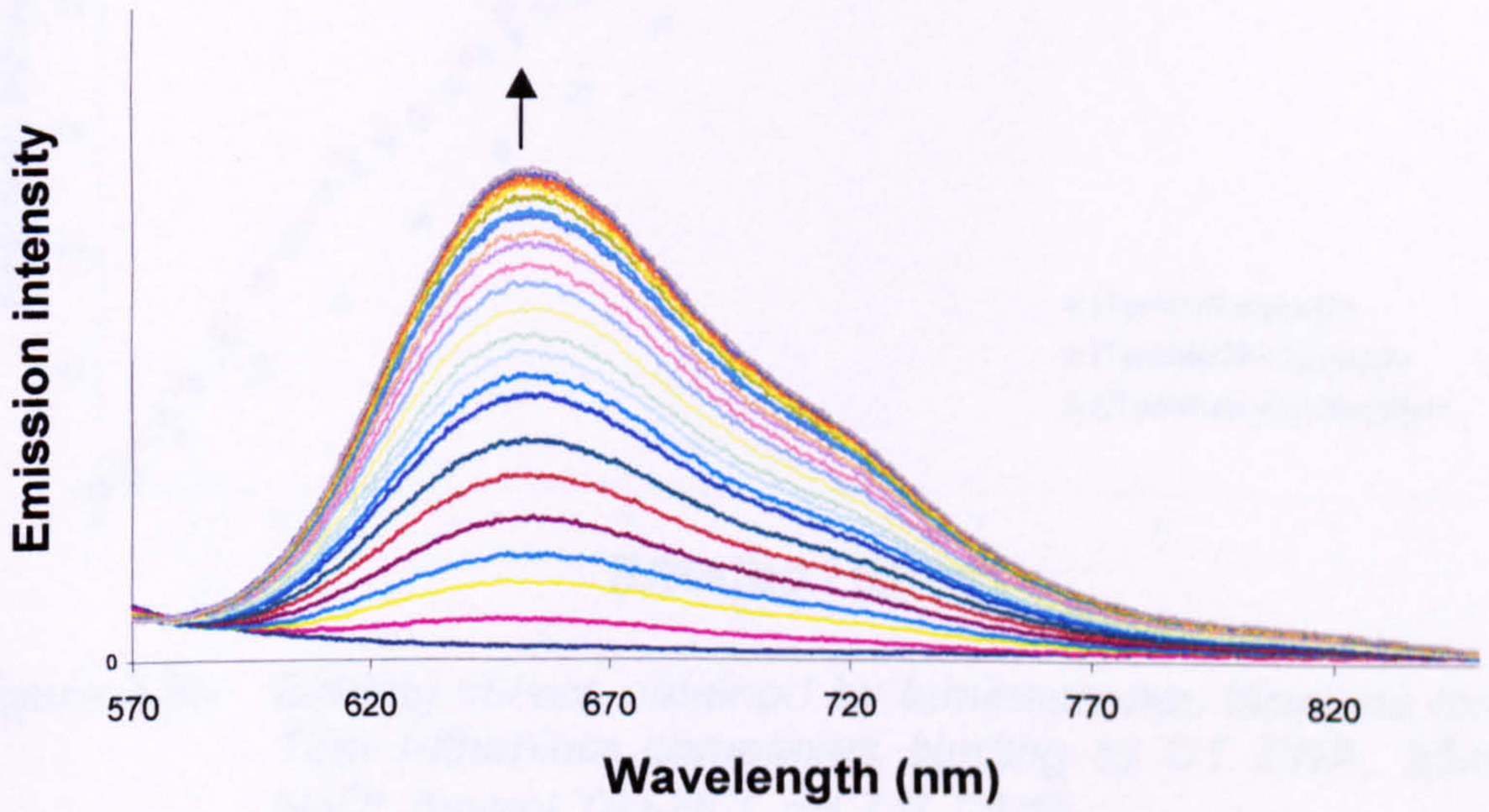

Figure 5.7:- *Raw titration data for the interaction of $[TpmPyRudppz]^{2+}$ with CT-DNA*

Analogous to $[(phen)_2Rudppz]^{2+}$, these complexes do not show any luminescence emission when they are in aqueous environments due to

deactivation of the excited state due to water hydrogen bonding to the phenazine nitrogens of dppz.

However, when bound to DNA the phenazine nitrogens are protected from water by the hydrophobic interior of the DNA grooves and the emission is switched on. Figure 5.7 shows the raw emission data for the titration of $[TpmPyRudppz]^{2+}$ with CT-DNA.

This raw data are typical of that obtained for all of the Tpm complexes. The rest of the plots can be found on the supplementary data CD.

When the data from the titrations are processed, saturation binding curves are produced and they are shown in Figure 5.8.

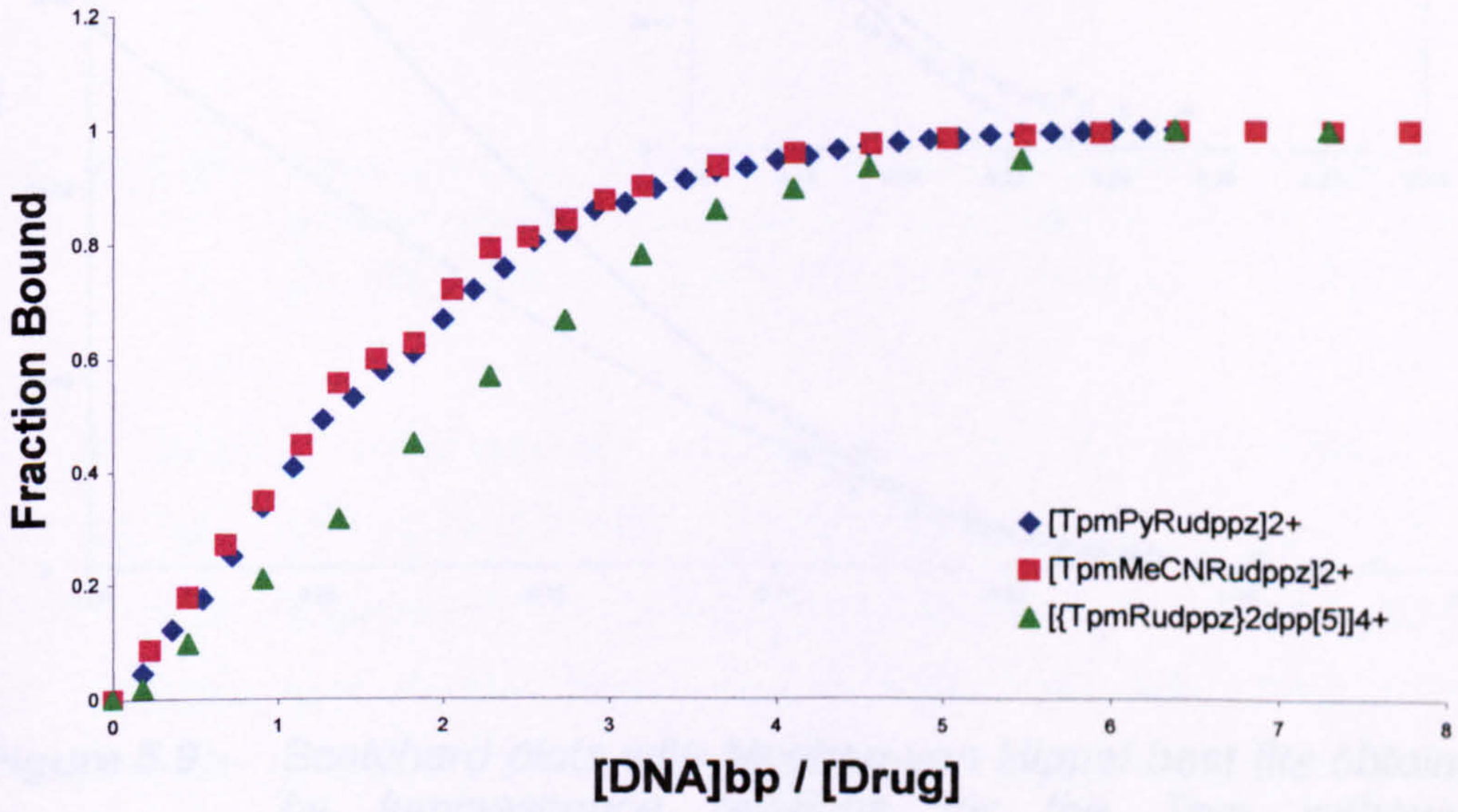

Figure 5.8:- *Binding curves obtained by luminescence titrations for the Tpm ruthenium complexes binding to CT DNA, 25mmol NaCl, 5mmol Tris-HCl, pH 7.0, 25°C.*

Intrinsic binding constants and binding site sizes were obtained from the Mcghee-von Hippel best fits of non-linear Scatchard plots (Figure 5.9).

Again the model fits the data well and the values obtained are in agreement with the values obtained from UV-Visible titrations. The

intrinsic binding constants for $[TpmPyRudppz]^{2+}$ and $[TpmMeCNRudppz]^{2+}$ were $4.73x10^6$ and $2.87x10^6$ $mol^{-1}dm^3$ with site sizes around 4 base pairs.

Unfortunately, the mono-cationic complex $[TpmClRudppz]^{+}$ did not show any emission when titrated with DNA so binding data could not be obtained from this method.

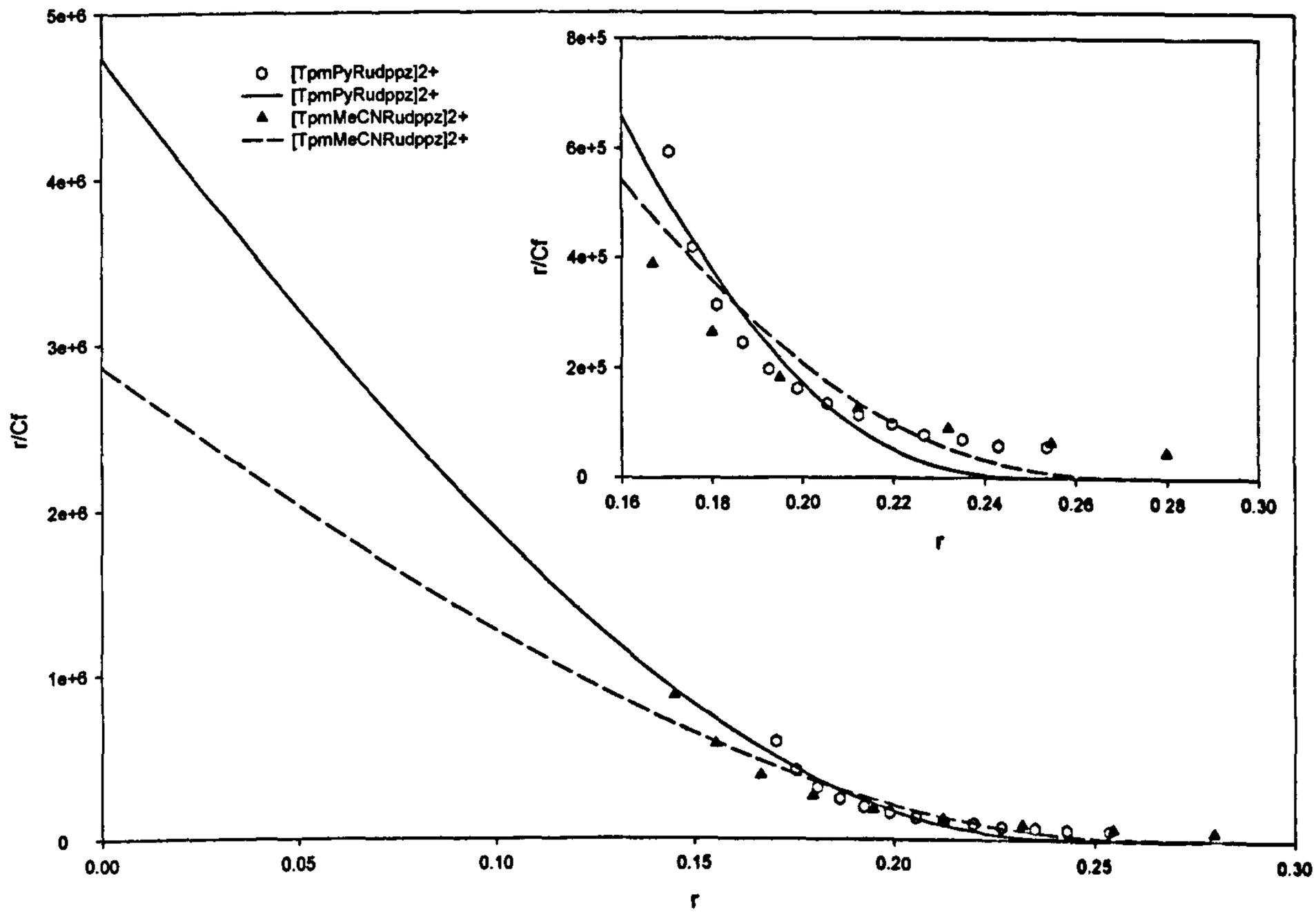

Figure 5.9:- *Scatchard plots with Mcghee-von Hippel best fits obtained by luminescence titrations for the Tpm ruthenium complexes binding to CT DNA, 25mmol NaCl, 5mmol Tris-HCl, pH 7.0, 25°C.*

In summary, the spectroscopic binding studies on the Tpm monometallic complexes reveal a good affinity for DNA with the dicationic complexes showing a 10-fold enhanced affinity over the monocationic complexes.

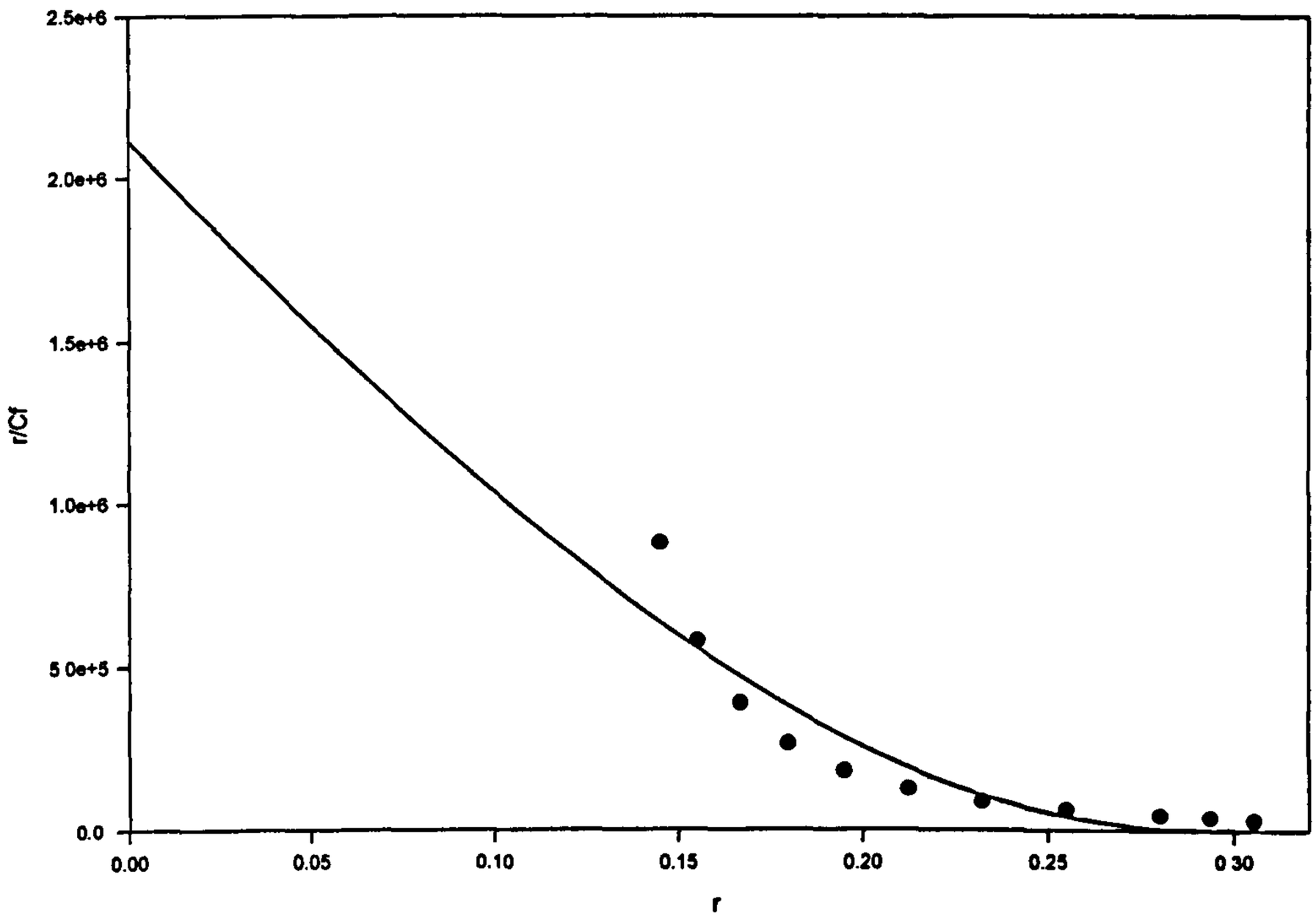

Figure 5.10:- *Scatchard plot with Mcghee-von Hippel best fit obtained by luminescence titration for the Tpm ruthenium clip binding to CT DNA, 25mmol NaCl, 5mmol Tris-HCl, pH 7.0, 25℃.*

These binding affinities are comparable to those obtained for $[(phen)_2Rudppz]^{2+}$ ($3.2x10^6$ and $1.7x10^6$ $mol^{-1}dm^3$ for the Δ- and Λ-enantiomers, respectively)[128]. As our complexes are completely achiral this suggests that chirality and shape selection has little effect on the ability of the complexes to interact with DNA. The difference in binding affinity between the mono and di-cationic species seems to indicate a significant electrostatic component is present in the overall binding affinity of these complexes with DNA. Salt dependence experiments are underway to try and quantify this further.

Although the monometallic complexes showed good affinity for DNA, the relatively small increase in affinity of the bimetallic $[\{TpmRudppz\}_2dpp[5]]^+$ ruthenium clip was disappointing. Analysis of the binding data obtained from the spectroscopic titrations (Table 5.1) and visual analysis of the

binding curves and Scatchard plots revealed that the binding parameters for the mono and bimetallic complexes were almost identical. Although this is possible it was thought extremely unlikely that this was the case, so the two systems were further investigated with ITC.

Table 5.1:- *Spectroscopic binding data for the Tpm complexes binding to CT-DNA, 25mmol NaCl, 5mmol Tris, pH 7.0*

Complex	UV-Visible			Luminescence		
	K (mol^{-1} dm^3)	S (bp)	%hyp	K (mol^{-1} dm^3)	S (bp)	I/I_0
$[TpmClRudppz]^{+a}$	$3.75x10^5$	2.51	33.38	-	-	-
$[TpmPyRudppz]^{2+}$	$5.17x10^6$	3.39	50.76	$4.73x10^6$	3.87	13.54
$[[TpmMeCNRudppz]^{2+}$	$4.89x10^6$	2.94	52.40	$2.87x10^6$	3.57	14.10
$[\{TpmRudppz\}_2dpp[5]]^{2+}$	$1.17x10^6$	2.95	60.59	$2.11x10^6$	3.27	9.04

[a] titration performed in 5% methanolic buffer

ITC was performed on both $[TpmPyRudppz]^{2+}$ and $[\{TpmRudppz\}_2dpp[5]]^{2+}$ with poly(dA).poly(dT) and poly(dG).poly(dC) natural homo-polymers. All the titration were performed at 25°C and the data are summarised in Table 5.2.

The raw ITC binding data and the binding isotherm for the interaction of $[TpmPyRudppz]^{2+}$ with poly(dA).poly(dT) is shown in Figure 5.11. The interaction shows a small positive enthalpy of 10.2 Kcal mol^{-1} indicating the interaction of $[TpmPyRudppz]^{2+}$ and poly(dA).poly(dT) is endothermic in nature[126].

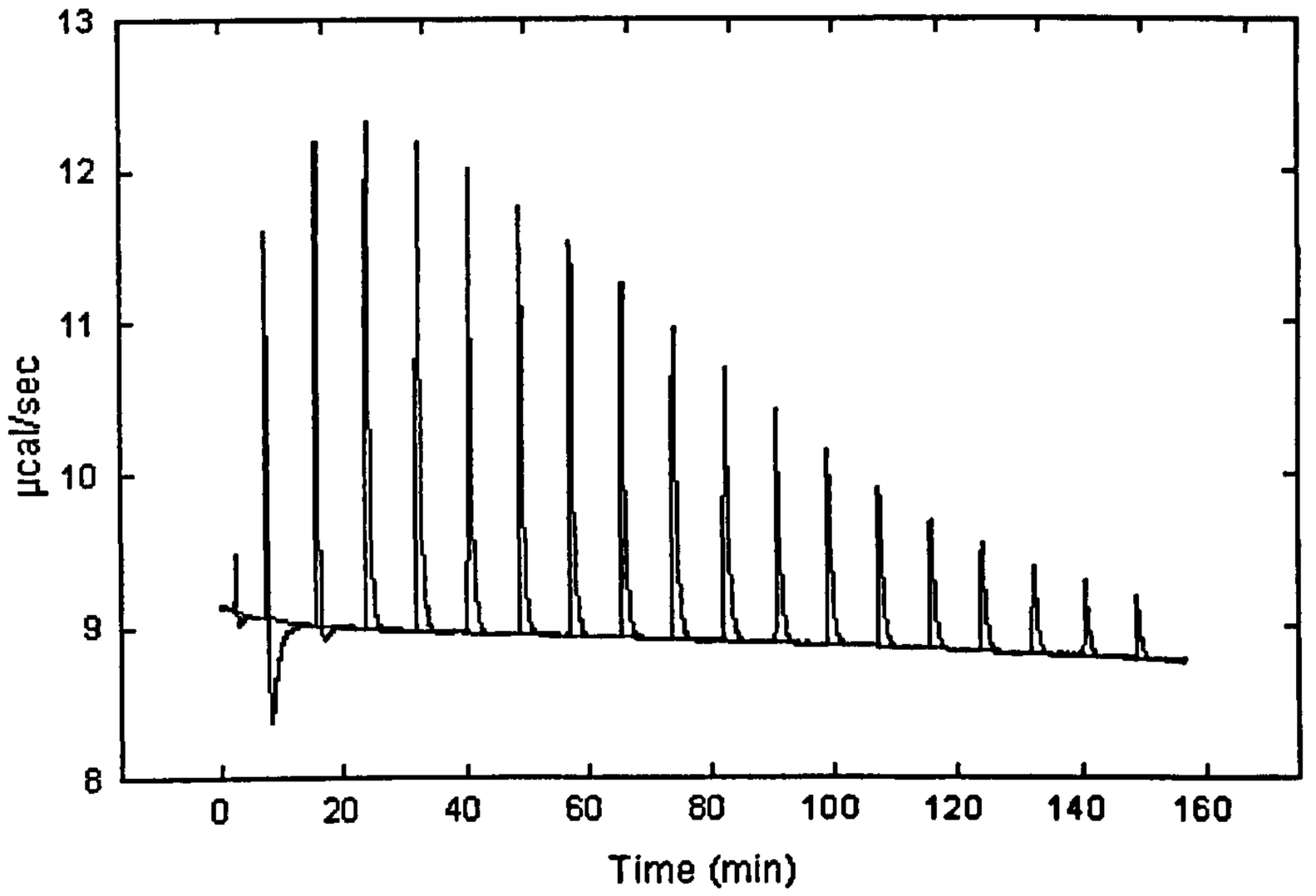

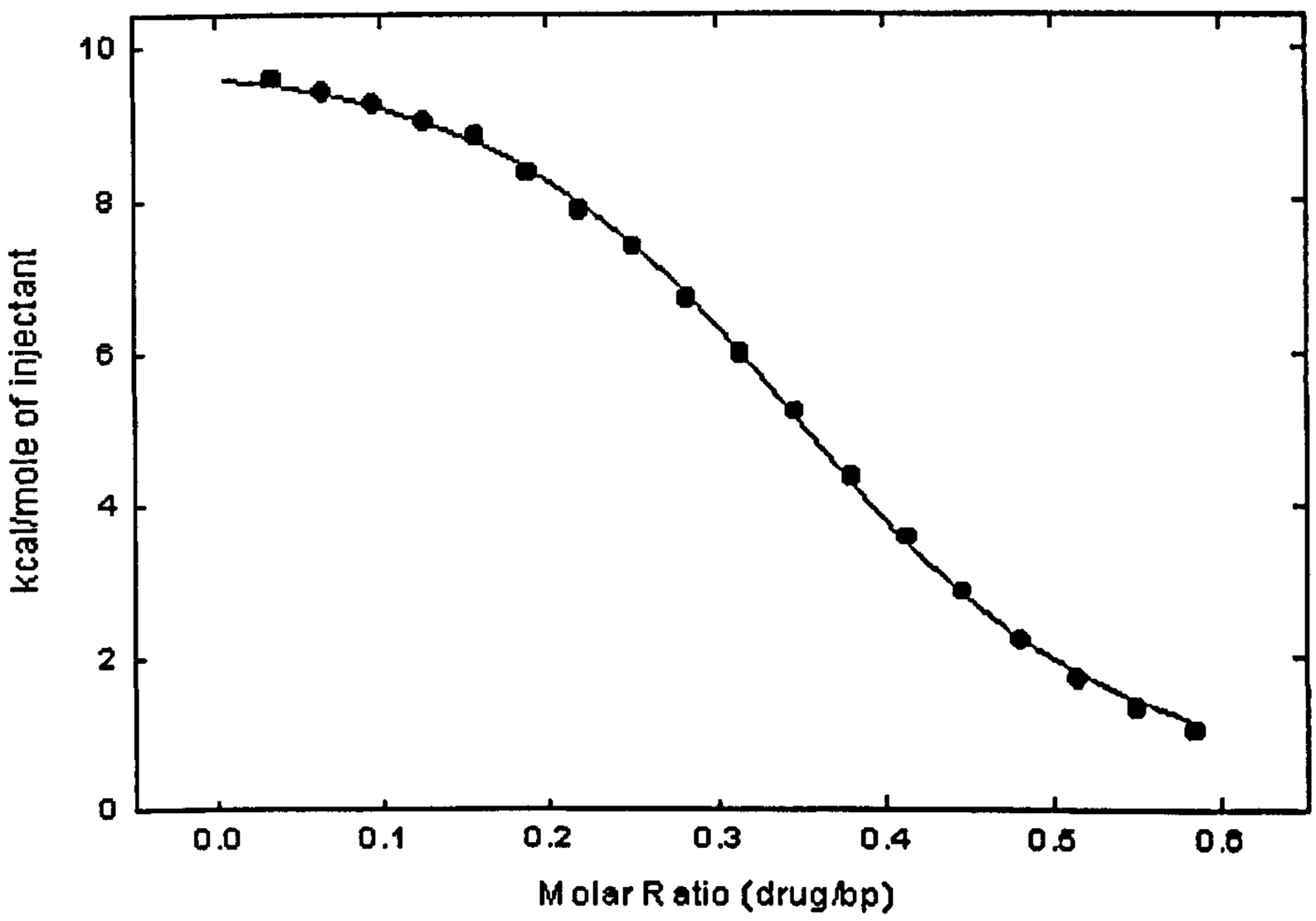

Figure 5.11:- *Raw ITC binding data (top) and binding isotherm (bottom) for the interaction of 0.823mmol [TpmPyRudppz]$^{2+}$ with 0.295 mmol(bp) poly(dA).poly(dT) at 25 °C*

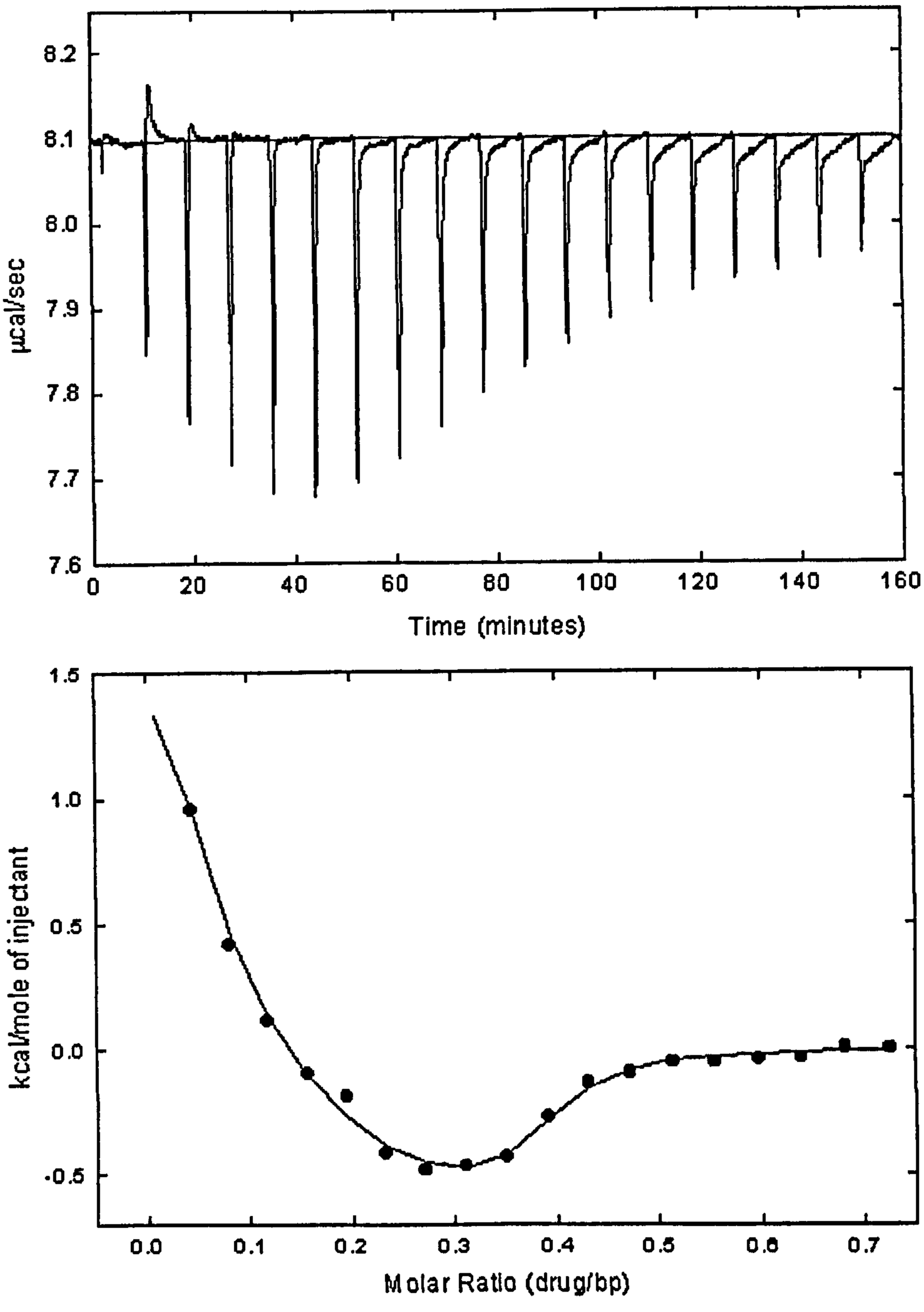

Figure 5.12:- *Raw ITC data (top) and Binding isotherm (bottom) for the interaction of 0.772 mmol [TpmPyRudppz]$^{2+}$ with 0.223 mmol(bp) poly(dG).poly(dC) at 25 °C*

The raw ITC data and the binding isotherm for the interaction of

$[TpmPyRudppz]^{2+}$ with poly(dG).poly(dC) is shown in Figure 5.12. The interaction produces a small negative binding enthalpy of –1.03 Kcal mol^{-1} indicating the interaction is exothermic[126].

The binding constants determined from the ITC experiments for $[TpmPyRudppz]^{2+}$ binding to poly(dA).poly(dT) and poly(dG).poly(dC) are $1.45x10^5$ and $1.12x10^6$ $mol^{-1}dm^3$, respectively. This means $[TpmPyRudppz]^{2+}$ has a near 8-fold preference for GC rich sequences of DNA over AT rich sequences. Moreover, the sign of the binding enthalpies indicates that binding of $[TpmPyRudppz]^{2+}$ to GC rich sequences is enthalpically driven and binding to AT sequences is driven by entropic contributions. The binding site size for binding to both poly(dA).poly(dT) and poly(dG).poly(dC) is around three base pairs which is typical of intercalators. The ITC data obtained for $[TpmPyRudppz]^{2+}$ binding to the homo-polymers is in good agreement with that obtained by the spectroscopic methods for binding to CT-DNA.

Table 5.2:- *ITC binding data for the Tpm ruthenium(II) complexes*

Complex (DNA)	ΔH_b (kcal mol^{-1})	K ($mol^{-1}dm^3$)	N (bp)
$[TpmPyRudppz]^{2+}$ (poly(dA).poly(dT))	+10.2	$1.45x10^5$	0.364 (2.7)
$[TpmPyRudppz]^{2+}$ (poly(dG).poly(dC))	-1.03	$1.12x10^6$	0.357 (2.8)
$[\{TpmRudppz\}_2dpp[5]]^{2+}$ (poly(dA).poly(dT))	$+2.38x10^4$	$4.23x10^5$	0.158 (6.38)
$[\{TpmRudppz\}_2dpp[5]]^{2+}$ (poly(dG).poly(dC))	+7260	$4.40x10^5$	0.132 (7.59)

The raw ITC data for both poly(dA).poly(dT) and poly(dG).poly(dC) show evidence of a second interaction before the main intercalation event. The first few injections in the poly(dG).poly(dC) titration can be used to estimate the binding parameters for this interaction. The binding constant is estimated at $3x10^7$ $mol^{-1}dm^3$ with a site size estimated at 100 base pairs. This indicates the homo-polymers contain a small number of highly

specific tight binding sites, which get saturated quickly, with the first few injections of the titration. The normal intercalation interaction then takes over. This phenomenon has bee observed before by Loontiens *et al.* in the interaction of Hoechst 33258 with poly(dA).poly(dT) and poly(dG).poly(dC)[129].

Figures 5.13 and 5.14 show the raw ITC data and binding isotherms for $[\{TpmRudppz\}_2dpp[5]]^{2+}$ binding to poly(dA).poly(dT) and poly(dG).poly(dC), respectively.

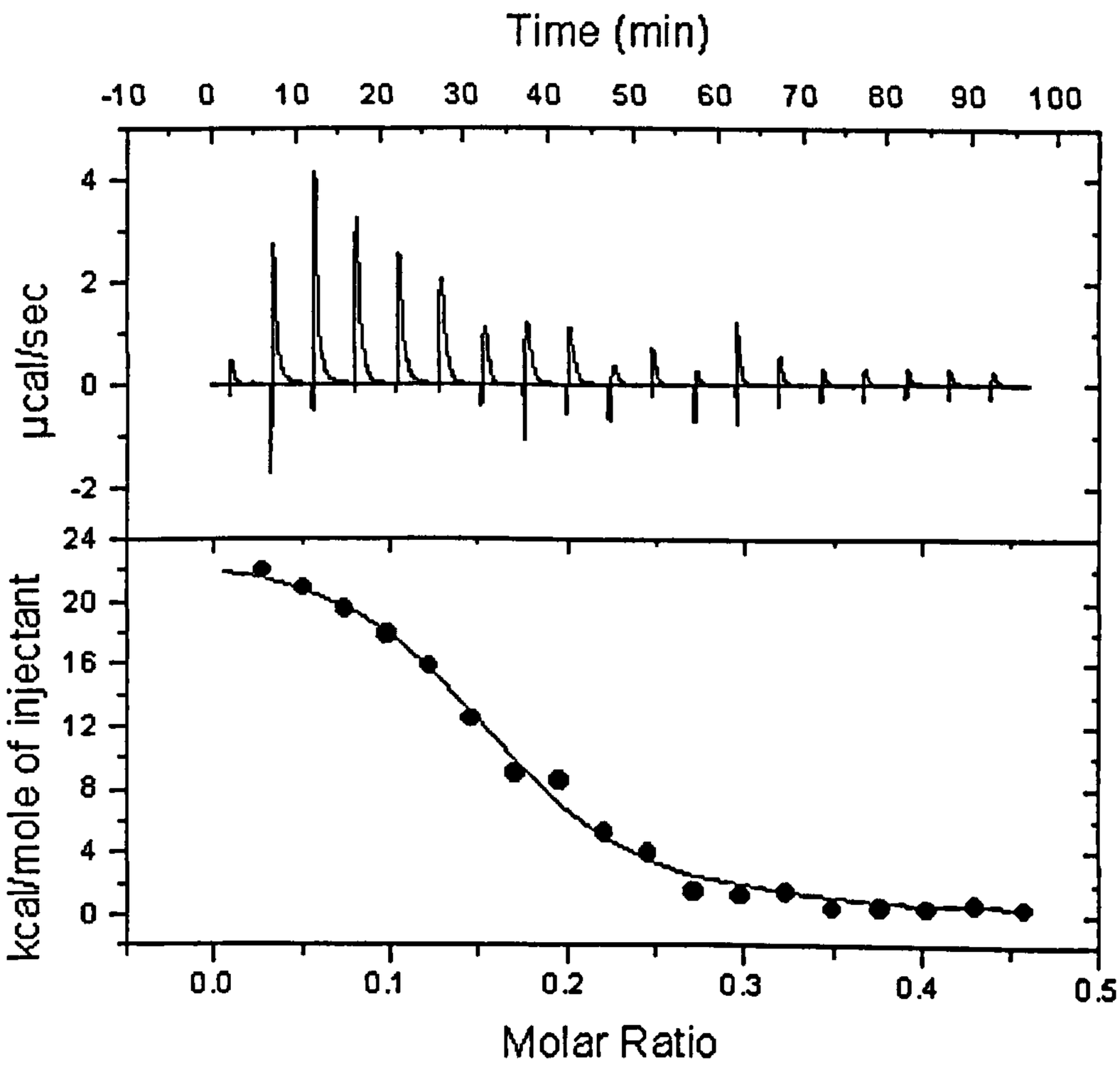

Figure 5.13:- *Raw ITC data (top) and binding isotherm (bottom) for the interaction of 0.80mmol $[\{TpmRudppz\}_2dpp[5]]^{4+}$ with 0.182mmol(bp) poly(dA).poly(dT) at 25℃*

Binding to both polymers results in a positive binding enthalpy, which

indicates the binding, is entropically driven. The binding constants for $[\{TpmRudppz\}_2dpp[5]]^{4+}$ binding to poly(dA).poly(dT) and poly(dG).poly(dC) are $4.23x10^5$ and $4.40x10^5$ $mol^{-1}dm^3$, respectively. This immediately shows that the sequence specificity shown in the monometallic complex is lost in the bimetallic complex. The magnitudes of the binding constants are again in good agreement with the spectroscopic data. Both ITC and spectroscopic studies show no significant increase in binding affinity for DNA between the monometallic and bimetallic complexes.

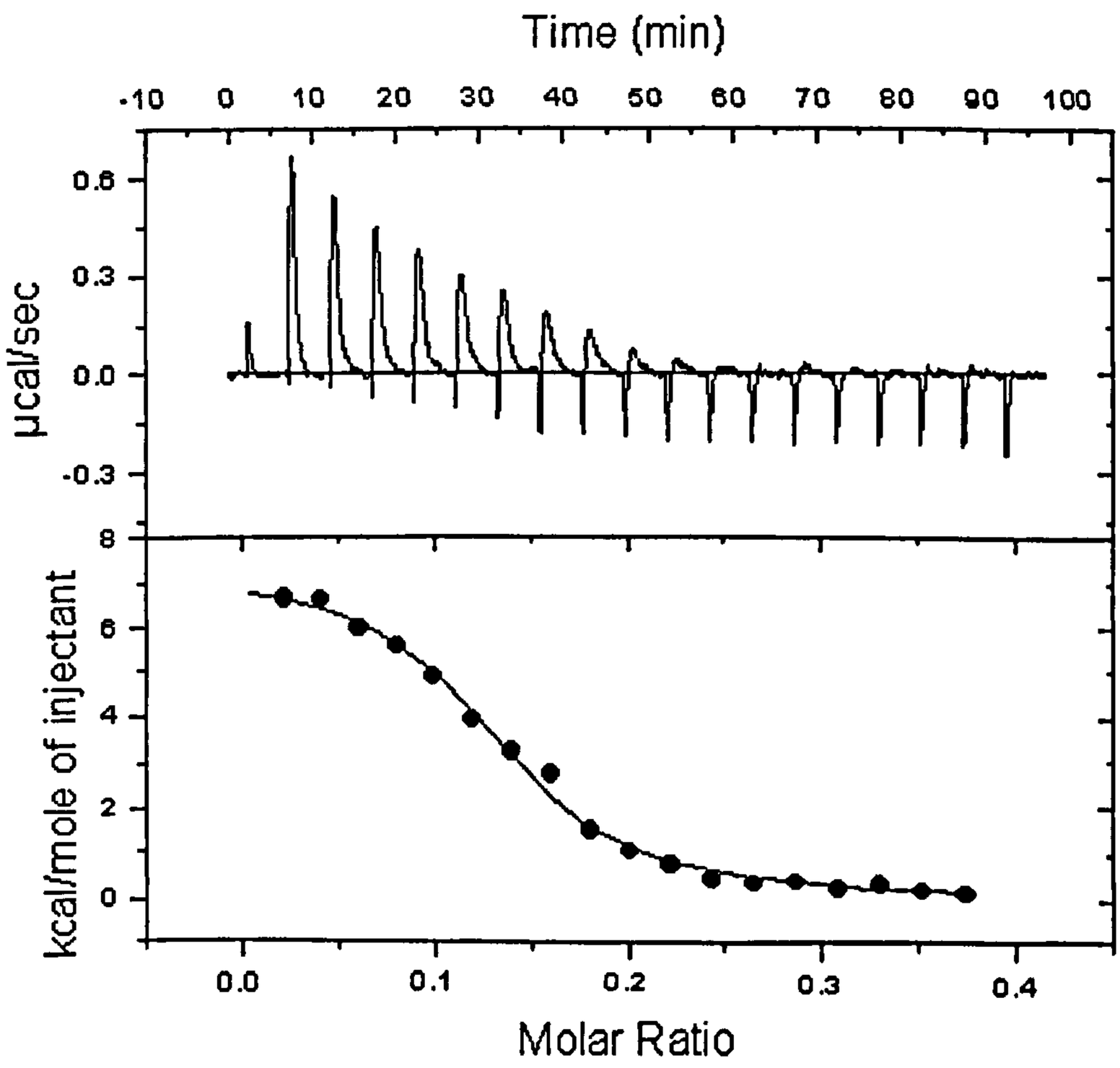

Figure 5.14:- *Raw ITC data (top) and binding isotherm (bottom) for the interaction of 0.80mmol* $[\{TpmRudppz\}_2dpp[5]]^{4+}$ *with 0.224mmol(bp) poly(dG).poly(dC) at 25°C*

ITC does, however, show a larger site size (6.4 and 7.5 for

poly(dA).poly(dT) and poly(dG).poly(dC), respectively) which shows that both of the metal centres are interacting with the DNA. The values of the binding constants and site sizes are comparable to those obtained by Kelly *et al.* [58] for the interaction of the bimetallic ruthenium(II) complex $[(phen)_2Ru(Mebipy)\text{-}(CH_2)_5\text{-}(bipyMe)Ru(phen)_2]^{4+}$ ($K = 2.4x10^5$ $mol^{-1}dm^3$, $S = 6.4$). This bimetallic complex has been shown to bind to DNA through electrostatic and groove binding interactions. It is probable, therefore, that $[\{TpmRudppz\}_2dpp[5]]^{4+}$ is binding in a similar manner within the grooves of the DNA. Instead of the increased binding affinity expected through cooperativity when two intercalators were joined together, we seem to be observing anti-cooperativity as neither of the metal centres are intercalating into DNA. Further synthetic studies are under way to lengthen the linker between the ruthenium centres to determine the optimum length to allow both centres to intercalate.

5.5.2 DNA binding studies on the rhenium mono- and bimetallic complexes

The interaction $[(CO)_3PyRedppz]^+$ with CT-DNA, poly(dA).poly(dT) and poly(dG).poly(dC) has been reported elsewhere[42]. Luminescence titrations reveal binding parameters of $4.2x10^4$ $mol^{-1}dm^3$ and a site size of 2 base pairs with CT-DNA after analysis of binding data with the Mcghee-von Hippel Model. Unfortunately the rhenium(I) bimetallic clip $[\{(CO)_3Redppz\}_2dpp[3]]^{2+}$ does not show any luminescence upon binding to DNA, so UV-Visible titrations are the only way to characterise the binding of these complexes spectroscopic ally. In order to carry out a comparative study, it was decided to synthesise the monometallic complexes $[(CO)_3MeCNRedppz]^+$ and $[(CO)_3PyRedppz]^+$ and re-investigate their DNA binding properties, along with the bimetallic clip by performing UV-Visible titrations under identical conditions.

As expected, all three of the complexes show saturation binding characteristics portrayed through hypochromic shifts in their dppz $\pi \rightarrow \pi^*$ transitions upon titration with CT-DNA. The raw binding data for $[(CO)_3MeCNRedppz]^+$ is shown in Figure 5.15.

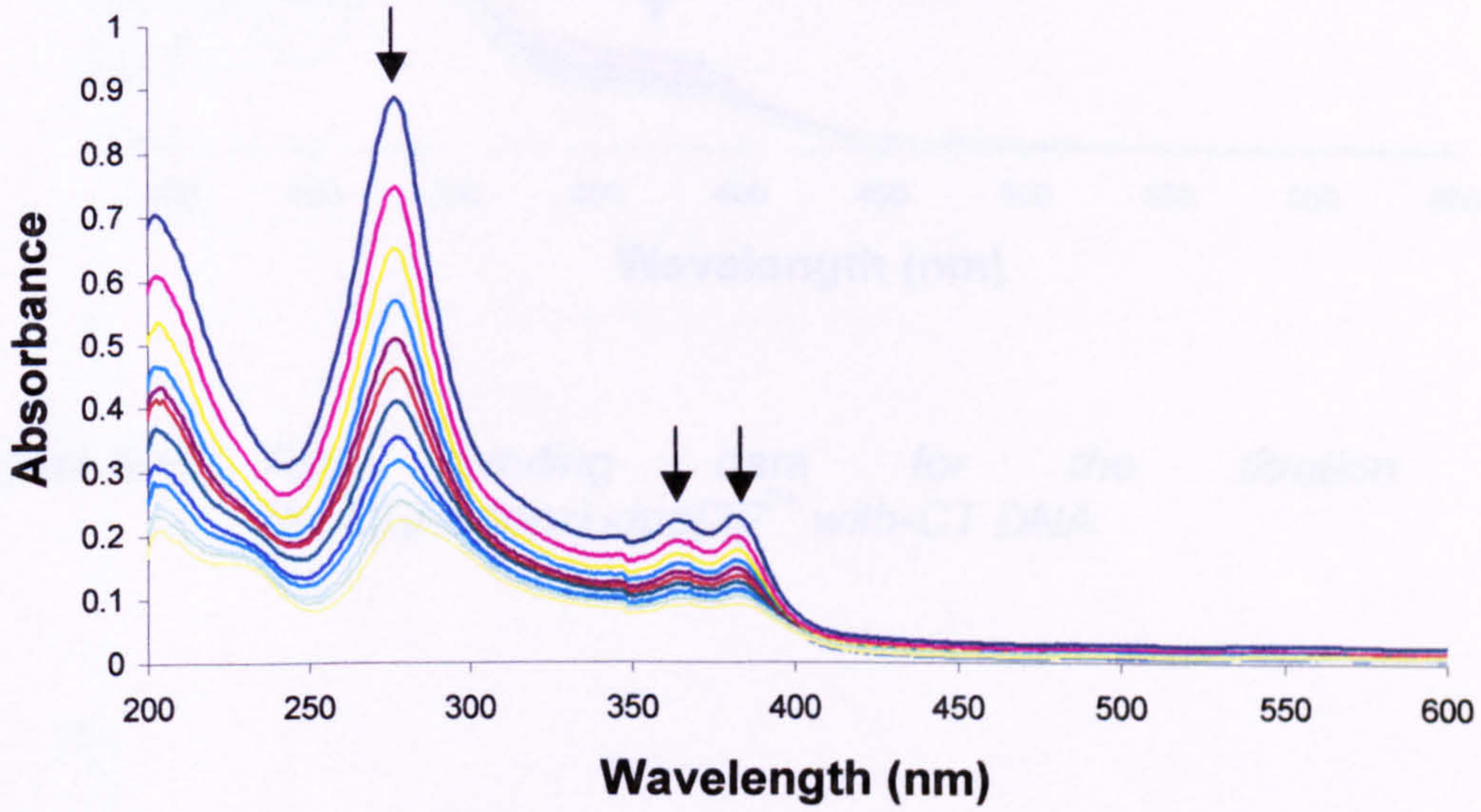

Figure 5.15:- *Raw binding data for the titration of $[(CO)_3MeCNRedppz]^+$ with CT-DNA*

The data for $[(CO)_3PyRedppz]^+$ are very similar and can be found on the supplementary data CD.

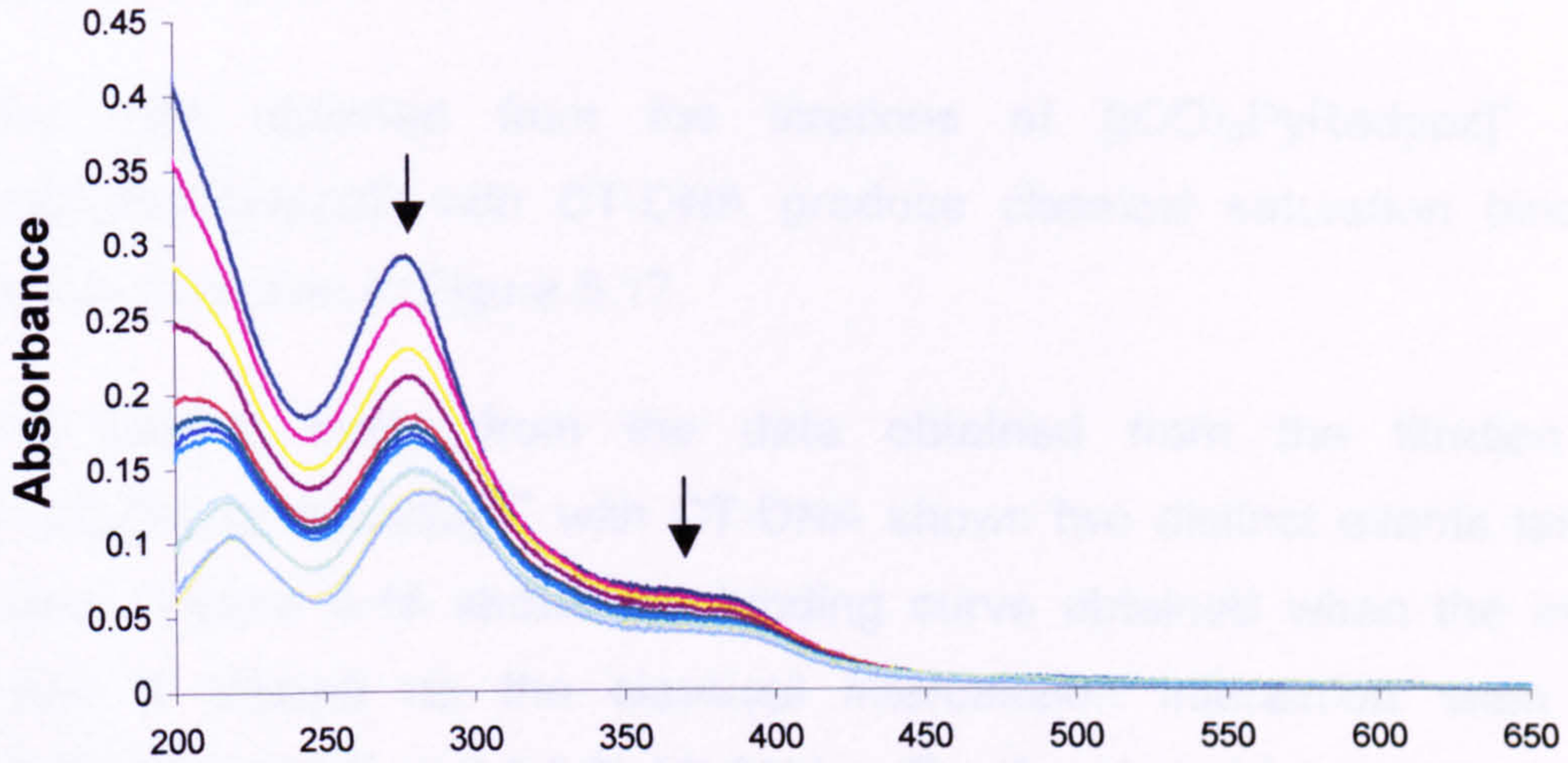

Figure 5.16:- *Raw binding data for the titration of $[\{(CO)_3Redppz\}_2dpp[3]]^{2+}$ with-CT DNA*

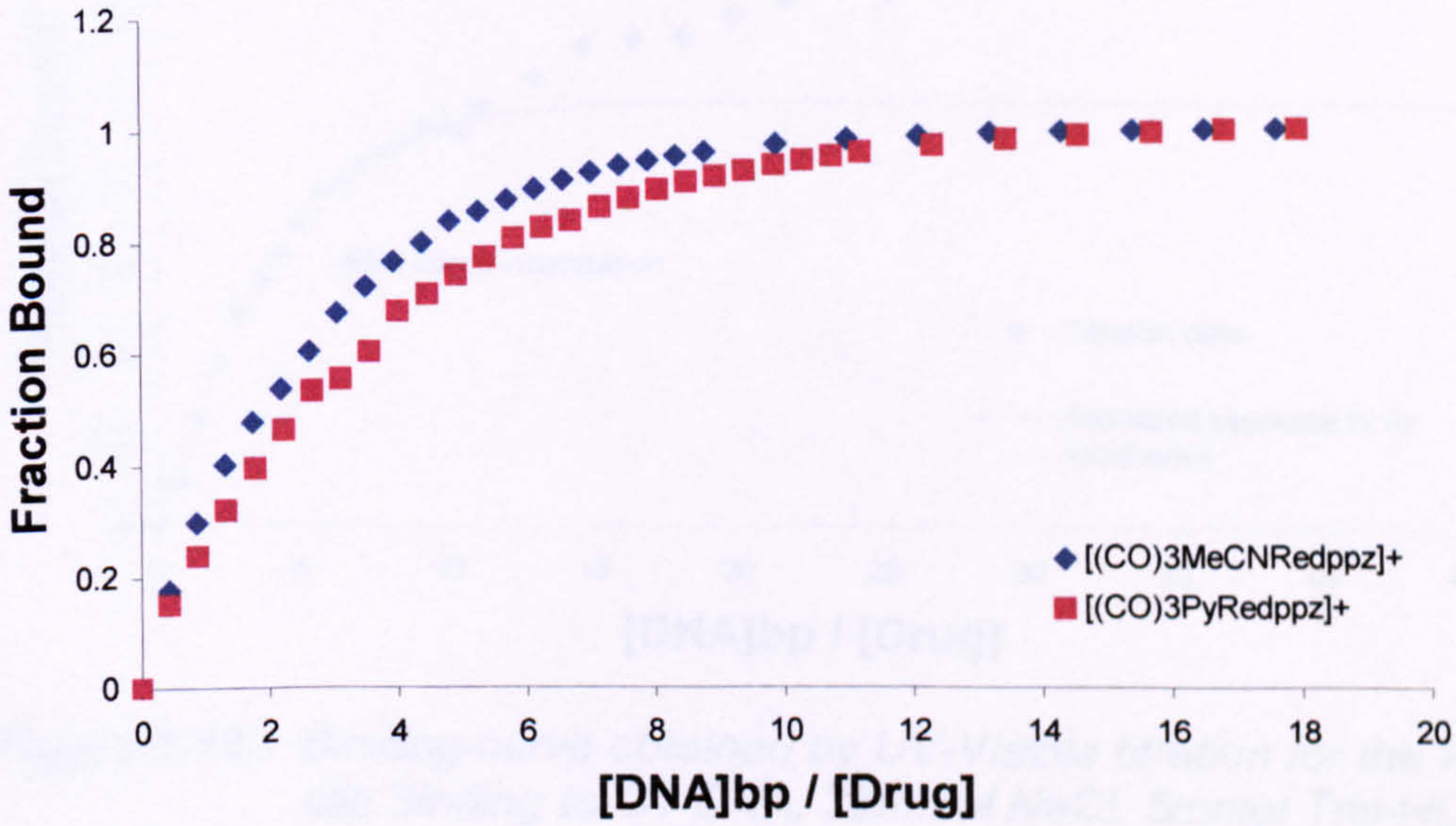

Figure 5.17:- *Binding curves obtained by luminescence titrations for the Re dppz monometallic complexes binding to CT DNA, 25mmol NaCl, 5mmol Tris-HCl, pH 7.0, 25°C.*

The data obtained from the titration of $[\{(CO)_3Redppz\}_2dpp[3]]^{2+}$ with CT-DNA were not, however, quite as simple. The raw titration data are

shown in Figure 5.16.

The data obtained from the titrations of $[(CO)_3PyRedppz]^+$ and $[(CO)_3MeCNdppz]^+$ with CT-DNA produce classical saturation binding curves as shown in Figure 5.17.

The binding curve from the data obtained from the titration of $[\{(CO)_3Redppz\}_2dpp[3]]^{2+}$ with CT-DNA shows two distinct events taking place. Figure 5.18 shows the binding curve obtained when the initial event is treated as the classical intercalation interaction seen for $[(CO)_3PyRedppz]^+$ and $[(CO)_3MeCNdppz]^+$. If a sigmoidal curve is fitted to the initial binding event, which saturates at a fraction bound of 1, the second event can clearly be seen.

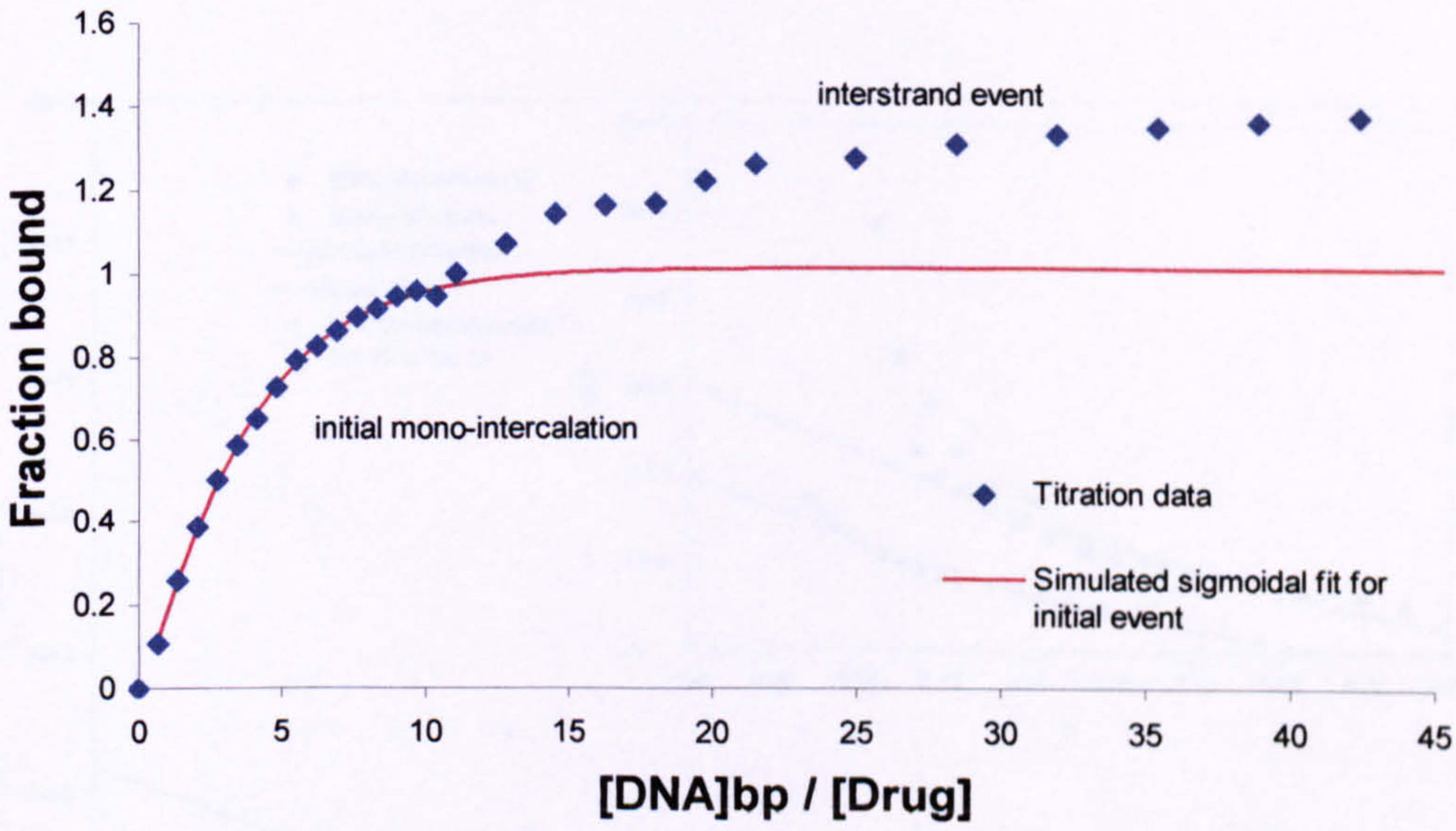

Figure 5.18:- *Binding curve obtained by UV-Visible titration for the Re [3] clip binding to CT DNA, 25mmol NaCl, 5mmol Tris-HCl, pH 7.0, 25℃.*

Table 5.3 summarises the binding parameters obtained from Mcghee-von Hippel best fits of non-linear Scatchard plots of the binding data (Figure 5.19). The % hypochromicity observed in the high-energy bands at *ca.* 278nm is approximately half (40%) in the bimetallic

$[\{(CO)_3Redppz\}_2dpp[3]]^{2+}$ than in the two monometallic complexes (86.36% and 88.88%, respectively, for $[(CO)_3PyRedppz]^+$ and $[(CO)_3MeCNdppz]^+$). As $[\{(CO)_3Redppz\}_2dpp[3]]^{2+}$ contains two identical intercalating domains, one would expect the % hypochromicity to be similar to the monometallic complexes if both rhenium centres are interacting with the CT-DNA. As $[\{(CO)_3Redppz\}_2dpp[3]]^{2+}$ only displays half the hypochromicity in the initial binding event, it suggests that only one rhenium binding domain is interacting with the DNA. We believe this is due to the steric constraints of the three carbon linker which does not allow sufficient freedom for both rhenium centres to intercalate into the DNA. It would, however, leave the second rhenium centre free to interact with a second DNA duplex

.

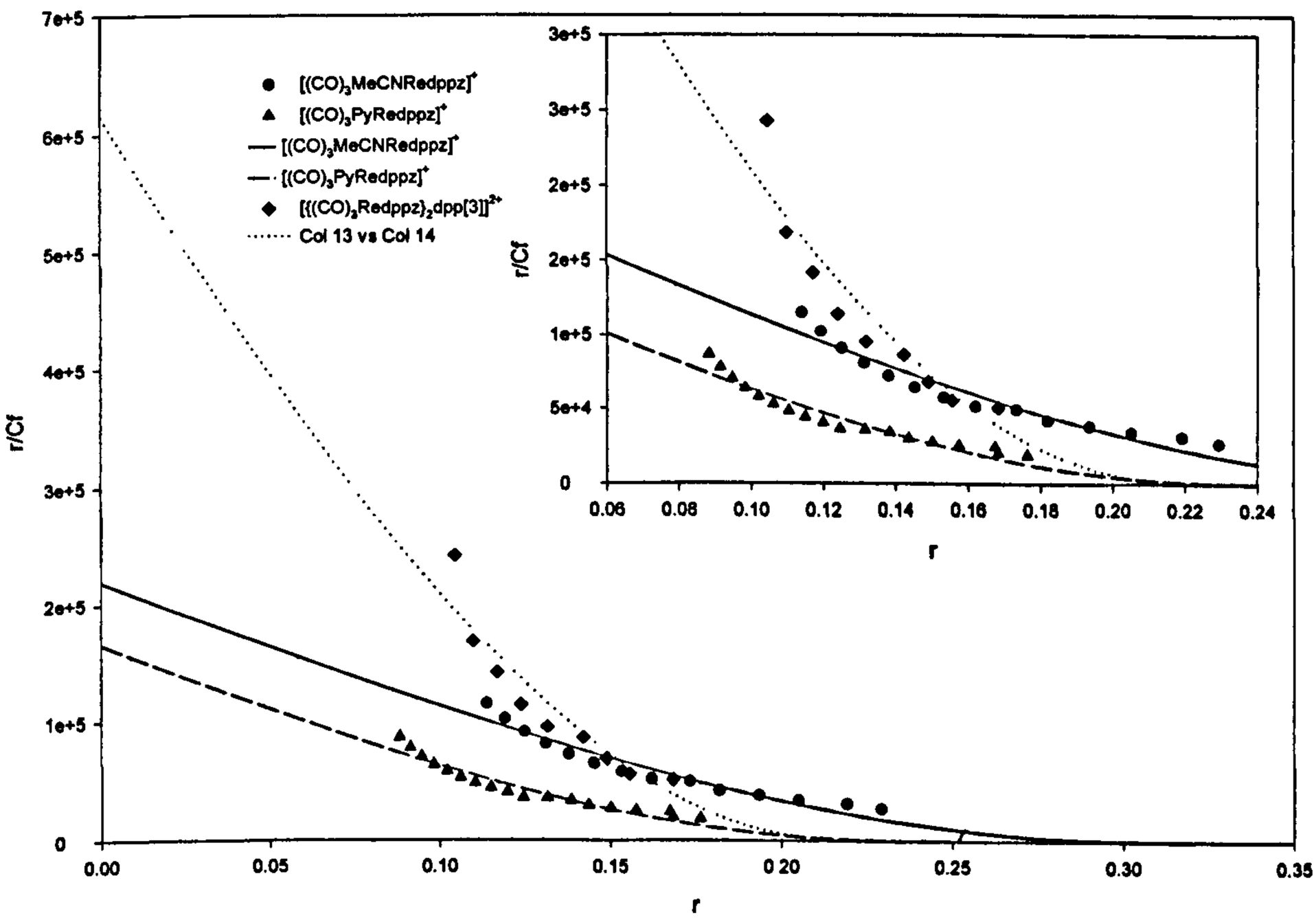

Figure 5.19:- *Scatchard plots with Mcghee-von Hippel best fits obtained by UV-Visible titrations for the Rhenium dppz complexes binding to CT DNA, 25mmol NaCl, 5mmol Tris-HCl, pH 7.0, 25°C.*

We believe the second binding event seen at higher concentrations of DNA is interstrand cross-linking of the second rhenium centre to a second DNA duplex.

Table 5.3:- *Spectroscopic binding data for the rhenium dppz mono- and bimetallic complexes binding to CT-DNA, 25mmol NaCl, 5mmol Tris, pH 7.0*

Complex	UV-Visible			Luminescence		
	K (mol^{-1} dm^3)	S (bp)	%hyp	K (mol^{-1} dm^3)	S (bp)	I/I_0
$[(CO)_3MeCNRedppz]^{+a}$	$2.20x10^5$	3.11	88.9	-	-	-
$[(CO)_3PyRedppz]^{+a}$	$1.66x10^5$	3.96	86.4	$4.20x10^{4,c}$	2[c]	13[c]
$[\{(CO)_3Redppz\}_2dpp[5]]^{+a,b}$	$7.17x10^5$	4.49	40.1	-	-	-

[a] Titration performed in 5% methanolic buffer
[b] Binding data is obtained from the initial binding event with DNA
[c] Data obtained from Yam *et al.*[42].

The binding parameters obtained from the titrations are consistent with the mono-intercalative nature of the initial binding event. The ratio of binding constants $[(CO)_3PyRedppz]^+$: $[\{(CO)_3Redppz\}_2dpp[3]]^{2+}$ is 4.3. If the both of the rhenium domains were intercalated to the DNA helix and the drug was acting as a bis-intercalator then an increase in binding affinity of at least 1000- fold would be expected as seen in other systems[57,58,130]. This 5 or so fold increase in binding affinity can again be attributed to an increased electrostatic interaction of di-cationic bimetallic over its mono-cationic monometallic analogue. The site size is only slightly bigger for the bimetallic (4.49bp compared to 3.96bp), which is again consistent with mono-intercalation.

Although $[\{(CO)_3Redppz\}_2dpp[5]]^{2+}$ has been synthesised, there has been insufficient time in this study to fully quantify its interaction with CT-DNA, and the work is still in progress.

5.5.3 DNA binding studies on the rhenium 4'-extended terpyridine complexes

The 4'-extended terpyridine complexes of rhenium(I) all showed hypochromic shifts in their UV-Visible spectra upon titration with CT-DNA. The raw titration data for $[(CO)_3MeCNReQtpy]^+$ is shown in Figure 5.20.

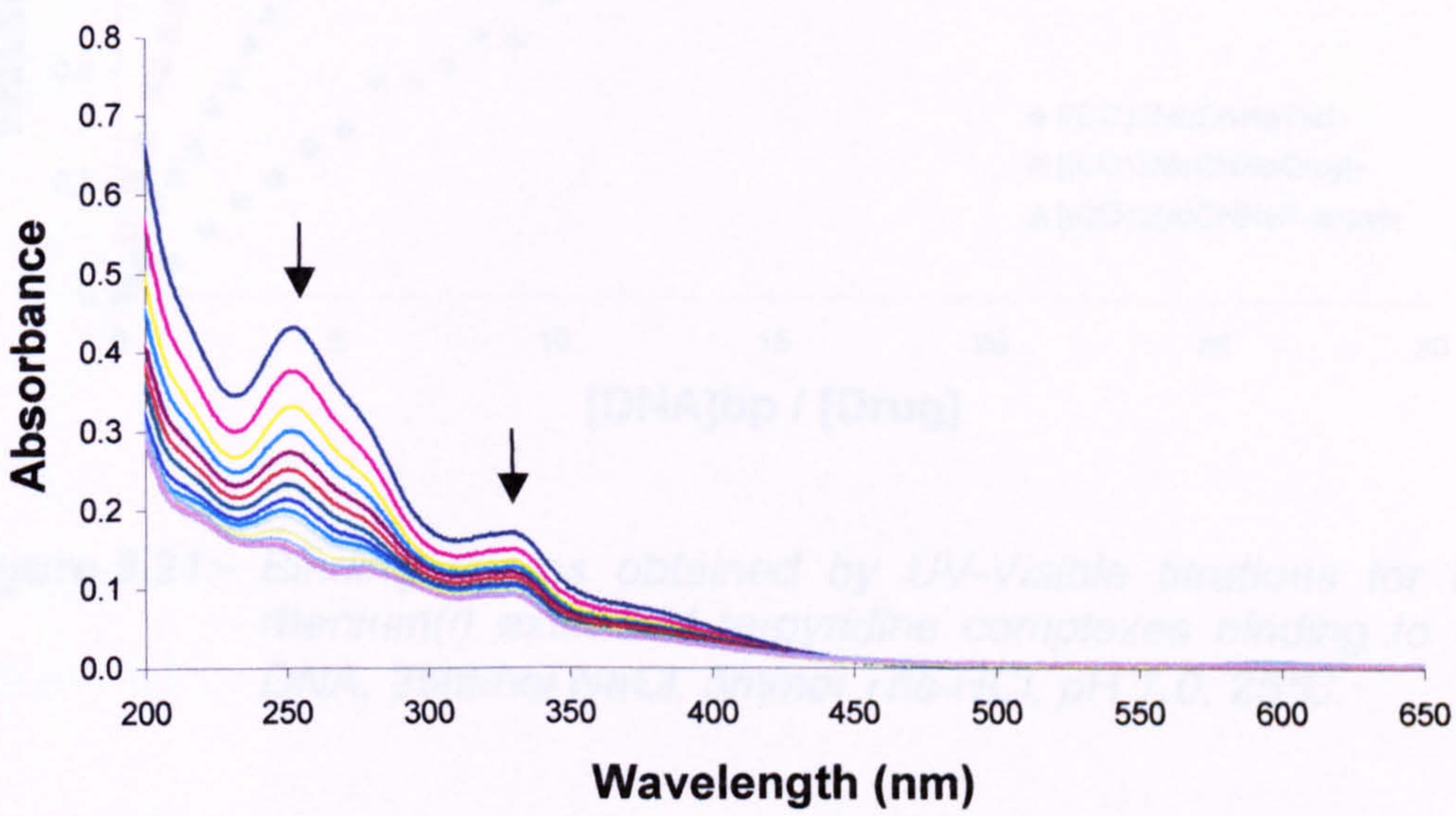

Figure 5.20:- *Raw binding data for the titration of $[(CO)_3MeCNReQtpy]^+$ with CT-DNA*

The UV-Visible spectrum shows hypochromicity in all of the transitions upon titration of CT-DNA. The raw data for the other two rhenium(I) complexes can be found on the supplementary data CD.

Manipulation of the spectral shifts produces saturation binding curves for all three of the rhenium(I) extended terpyridine complexes (Figure 5.21). $[(CO)_3MeCNReQtpy]^+$ and $[(CO)_3MeCNReP\text{-}terpy]^+$ show well defined curves reaching saturation between 5-10 base pairs per drug. The binding of $[(CO)_3MeCNReTpt]^+$ to CT-DNA produces a significantly different binding curve, which is more linear in nature. Saturation is not

achieved until a ratio of about 20-25 base pairs per drug is reached.

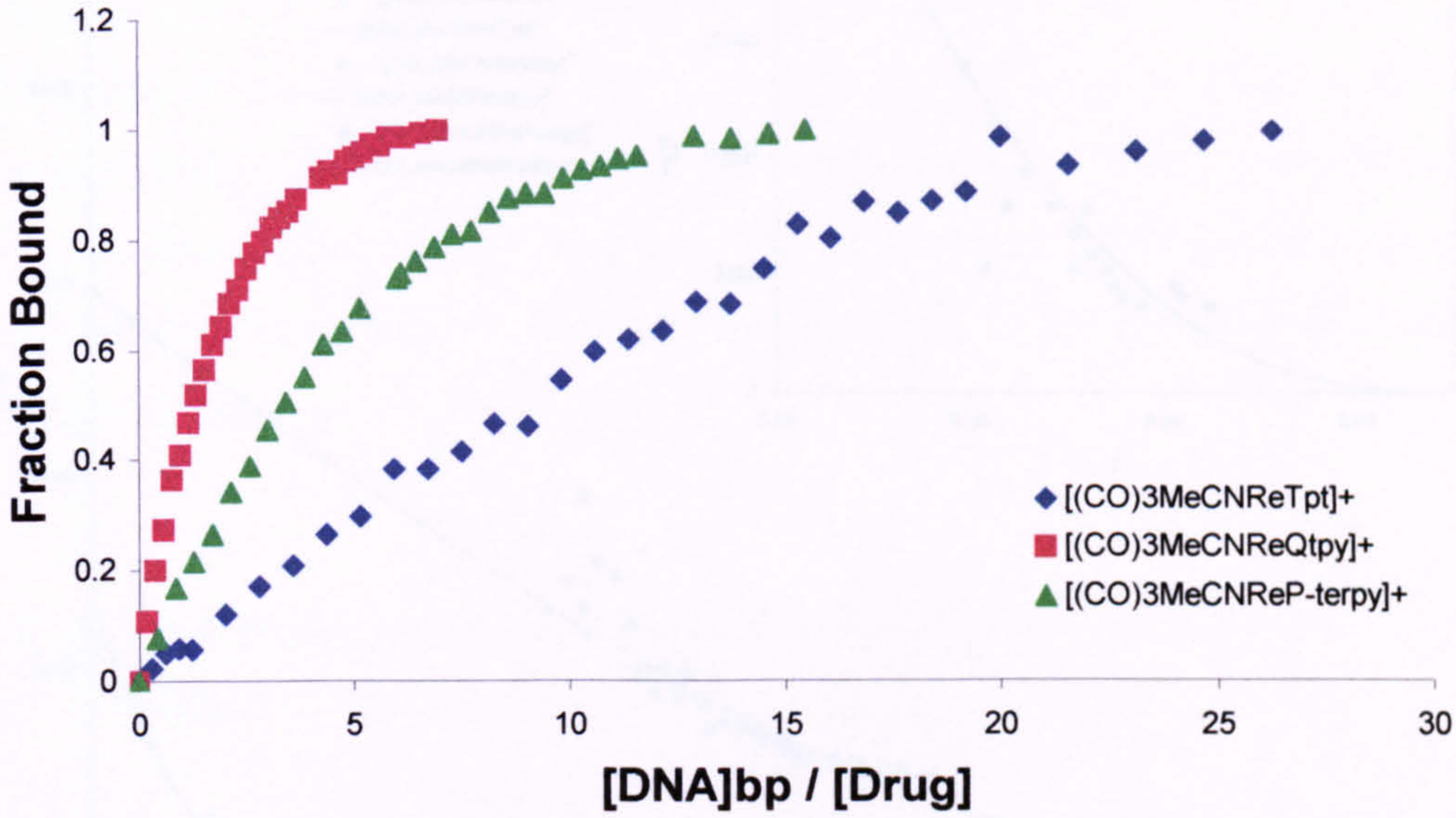

Figure 5.21:- *Binding curves obtained by UV-Visible titrations for the rhenium(I) extended terpyridine complexes binding to CT DNA, 25mmol NaCl, 5mmol Tris-HCl, pH 7.0, 25°C.*

The binding parameters were again determined from non-linear least-squares fits of the Mcghee-von Hippel model to the non-linear binding isotherms obtained from Scatchard plots (Figure 5.22). The data are summarised in Table 5.4.

Table 5.4:- *Spectroscopic binding data for the rhenium 4'-extended terpyridine complexes binding to CT-DNA, 25mmol NaCl, 5mmol Tris, pH 7.0*

Complex	UV-Visible		
	K (mol^{-1} dm^3)	S (bp)	%hyp
$[(CO)_3MeCNReTpt]^{+,a}$	$1.34x10^5$	12.19	17.8
$[(CO)_3MeCNReQtpy]^{+,a}$	$2.97x10^5$	2.04	64.8
$[(CO)_3MeCNReP\text{-}terpy]^{+,a}$	$4.32x10^5$	2.24	79.2

[a] titration performed in 5% methanolic buffer

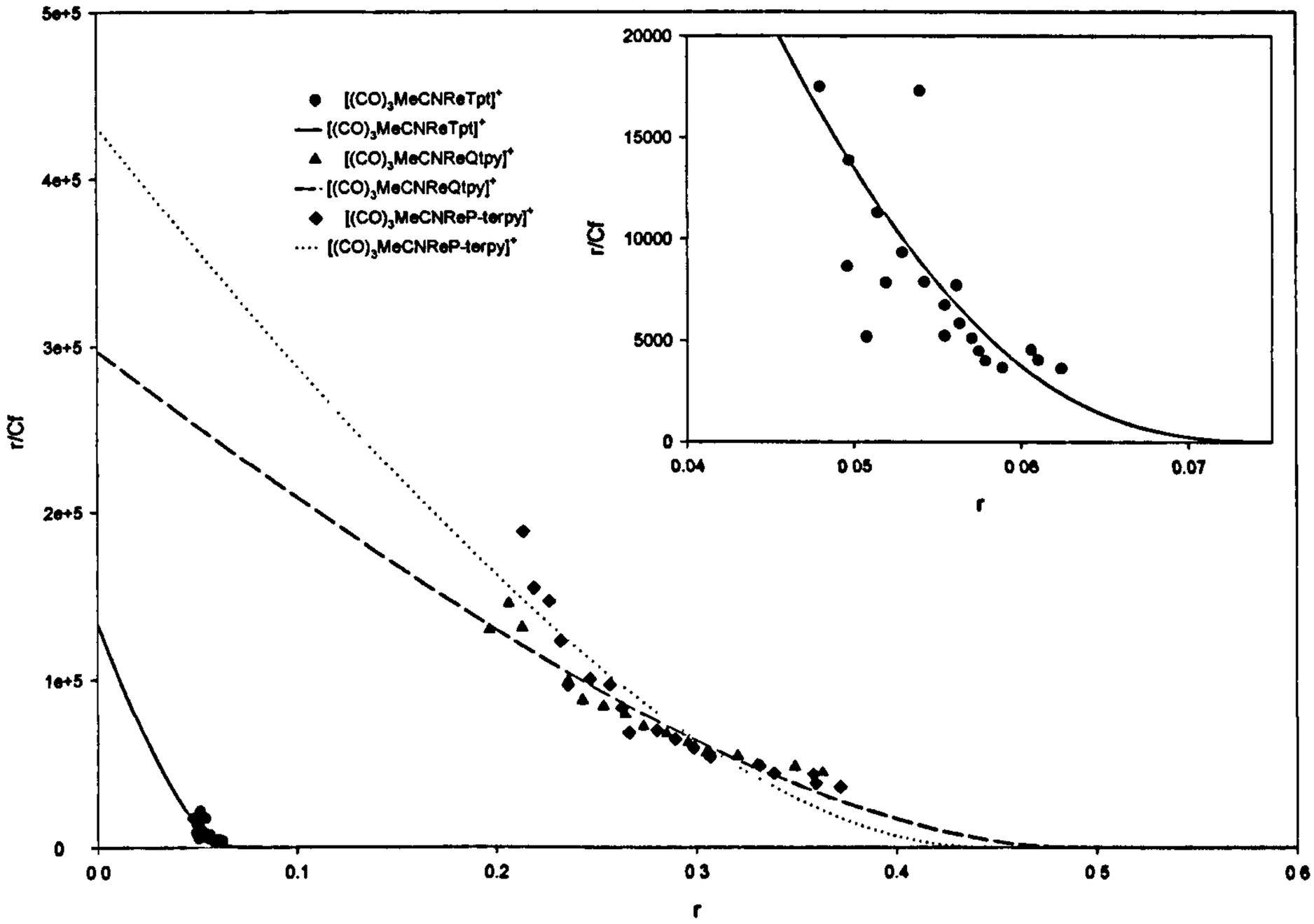

Figure 5.22:- *Scatchard plots with Mcghee-von Hippel best fits obtained by UV-Visible titrations for the Tpm ruthenium complexes binding to CT DNA, 25mmol NaCl, 5mmol Tris-HCl, pH 7.0, 25℃.*

The Mcghee-von Hippel best fits show immediately that $[(CO)_3MeCNReTpt]^+$ is interacting with the DNA in a different manner to $[(CO)_3MeCNReQtpy]^+$ and $[(CO)_3MeCNReP\text{-}terpy]^+$, which show all the hallmarks of a classical intercalative interaction with DNA. The magnitude of the intrinsic binding constants ($2.97x10^5$ and $4.32x10^5$ $mol^{-1}dm^3$, respectively for $[(CO)_3MeCNReQtpy]^+$ and $[(CO)_3MeCNReP\text{-}terpy]^+$) are typical of those expected for intercalation as are the site sizes (2.04 and 2.24 for $[(CO)_3MeCNReQtpy]^+$ and $[(CO)_3MeCNReP\text{-}terpy]^+$ respectively)[9]. In contrast, the site size determined for $[(CO)_3MeCNReTpt]^+$ is 12.19 base pairs which is extremely large for a small molecule binding to DNA, especially is intercalation is the suspected mode of interaction. The binding constant is $1.34x10^5$, which is comparable to the other two complexes. The percentage hypochromicity

when fully bound is also small (17.75%) compared to 64.8 % for $[(CO)_3MeCNReQtpy]^+$ and 79.2% for $[(CO)_3MeCNReP\text{-}terpy]^+$. All the evidence points to a non-intercalative mode of interaction for $[(CO)_3MeCNReTpt]^+$ with CT DNA, except for the high binding constant. The preference of $[(CO)_3MeCNReTpt]^+$ for a small number of very specific tight binding sites could explain the abnormal binding parameters associated with complex. Further studies need to be undertaken before this hypothesis can be confirmed.

5.5.4 DNA binding studies on the $TerpyRu^{2+}$ extended terpyridine complexes

All five of the achiral $terpyRu^{2+}$ extended terpyridine complexes showed hypochromic shifts in their UV-Visible spectrum upon titration with CT-DNA.

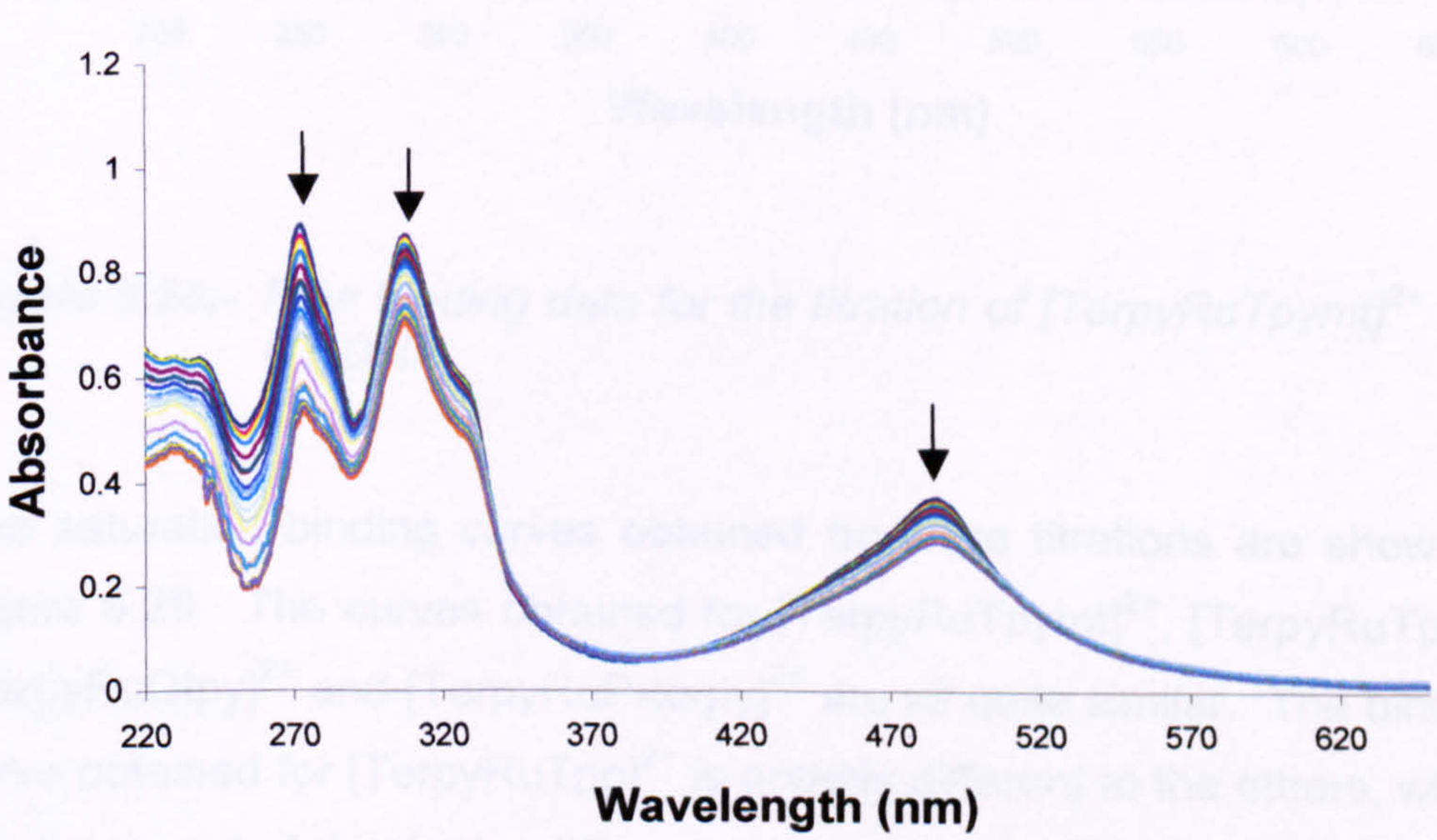

Figure 5.23:- *Raw binding data from the titration of $[TerpyRuQtpy]^{2+}$ with CT-DNA*

Figure 5.23 shows the raw data from the titration of $[TerpyRuQtpy]^{2+}$ with

CT-DNA. Hypochromicity is seen in both the high energy ligand centred bands (<320nm) and the MLCT band. This is not the case for all of the extended terpyridine complexes as $[TerpyRuTpymt]^{2+}$ and $[TerpyRuTpt]^{2+}$ show no hypochromic shifts in the MLCT band, with only the higher energy ligand centred band showing any significant hypochromicity. Figure 5.24 shows the raw binding data for $[TerpyRuTpymt]^{2+}$ interacting with CT-DNA.

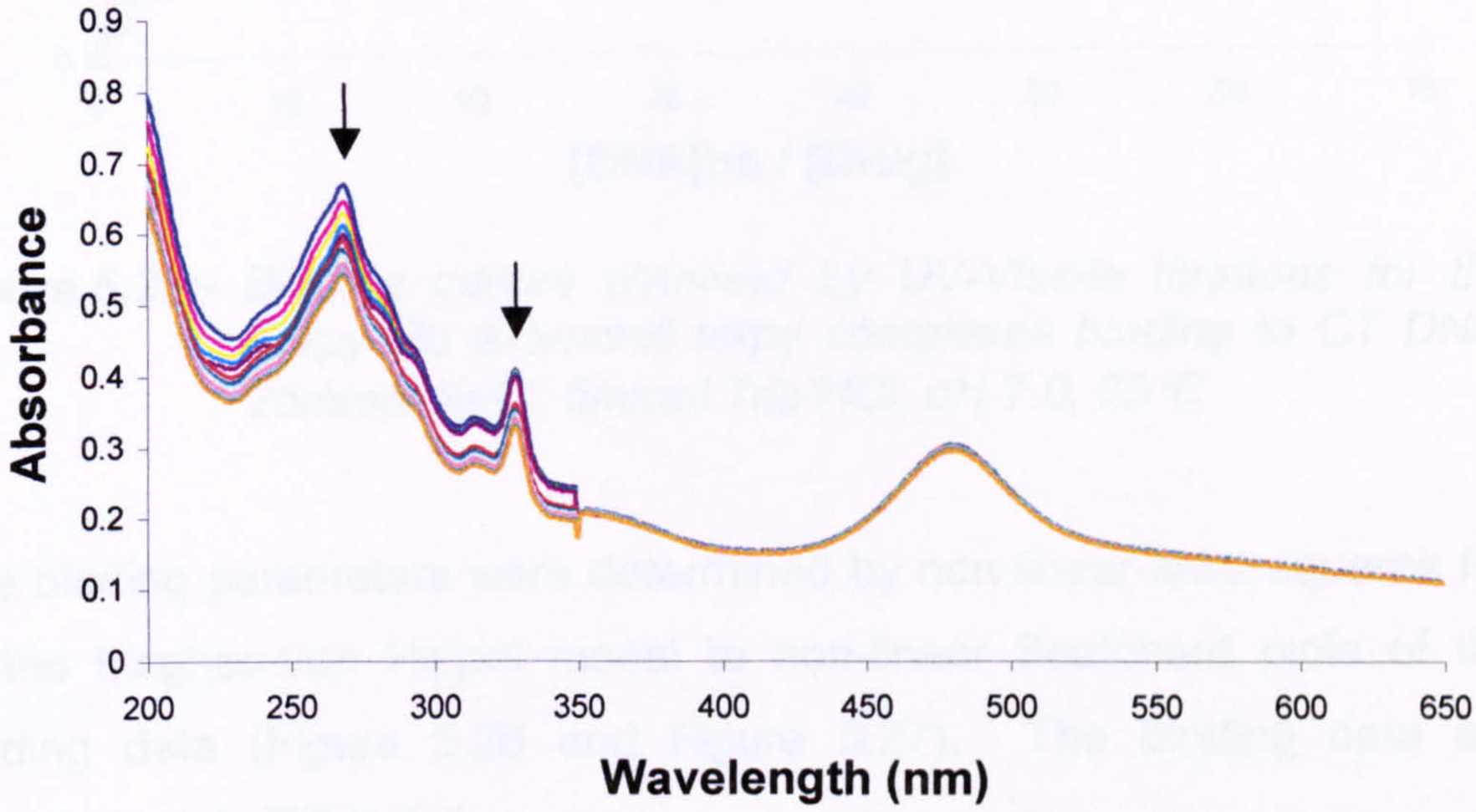

Figure 5.24:- *Raw binding data for the titration of $[TerpyRuTpymt]^{2+}$ with CT-DNA*

The saturation binding curves obtained from the titrations are shown in Figure 5.25. The curves obtained for $[TerpyRuTpymt]^{2+}$, $[TerpyRuTpt]^{2+}$, $[TerpyRuQtpy]^{2+}$ and $[TerpyRuP\text{-}terpy]^{2+}$ are all quite similar. The binding curve obtained for $[TerpyRuTpp]^{2+}$ is notably different to the others, which can be expected due to the different geometry of the Tpp ligand.

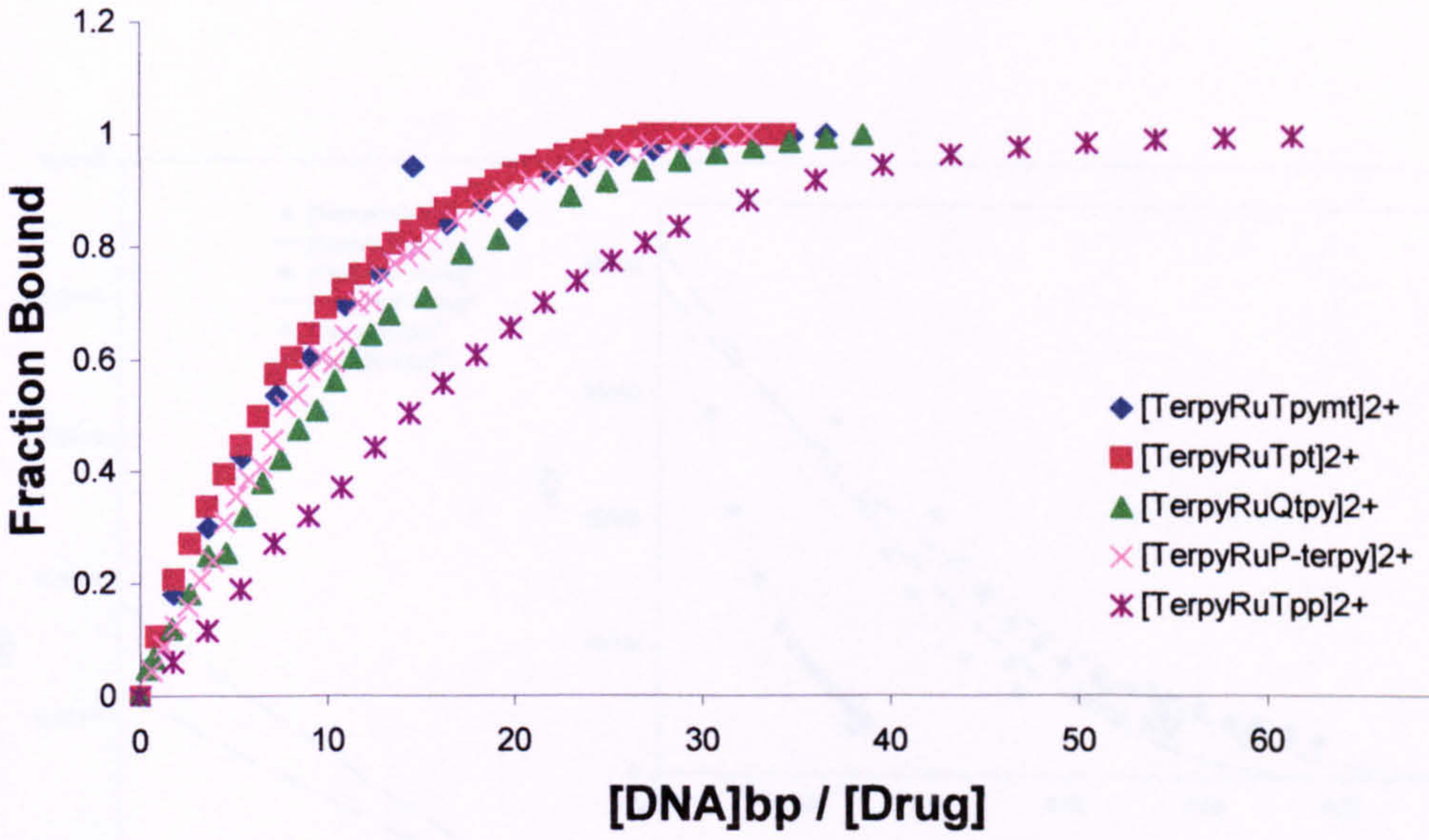

Figure 5.25:- *Binding curves obtained by UV-Visible titrations for the Terpy Ru extended terpy complexes binding to CT DNA, 25mmol NaCl, 5mmol Tris-HCl, pH 7.0, 25°C.*

The binding parameters were determined by non-linear least-squares fits of the Mcghee-von Hippel model to non-linear Scatchard plots of the binding data (Figure 5.26 and Figure 5.27). The binding data are summarised in Table 5.5.

Table 5.5:- *Spectroscopic binding data for the $TerpyRu^{2+}$ extended terpyridine complexes binding to CT-DNA, 25mmol NaCl, 5mmol Tris, pH 7.0*

Complex	UV-Visible		
	K (mol^{-1} dm^3)	S (bp)	%hyp
$[TerpyRuTpymt]^{2+}$ [a]	$8.14x10^4$	8.43	19.8
$[TerpyRuTpt]^{2+}$	$8.28x10^4$	9.79	15.9
$[TerpyRuQtpy]^{2+}$	$7.63x10^4$	12.67	48.4
$[TerpyRuP\text{-}terpy]^{2+}$	$6.38x10^4$	10.96	49.4
$[TerpyRuTpp]^{2+}$ [a]	$1.28x10^5$	20.71	31.5

[a] titration performed in 5% methanolic buffer

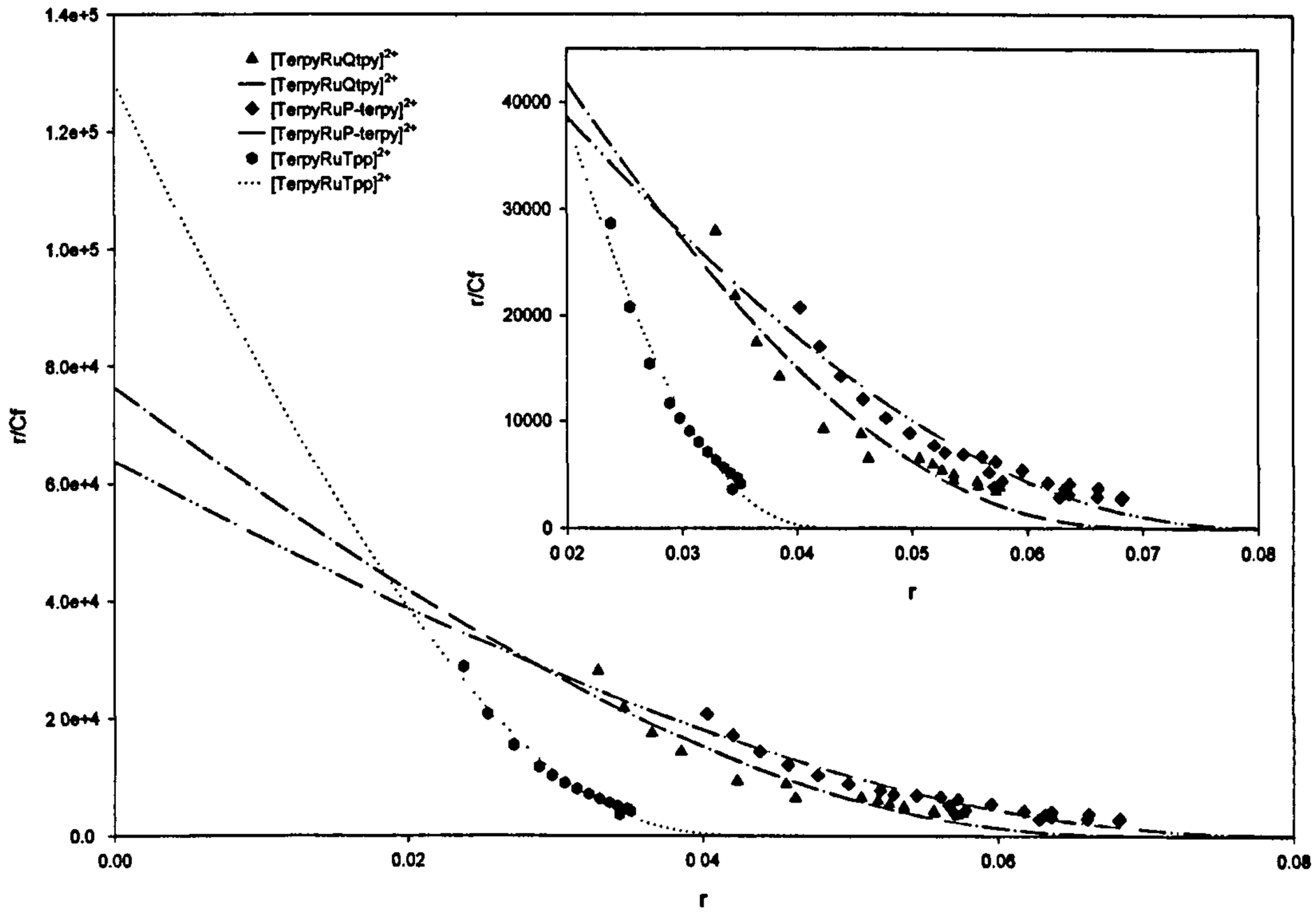

Figure 5.26:- *Scatchard plots with Mcghee-von Hippel best fits obtained by UV-Visible titrations for the Terpy ruthenium tetrazine complexes binding to CT DNA, 25mmol NaCl, 5mmol Tris-HCl, pH 7.0, 25°C.*

Analysis of the binding parameters and the Scatchard plots reveals three distinct types of interaction with the CT-DNA. The % hypochromicity seen in the UV-Visible spectrum of $[TerpyRuTpymt]^{2+}$ and $[TerpyRuTpt]^{2+}$ is less than half of that seen for $[TerpyRuQtpy]^{2+}$ and $[TerpyRuP\text{-}terpy]^{+}$ (19.77% and 15.93% compared to 48.36% and 49.37%, respectively). The binding site size is also slightly smaller for $[TerpyRuTpymt]^{2+}$ and $[TerpyRuTpt]^{2+}$ than it is for $[TerpyRuQtpy]^{2+}$ and $[TerpyRuP\text{-}terpy]^{+}$. This suggests that the triazines interact in a slightly different mode to the terpyridines. The binding constants for all four of the extended terpyridine type complexes are similar but there is a definite trend to a higher binding affinity with increased nitrogens.

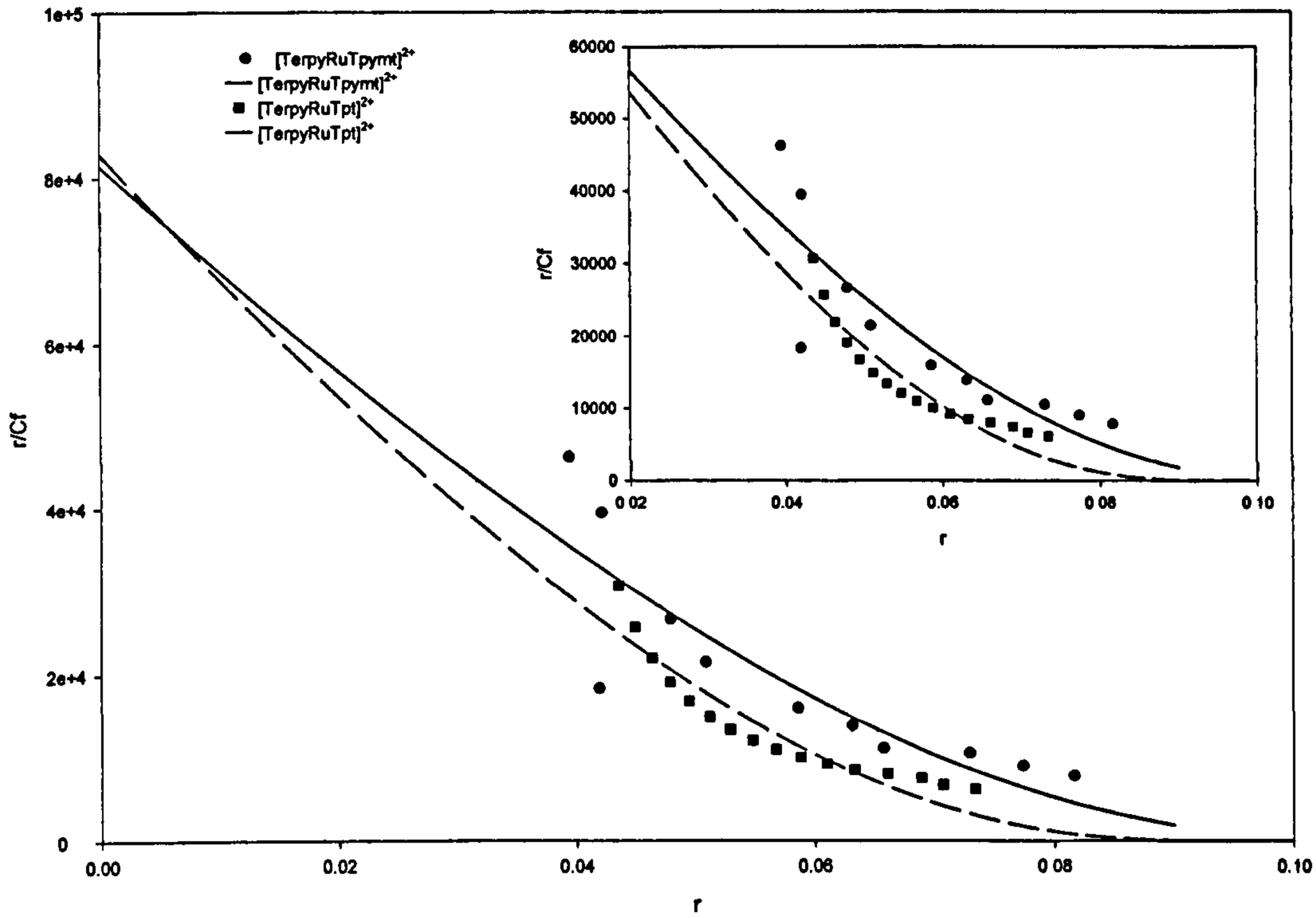

Figure 5.27:- *Scatchard plots with Mcghee-von Hippel best fits obtained by UV-Visible titrations for the Terpy ruthenium terpyridine complexes binding to CT DNA, 25mmol NaCl, 5mmol Tris-HCl, pH 7.0, 25℃.*

From Figure 5.26 it is clear that $[TerpyRuTpp]^{2+}$ interacts with CT-DNA in a very different mode than the other complexes. The binding site size is over twice as big as for the other complexes and it also has the greatest binding affinity ($1.28x10^5$ $mol^{-1}dm^3$). Again this is probably due to the extra aromatic ring present in Tpp and not the other ligands.

5.5.5 DNA binding studies on the $(phen)_2Ru^{2+}$ extended terpyridine complexes

All four of the $(phen)_2Ru^{2+}$ extended terpyridine complexes showed both hypochromic shifts in their UV-Spectra and increased emission in their luminescence spectra upon binding to CT-DNA. The raw binding data

from the titration of $[(phen)_2RuP\text{-}terpy]^{2+}$ with CT-DNA is shown in Figure 5.28.

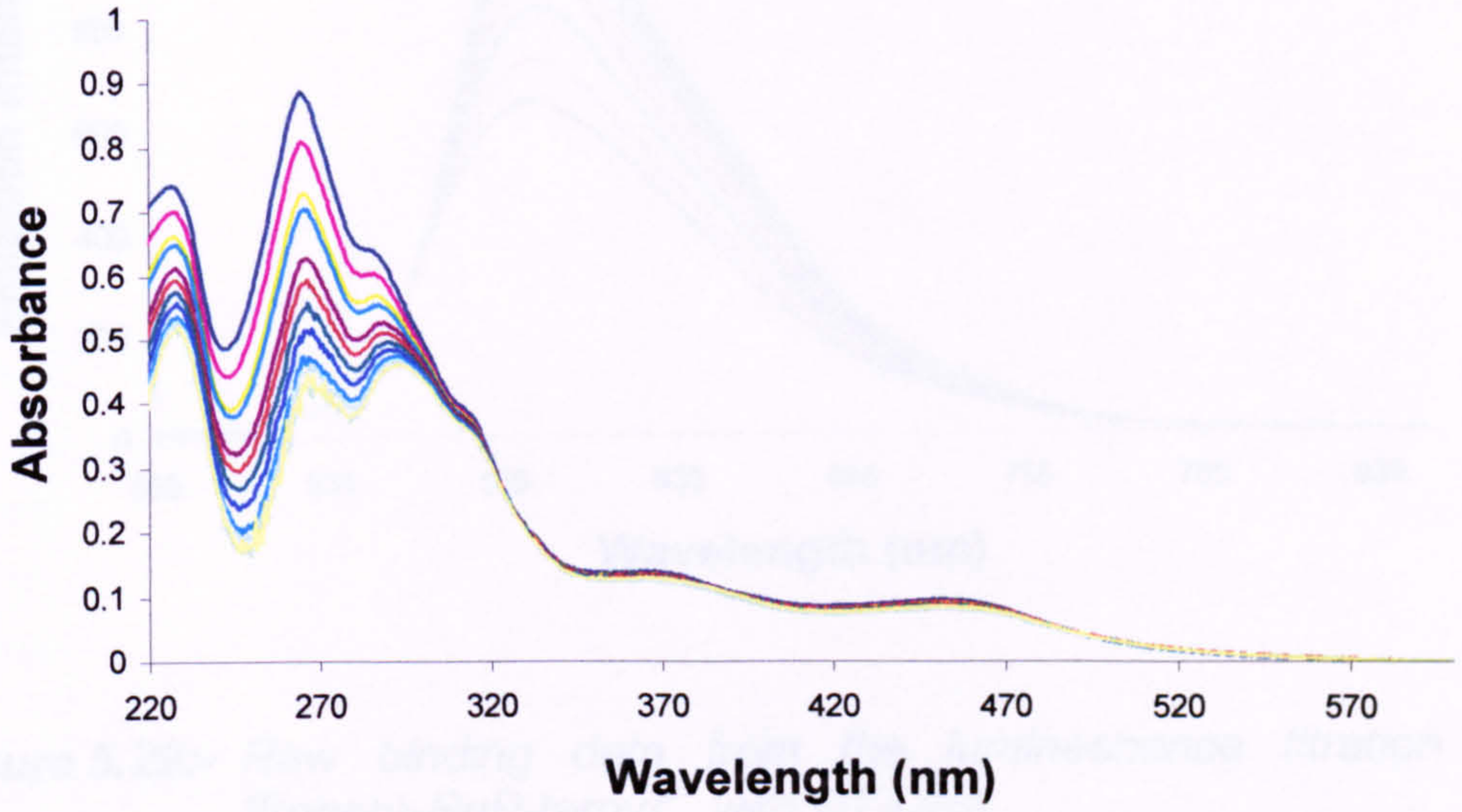

Figure 5.28:- *Raw data from the titration of $[(phen)_2RuP\text{-}terpy]^{2+}$ with CT-DNA*

Again all of the $(phen)_2Ru^{2+}$ complexes show little or no hypochromicity in the low energy MLCT bands. They do however show pronounced hypochromicity in the higher energy ligand centred transitions. The % hypochromicity observed in $[(phen)_2RuTpt]^{2+}$ is about half of that shown in the other complexes. This again is an indication of a different interaction of the triazine and terpyridine complexes with CT-DNA.

The emission titration raw data for the titration of $[(phen)_2RuP\text{-}terpy]^{2+}$ with CT-DNA is shown in Figure 5.29.

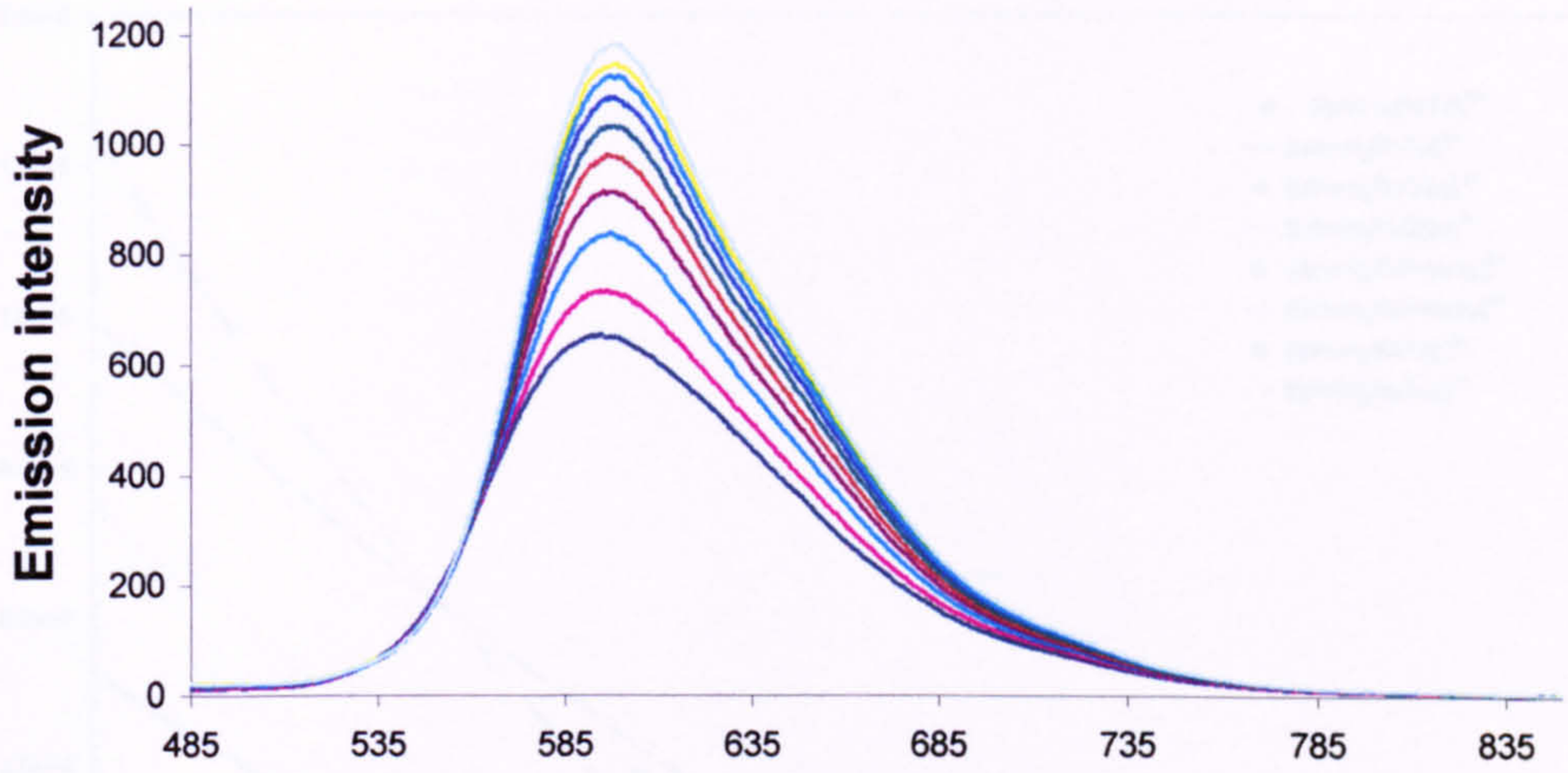

Figure 5.29:- *Raw binding data from the luminescence titration of $[[(phen)_2RuP\text{-}terpy]^{2+}$ with CT-DNA*

The $(phen)_2Ru^{2+}$ complexes with the extended terpyridine ligands cannot be described as molecular light switches for DNA, as they show considerable luminescence without any DNA present. They do, however, show an increased emission when bound to CT-DNA.

The binding data for both the UV-Visible and luminescence titrations are summarised in Table 5.6. The data were once again obtained from non-linear least-squares fits of the Mcghee-von Hippel model to non-linear Scatchard plots of the binding data. Figure 5.30 shows the Scatchard plots for the UV-Visible binding data and Figure 5.31 shows the Scatchard plots for the luminescence binding data.

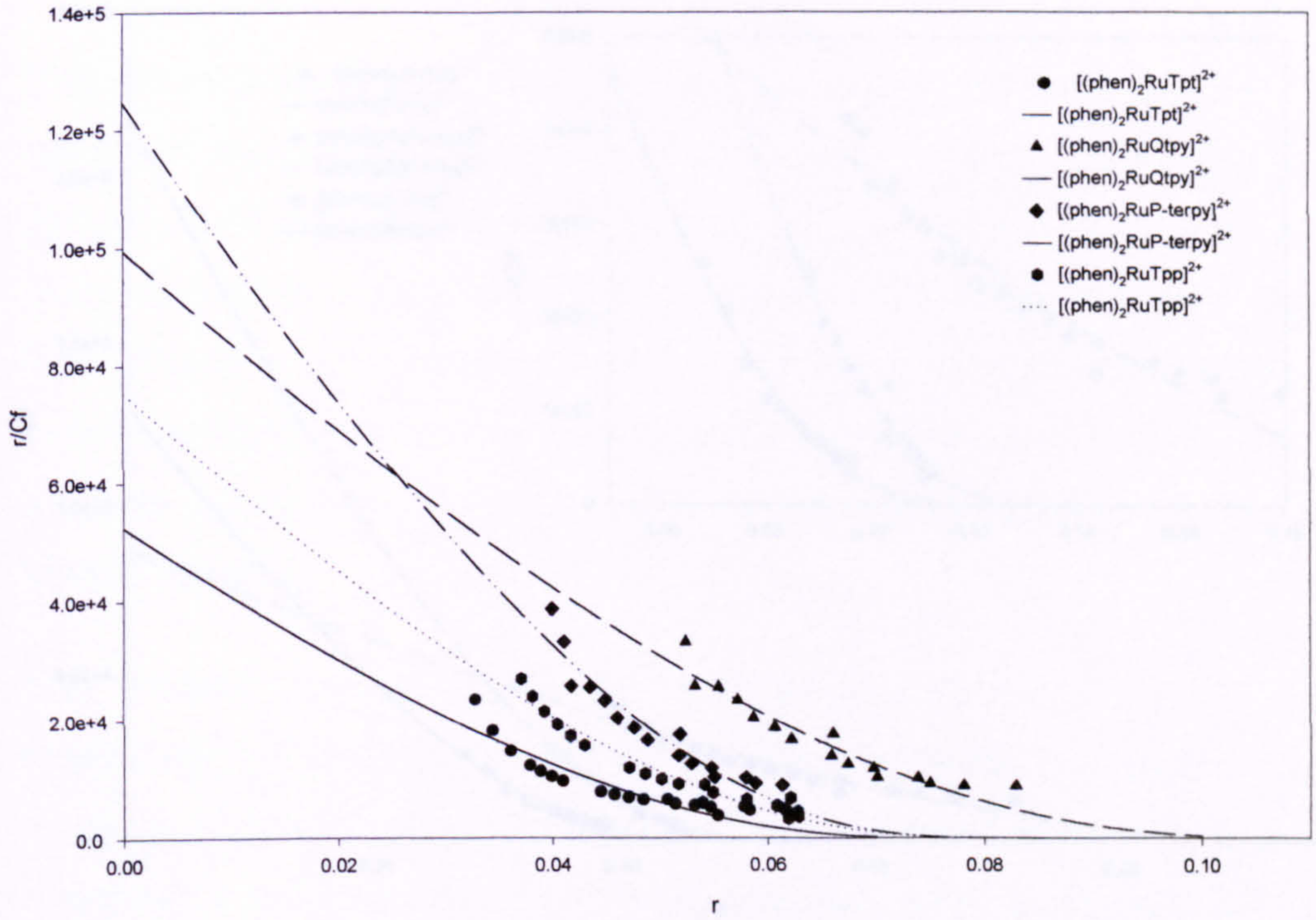

Figure 5.30:- *Scatchard plots with Mcghee-von Hippel best fits obtained by UV-Visible titrations for the $(phen)_2Ru^{2+}$ extended terpyridine complexes binding to CT DNA, 25mmol NaCl, 5mmol Tris-HCl, pH 7.0, 25°C.*

Table 5.6:- *Spectroscopic binding data for the $(phen)_2Ru^{2+}$ extended terpyridine complexes binding to CT-DNA, 25mmol NaCl, 5mmol Tris, pH 7.0*

Complex	UV-Visible			Luminescence		
	K (mol^{-1} dm^3)	S (bp)	%hyp	K (mol^{-1} dm^3)	S (bp)	I/I_0
$[(phen)_2RuTpt]^{2+}$ [a]	$5.24x10^4$	11.8	31.9	$1.30x10^5$	7.77	6.4
$[(phen)_2RuQtpy]^{2+}$	$9.94x10^4$	10.63	57.7	$1.97x10^5$	7.24	17.9
$[(phen)_2RuP\text{-}terpy]^{2+}$	$1.25x10^5$	11.38	57.7	$2.17x10^5$	6.99	18.2
$[(phen)_2RuTpp]^{2+}$ [a]	$7.54x10^5$	11.19	28.2	$8.73x10^4$	3.83	16.5

[a] titration performed in 5% methanolic buffer

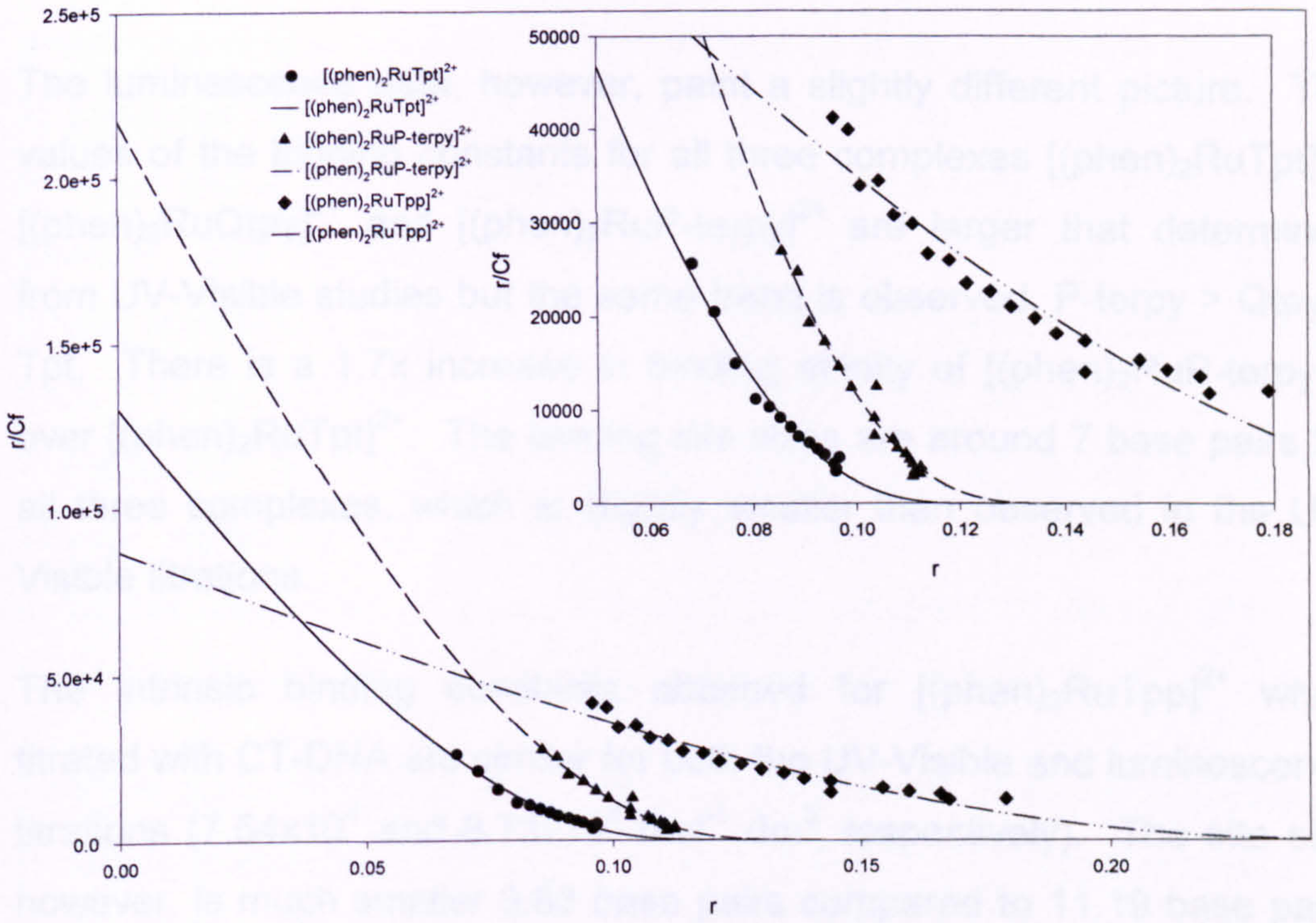

Figure 5.31:- *Scatchard plots with Mcghee-von Hippel best fits obtained by luminescence titrations for the $(phen)_2Ru^{2+}$ extended terpyridine complexes binding to CT DNA, 25mmol NaCl, 5mmol Tris-HCl, pH 7.0, 25°C.*

Analysis of the binding parameters for the $(phen)_2Ru^{2+}$ extended terpyridine complexes with CT-DNA shows that they all bind moderately well to CT-DNA. The association constants for the complexes increase as the number of nitrogens in the extended terpyridine ligand decreases. $[(phen)_2RuTpt]^{2+}$ has an intrinsic binding constant of $5.24x10^4$ mol^{-1} dm^3, whilst $[(phen)_2RuP\text{-}terpy]^{2+}$ has an intrinsic binding constant of $1.25x10^5$ mol^{-1} dm^3. This shows a 2.3x increase in affinity. $[(phen)_2RuTpp]^{2+}$ has an intrinsic binding constant of $7.54x10^4$ mol^{-1} dm^3 which is between $[(phen)_2RuTpt]^{2+}$ and $[(phen)_2RuQtpy]^{2+}$. The binding site size is between 9 and 11 for all four of the complexes. This value is quite high for the classical intercalation of relatively small monometallic complexes to CT-DNA. This suggests that the mode of interaction is not classical intercalation but more likely some kind of groove binding association, or

possible a combination of the two.

The luminescence data, however, paint a slightly different picture. The values of the binding constants for all three complexes $[(phen)_2RuTpt]^{2+}$, $[(phen)_2RuQtpy]^{2+}$ and $[(phen)_2RuP\text{-}terpy]^{2+}$ are larger that determined from UV-Visible studies but the same trend is observed, P-terpy > Qtpy > Tpt. There is a 1.7x increase in binding affinity of $[(phen)_2RuP\text{-}terpy]^{2+}$ over $[(phen)_2RuTpt]^{2+}$. The binding site sizes are around 7 base pairs for all three complexes, which is slightly smaller than observed in the UV-Visible titrations.

The intrinsic binding constants obtained for $[(phen)_2RuTpp]^{2+}$ when titrated with CT-DNA are similar for both the UV-Visible and luminescence titrations ($7.54x10^4$ and $8.73x10^4$ mol^{-1} dm^3, respectively). The site size however, is much smaller 3.83 base pairs compared to 11.19 base pairs obtained from UV-Visible titrations. The nature of the Scatchard plot for $[(phen)_2RuTpp]^{2+}$ compared to the other $(phen)_2Ru^{2+}$ also shows that a very different mode of interaction with $[(phen)_2RuTpp]^{2+}$ and CT-DNA. The site size and magnitude of the binding constant are consistent with those observed in this study and others for classical intercalation. It is, however, impossible to determine the exact nature of the interactions from these simple spectroscopic assays alone.

5.6 Conclusions and future work

In this study a number of novel metallo DNA binding agents have been synthesised and their DNA binding studies reported. This study is one of the few examples where achiral metal complexes have been assayed alongside chiral complexes. It is clear from this study that chirality forms a minor role in determining how well these complexes bind to DNA.

Other factors such steric bulk, charge and the nature of the intercalating domain dominate the ability of these complexes to bind to the DNA helix. In particular the mono- and bimetallic ruthenium and rhenium complexes of dppz show great potential for further development as DNA binding agents. The complex $[TpmPyRudppz]^{2+}$ has been shown to have a strong preference for GC rich sequences of DNA over AT rich sequences. This is in contrast to the related complex $[(phen)_2Rudppz]^{2+}$ which shows a preference for AT rich sequences. Along with the contrast in binding affinity, trends of the terpyRu extended terpy and $(phen)_2Ru$ extended terpy this show that very minor changes in structure of the complex can have a profound effect on its DNA binding characteristics.

There is no better example of this than the two sets of bimetallic systems. Previous studies show that joining two binding agents together increases their affinity for DNA, due to cooperativity by several orders of magnitude[59-61]. In this case the length of the linkers were not optimised to afford bis-intercalation so no significant cooperative effects were observed. In the future molecular modelling studies would serve to determine the optimum linker length.

The difference in binding affinity between $[TpmClRudppz]^{2+}$ and $[TpmPyRudppz]^{2+}$ has highlighted how important electrostatic contributions are to the overall affinity of the complexes for DNA. Further tuning of the charge by incorporating rhodium(III) or iridium(III) could enable the binding properties to be modulated even further.

Chapter 6

Experimental techniques and synthetic procedures

6.1 Chemicals

All chemicals were purchased from commercial sources and were used as supplied unless otherwise stated.

6.2 Solvents

Solvents were obtained from commercial sources and were dried and purified using standard literature methods[131].

6.3 Reaction conditions

Unless otherwise stated all reactions were carried out under an oxygen free nitrogen atmosphere.

6.4 Chromatography

Alumina column chromatography was carried out on either grade I or grade II with acetonitrile / toluene solvent systems.

Silica chromatography was carried out with acetonitrile / water / KNO_3 solvent systems.

Size exclusion chromatography was carried out on Sephadex LH-20 resin with acetonitrile / toluene solvent systems.

Ion exchange chromatography was carried out on Sephadex CM-C25 cation exchange resin with a 5:3 water / acetone solvent system containing varying amounts of NaCl.

All column sizes were approx. 15cm x 3cm unless otherwise stated except the LH-20 column which was 1m x 1cm.

6.5 Nuclear magnetic resonance spectra

Standard ^1H NMR spectra were recorded on a Brucker AM250 machine, working in Fourier transform mode.

More complex ^1H NMR experiments including COSY experiments were perfomed by Sue Bradshaw in the NMR service within the department. The spectra were recorded on a Brucker AMX2400 machine.

The following abbreviations are used in the annotation of ^1H spectra.

br- broad, s- singlet, d- doublet, dd- double doublet, dt- double triplet, t- triplet, q- quartet and m- multiplet.

6.6 Mass spectra

FAB mass spectra were obtained on a Kratos MS80 machine working in positive ion mode, with a m-nitrobenzyl alcohol matrix

6.7 Electrochemistry studies

Cyclic voltammograms were recorded using an EG&G model 362 potentiostat and either the condecon 310 hardware/software package or the EG&G electrochemistry power suite software package.

Measurements were made using approx. 2mmol solutions of material made up in freshly distilled acetonitrile that contained 0.1M Bu_4NPF_6 as the support electrolyte.

Potentials were measured against a Ag/AgCl reference electrode and ferrocene was used as an internal reference.

All CV's were software corrected for internal resistance

6.8 UV-Visible absorption spectra

General UV-Visible spectra were recorded on a Unicam UV2 spectrometer in twin beam mode. Spectra were recorded in matched quartz cells (Helmer) and were baseline corrected.

UV-Titrations were performed on a Varian-Carey bio-3 UV-Visible spectrometer connected to a Viglen PC running Carey Win UV software.

The spectrometer was operating in twin beam mode and the spectra were baseline corrected.

6.9 Emission spectra

Emission spectra were recorded on a Hitachi F4500 spectrophotometer operating in luminescence wavelength scan mode. The photomultipler tube was set to a potential of 700V, the excitation and emission slit widths were both 10nm, the scan speed was 240nms^{-1} and the response time was set to 0.05s.

6.10 Isothermal Titration Calorimetry

ITC was performed using a Microcal VP-ITC micro-calorimater connected to a Gateway 200 PC. Microcal Origin was used to analyse the data.

6.11 Synthetic procedures

6.11.1 Preparation of 2-cyanopyrimidine (2.1)[94]

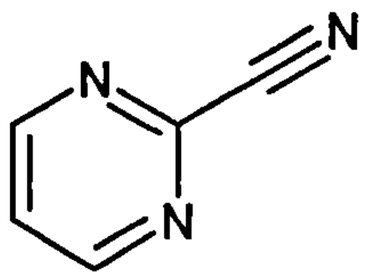

184

DABCO (1.9g, 17mmol) and NaCN (11.07g, 0.178mol) were added to freshly distilled DMSO at 35°C and allowed to stir for 1 hour. To the resulting suspension 2-chloropyrimidine (20g, 0.175mol) was added in three portions at 15 minute intervals. The mixture was allowed to stir at 40°C for 4h after which it was treated with water (150ml) and allowed to cool to room temperature. The resulting dark red solution was then extracted with diethylether (6x100ml), with the combined organics being further washed with water (50ml). The solution dried ($MgSO_4$) and the ether was removed under vacuum to give 17.5g (96.38%) of a waxy white solid. ^1H NMR ($CDCl_3$): δ_H = 7.62 (t, J= 5.6Hz, 1H), 8.89 (d, J= 9Hz, 2H). –MS; m/z (%): 105 (75) [M^+].

6.11.2 Preparation of tris(2'-pyrimidine)-2,4,6-triazine (2.2)[93]

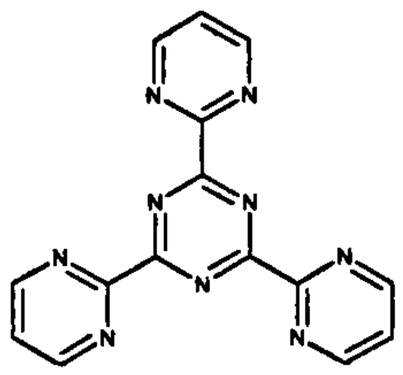

2-Cyanopyrimidine (10g, 98.01mmol) was heated under a N_2 atmosphere to 150°C for 3 days in a dry round-bottomed flask. After cooling, the black solid was crushed and treated with diethylether (50ml) to remove any starting material. The solid was dissolved in 6M HCl and filtered to remove a fine black solid. The hydrochloride salt was precipitated by addition of acetone (1l) and collected on a sinter. The salt was taken up into water (10ml) and deprotonated by addition of concentrated ammonia solution, upon which the free base precipitated and was collected and dried giving 4.45g (43.24%) of 2.2. Fine cream solid. ^1H NMR (DCl/D_2O): δ_H = 6.48 (t, J= 5 Hz, 3H), 7.57 (d, J= 9Hz, 6H). –MS; m/z (%): 316 (70) [M^+].

6.11.3 Preparation of β-(dimethylamino)-2-pyridyl-ketone (2.3)[132]

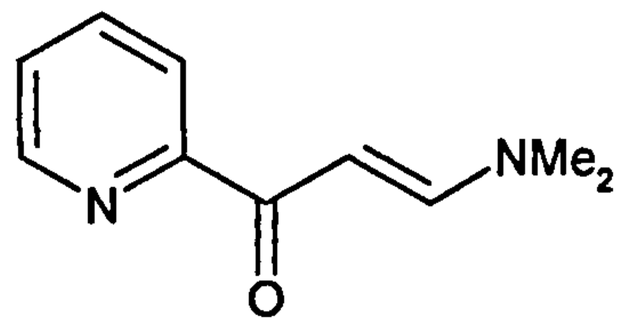

A solution of 2-acetylpyridine (20g, 0.165mol) and *N-N*-di-methylformamide-di-methylacetal (24g, 0.201mol) were heated to reflux with stirring in toluene (100ml). Methanol was gradually distilled off over 24 hours using a Dean Stark trap. The yellow solution was then cooled and toluene was removed under vacuum leaving a yellow oil, which crystallised upon addition of cyclohexane (50 ml) and overnight cooling. The pale yellow crystals were collected by filtration and air-dried, 16.5g (56.82%). Mp 125-127°C (lit mp 125-127°C). -^{1}H NMR ($CDCl_3$): δ_H = 3.06 (br d, 6H), 6.45 (d, 1H), 7.24-7.44 (m, 1H), 7.78 (dt, 1H), 7.90 (d, 1H), 8.15 (d, 1H), 8.59 (dd, 1H).

6.11.4 Preparation of 2,2':6',2'' terpyridine (2.4)[132]

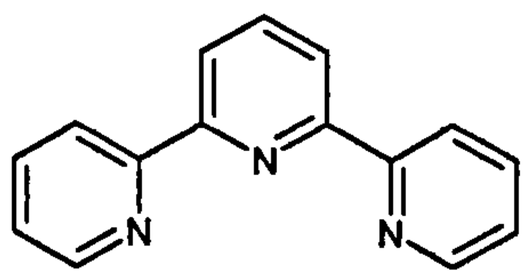

Potassium tertiary butoxide (3.25g, 28.7mmol) was added to a stirred solution of 2-acetylpyridine (1.73g, 14.3mmol) in THF (80ml). After two hours β-(dimethylamino)-2-pyridyl-ketone (2.53g, 14.4mmol) was added to the lilac solution and stirred for 18 hours. The deep red solution was then treated with ammonium acetate (10.8g, 140mmol) in acetic acid (200ml) and the mixture was refluxed for 2.5 hours. The solution was

colled and the solvent removed under vacuum leaving a thick black oil which was taken up into water (80ml) and made alkaline by the addition of sodium carbonate. The aqueous solution was extracted with dichloromethane (3x50ml) with the combined organic extracts being dried over $MgSO_4$ and evaporated to dryness. The resulting black tar was taken up in toluene and filtered through celite to remove a fine black solid. The mother liquor was concentrated and passed through a short grade II alumina chromatography column (3x3cm) with 1:1 hexane DCM as the elluent. The solvent was removed under vacuum and the tan oil was recrystallised from ethanol giving tan crystals, 1.75g (52.5%), which were collected, and air-dried. Mp 84-86°C (lit mp 84-86°C). -^{1}H NMR ($CDCl_3$): δ_H = 7.29 (dd, 2H), 7.81 (td, 2H), 7.91 (t, 1H), 8.45 (d, 2H), 8.62 (d, 2H), 8.69 (dm, 2H).

6.11.5 Preparation of 4'-phenyl-2,2':6,2''-terpyridine (2.5)[95]

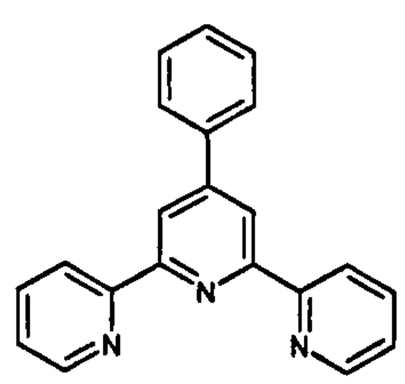

2-Acetylpyridine (25cm^3, 0.33mol) was added dropwise to a stirred solution emulsion of benzaldehyde (11.5cm^3, 0.11mol) in EtOH (100cm^3) and NaOH(aq) (150cm^3, 1.5M). The mixture was stirred for 24hr at room temperature, after which the white precipitate was collected by filtration, and washed with EtOH. The white solid was refluxed in EtOH with ammonium acetate (40g) for a further three hours then cooled to 0°C. The resulting precipitate was collected and washed with boiling water (100ml) and EtOH (100ml) then recrystalised from 10% DMF in EtOH. The white crystals were dried *in vacuo* to give 25.4g (74%) of 2.5. ^{1}H NMR ($CDCl_3$): δ_H = 7.34 (tm, 2H), 7.43-7.55 (m, 3H), 7.83-7.74 (m, 4H),

8.66 (dd, 2H), 7.7-7.77 (m, 4H).

6.11.6 Preparation of 2,2':4,4'':6,2''-quaterpyridine (2.6)[96]

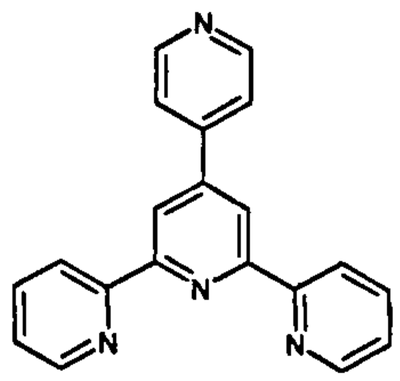

To a stirring solution of 2-pyridinecarboxaldehyde (0.1047mmol) in MeOH (40cm^3) cooled to -15°C, 2-acetylpyridine in 20cm^3 MeOH and 20% NaOH(aq) (40cm^3) were added simultaneously dropwise over 20 mins. The mixture was stirred for 3hr at -15°C, then slowly warmed to room temperature and filtered. The filtrate solution was refluxed with ammonium acetate (40g) for 4 hr. The resulting precipitate was collected and washed with boiling water (100cm^3) and hot EtOH (100cm^3). The crude product was recrystalised from 15%DMF in EtOH and dried in vacuo. Mass = 9.46g (69%) white solid. Mp 214-215°C (lit mp 216-218°C). -^{1}H NMR ($CDCl_3$): δ_H = 7.36 (td, 2H), 7.77 (dd, 2H), 7.86 (td, 2H), 8.64 (dd, 2H), 8.73 (m, 4H).

6.11.7 Preparation of 2,3,5,6-tetrakis-(2-pyridyl)pyrazine (2.7)[97]

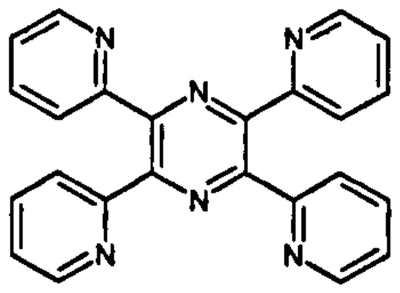

Pyridoin (20g) and ammonium acetate (90g) were heated 180°C for 2 hours with stirring. The green melt containing yellow crystals was allowed

to cool to room temperature and the solid was filtered off. The pale yellow product was washed with ETOH (100cm^3) and dried in vacuo. Mass = 5.68g (27.5%). Mp 280-283°C (lit mp 284C). -^{1}H NMR ($CDCl_3$): δ_H = 7.24 (dd, 4H), 7.77 (td, 4H), 8.04 (d, 4H), 8.37 (dd, 4H).

6.11.8 Preparation of TerpyRuCl$_3$.3 H$_2$O (2.8)

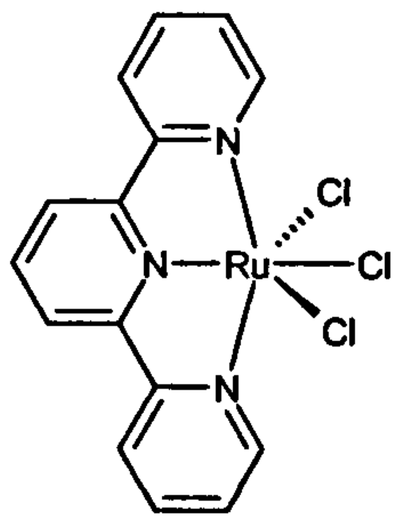

Ruthenium(III) trichloride tri-hydrate (522mg, 2.52mmol) and terpyridine (466mg, 2mmol) were refluxed for 3 hours in ethanol (250cm^3). The solution was cooled to 4°C for 18 hours then filtered leaving a dark green solid which was washed with ice-cold ethanol (2x25cm^3) and diethylether (2x25 cm^3) and air-dried, 685mg (78%). MS; m/z (%): 406 (90) [M$^+$- Cl]

6.11.9 Preparation of [TerpyRuTpt][PF$_6$]$_2$ (2.9)[98]

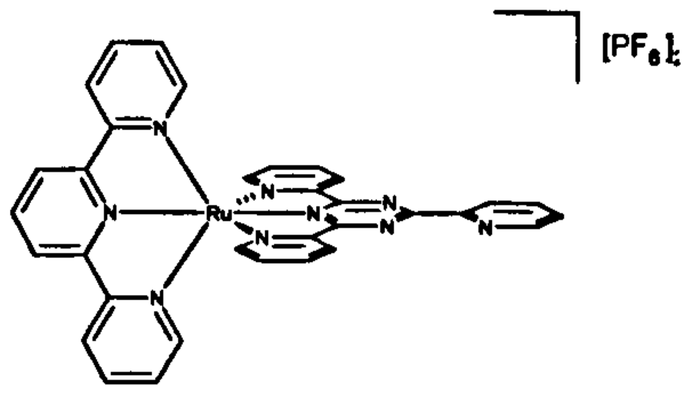

TerpyRyCl$_3$.3H$_2$O (110mg, 0.25mmol) and Tpt (2eq, 160mg, 0.50mmol) were refluxed for 24 hours in 1:1 EtOH/H$_2$O (25cm^3). After cooling to 0°C the purple solution was filtered, concentrated and the crude product was

precipitated by adding NH_4PF_6. The crude product was collected and chromatographed on grade II alumina using 1:1 toluene/MeCN as the eluent. The fractions containing the product were concentrated and Et_2O was added to precipitate the product which was collected by filtration and dried *in vacuo*. Mass = 134mg (57%) purple solid. ^1H NMR (d^3- MeCN): δ_H = 7.13 (dd, 2H), 7.45 (m, 4H), 7.61 (dd, 2H), 7.77 (dd, 1H), 7.94 (td, 2H), 8.13 (td, 2H), 8.24 (td, 1H), 8.49-8.54 (m 4H), 8.8 (d, 2H), 9.04-9.16 (m, 4H) –MS; m/z (%): 791 (35) $[M^+-[PF_6]]$, 646 (80) $[M^+-2[PF_6]]$.

6.11.10 Preparation of [TerpyRuP-terpy][PF_6]$_2$ (2.10)[85]

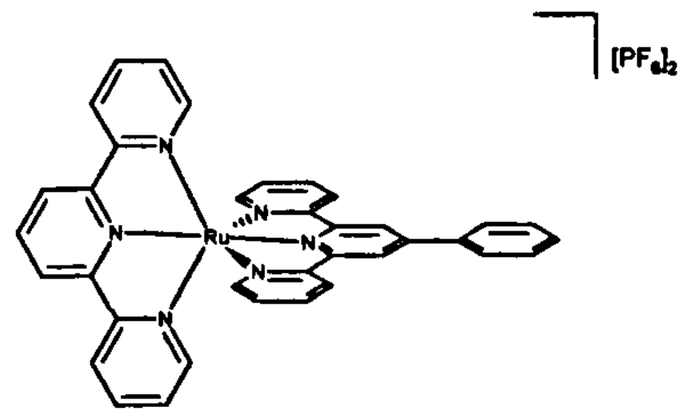

$TerpyRuCl_3.3H_2O$ (100mg, 0.23mmol) and P-terpy (71mg, 0.23mmol) were added to methanol (30cm^3) with stirring and brought to reflux. After 10 minutes 5 drops on *N*-methylmorpholine was added and the solution was refluxed for a further hour. The purple solution was then cooled and filtered, and reduced to 5cm^3. Aqueous NH_4PF_6 was added to induce precipitation of a purple solid which was chromatographed on silica eluted with 7:1:1, acetonitrile:water:KNO_3(sat). The fractions containing the product were combined and reduced in volume to 5ml, and treated with NH_4PF_6 to precipitate the product. The precipitate was collected by filtration, washed with water (2x 20cm^3), diethylether (2x 20cm^3) and then dried *in vacuo*. Mass = 108mg (50%) purple solid. ^1H NMR (d^3- MeCN): δ_H = 7.16 (m, 4H), 7.34 (dd, 2H), 7.43 (dd, 2H), 7.64-7.73 (m, 3H), 7.92 (m, 4H), 8.18 (dd, 2H), 8.39 (t, 1H), 8.48 (dd 2H), 8.63 (dd, 2H), 8.74 (d, 2H), 9.01 (s, 2H). –MS; m/z (%): 789 (53) $[M^+-[PF_6]]$, 644 (100) $[M^+-2[PF_6]]$.

6.11.11 Preparation of [TerpyRuTpp][PF_6]$_2$ (2.11)[99]

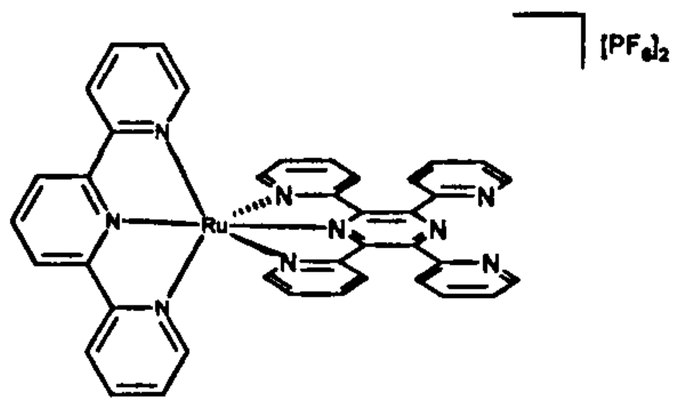

$TerpyRuCl_3.3H_2O$ (152mg, 0.345mmol) and Tpp (3eq, 413mg, 1.06mmol) were refluxed in 2:1 $EtOH/H_2O$ (30cm^3) with triethylamine (1.5cm^3) with stirring for 5 hrs. The purple solution was cooled and filtered, and reduced to 5 ml. Aqueous NH_4PF_6 was added resulting in the precipitation of the crude product as a purple solid. The crude product was chromatographed on grade II alumina using 1:1 MeCN/toluene as the eluent. The main purple fraction was reduced in volume and adding Et_2O precipitated the product. The product was collected by filtration, washed with water (2x 20cm^3), diethylether (2x 20cm^3) and dried *in vacuo*. Mass = 143mg (61.4%) purple solid. ^1H NMR (d^3- MeCN): δ_H = 7.29 (m, 2H), 7.37 (m, 2H), 7.63-7.88 (m, 8H), 7.98 (dd, 1H), 8.11 (dd, 2H), 8.80 (td, 2H), 8.48 (dd, 2H), 8.66 (t 2H), 8.76 (m, 2H), 8.87 (d, 2H), 9.16 (d, 2H). –MS; m/z (%): 869 (80) [M^+-[PF_6]], 723 (100) [M^+-2[PF_6]].

6.11.12 Preparation of [TerpyRuQtpy][PF_6]$_2$ (2.12)

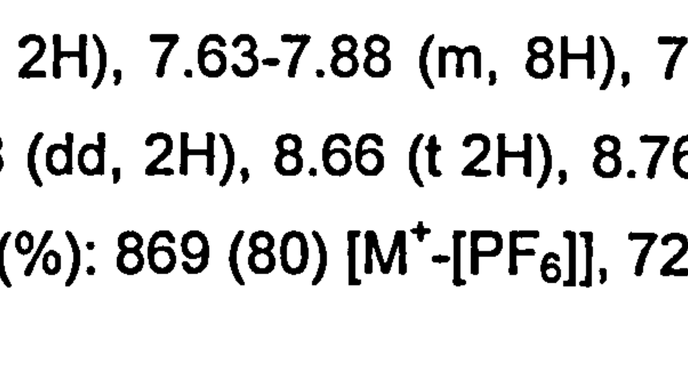

$TerpyRuCl_3.3H_2O$ (220mg, 0.50mmol) and Qtpy (2eq, 310mg, 1.0mmol)

were heated to 180°C with stirring in freshly distilled ethylene glycol (15cm^3) for 2 hours. The cooled purple solution was diluted with water (20ml) and filtered to remove a fine black precipitate. The solution was the treated with NH_4PF_6 (3eq), which resulted in the precipitation of a purple solid, which was collected on a sinter, washed with water (2 x 20cm^3) and diethylether (2 x 20cm^3) and air dried. The crude product was dissolved in acetonitrile (2cm^3) and chromatographed on silica eluted with 7:1:1, acetonitrile:water:KNO_3(sat).The main purple band containing the product was reduced in volume to 5cm^3, and treated with NH_4PF_6 to precipitate the product. The precipitate filtered, washed with water (2x 20cm^3), diethylether (2x 20cm^3) and dried *in vacuo*. Mass = 240mg (51.3%) purple solid. ^{1}H NMR (d^3- MeCN): δ_H = 7.10-7.25 (m, 4H), 7.38 (dd, 2H), 7.43 (dd, 2H), 7.88-8.03 (m, 4H), 8.41 (dd, 2H), 8.51 (dm, 2H), 8.67 (m, 2H), 8.75 (dd 2H), 9.02 (m, 3H), 9.08 (d, 2H). –MS; m/z (%): 791 (80) [M$^+$-[PF_6]], 646 (100) [M$^+$-2[PF_6]]. Anal. Calcd. for $C_{35}H_{25}N_7RuPF_6$ (M$^+$ -[PF_6]): 790.0858. Found: 790.0792.

6.11.13 Preparation of [TerpyRuTpymt][PF_6]$_2$ (2.13)

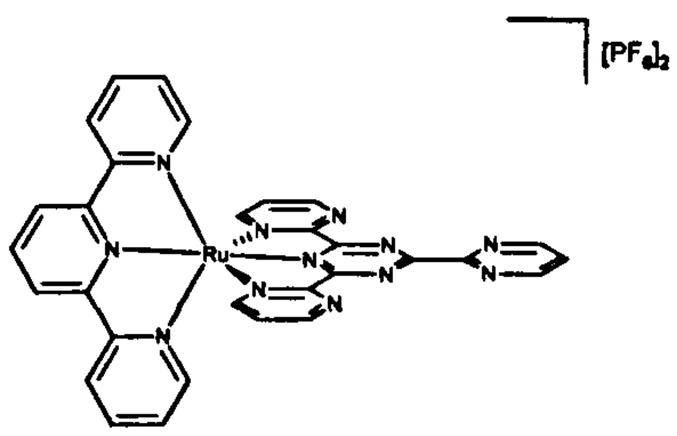

$TerpyRuCl_3.3H_2O$ (200mg, 0.45mmol) and Tpymt (3eq, 429mg, 1.362mmol) were heated to 180°C in freshly distilled ethylene glycol (20cm^3) for 1 hour. The purple solution was diluted with water (20cm^3) and filtered to remove unreacted ligand. NH_4PF_6 was added in excess until precipitation of a purple solid was complete, which was collected by filtration and washed with ice-cold water (2x20cm^3) and air-dried. The

crude product was taken up in the minimum amount of 5:3 water: acetone and loaded onto a Sephadex CM-C25 ion exchange chromatography column and eluted with 0.05M NaCl in 5:3 water: acetone to remove a brown impurity which was discarded. The desired product was eluted as a purple band with 0.1M NaCl in the solvent, and was recovered by reducing the volume of eluent and precipitation with NH_4PF_6 and filtration. The product was washed with ice-cold water (2x20cm^3) and dried *in vacuo*. Mass = 209mg (49.46%) purple solid. X-Ray quality crystals were grown from nitromethane / diethylether solvent diffusion. ^1H NMR (d^3-$MeNO_2$): δ_H = 7.15 (td, 2H), 7.42 (dd, 2H), 7.54 (dd, 2H), 7.88 (t, 1H), 8.00 (td, 2H), 8.17 (dd, 2H), 8.60 (d, 2H), 8.64 (t, 1H), 8.91 (d, 2H), 9.14 (dd, 2H), 9.31 (d, 2H). –MS; m/z (%): 795 (30) [M^+-[PF_6]], 325 (100) [M^{2+}-2[PF_6]]. Anal. Calcd. for $C_{30}H_{20}N_{12}RuPF_6$ (M^+ -[PF_6]): 795.0619. Found: 795.0590.

6.11.14 Preparation of $(phen)_2RuCl_2.2H_2O$ (2.14)

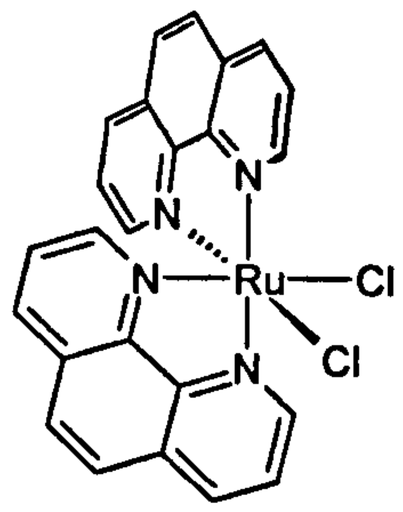

Ruthenium(III) chloride trihydrate (10g, 38.2mmol), 1,10 phenanthroline (13.84g, 76.9mmol) and LiCl (11g) were dissolved in anhydrous sure seal DMF (60cm^3) and refluxed for 8 hours. The purple solution was then cooled and poured into stirred acetone (200cm^3) and cooled to 4°C for 18 hours. The dark solid was collected by filtration and washed with water (3x25cm^3) and diethylether (3x25cm^3) then dried *in vacuo*. Mass= 14.5g,

(66.8%) brown-green solid. MS; m/z (%): 532 (45) [M^+], 497 (80) [M^+ - Cl].

6.11.15 Preparation of $[(phen)_2RuTpt][PF_6]_2$ (2.15)

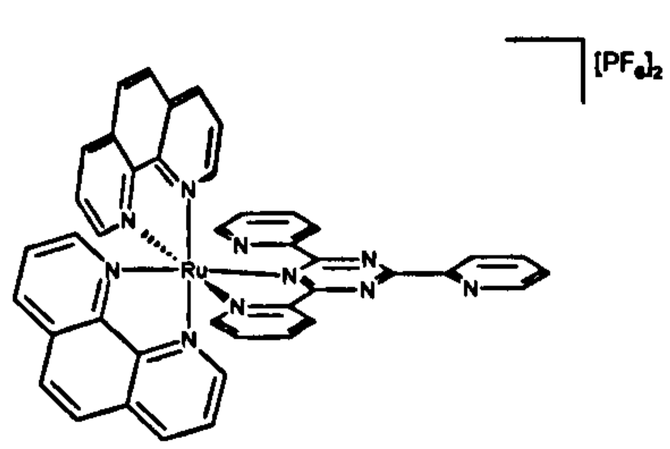

$(phen)_2RuCl_2.2H_2O$ (300mg, 0.53mmol) and Tpt (2eq, 1.06mmol, 329mg) were suspended MeOH (40cm^3) and purged with nitrogen for 10 minutes. The suspension was then brought to reflux for 10 hours after which the cooled solution was concentrated and loaded onto a silica chromatography column. The product was eluted with 7:1:0.5 acetonitrile/ water/ KNO_3(sat), with the desired product being collected as the first main red band. The fractions containing the product were concentrated and addition of NH_4PF_6 afforded precipitation of the product as its hexafluorophosphate salt, which was collected, washed with iced water (2.25 ml) and dried *in vacuo.* Mass=109mg (19.35%) red solid. ^1H NMR (d^6- acetone): δ_H = 6.94 (dd, 1H), 7.18 (m, 2H), 7.37 (td, 1H), 7.50 (dd, 1H), 7.59 (dd, 1H), 7.66 (td, 1H), 7.73 (td, 1H), 7.85 (dd, 1H), 7.96 (m, 2H), 8.06-8.25(m, 4H), 8.33-8.51 (m, 6H), 8.69 (dd,1H), 8.77 (dd, 1H), 8.84 (dd, 1H), 8.91 (dd, 1H), 8.96 (dd, 1H), 9.42 (dd, 1H), 9.94 (dd, 1H) – MS; m/z (%): 919 (40) [M^+-[PF_6]], 774 (40) [M^{2+}-2[PF_6]]. Anal. Calcd. for $C_{42}H_{28}N_{10}RuPF_6$ (M^+ -[PF_6]): 919.1184. Found: 915.1129

6.11.16 Preparation of $[(phen)_2RuQtpy][PF_6]_2$ (2.16)

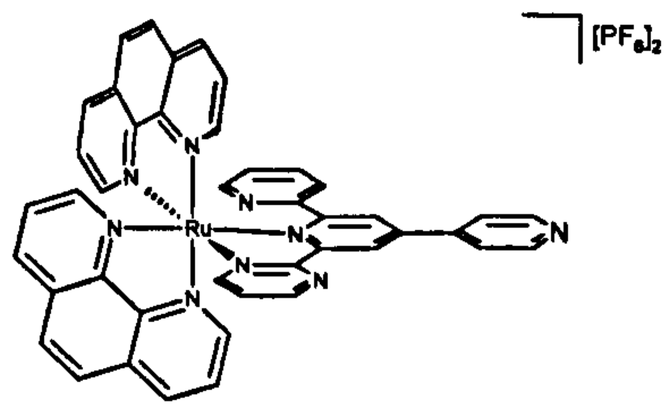

(2.16) was prepared in an analogous way to (2.15) with $(phen)_2RuCl_2.2H_2O$ (150mg, 0.264mmol) and Qtpy (2eq, 166mg, 0.528mmol). Mass = 88mg (31.4%) red solid. ^1H NMR (d^6- acetone): δ_H = 7.27 (td, 1H), 7.44 (dd, 1H), 7.74 (dd, 1H), 7.81 (dd, 1H), 7.92-8.06 (m, 4H), 8.23 (m, 4H), 7.36-8.55 (m, 7H), 8.22 (dd, 1H), 8.29 (dd, 1H), 8.32(dd, 2H), 8.36 (m, 4H), 9.02 (dd,1H), 9.23 (s, 2H), 9.39 (dd, 1H). – MS; m/z (%): 916 (25) $[M^+-[PF_6]]$, 772 (40) $[M^{2+}-2[PF_6]]$. Anal. Calcd. for $C_{44}H_{32}N_8RuPF_6$ (M^+ -$[PF_6]$): 919.1435. Found: 915.1478.

6.11.17 Preparation of $[(phen)_2RuP\text{-}terpy][PF_6]_2$ (2.17)

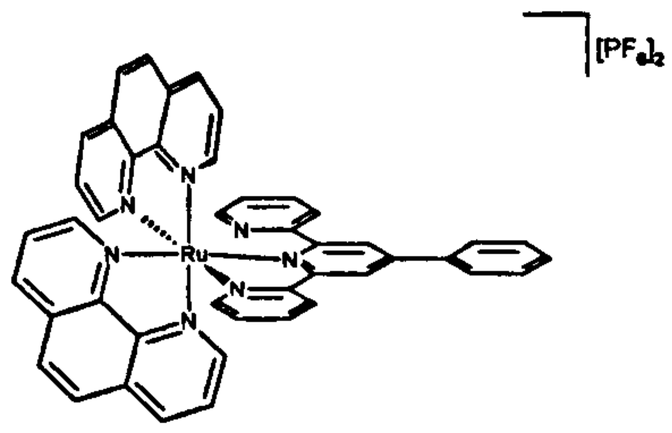

(2.17) was prepared in an analogous way to (2.15) with $(phen)_2RuCl_2 . 2H_2O$ (300mg, 0.53mmol) and P-terpy (163mg, 0.53mmol. Mass= 210mg (37.4%) orange solid. X-ray quality crystals were grown from Et_2O/acetone vapour diffusion. ^1H NMR (d^3- MeCN): δ_H = 6.79 (td, 1H), 6.80 (m, 2H), 6.99 (dd, 1H), 7.21 (td, 1H), 7.32 (m, 2H), 7.46 (dd, 1H), 7.57 (m, 2H), 7.76 (dd, 1H), 7.80 (dd, 1H), 7.94 (m, 3H), 8.01-8.34 (m, 8H), 8.41 (dd,1H), 8.58 (dd, 1H), 8.71 (dd, 1H), 8.74 (dd, 1H), 8.79 (d,

1H), 8.87 (d, 2H). –MS; m/z (%): 771 (15) [M^{2+}-2[PF_6]], 591 (30) (M^+-phen-2[PF_6]). Anal. Calcd. for $C_{45}H_{31}N_7RuPF_6$ (M^+ -[PF_6]): 916.1326. Found: 916.1348.

6.11.18 Preparation of [(phen)$_2$RuTpp][PF_6]$_2$ (2.18)

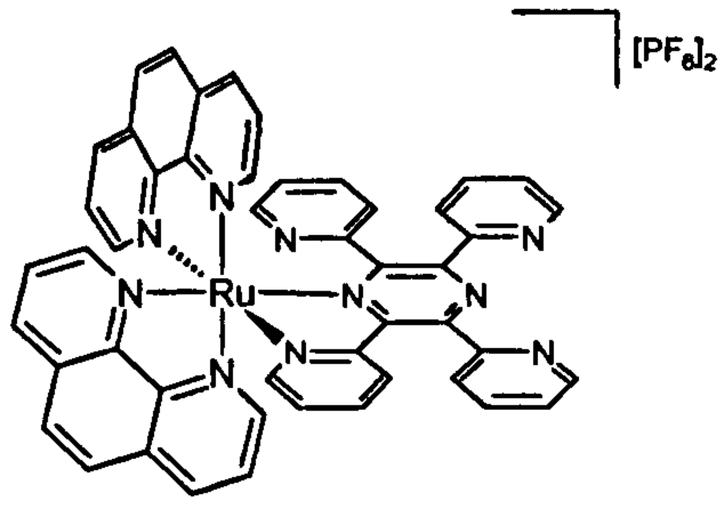

(2.18) was prepared in an analogous way to (2.15) with (phen)$_2$$RuCl_2$.2$H_2O$ (300mg, 0.53mmol) and P-terpy (2eq, 403mg, 1.04mmol). Mass= 110mg (18.3%) orange solid. X-ray quality crystals were grown from Et_2O/acetone vapour diffusion. 1H NMR (d^6- acetone): δ_H = 6.73 (br, 1H), 6.92 (br, 1H), 7.17 (m, 1H), 7.22 (td, 1H), 7.51 (dd, 1H), 7.57-7.91 (m, 9H), 8.04 (dd, 1H), 8.12 (m, 2H), 8.18-8.48 (m, 10H), 8.64 (dd, 1H), 8.75-8.84 (m, 2H), 8.98 (dd,1H), 9.16 (br, 1H). –MS; m/z (%): 850 (60) [M^{2+}-2[PF_6]], 670 (80) (M^+-phen-2[PF_6]). Anal. Calcd. for $C_{48}H_{32}N_{10}RuPF_6$ (M^+ -[PF_6]): 995.1497. Found: 995.1511.

6.11.19 Preparation of (CO)$_3$ClReTpt (2.19)

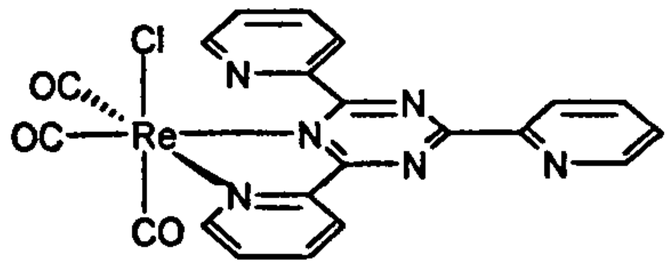

Tpt (3eq, 646mg, 2.08mmol) was added to a refluxing solution of (CO)$_5$ReCl (250mg, 0.69mmol) in toluene (100cm^3). The mixture was

refluxed under N_2 for 4 hours and then cooled. The resulting precipitate was collected by filtration and was stirred in DCM ($50cm^3$) for 10 min to remove any unreacted ligand. The orange solid was filters and washed with DCM ($2x20cm^3$) and Et_2O ($2x20cm^3$) and dried *in vacuo*. Mass = 225mg (92%) orange solid. –MS; m/z (%): 618 (35) [M^+]], 590 (75) (M^+-CO), 582 (75) (M^+-Cl), 562 (30) (M^+-2CO), 555 (80) (M^+-CO-Cl). Anal. Calcd. for $C_{21}H_{13}ClN_6O_3Re$ (MH^+): 619.0295. Found: 619.0295.

6.11.20 Preparation of $(CO)_3ClReQtpy$ (2.20)

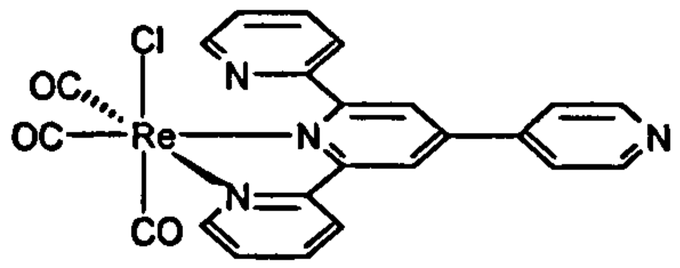

(2.20) was prepared in an analogous way to (2.19) using Qtpy (3eq, 646mg, 2.08mmol) and $(CO)_5ReCl$ (250mg, 0.69mmol). Mass = 230mg (92%) yellow solid. 1H NMR (d^6- DMSO): δ_H = 7.63 (td, 1H), 7.79 (t, 1H), 7.90 (dd, 1H), 8.07 (t, 1H), 8.28-8.52 (m, 4H), 8.79 (d, 1H), 8.96 (m, 2H), 9.11 (m, 2H), 9.27 (s, 1H). –MS; m/z (%): 617 (100) [M^+], 589 (15) (M^+-CO). Anal. Calcd. for $C_{23}H_{15}ClN_4O_3Re$ (MH^+): 617.0390. Found: 617.0382.

6.11.21 Preparation of $(CO)_3ClReP$-terpy (2.21)

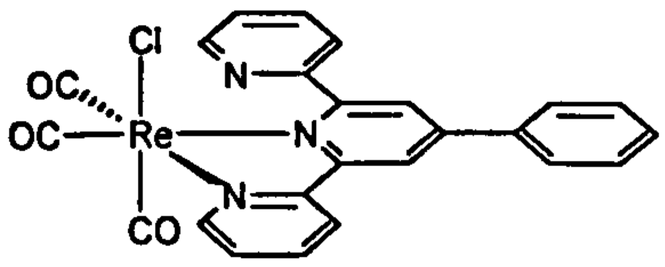

(2.21) was prepared in an analogous way to (2.19) using P-terpy (256mg, 0.83mmol) and $(CO)_5ReCl$ (300mg, 0.83mmol). Mass= 480mg (94.1%)

yellow solid. ^{1}H NMR (d^6- DMSO): δ_H = 7.63 (m, 3H), 7.78 (t, 1H), 7.92 (dd, 1H), 8.06 (t, 1H), 8.21 (m, 3H), 8.49 (td, 1H), 8.81 (dd, 1H), 9.12 (m, 3H). –MS; m/z (%): 615 (30) [M^+], 587 (80) (M^+-CO) 879 (100) [M^+-Cl], 552 (30) [M^+ -CO-Cl]. Anal. Calcd. for $C_{24}H_{16}ClN_3O_3Re$ (MH^+): 616.0438. Found: 616.0441.

6.11.22 Preparation of $(CO)_3ClReTpp$ (2.22)

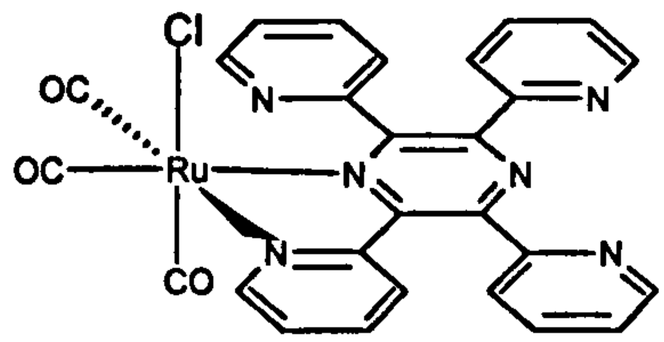

(2.22) was prepared in an analogous way to (2.19) using P-terpy (3rq, 960mg, 2.49mmol) and $(CO)_5ReCl$ (300mg, 0.83mmol). Mass= 345mg (59.9%) yellow solid. –MS; m/z (%): 694 (5) [M^+], 666 (10) (M^+-CO) 638 (10) [M^+-2CO], 610 (15) [M^+ -3CO]. Anal. Calcd. for $C_{27}H_{17}ClN_6O_3Re$ (MH^+): 695.0608. Found: 695.0601.

6.11.23 Preparation of $[(CO)_3MeCNReTpt][CF_3SO_3]$ (2.23)

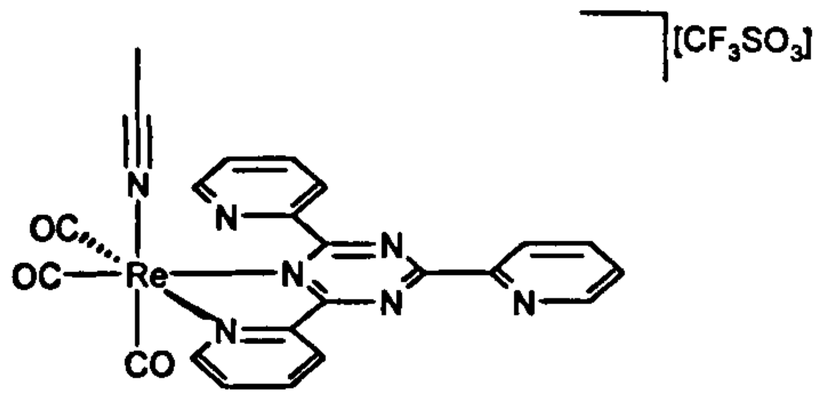

$(CO)_3ClReTpt$ (230mg, 0.37mmol) and $AgCF_3S\ O_3$ (96mg, 0.37mmol) were refluxed for 10 hours in freshly distilled acetonitrile. After cooling the green solution, the solvent was removed. The green solid was taken up into DCM (10cm^3) and filtered through Celite to remove the insoluble

AgCl. The mother liquor was reduced to 1 cm^3 then added to cold pentane (100cm^3), which resulted in precipitation of the product, which was filtered and dried *in vacuo*. Mass = 193mg (67%) green solid. ^1H NMR (d^3- $MeNO_2$): δ_H = 2.14 (s, 3H), 7.8 (m, 2H), 8.06 (td, 1H), 8.19 (m, 1H), 8.30 (d, 1H), 8.98 (m, 4H), 9.25 (m, 2H). –MS; m/z (%): 624 (10) [M^+-CF_3SO_3], 583 (60) [M^+-CF_3SO_3-MeCN] 555 (30) [M^+-CF_3SO_3-MeCN-CO], 532 (10) [M^+-CF_3SO_3-MeCN-2CO]. Anal. Calcd. for $C_{23}H_{15}N_7O_3Re$ (M^+-CF_3SO_3): 624.0794. Found: 624.0810.

6.11.24 Preparation of [$(CO)_3$MeCNReQtpy][CF_3SO_3] (2.24)

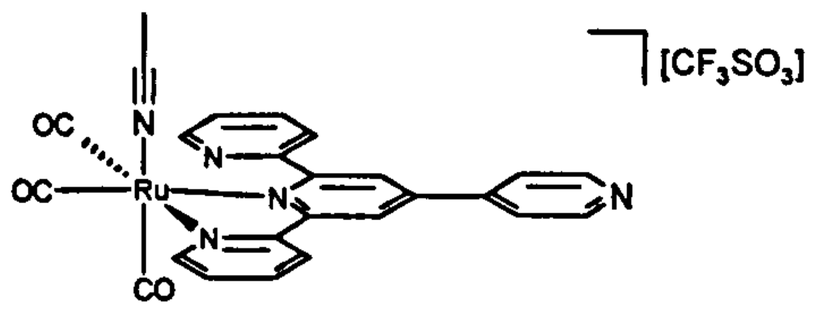

(2.24) was prepared in an analogous way to (2.23) using $(CO)_3$ClReQtpy (150mg, 0.242mmol) and $AgCF_3SO_3$ (63mg, 0.242mmol) Mass = 135mg (72%) pale yellow solid. ^1H NMR (d^6- acetone): δ_H = 2.09 (s, 3H), 7.64 (m, 3H), 7.78 (td, 1H), 7.89 (td, 1H), 8.05-8.28 (m, 3H), 8.41 (t, 1H), 8.52 (td, 1H), 8.90 (d, 1H), 9.11-9.34 (m, 3H). –MS; m/z (%): 582 (40) [M^+-CF_3SO_3-MeCN] 554 (50) [M^+-CF_3SO_3-MeCN-CO], 525 (30) [M^+-CF_3SO_3-MeCN-2CO]. Anal. Calcd. for $C_{25}H_{19}N_5O_3Re$ (M^+-CF_3SO_3): 624.1046. Found: 624.1051.

6.11.25 Preparation of $[(CO)_3MeCNReP\text{-}terpy][CF_3SO_3]$ (2.25)

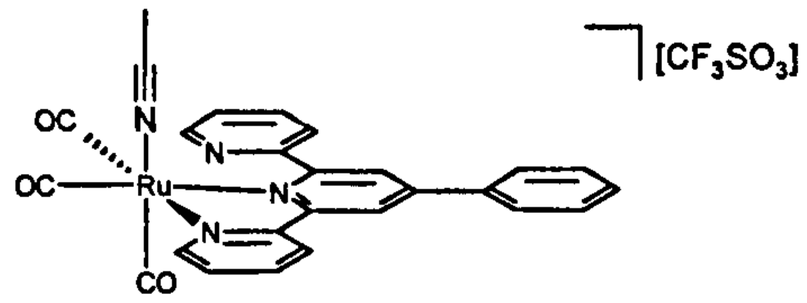

(2.25) was prepared in an analogous way to (2.23) using $(CO)_3ClReP\text{-}terpy$ (150mg, 0.242mmol) and $AgCF_3S\ O_3$ (63mg, 0.242mmol) Mass = 135mg (72%) pale yellow solid. ^1H NMR (d^6- acetone): δ_H = 2.09 (s, 3H), 7.32 (dd, 1H), 7.63 (m, 3H), 7.76 (td, 1H), 7.96 (t, 1H), 8.11-8.24 (m, 3H), 8.42 (dd, 1H), 8.51 (td, 1H), 8.91 (dd, 1H), 9.1-9.35 (m, 3H). –MS; m/z (%): 702 (30) [M^+-MeCN-CO], 674 (100) [M^+-MeCN-CO], 552 (80) [M^+-CF_3SO_3-MeCN-2CO]. Anal. Calcd. for $C_{26}H_{18}N_4O_3Re$ (M^+-CF_3SO_3): 621.0937. Found: 621.0947.

6.11.26 Preparation of 1,10 phenanthroline-5,6-dione (3.1)[27]

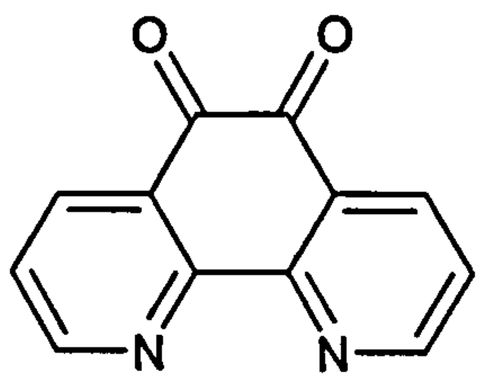

1,10-phenanthroline (5g, 27.8mmol) was dissolved in small portions into concentrated sulfuric acid (30cm^3). Sodium bromide (2.5g) and nitric acid (15cm^3) were then carefully added and the mixture was refluxed for 40 minutes. The condenser was then removed and the mixture was allowed to simmer until all of the bromine had vented off. The golden solution was cooled and poured over ice (400g) and neutralised to pH 7.0 by addition of 10M NaOH. The mixture was filtered and the solid was

extracted into boiling water. when cool all the aqueous layers were combined and extracted with DCM (5 x 100cm^3). The combined organic layers were washed with water (50cm^3) and dried with $MgSO_4$. The solvent was removed and the yellow product was recrystalised from water/methanol. Mass = 2.4g (41.1%) yellow solid. ^{1}H NMR ($CDCl_3$): δ_H = 7.56 (dd, 2H), 8.47 (dd, 2H), 9.07 (dd, 2H). –MS; m/z (%): 211 (100) [MH^+].

6.11.27 Preparation of dipyrido[3,2-a:2',3'-c]phenazine (3.2)

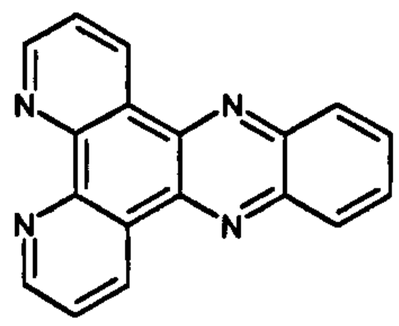

1,10 phenanthroline-5,6-dione (500mg, 2.38mmol) and *o*-phenylene-diamine (257mg, 2.38mg) were refluxed in EtOH (150cm^3) for 20 minutes. Upon cooling at 4°C for 18 hours a yellow solid formed in the dark solution, which was collected by filtration. The solid was recrystalised from 1:1 water/EtOH. Mass = 640mg (95.1%) yellow fluffy solid. ^{1}H NMR (d^6-DMSO): δ_H = 7.93 (dd, 2H), 8.06 (dd, 2H), 8.37 (dd, 2H), 9.21 (dd, 2H), 9.49 (dd, 2H). –MS; m/z (%): 282 (100) [M^+].

6.11.28 Preparation of $TpmRuCl_3$ (3.4)[111]

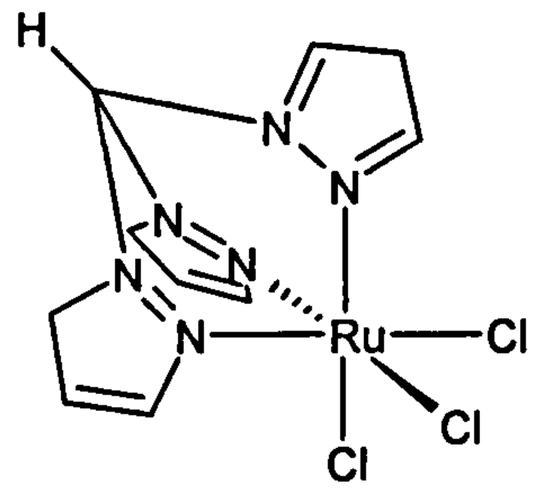

Tris(1-pyrazoyl)methane (1g, 4.67mmol) and $RuCl_3.3H_2O$ (1.22g, 4.67mmol) were refluxed in ethanol ($500cm^3$) for 3 hours. After cooling the dark precipitate was filtered and washed with cold ethanol ($2x20cm^3$) and Et_2O ($2x20cm^3$) and dried *in vacuo*. Mass = 1.45g (73.8%) brown solid. –MS; m/z (%): 386 (20) [M^+-Cl].

6.11.29 Preparation of $[TpmRuCldppz][PF_6]$ (3.5)

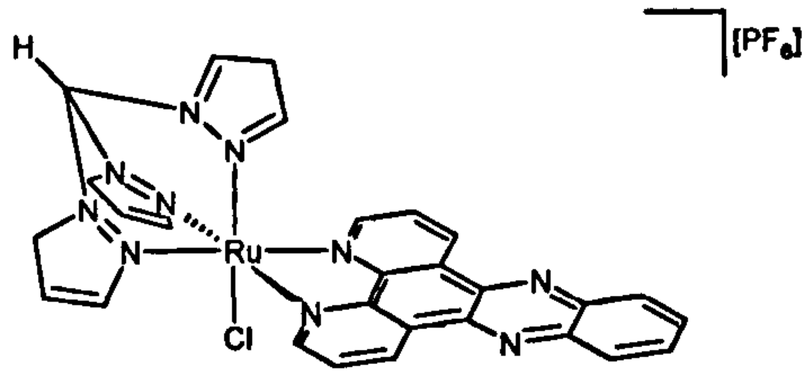

$TpmRuCl_3$ (500mg, 1.19mmol), dppz (1.1eq, 371mg , 1.31mmol) and LiCl (400mg) were heated to reflux in 3:1 ethanol:H_2O ($100cm^3$) for 10mins. 12 drops of triethylamine were added and refluxing continued for 3 hours. After cooling, the solvent was removed and the black residue was dissolved in methanol (20ml) and a fine black solid was filtered out. The product was precipitated by addition of aqueous NH_4PF_6 and collected by filtration. The crude product was chromatographed on grade I alumina with 1:1 acetonitrile. The deep purple band was collected and concentrated. Addition of Et_2O precipitated the product as a purple solid. Mass = 440mg (48.8%) purple solid. ^1H NMR (d^6- acetone): δ_H = 6.30 (td,

1H), 6.87 (m, 3H), 8.06 (dd, 2H), 8.17 (dd, 2H), 8.42 (dd, 2H), 8.52 (dd, 2H), 8.57 (m, 3H), 9.17 (dd, 2H), 9.57 (dd, 2H), 9.63 (s, 1H). –MS; m/z (%): 633 (100) [M^+-PF_6], 597 (30) [M^+-PF_6-Cl]. Anal. Calcd. for $C_{28}H_{20}ClN_{10}Ru$ (M^+-PF_6): 633.0604. Found: 633.0612.

6.11.30 Preparation of [TpmpyRudppz][PF_6]$_2$ (3.6)

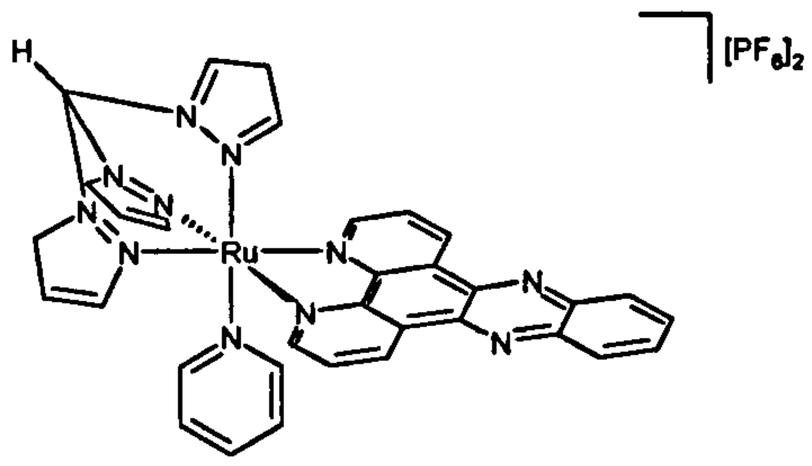

[TpmClRudppz][Cl] (70mg, 0.90mmol) and $AgNO_3$ (2.1eq, 1.89mmol, 32mg) were refluxed in 1:1 water/EtOH for 4 hours. Excess pyridine (1cm^3) was added and the refluxing was continued for a further 4 hours. The cooled solution was then filtered through celite to remove AgCl. NH_4PF_6 was added to precipitate the product, which was collected by filtration and washed with water (2x20cm^3) and Et_2O (2x20cm^3) then dried *in vacuo*. Mass = 68mg (78.1%) orange solid. ^{1}H NMR (d^6- acetone): δ_H = 6.30 (dd, 1H), 6.93 (dd, 1H), 6.98 (m, 2H), 7.15 (dd, 2H), 7.76 (dd, 2H), 7.80 (t, 1H), 8.21 (dd, 2H), 8.24 (dd, 2H), 8.52 (dd, 2H), 8.56 (m, 2H), 8.58 (dd, 1H), 8.85 (dd, 2H), 9.42 (dd, 2H), 9.87 (dd, 2H), 9.93 (s, 1H). –MS; m/z (%): 676 (50) [M^+-2PF_6], 752 (100) [M^+-Tpm], 598 (30) [M^+-2PF_6-Py]. Anal. Calcd. for $C_{33}H_{25}N_{11}RuPF_6$ (M^+-PF_6): 822.0910. Found: 822.0902.

6.11.31 Preparation of [TpmMeCNRudppz][PF_6]$_2$ (3.7)

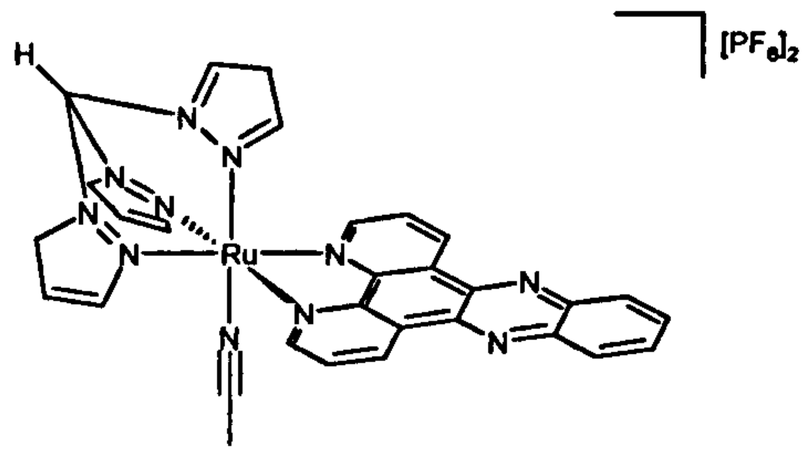

[TpmClRudppz][PF_6] (100mg, 0.128mmol) and $AgCF_3SO_3$ (1.1eq, 0.141mmol, 36mg) were refluxed in freshly distilled acetonitrile (50cm^3) for 10 hours. After cooling the solvent was removed and the residue was taken up into methanol (20 ml) and filtered through celite to remove AgCl. The mother liquor was treated with aqueous NH_4PF_6 to induce the precipitation of the product, which was collected by filtration and dried *in vacuo*. Mass = 119mg (98%) red solid. ^{1}H NMR (d^6- acetone): δ_H = 2.29 (s, 3H), 6.37 (dd, 1H), 6.95 (dd, 2H), 7.07 (dd, 1H), 8.22 (dd, 2H), 8.27 (dd, 2H), 8.56 (t, 2H), 8.62 (dd, 1H), 8.80 (dd, 2H), 9.42 (dd, 2H), 9.86 (dd, 2H), 9.87 (dd, 2H), 10.01 (s, 1H). –MS; m/z (%): 784 (100) [M^+-PF_6], 638 (70) [M^+-PF_6], 597 (80) [M^+-PF_6-MeCN]. Anal. Calcd. for $C_{33}H_{25}N_{11}RuPF_6$ (M^+-PF_6): 784.0823. Found: 784.0836.

6.11.32 Preparation of 1,5-di(4-pyridyl)pentane (4.1)[115]

To 250cm^3 of liquid ammonia cooled by a CO_2/acetone bath was added portion wise over a period of 30 mins 7g of potassium metal, followed by 200mg $Fe(NO_2)_3.9H_2O$. After 30 minutes stirring, the intense blue colour had been replaced by a grey suspension indicating the formation of potassium amide. 4-picoline (11.75g, 0.126mol) was added dropwise

over 30 minutes. After a further 30 minutes stirring 1,5-dibromopentane (12.75g, 0.063mol) in Et_2O was added drop wise over 30 minutes. Stirring was continued for 3 hours at –78°C, then ammonium chloride (10g) was added and the cooling bath removed. After all the ammonia had evaporated, the residue was taken up in water (100cm^3) and extracted with Et_2O. After drying with Na_2CO_3, the solvent was removed yielding a tan solid. Mass = 10.07g (70.7%) tan solid. ^1H NMR ($CDCl_3$): δ_H = 1.35 (t, 2H), 1.61 (m, 4H), 2.59 (t, 4H), 7.05 (d, 4H), 8.44 (d, 4H).

6.11.33 Preparation of $(CO)_3$ClRedppz (4.2)[42]

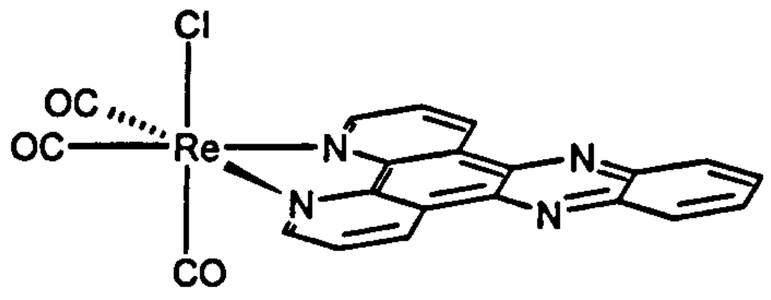

$(CO)_5ReCl$ (120mg, 0.425mmol) and dppz (0.425mmol, 154mg) were refluxed in toluene (50cm^3) for 6 hours. After cooling to room temperature, a yellow precipitate formed which was collected by filtration, washed with toluene (2x25cm^3) and Et_2O (2x25cm^3) and dried *in vacuo*. Mass = 235mg (94%). –MS; m/z (%): 588 (15) [M^+], 560 (90) [M^+-CO], 524 (100) [M^+-CO-Cl].

6.11.34 Preparation of $[(CO)_3MeCNRedppz][CF_3SO_3]$ (4.3)[42]

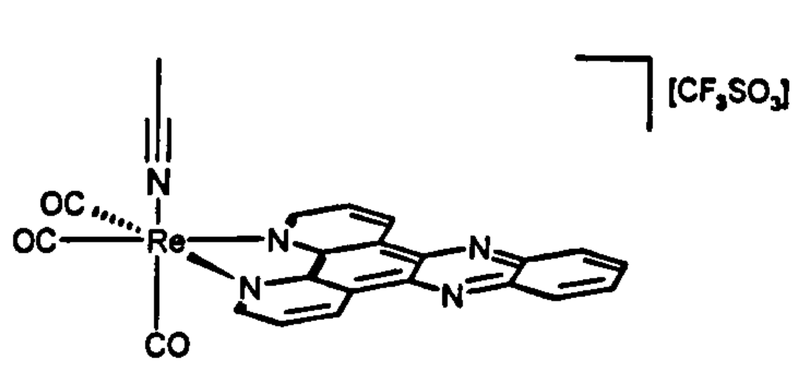

$(CO)_3$ClRedppz (360mg, 0.613mmol) and $AgCF_3SO_3$ (158mg,

0.613mmol) were suspended in freshly distilled MeCN (50cm^3) which had been purged with N_2 for 10 mins. The mixture was brought to reflux for 10 hours and cooled. The solvent was removed and the residue was taken up in DCM, and filtered through celite to remove AgCl. The filtrate was added to 100 cm^3 of cold pentane and the resulting precipitate was collected, washed with Et_2O and dried *in vacuo*. Mass = 430mg (94.5%) yellow-green solid. ^{1}H NMR (d^3-$MeNO_2$): δ_H = 2.16 (s, 3H), 8.14(dd, 2H), 8.26 (dd, 2H), 8.45 (dd, 2H), 9.94 (dd, 2H).

6.11.36 Preparation of $[(CO)_3PyRedppz][CF_3SO_3]$ (4.4)[42]

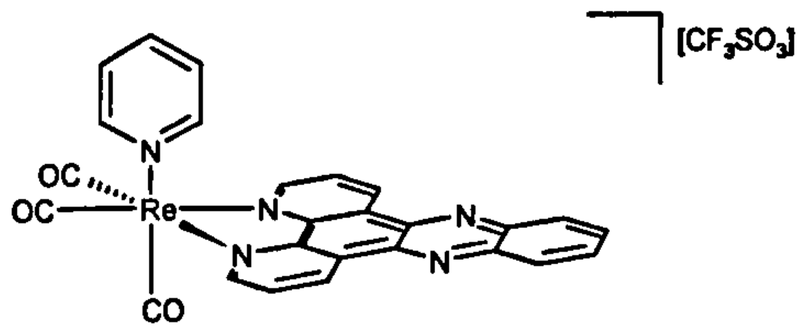

$[(CO)_3MeCNRedppz][CF_3SO_3]$ (150mg, 0.202mmol) and an excess of pyridine (1cm^3) were refluxed in THF (50cm^3) for 4 hours. Upon cooling the solution was filtered, then added to cold pentane (200cm^3). The resulting precipitate was collected and washed with Et_2O (2x25cm^3) and dried *in vacuo*. Mass = 125mg (79.3%) green solid. ^{1}H NMR (d^6-acetone): δ_H = 7.42 (t, 2H), 7.92 (t, 1H), 8.16 (dd, 2H), 8.37-8.56 (m, 4H), 8.71 (dd, 2H), 9.98 (m, 4H).

6.11.37 Preparation of $[\{(CO)_5Re\}_2dpe[2]][CF_3SO_3]_2$ (4.5)

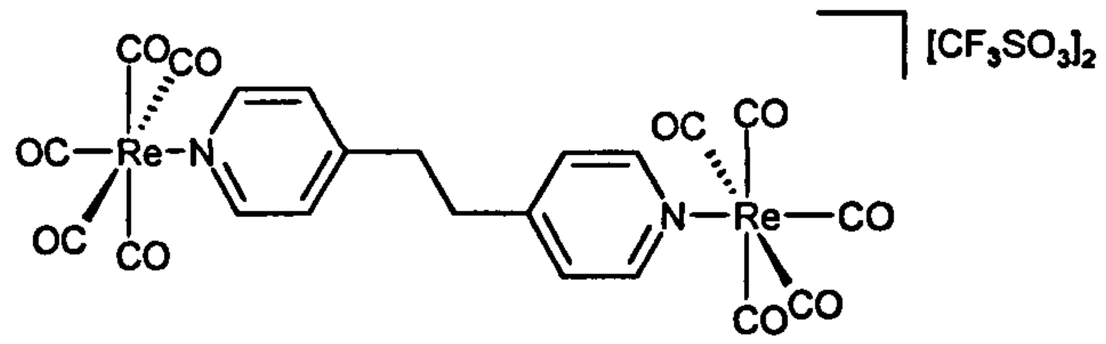

$(CO)_5ReCl$ (0.5g, 1.38mmol) and $AgCF_3SO_3$ (355mg, 1.38mmol) were dissolved in DCM (50cm^3) and stirred at room temperature under N_2 for 18 hours. The solution was filtered through celite to remove AgCl, with the mother liquor being returned to the flask. 1,2-Di(4-pyridyl)ethane (1/2 eq, 119mg, 0.65mmol) was added and the mixture was stirred in the dark under N_2 for 4 days after which a white precipitate was removed by filtration, washed with DCM (2x20cm^3) and dried *in vacuo*. Mass = 390mg (71.7%) white solid. ^{1}H NMR (d^6-acetone): δ_H = 3.25 (s, 4H), 7.74 (d, 4H), 9.21 (d, 4H). –MS; m/z (%): 986 (40) [M^+-CF_3SO_3], 837 (90) [M^+-CF_3SO_3]. Anal. Calcd. for $C_{23}H_{12}N_2O_{13}SF_3Re_2$ (M^+-CF_3SO_3): 986.9128. Found: 986.8452.

6.11.38 Preparation of $[\{(CO)_5Re\}_2dpp[3]][CF_3SO_3]_2$ (4.6)

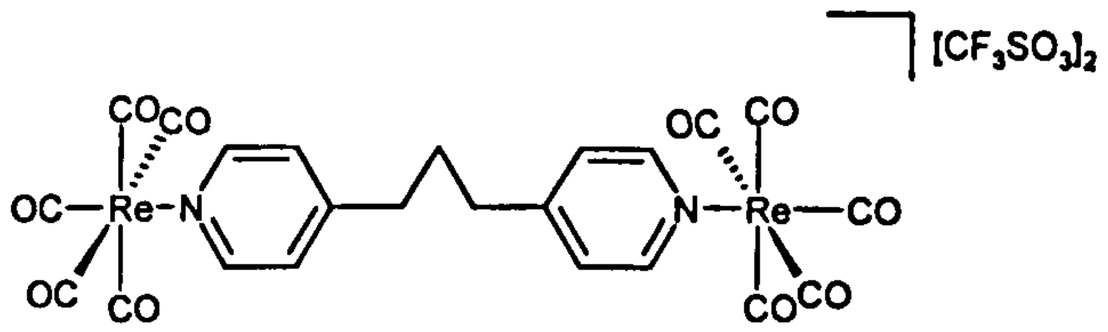

(4.6) was prepared in an analogous way to (4.5) using $(CO)_5ReCl$ (0.1g, 2.76mmol) and $AgCF_3SO_3$ (709mg, 2.76mmol) and 1,3-di(4-pyridyl)propane (1/2 eq, 274mg, 1.38mmol). Mass = 1200mg (75.7%) white solid. ^{1}H NMR (d^6-acetone): δ_H = 2.07 (m, 2H), 2.93 (t, 4H), 7.64 (d, 4H), 9.17 (d 4H). –MS; m/z (%): 999 (50) [M^+-CF_3SO_3], 850 (70) [M^+-CF_3SO_3]. Anal. Calcd. for $C_{24}H_{14}N_2O_{13}SF_3Re_2$ (M^+-CF_3SO_3): 1000.9284.

Found: 1000.9281.

6.11.39 Preparation of $[\{(CO)_5Re\}_2dpp[5]][CF_3SO_3]_2$ (4.7)

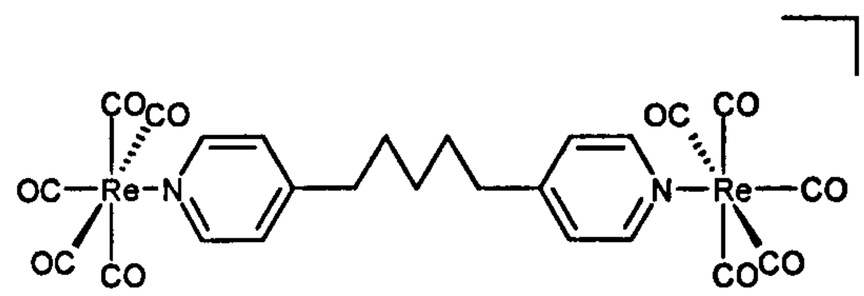

(4.7) was prepared in an analogous way to (4.5) using $(CO)_5ReCl$ (0.5g, 1.38mmol) and $AgCF_3SO_3$ (355mg, 1.38mmol) and 1,5-di(4-pyridyl)pentane (1/2 eq, 156mg, 0.69mmol). Mass = 639mg (78.7%) white solid. ^1H NMR (d^6-acetone): δ_H = 1.49 (m, 2H), 1.74 (m, 4H), 2.84 (t, 4H), 7.62 (d 4H), 9.16 (d, 4H). –MS; m/z (%): 1028 (20) $[M^+-CF_3SO_3]$, 879 (80) $[M^+-CF_3SO_3]$. Anal. Calcd. for $C_{26}H_{18}N_2O_{13}SF_3Re_2$ ($M^+-CF_3SO_3$): 1028.9597. Found: 1028.9639.

6.11.40 Preparation of $[\{(CO)_3Redppz\}_2dpe[2]][CF_3SO_3]_2$ (4.8)

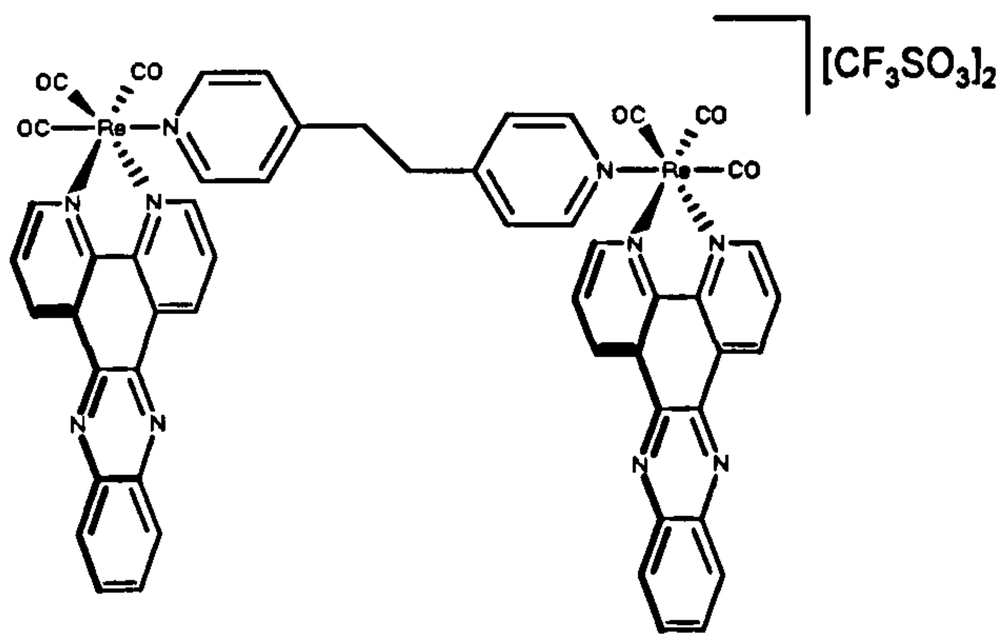

$[\{(CO)_3Redppz\}_2dpe[2]][CF_3SO_3]_2$ (100mg, 0.120mmol) and dppz (2 eq, 69mg, 0.240mmol) were dissolved in nitromethane ($30cm^3$) and heated at 70°C for 2 days with stirring. After cooling to solution was concentrated to

5ml and the product was precipitated by the addition of diethylether (100ml). The pale yellow solid was collected by filtration and was purified by column chromatography on Sephadex LH20 size exclusion resin (1mx 1 cm) with 2.5:1 toluene/acetonitrile as the eluent. The fractions containing the product were combined and the solvent concentrated to 5 ml, with addition of Et_2O ($100cm^3$) to precipitate the product, which was collected by filtration and dried *in vacuo*. 95mg (49.9%) yellow solid. ^1H NMR (d^6-DMSO): δ_H = 2.63 (m, 4H), 7.17 (d, 4H), 8.17 (dd, 4H), 8.38 (m, 4H), 8.41 (d, 4H), 8.50 (dd, 4H), 9.76 (dd 4H), 9.85 (dd, 4H). –MS; m/z (%): 1438 (20) [M^+-CF_3SO_3], 1289 (25) [M^+-$2CF_3SO_3$]. Anal. Calcd. for $C_{55}H_{32}N_{10}O_9SF_3Re_2$ (M^+-CF_3SO_3): 1439.1142. Found: 1439.1089.

6.11.41 Preparation of [{$(CO)_3$Redppz}$_2$dpp[3]][CF_3SO_3]$_2$ (4.9)

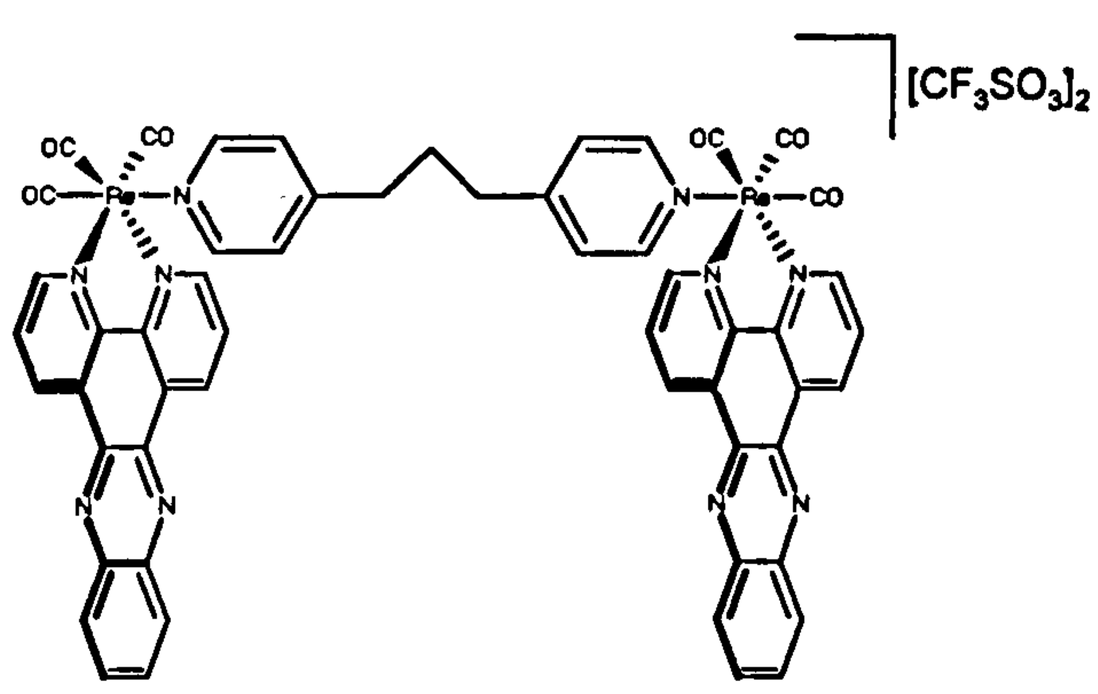

(4.9) was prepared in an analogous way to (4.8) using [{$(CO)_3$Redppz}$_2$dpp[3]][CF_3SO_3]$_2$ (600mg, 0.523mmol) and dppz (2.1 eq, 295mg, 1.0450mmol). Mass = 240mg (49.9%) yellow solid. ^1H NMR (d^6-acetone): δ_H = 1.55 (m, 2H), 2.39 (m, 4H), 7.13 (d, 4H), 8.10 (dd 4H), 8.23 (m, 4H), 8.39 (dd, 4H), 8.46 (d, 4H), 9.71 (dd 4H), 9.88 (dd, 4H). –MS; m/z (%): 1452 (40) [M^+-CF_3SO_3], 1303 (50) [M^+-$2CF_3SO_3$]. Anal. Calcd. for $C_{55}H_{34}N_{10}O_6PF_6Re_2$ (as PF_6 salt) (M^+-PF_6): 1449.1420. Found: 1449.1403.

6.11.41 Preparation of [{(CO)$_3$Redppz}$_2$dpp[5]][CF$_3$SO$_3$]$_2$ (4.10)

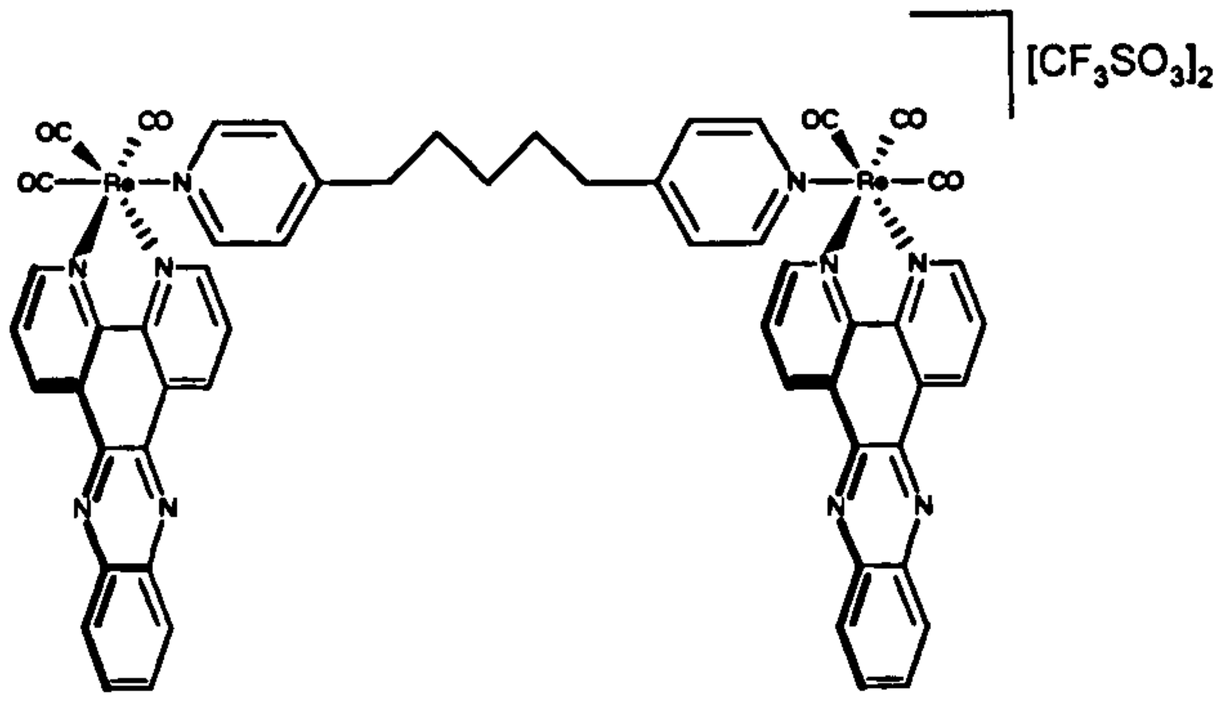

(4.10) was prepared in an analogous way to (4.8) using [{(CO)$_3$Redppz}$_2$dpp[5]][CF$_3$SO$_3$]$_2$ (500mg, 0.43mmol) and dppz (3 eq, 360mg, 1.29mmol). Further purification was achieved by recrystalisations from 1:1 H_2O/acetone. Mass = 40mg (49.9%) yellow solid. ^{1}H NMR (d^6-acetone): δ_H = 1.10 (m, 2H), 1.31 (m, 4H), 2.37 (m, 4H), 7.16 (d, 4H), 8.16 (dd 4H), 8.40 (dd, 4H), 8.45 (dd, 4H), 8.47 (d, 4H), 9.91 (dd 4H), 9.97 (dd, 4H). –MS; m/z (%): 1480 (15) [M$^+$-CF$_3$SO$_3$], 1331 (20) [M$^+$-2CF$_3$SO$_3$]. Anal. Calcd. for $C_{58}H_{38}N_{10}O_9F_3SRe_2$ (M$^+$-CF$_3$SO$_3$): 1481.1611. Found: 1481.1647.

6.11.42 Preparation of [Tpmdpp[5]Rudppz]Cl$_2$ (4.11)

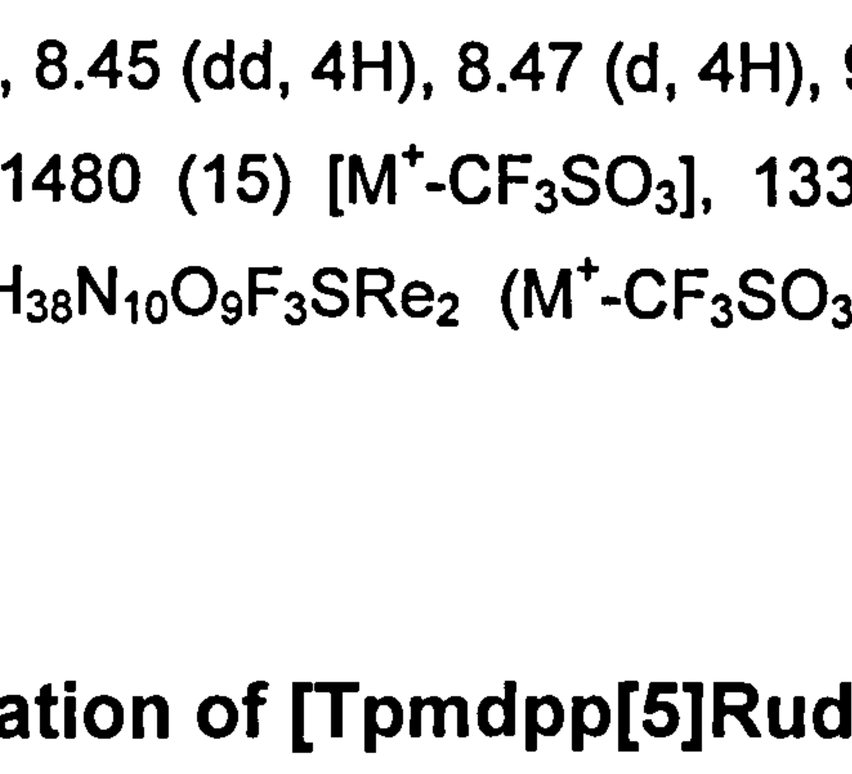

[TpmClRudppz]Cl (450mg, 0.59mmol) and $AgNO_3$ (2.1eq, 1.22mmol,

191mg) were refluxed in 1:1 EtOH/water (100cm^3) for 3 hours. The solution was cooled and filtered through celite to remove AgCl. The filtrate was returned to the flask along with dpp[5] (10eq, 5.792mmol, 1.31g) and the mixture was refluxed for 10 hours. After cooling, the solution was concentrated and NH_4PF_6 was added until the complex precipitated. After collection by filtration the crude product was dissolved in acetone (5cm^3). Bu_4NCl was added to precipitate the product as a dichloride salt which was collected by filtration and copiously washed with acetone to remove excess dpp[5]. The red solid was dried *in vacuo*. Mass = 454mg (66.6%). A small amount of the product was converted to its PF_6^- for analysis. ^{1}H NMR (d^6-acetone): δ_H = 1.25 (m, 2H), 1.51 (m, 2H), 1.59 (m, 2H), 2.54 (m, 2H), 2.59 (m, 2H), 6.30 (t, 1H), 6.92 (dd, 1H), 6.98 (m, 4H), 7.23 (dd 2H), 7.61 (dd, 2H), 8.23 (m, 4H), 8.44 (dd, 2H), 8.46 (dd, 2H), 8.58 (m, 4H), 8.85 (dd, 2H), 9.42 (dd, 2H), 9.89 (dd, 2H), 9.91 (s, 1H). –MS; m/z (%): 1114 (5) [M$^+$], 969 (40) [M$^+$-PF_6], 824 (50) [M$^+$-2PF_6]. Anal. Calcd. for $C_{43}H_{38}N_{12}PF_6Ru$ (M$^+$-PF_6): 1114.1670. Found: 1114.1677.

6.11.43 Preparation of [{TpmRudppz}$_2$dpp[5]][PF_6]$_4$ (4.12)

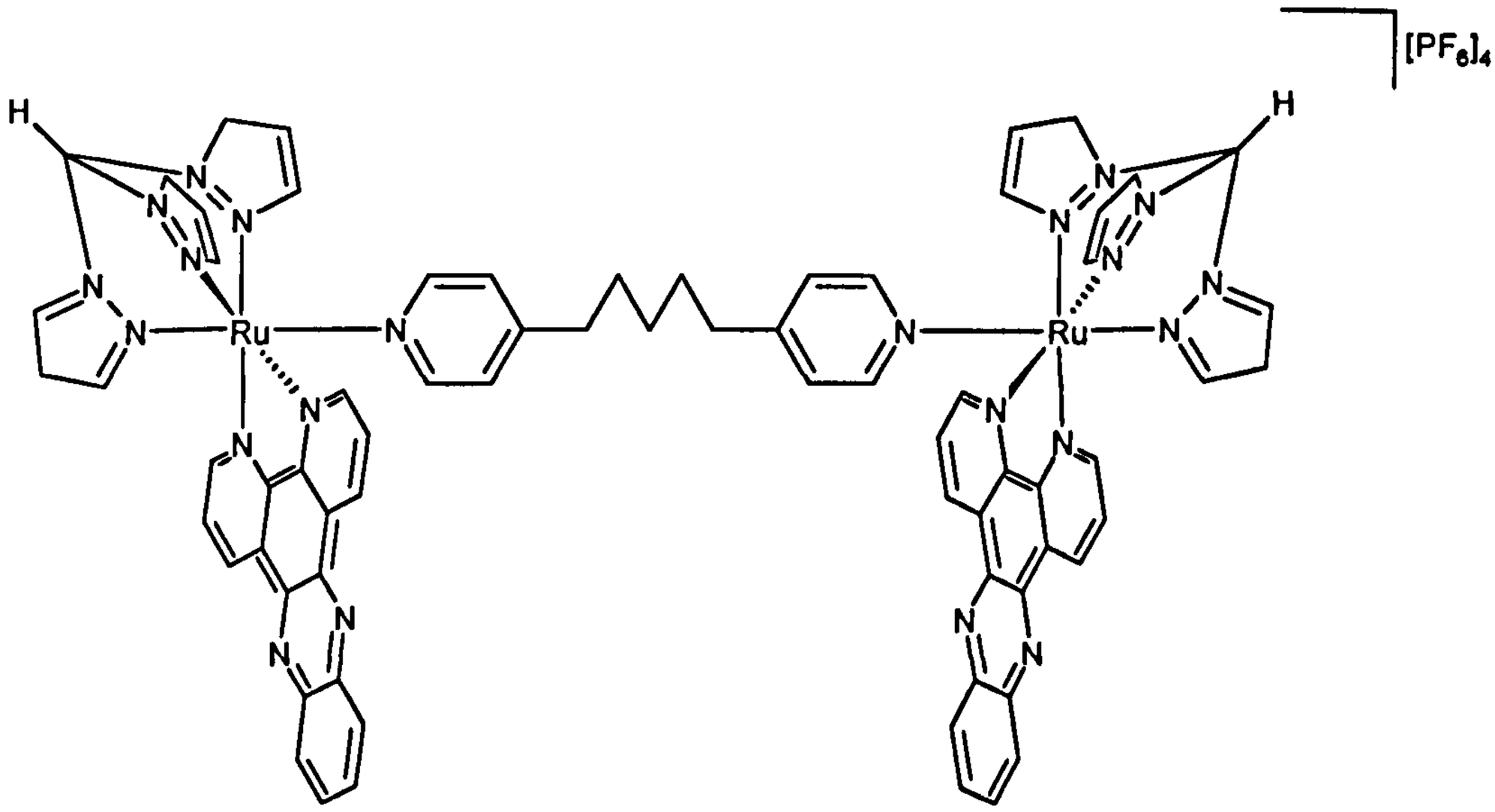

[TpmClRudppz]Cl (100mg, 0.13mmol) and $AgNO_3$ (2.05eq, 42mg, 0.264mmol) were refluxed in 1:1 EtOH/water (30cm^3) for 3 hours. The cooled solution was filtered through celite to remove AgCl. The filtrate was added dropwise to a refluxing solution of [Tpmdpp[5]Rudppz]Cl_2 (0.257mmol, 230mg) in 1:1 EtOH/water (30cm^3). The solution was left to reflux for 3 days. The cooled solution was concentrated and chromatographed on Sephadex CM-C25 ion exchange resin. The product was the first band eluted from the column with 0.1M NaCl in 5:3 water: acetone. The fractions containing the product were concentrated and the product was precipitated by addition of NH_4PF_6. The product was collected by centrifugation, washed with water, Et_2O and dried in vacuo. Mass = 43mg (16.5%) red powder. ^{1}H NMR (d^6-acetone): δ_H = 1.19 (m, 2H), 1.40 (m, 4H), 2.44 (t, 4H), 6.28 (t, 2H), 6.89 (dd, 2H), 6.93 (m, 8H), 7.55 (dd 4H), 8.18 (dd, 4H), 8.24 (dd, 4H), 8.42 (dd, 4H), 8.57 (m, 6H), 8.86 (dd, 4H), 9.37 (dd, 4H), 9.86 (dd, 4H), 10.10 (s, 2H).). –MS; m/z (%): 1858 (10) [M^+-PF_6], 857 (50) [M^{2+}-$2PF_6$). Anal. Calcd. for $C_{71}H_{58}N_{22}P_3F_{18}Ru_2$ (M^+-PF_6): 1857.2227. Found: 1857.2277.

Chapter 7

References

(1) McMurry, J. *Organic Chemistry*; 3 ed.; Brooks/Cole:, 1992.

(2) Stryer, L. *Biochemistry*; 4 ed.; W.H. Freeman:, 1999.

(3) Johnson, D. S.; Boger, D. L. Chapter 3 In *Comprehensive Supramolecular Chemistry*; Lehn, J. -M.; Murakami, Y., Ed.; Pergamon Press: Oxford, 1996; Vol. 4, p 73.

(4) Travers, A. *DNA-Protein interactions*; Chapman and Hall: London, 1993.

(5) Schmid, N.; Behr, J. P. *Biochemistry* **1991**, *30*, 4357.

(6) Goddard, W.; Plaxco, K. *Biochemistry* **1993**, *33*, 3050.

(7) Zimmer, C.; Wahnert, U. *Prog. Biophys. Mol. Biol.* **1986**, *47*, 31.

(8) Berman, H. M. *Curr. Opin. Struct. Biol.* **1994**, *4*, 345.

(9) Long, E. C.; Barton, J. K. *Accounts Chem. Res.* **1990**, *23*, 271-273.

(10) Jenette, K. W.; Lippard, S. J.; Vassiliades, G. A.; Bauer, W. R. *Proc. Natl. Acad. Sci. U. S. A.* **1974**, *71*, 3839.

(11) Barton, J. K.; Dannenberg, J. J.; Raphael, A. L. *J. Am. Chem. Soc.* **1982**, *104*, 4967-4969.

(12) Barton, J. K.; Danishefsky, A. T.; Goldberg, J. M. *J. Am. Chem. Soc.* **1984**, *106*, 2172-2176.

(13) Rehmann, J. P.; Barton, J. K. *Biochemistry* **1990**, *29*, 1701-1709.

(14) Barton, J. K.; Goldberg, J. M.; Kumar, C. V.; Turro, N. J. *J. Am. Chem. Soc.* **1986**, *108*, 2081-2088.

(15) Kumar, C. V.; Barton, J. K.; Turro, N. J. *J. Am. Chem. Soc.* **1985**, *107*, 5518-5523.

(16) Erikkon, M.; Leijon, M.; Hiort, C.; Norden, B.; Graslund, A. *J. Am. Chem. Soc.* **1992**, *114*, 4933.

(17) Satyanarayana, S.; Dabrowiak, J. C.; Chaires, J. B. *Biochemistry* **1992**, *31*, 9315.

(18) Coggan, D. Z. M.; Haworth, I. S.; Bates, P. J.; Robinson, A.; Rodger, A. *Inorg. Chem.* **1999**, *38*, 4486-4497.

(19) Barton, J. K.; Basile, L. A.; Danishefsky, A.; Alexandrescu, A. *Proc. Natl. Acad. Sci. U. S. A.* **1984**, *81*, 1961-1965.

(20) Kim, H. K.; Lincoln, P.; Norden, B.; Tuite, E. *Chem. Commun.* **1997**, 2375-2376.

(21) Friedman, A. E.; Chambron, J. C.; Sauvage, J. P.; Turro, N. J.; Barton, J. K. *J. Am. Chem. Soc.* **1990**, *112*, 4960-4962.

(22) Fees, J.; Ketterle, M.; Klein, A.; Fiedler, J.; Kaim, W. *J. Chem. Soc. Dalton Trans.* **1999**, 2595-2599.

(23) Fees, J.; Kaim, W.; Moscherosch, M.; Matheis, W.; Klima, J.; Krejcik, M.; Zalis, S. *Inorg. Chem.* **1993**, *32*, 166-174.

(24) Amouyal, E.; Homsi, A.; Chambron, J. C.; Sauvage, J. P. *J. Chem. Soc. Dalton Trans.* **1990**, 1841-1845.

(25) Jenkins, Y.; Friedman, A. E.; Turro, N. J.; Barton, J. K. *Biochemistry* **1992**, *31*, 10809-10816.

(26) Dupureur, C. M.; Barton, J. K. *J. Am. Chem. Soc.* **1994**, *116*, 10286-10287.

(27) Hiort, C.; Lincoln, P.; Norden, B. *J. Am. Chem. Soc.* **1993**, *115*, 3448.

(28) Tuite, E.; Lincoln, P.; Norden, B. *Journal of American Chemical Society* **1997**, *119*, 239.

(29) Holmlin, R. E.; Stemp, E. D. A.; Barton, J. K. *Inorg. Chem.* **1998**, *37*, 29-34.

(30) Collins, J. G.; Sleeman, A. D.; Aldrich-Wright, J. R.; Greguric, I.; Hambley, T. W. *Inorg. Chem.* **1998**, *37*, 3133-3141.

(31) Moucheron, C.; Kirsch-De Mesmaeker, A.; Choua, S. *Inorg. Chem.* **1997**, *36*, 584-592.

(32) Kirsch-De Mesmaeker, A.; Nasielskihinkens, R.; Maetens, D.; Pauwels, D.; Nasielski, J. *Inorg. Chem.* **1984**, *23*, 377-379.

(33) Masschelein, A.; Jacquet, L.; Kirsch-De Mesmaeker, A.; Nasielski, J. *Inorg. Chem.* **1990**, *29*, 855-860.

(34) Jacquet, L.; Kirschdemesmaeker, A. *J. Chem. Soc.-Faraday Trans.* **1992**, *88*, 2471-2480.

(35) Nunez, M. E.; Barton, J. K. *Curr. Opin. Chem. Biol.* **2000**, *4*, 199-206.

(36) Pyle, A. M.; Long, E. C.; Barton, J. K. *J. Am. Chem. Soc.* **1989**, *111*, 4520-4522.

(37) Jackson, B. A.; Alekseyev, V. Y.; Barton, J. K. *Biochemistry* **1999**, *38*, 4655-4662.

(38) Jackson, B. A.; Barton, J. K. *J. Am. Chem. Soc.* **1997**, *119*, 12986-12987.

(39) Kisko, J. L.; Barton, J. K. *Inorg. Chem.* **2000**, *39*, 4942-4949.

(40) Stoeffler, H.; Thornton, N.; Temkin, S.; Schanze, K. *J. Am. Chem. Soc.* **1995**, *117*, 7119.

(41) Yam, V. W. W.; Lo, K. K. W.; Cheung, K. K.; Kong, R. Y. C. *Chem. Commun.* **1995**, 1191-1193.

(42) Yam, V. W. W.; Lo, K. K. W.; Cheung, K. K.; Kong, R. Y. C. *J. Chem. Soc. Dalton Trans.* **1997**, 2067-2072.

(43) Stinner, C.; Wightman, M. D.; Kelley, S. O.; Hill, M. G.; Barton, J. K. *Inorg. Chem.* **2001**, *40*, 5245-5250.

(44) Pyle, A. M.; Morii, T.; Barton, J. K. *J. Am. Chem. Soc.* **1990**, *112*, 9432-9434.

(45) Campisi, D.; Morii, T.; Barton, J. K. *Biochemistry* **1994**, *33*, 4130-4139.

(46) Krotz, A. H.; Kuo, L. Y.; Shields, T. P.; Barton, J. K. *J. Am. Chem. Soc.* **1993**, *115*, 3877-3882.

(47) Krotz, A. H.; Kuo, L. Y.; Barton, J. K. *Inorg. Chem.* **1993**, *32*, 5963-5974.

(48) Krotz, A. H.; Hudson, B. P.; Barton, J. K. *J. Am. Chem. Soc.* **1993**, *115*, 12577-12578.

(49) Hudson, B. P.; Dupureur, C. M.; Barton, J. K. *J. Am. Chem. Soc.* **1995**, *117*, 9379-9380.

(50) Hudson, B. P.; Barton, J. K. *J. Am. Chem. Soc.* **1998**, *120*, 6877-

6888.

(51) Kielkopf, C. L.; Erkkila, K. E.; Hudson, B. P.; Barton, J. K.; Rees, D. C. *Nat. Struct. Biol.* **2000**, *7*, 117-121.

(52) Bobba, G.; Kean, S. D.; Parker, D.; Beeby, A.; Baker, G. *J. Chem. Soc. Perkin Trans. 2* **2001**, 1738-1741.

(53) Govenlock, L. J.; Mathieu, C. E.; Maupin, C. L.; Parker, D.; Riehl, J. P.; Siligardi, G.; Williams, J. A. G. *Chem. Commun.* **1999**, 1699-1700.

(54) Bobba, G.; Dickins, R. S.; Kean, S. D.; Mathieu, C. E.; Parker, D.; Peacock, R. D.; Siligardi, G.; Smith, M. J.; Williams, J. A. G.; Geraldes, C. *J. Chem. Soc. Perkin Trans. 2* **2001**, 1729-1737.

(55) Carlson, D. L.; Huchital, D. H.; Mantilla, E. J.; Sheardy, R. D.; Murphy, W. R. *Abstr. Pap. Am. Chem. Soc.* **1992**, *204*, 324-INOR.

(56) Carlson, D. L.; Huchital, D. H.; Mantilla, E. J.; Sheardy, R. D.; Murphy, W. R. *J. Am. Chem. Soc.* **1993**, *115*, 6424-6425.

(57) Oreilly, F.; Kelly, J.; KirschDeMesmaeker, A. *Chem. Commun.* **1996**, 1013-1014.

(58) O'Reilly, F. M.; Kelly, J. M. *New J. Chem.* **1998**, *22*, 215-217.

(59) Lincoln, P.; Norden, B. *Chem. Commun.* **1996**, 2145-2146.

(60) Önfelt, B.; Lincoln, P.; Norden, B. *J. Am. Chem. Soc.* **1999**, *121*, 10846-10847.

(61) Önfelt, B.; Lincoln, P.; Norden, B. *J. Am. Chem. Soc.* **2001**, *123*, 3630-3637.

(62) Foley, F. M.; Keene, F. R.; Collins, J. G. *J. Chem. Soc. Dalton*

Trans. **2001**, 2968-2974.

(63) Hannon, M. J.; Moreno, V.; Prieto, M. J.; Moldrheim, E.; Sletten, E.; Meistermann, I.; Isaac, C. J.; Sanders, K. J.; Rodger, A. *Angew. Chem. Int. Ed. Engl.* **2001**, *40*, 880-884.

(64) Balzani, V.; Juris, A. *Coord. Chem. Rev.* **2001**, *211*, 97-115.

(65) Balzani, V.; Campagna, S.; Denti, G.; Juris, A.; Serroni, S.; Venturi, M. *Accounts Chem. Res.* **1998**, *31*, 26-34.

(66) Balzani, V.; Ceroni, P.; Juris, A.; Venturi, M.; Campagna, S.; Puntoriero, F.; Serroni, S. *Coord. Chem. Rev.* **2001**, *219*, 545-572.

(67) Taube, H. *Advances in Chemistry Series* **1997**, *253*, 1-17.

(68) Taube, H. *Angew. Chem. Int. Ed. Engl.* **1984**, *23*, 329-339.

(69) Venturi, M.; Serroni, S.; Juris, A.; Campagna, S.; Balzani, V. *Dendrimers* **1998**, *197*, 193-228.

(70) Di Bella, S. *Chem. Soc. Rev.* **2001**, *30*, 355-366.

(71) Lacroix, P. G. *Eur. J. Inorg. Chem.* **2001**, 339-348.

(72) Lehn, J. M. *Nonlinear Opt. Prop. Org. Mol. Cryst.* **1987**, *2*, 215-220.

(73) Lehn, J. M. *Int. Congr. Catal., [Proc.], 8th* **1984**, *1*, I63-I83.

(74) Fujita, M. *Chem. Soc. Rev.* **1998**, *27*, 417-425.

(75) Erkkila, K. E.; Odom, D. T.; Barton, J. K. *Chem. Rev.* **1999**, *99*, 2777-2795.

(76) Seddon, K. R.; Seddon, E. R. *The Chemistry Of Ruthenium*; Elsevier: Amsterdam, 1984.

(77) Schroder, M.; Stephenson, T. A. *Comprehensive Coordination*

Chemistry; Pergamon: Oxford, 1987; Vol. 4.

(78) Sullivan, B. P.; Salmon, D. J.; Meyer, T. J. *Inorg. Chem.* **1978**, *17*, 3334.

(79) Balzani, V.; Juris, A.; Venturi, M.; Campagna, S.; Serroni, S. *Chem. Rev.* **1996**, *96*, 759-833.

(80) Chotalia, R.; Constable, E. C.; Hannon, M. J.; Tocher, D. A. *J. Chem. Soc. Dalton Trans.* **1995**, 3571-3580.

(81) Constable, E. C. *Adv. Inorg. Chem.* **1986**, *30*, 69-121.

(82) Constable, E. C.; Steel, P. J. *Coord. Chem. Rev.* **1989**, *93*, 205-223.

(83) Barigelletti, F.; Flamigni, L.; Balzani, V.; Collin, J. P.; Sauvage, J. P.; Sour, A.; Constable, E. C.; Thompson, A. *Coord. Chem. Rev.* **1994**, *132*, 209-214.

(84) Constable, E. C. *Progress in Inorganic Chemistry,* **1994**, *42*, 67-138.

(85) Constable, E. C.; Thompson, A.; Tocher, D. A.; Daniels, M. A. M. *New J. Chem.* **1992**, *16*, 855-867.

(86) Striplin, D. R.; Crosby, G. A. *Coord. Chem. Rev.* **2001**, *211*, 163-175.

(87) Sun, S. S.; Lees, A. J. *J. Am. Chem. Soc.* **2000**, *122*, 8956-8967.

(88) Coe, B. J.; Glenwright, S. J. *Coord. Chem. Rev.* **2000**, *203*, 5.

(89) Gelling, A.; Orrell, K. G.; Osborne, A. G.; Sik, V. *Polyhedron* **1999**, *18*, 1285-1291.

(90) Gelling, A.; Olsen, M. D.; Orrell, K. G.; Osborne, A. G.; Sik, V. *J.*

Chem. Soc.-Dalton Trans. **1998**, 3479-3488.

(91) Gelling, A.; Orrell, K. G.; Osborne, A. G.; Sik, V.; Hursthouse, M. B.; Hibbs, D. E.; Malik, K. M. A. *Polyhedron* **1998**, *17*, 2141-2151.

(92) Gelling, A.; Orrell, K. G.; Osborne, A. G.; Sik, V. *J. Chem. Soc. Dalton Trans.* **1998**, 937-945.

(93) Lippard, S. J.; Lerner, E. I. *J. Am. Chem. Soc.* **1976**, *98*, 5397.

(94) Gohring, W.; Schildknecht, J.; Federspiel, M. *Chimia* **1996**, *50*, 583.

(95) Constable, E. C.; Lewis, J.; Liptrot, M. C.; Raithby, P. R. *Inorg. Chim. Acta* **1990**, *178*, 47-54.

(96) Persaud, L.; Barbiero, G. *Can. J. Chem.* **1991**, *69*, 315.

(97) Goodwin, H. A.; Lions, F. *J. Am. Chem. Soc.* **1959**, *81*, 6415.

(98) Chirayil, S.; Hedge, V.; Jahng, Y.; Thummel, R. P. *Inorg. Chem.* **1991**, *30*, 2821.

(99) Vogler, L. M.; Scott, B.; Brewer, K. J. *Inorg. Chem.* **1993**, *32*, 898.

(100) Shaver, R. J.; Perkovic, M. W.; Rillema, D. P.; Woods, C. *Inorg. Chem.* **1995**, *34*, 5446.

(101) Sauvage, J. P.; Collin, J. P.; Chambron, J. C.; Guillerez, S.; Coudret, C.; Balzani, V.; Barigelletti, F.; Decola, L.; Flamigni, L. *Chem. Rev.* **1994**, *94*, 993-1019.

(102) Holmlin, R. E.; Barton, J. K. *Inorg. Chem.* **1995**, *34*, 7-8.

(103) Zou, X. H.; Ye, B. H.; Li, H.; Zhang, Q. L.; Chao, H.; Liu, J. G.; Ji, L. N.; Li, X. Y. *J. Biol. Inorg. Chem.* **2001**, *6*, 143-150.

(104) Barker, K. D.; Benoit, B. R.; Bordelon, J. A.; Davis, R. J.; Delmas, A. S.; Mytykh, O. V.; Petty, J. T.; Wheeler, J. F.; Kane-Maguire, N. A. P. *Inorg. Chim. Acta* **2001**, *322*, 74-78.

(105) Tuite, E.; Lincoln, P.; Norden, B. *J. Am. Chem. Soc.* **1997**, *119*, 239-240.

(106) Lincoln, P.; Norden, B. *J. Phys. Chem. B* **1998**, *102*, 9583-9594.

(107) Terbrueggen, R. H.; Barton, J. K. *Biochemistry* **1995**, *34*, 8227-8234.

(108) Franklin, S. J.; Barton, J. K. *Biochemistry* **1998**, *37*, 16093-16105.

(109) Szalda, D. J.; Keene, F. R. *Inorg. Chem.* **1986**, *25*, 2795.

(110) Reger, D. L.; Grattan, C. T.; Brown, K. J.; Little, C. A.; Lamba, J. J. S.; Rheingold, A. L.; Sommer, R. D. *J. Organomet. Chem.* **2000**, *607*, 120.

(111) Llobet, A.; Doppelt, P.; Meyer, T. J. *Inorg. Chem.* **1993**, *27*, 514.

(112) Dickenson, J. E.; Summers, L. A. *Aust. J. Chem.* **170**, *23*, 1023.

(113) Hartshorn, R. M.; Barton, J. K. *J. Am. Chem. Soc.* **1992**, *114*, 5919-5925.

(114) Casper, J. V.; Meyer, T. J. *J. Phys. Chem.* **1983**, *87*, 952.

(115) Jampolsky, L. M.; Baum, M.; Kaiser, S.; Sternbach, L. H.; Goldberg, M. W. *J. Am. Chem. Soc.* **1952**, *74*, 5222.

(116) Appel, M.; Sacher, W.; Beck, W. *J. Organomet. Chem.* **1987**, *333*, 237-244.

(117) Duveneck, G. L.; Kumar, C. V.; Turro, N. J.; Barton, J. K. *J. Phys. Chem.* **1988**, *92*, 2028-2032.

(118) Scatchard, G. *Ann. N. Y. Acad. Sci.* **1949**, *51*, 660.

(119) Latt, S. A.; Sober, H. A. *Biochemistry* **1967**, *6*, 3293.

(120) Lifson, S. *J. Chem. Pys.* **1964**, *40*, 3705.

(121) Crothers, D. M. *Biopolymers* **1968**, *6*, 575.

(122) Zasedatelev, A. S.; Gurskii, G. V.; Volkenshtein, M. V. *Mol. Biol* **1971**, *5*, 245.

(123) Schellman, J. A. *Israeli J. Chem.* **1974**, *5*, 84.

(124) McGhee, J. D.; von Hippel, P. H. *J. Mol. Biol.* **1974**, *86*, 469.

(125) Ladbury, J. E.; Chowdhry, B. Z. *Chem. Biol.* **1996**, *3*, 791.

(126) Haq, I.; Chowdhry, B. Z.; Jenkins, T. C. *Method Enzymol.* **2001**, *340*, 109.

(127) Sambrook, J.; Fritsch, E. F.; Maniatis, T. *Molecular Cloning: A Laboratory Manual*; Cold Spring Harbor Laboratory Press: New York, 1989; Vol. 1, 2, 3.

(128) Haq, I.; Lincoln, P.; Suh, D. C.; Norden, B.; Chowdhry, B. Z.; Chaires, J. B. *J. Am. Chem. Soc.* **1995**, *117*, 4788-4796.

(129) Loontiens, F. G.; Regenfuss, P.; Zechel, A.; Dumortier, L.; Clegg, R. M. *Biochemistry* **1990**, *29*, 9029-9039.

(130) O'Reilly, F. M.; Kelly, J. M. *J. Phys. Chem. B* **2000**, *104*, 7206-7213.

(131) Perrin, D. D.; Armarego, D. R.; Perrin, D. R. *Purification of laboratory chemicals*; 2nd Edition ed.; Pergamon Press: Oxford, 1980.

(132) Jameson, D. L.; Guise, L. E. *Tetrahedron Lett.* **1991**, *32*, 1999.